

Tactile Displays, Design and Evaluation

Dissertation zur Erlangung des akademischen Grades eines
Doktors der Ingenieurwissenschaften (Dr.-Ing.) an der Technischen
Fakultät der Universität Bielefeld.

vorgelegt von

Michael Fritschi

Februar 2016

1. Gutachter: Prof. Dr. Helge Ritter
Technische Fakultät / Neuroinformatics Group
Universität Bielefeld

2. Gutachter: Prof. Dr. Marc Ernst
Fakultät für Biologie / Kognitive Neurowissenschaften
Universität Bielefeld

Foreword

Upon the completion of this work, first I would like to express my gratitude for the contribution of my scientific advisors, Prof. Marc Ernst, Prof. Martin Buss, and Prof. Helge Ritter. Also, I am obliged to the other committee members, Prof. Ulrich Rückert and Dr. Andreas Kipp.

This thesis was a result of the EU project TOUCH-HapSys, and I would like to sincerely thank all members of this consortium for their valuable input and inspiring discussions.

The interdisciplinary nature of this European project, as well as the migration of entire research groups from one location to another, made it possible for me to experience the scientific environment at different institutions. Particularly, I have to name the control systems group (RS) at TU Berlin, the Institute of Automatic Control Engineering (LSR) at Technische Universität München, the Max-Planck Institute for Biological Cybernetics in Tübingen, and the Cluster of Excellence Cognitive Interaction Technology (CITEC) at Universität Bielefeld. Many former colleagues are now dear friends to me.

I deeply appreciate the scientific contribution of diverse close colleagues to this work, particularly of Marco Vitello and Knut Drewing. Special thanks go to the mechanical and electrical workshops in München and Tübingen, who enabled the realization of the devices described in this thesis.

I would also like to thank all the master students who contributed to this research, particularly Zlatko Marik and Hubert Brückner. Furthermore, I am indebted to all subjects who took part in the studies.

Finally, and most importantly, I dedicate this thesis to my wife and to my parents, who tirelessly supported me throughout these years.

Delft, 2016.

Michael Fritschi

Abstract

This thesis presents the design and development of several tactile displays, as well as their eventual integration into a framework of tactile and kinesthetic stimulation. As a basis for the design of novel devices, an extensive survey of existing actuator principles and existing realizations of tactile displays is complemented by neurobiological and psychophysical findings. The work is structured along three main goals: First, novel actuator concepts are explored whose performance can match the challenging capabilities of human tactile perception. Second, novel kinematic concepts for experimental platforms are investigated that target an almost unknown sub-modality of tactile perception: The perception of shear force. Third, a setup for integrated tactile-kinesthetic displays is realized, and a first study on the psychophysical correlation between the tactile and the kinesthetic portion of haptic information is conducted. The developed devices proved to exceed human tactile capabilities and have already been used to learn more about the human tactile sense.

Zusammenfassung

Diese Arbeit präsentiert die Konzeption und Konstruktion verschiedener taktiler Displays und schlussendlich ihre Integration in eine modulare Struktur taktiler und kinesthetischer Stimulation. Als Basis für die Entwicklung neuartiger Geräte wird ein ausführlicher Überblick über bereits bestehende Aktuierungskonzepte und bisherige Realisierungen taktiler Displays ergänzt durch neurobiologische und psychophysische Erkenntnisse. Diese Arbeit ist entlang dreier Hauptziele strukturiert: Zuerst werden neue Aktuierungskonzepte erforscht, deren Performanz den beeindruckenden Fähigkeiten menschlicher taktiler Wahrnehmung gewachsen ist. Zweitens werden neuartige kinematische Konzepte für Experimentalplattformen untersucht, welche eine fast unbekannt Sub-Modalität taktiler Wahrnehmung betreffen: Die Wahrnehmung von Scherkräften. Drittens wird ein Konzept für integrierte taktil-kinesthetische Displays realisiert, und eine erste Studie zum psychophysischen Zusammenhang zwischen dem taktilen und dem kinesthetischen Anteil haptischer Information durchgeführt. Die entwickelten Geräte erwiesen sich als den menschlichen taktilen Fähigkeiten überlegen, und sie wurden dementsprechend bereits eingesetzt, um mehr über den menschlichen taktilen Sinn zu erfahren.

Contents

1	Introduction	1
1.1	Terminology	1
1.2	The Human Tactile Sense	2
1.2.1	Anatomy of the Human Skin	3
1.2.2	The Somatosensory System	4
1.2.3	The Somatosensory Pathway	10
1.2.4	Psychophysics	14
1.2.5	Tactile Exploration	20
1.3	State of the Art in Actuator Technology and Tactile Displays	21
1.3.1	Actuator Types and Applications	22
1.3.2	Classification and Evaluation Criteria for Mechanical Tactile Actuators	23
1.3.3	Actuators based on Magnetic Fields	25
1.3.4	Actuators based on Electric Fields	29
1.3.5	Fluid Actuators	33
1.3.6	Thermal Actuators	34
1.3.7	Thermo-Tactile Actuators	35
1.3.8	Electro-Tactile Actuators	36
1.3.9	Conclusion	37
1.4	Contribution and Outline of this Thesis	41
2	Normal Force Display: The Multi-Actuated Pin	43
2.1	Design Concept	43
2.1.1	Guidelines from Tactile Perception	44
2.1.2	The Multi-Actuator Concept	46
2.1.3	Control Strategy	49
2.2	Low-Frequency Module	50
2.2.1	Construction	50
2.2.2	Position Sensor	54
2.2.3	Model Identification	55
2.2.4	Control Concept	63
2.2.5	Controller Performance	67
2.3	High-Frequency Module	71
2.3.1	Position Control	71
2.3.2	Controller Performance	72
2.4	Conclusion	74

3	Lateral Force Displays	77
3.1	Shear-Force Display	78
3.1.1	Concept and Specification	78
3.1.2	Hardware Setup	80
3.1.3	Evaluation Experiment	88
3.2	Slip-Friction Display	92
3.2.1	Concept and Specification	93
3.2.2	Hardware Setup	95
3.3	Conclusion	95
4	Integrated Kinesthetic and Tactile Stimulation	97
4.1	Combining Tactile and Kinesthetic Displays	98
4.1.1	Link Configuration	98
4.1.2	Kinesthetic Feedback: ViSHaRD 10	101
4.1.3	Tactile Feedback	101
4.1.4	Hardware Integration	103
4.2	Evaluation and Application	106
4.2.1	Evaluation of the Integrated Kinesthetic–Tactile Setups	106
4.2.2	Psychophysical Application: Perception of Virtual Stairs	110
4.3	Conclusion	113
5	Conclusion and Perspective	115
5.1	Investigating Mechanisms of Human Perception	115
5.1.1	Selective Attention	115
5.1.2	Interplay of Somatosensory Modalities	115
5.1.3	Interplay of Haptic Sub-Modalities	116
5.2	Outlook on Future Device Design	116
5.2.1	Exploiting Perception Phenomena to Reduce Complexity	117
5.2.2	Tailoring Tactile Devices to Convey Information in Novel Applications	118
5.2.3	The First Step	119
A	Technical Documents: Low-Frequency Actuator	121
B	Technical Documents: High-Frequency Actuator	123
C	Technical Documents: Pin-Based Shear Force Display	125

Notations

Abbreviations

CNS	central nervous system
DC	direct current
DEA	dielectric elastomer actuator
DOF	degrees of freedom
ER-fluids	electro rheological fluids
EAP	electromechanically active polymers
FA	fast adapting
FA-I	fast adapting type 1
FA-II	fast adapting type 2
FEM	finite element method
FNS	functional neuromuscular stimulation
HBB	haptic black box
JND	just noticeable difference
MEMS	micro electromechanical systems
MMMS	micromagnetomechanical systems
MR-fluids	magneto rheological fluids
PDMS	Polydimethylsiloxane
PMN-PT	lithium niobate crystals lead magnesium niobate-lead titanate
PSD	position sensitive diode
PWM	pulse wide modulation
PZN-PT	lead zinc niobate-lead titanate (ceramic perovskite material)
PZT	lead-zirconium-titanate (ceramic perovskite material)
RA	rapidly adapting
RC	radio controlled
RL	stimulus threshold
RMS	root mean square
SA	slow adapting
SA-I	slow adapting type 1
SA-II	slow adapting type 2
SMA	Shape Memory Alloys
SMT	surface-mount technology

Conventions

Scalars, Vectors, and Matrices

Scalars are denoted by upper and lower case letters in italic type. *Vectors* are denoted by lower case letters in boldface type, as the vector \mathbf{x} is composed of elements x_i . *Matrices* are denoted by upper case letters in boldface type, as the matrix \mathbf{M} is composed of elements M_{ij} (i -th row, j -th column).

x	scalar
\mathbf{x}	vector
\mathbf{X}	matrix
\mathbf{X}_+	positive definite matrix
$f(\cdot)$	scalar function
$\mathbf{f}(\cdot)$	vector function
$\dot{\mathbf{x}}, \ddot{\mathbf{x}}$	equivalent to $\frac{d}{dt}\mathbf{x}$ and $\frac{d^2}{dt^2}\mathbf{x}$
\mathbf{x}^T	transposed vector
$w'(x), w''(x)$	equivalent to $\frac{d}{dx}w$ and $\frac{d^2}{dx^2}w$

Subscripts and Superscripts

$\hat{\mathbf{A}}, \hat{\mathbf{b}}, \hat{\mathbf{c}}, \hat{\mathbf{x}}$	observer state space system
\overline{AB}	distance between point A and B
c_A	torsional stiffness coefficient at point A
c_{AB}	bending stiffness coefficient between point A and B
d_A	torsional damping coefficient at point A
d_{AB}	bending damping coefficient between point A and B
i_{AB}	transmission ratio between point A and B
I_i	transmission ratio of the i -th reduction gear
J_{AB}	inertia of the material between point A and B
l_{AB}	length between point A and B
m_{AB}	mass of the material between point A and B
M_0	momentum at position $x = 0$
n_{AB}	transmission ratio between point A and B
φ_A	angle at point A
U_i	i -th voltage value
$\tilde{\mathbf{x}}$	state vector error
Δx_A	displacement in x -direction at point A
Δy_A	displacement in y -direction at point A
y_{AB}	y -position shift of the center points of gravity between point A and B

Symbols and Abbreviations

\mathbf{A}	state space system matrix
\mathbf{b}	input vector of the state space system
b	width
b_s	damping coefficient (staircase experiment)
c	constant value of the Weber fraction
c_P	stiffness coefficient of the piezo actuator
C_P	piezo capacity
D_1, D_{12}, D_2, D_{21}	simplified, inertia related damping values
E	elastic modulus
E_{pot}	potential energy
F	force (staircase experiment)
F_{ext}	external force
f_{max}	maximum frequency
F_P	piezo force
ΔF_P	maximum piezo force shift
g	gravitational constant
h	hight
I	moment of inertia
I_P	piezo current
\mathbf{k}	gain vector
k	constant value of the Fechner's law
k_g	piezo command value–voltage gain
k_I	gain value (type I system)
K_P	piezo voltage–force constant
k_s	spring coefficient (staircase experiment)
\mathbf{l}	Kalman gain vector
l	length
L	Lagrangian function
l_i	length of the i -th link
l_{lower}	length of the lower lever of the low frequency actuator
l_{upper}	length of the upper lever of the low frequency actuator
M	momentum
M_{ext}	external torque
\mathbf{q}	generalized Lagrangian coordinates
\mathbf{Q}	weight matrix
Q_i	external torque

r	weight coefficient
R	dissipation energy
R_i	internal resistance
t, t_i	time
T	kinetic energy
u	input signal
U_{max}	maximum voltage
U_P	piezo voltage
\dot{U}_P	derivation of the piezo voltage
U_0	supply voltage
ΔU_0	maximum supply voltage shift
\mathbf{V}	weight matrix Kalman-Bucy filter
V	potential energy
v_{exp}	exploration velocity
v_s	avatar velocity (staircase experiment)
w'_l	bending deflection at position $x = l$
$w''(x)$	beam deflection
\mathbf{x}	state vector of the state space system
x_s	indentation depth (staircase experiment)
y	output signal
y_{begin}	start position of stimulus
y_{end}	end position
y_{start}	start position
\mathbf{z}	disturbance vector of the state space system
α, β, γ	angles related to the pivot points A, D, G
Π	covariance matrix (Matrix-Riccati-Equation)
φ	angle
Φ	physical stimulus intensity
$\Delta\Phi$	just noticeable difference
Φ_0	baseline intensity of physical stimulus
σ	stability margin
Ψ	magnitude of perceived sensation

List of Figures

1.1	Anatomic terminology of the human hand.	2
1.2	Cross-section of human skin. Reprinted from [128].	4
1.3	Glabrous Skin, Reprinted from [92], with permission from Elsevier.	4
1.4	Mechanoreceptors of the human glabrous skin, drawings by Henry Vandyke Carter, adapted from [66].	6
1.5	Types of mechanoreceptive response behavior. Adapted from [92], with permission from Elsevier.	7
1.6	Densities of the four types of mechanoreceptors. Adapted from [90], reprinted by permission of John Wiley & Sons.	8
1.7	Dorsal column - Medial lemniscal system. Reprinted from [135], with permission from Dr. Diana Weedman Molavi.	11
1.8	Approximate representation of sensory and motor information in the neocortex. Reprinted from [98] with permission from Cengage.	12
1.9	Frequency dependency of the thresholds for sinusoidal stimuli of FA-I, FA-II, and SA-I mechanoreceptors. Redrawn from [82], with permission from Cambridge University Press.	19
1.10	Selection of exploration procedures (EP's), reprinted from [113], with permission from Elsevier.	21
2.1	Parallel configuration	48
2.2	One common HF-Module	48
2.3	Stack piezo configuration. Reprinted from [154], with permission from Piezo Systems, Inc.	49
2.4	Stack piezo actuator	51
2.5	One-lever transmission	51
2.6	Cascaded two-lever transmission	51
2.7	First layout of combined lever system	52
2.8	First FEM design loop of the combined lever system	52
2.9	Final FEM design loop of the combined lever system	53
2.10	Final combined lever system with stack piezo	54
2.11	Schematic drawing of the position sensor concept (pin in upper position)	55
2.12	Mechanical model	56
2.13	Electrical model of the piezo, attached to the power supply	58
2.14	Open-loop frequency response, measured in experiment	62
2.15	Step response of the real system compared to the model.	63
2.16	Control structure	64
2.17	Standardized step response at different stability margins	65
2.18	Standardized computed actuating value at different stability margins	66
2.19	Kalman-Bucy-Filter block diagram [176]	67

2.20	Closed-loop response to a reference step from 1100 μm to 250 μm	68
2.21	Control input for a reference step from 1100 μm to 250 μm with respect to U_{max}	69
2.22	Closed loop step response from 250 μm to 1100 μm	69
2.23	Control input at a step from 250 μm to 1100 μm with respect to U_{max}	70
2.24	Complete setup of the low-frequency module	70
2.25	High-frequency stack piezo	71
2.26	High-frequency module control structure	72
2.27	Hysteresis of the stack piezo	73
2.28	Pulse signal tracking performance at 250 Hz	73
2.29	Sine wave tracking performance at 250 Hz	74
3.1	Functional principle of the Shear-Force Display.	80
3.2	Realization of one pin on top of a base rod with fixation points for the steering rods; top view of the arrangement of the four pins with base and control rods.	82
3.3	Kinematic actuation chain for the x - axis (left) and y - axis (right) of one pin.	83
3.4	Position error in dependence of the servo motor lever angle	85
3.5	Mechanical details of the prototype setup.	86
3.6	Hardware setup of the pin-based Shear-Force Display	86
3.7	Structure of the computer interface.	87
3.8	Composition of the PWM-signal	87
3.9	Connecting cable	87
3.10	Setup in Experiment 1.	89
3.11	Medians and quartiles of 84%-thresholds by standard direction.	90
3.12	Setup in Experiment 2.	91
3.13	Medians and quartiles of 84%-thresholds by standard direction and pin number.	92
3.14	Design of the sphere-based tactile Slip-Friction Display	94
3.15	Hardware setup of the tactile Slip-Friction Display	95
4.1	Serial kinematic approach; adapted from [108].	99
4.2	Parallel kinematic approach; adapted from [108].	99
4.3	ViSHaRD 10 with standard end-effector.	102
4.4	VirTouch Mouse [124].	103
4.5	Mounting mechanism on ViSHaRD 10.	104
4.6	Slip-Friction Display mounted on ViSHaRD 10.	105
4.7	Shear-Force Display mounted on ViSHaRD 10.	105
4.8	VirTouch Mouse mounted on ViSHaRD 10.	106
4.9	ViSHaRD 10 + Shear-Force Display.	109
4.10	ViSHaRD 10 + Slip-Friction Display.	109
4.11	ViSHaRD 10 + VirTouch Mouse.	110
4.12	Virtual stairs.	111
4.13	Edge stimuli for haptic rendering in the evaluation task.	112
4.14	Mean ratings and SD for five ratings each of different steepness. Data of one subject in condition with and without additional tactile feedback.	113

A.1	Technical drawing of the lever system (unit of length = mm)	121
A.2	Circuit diagram of the IR-Position sensor	122
B.1	Connector pin assignment of the strain gauge (full Wheatstone bridge) of the PSt 150/5/40 piezo actuator module, taken from [155]	123
B.2	Circuit diagram of the strain gauge amplifier	124

List of Tables

1.1	Classification of nerve fibers, according to Erlanger and Gasser. Adapted from [138]	5
1.2	Summary of the functional features of the four types of mechanoreceptors, extracted by neurobiological investigations.	9
1.3	Magnetic field principles that can be used for tactile displays	38
1.4	Electric field and thermal actuation principles that can be used for tactile displays	39
1.5	Fluid principles that can be used for tactile displays	40
2.1	Stack piezo data	51
2.2	Stiffness coefficients	60
2.3	Deviations and masses of the combined lever system	61
2.4	Stack piezo data	71
3.1	Specifications for the Shear-Force Display.	79
3.2	Performance data of the RC-servo motor DS 3781	81
3.3	Dimensions of the kinematic chain	83
3.4	Technical data of the Shear-Force Display.	88
4.1	Specifications of ViSHaRD 10	101

1 Introduction

To enhance the immersion of a human user into a virtual or telepresent environment, it is effective to stimulate as many senses as possible. Compared to visual and auditory feedback, *haptic* (and herein especially *tactile*) feedback represents a relatively young technology, yet it is a key requirement for a realistic impression. This chapter provides background information on the human tactile perception and ways to stimulate it. This information is given from a multidisciplinary point of view: First, the biological functionality of the haptic sense, second, psychophysical investigations on haptic perception, third, technical possibilities and state-of-the-art devices to stimulate the tactile sense.

1.1 Terminology

A problem that arises in cross-disciplinary research is the varying connotation of key terms in the different fields. Probably the most critical part in this case concerns the essential concept of haptics and its several sub-classifications. The definitions as they are used in this thesis are:

tactile [lat. *tāctilis*, from *tāct(us)*, past participle of *tangere*, 'to touch'] connected with the sense of touch. Perceptible or designed to be perceived by touch [185].

cutaneous [lat. *cutis*, 'skin'] having to do with the skin [185].

kinesthetic [gr. *kīnein*, to move + *esthesia*, the ability to feel or perceive sensations.] The sense that detects bodily position, especially force and movement of the muscles, tendons, and joints. The sensation of moving in space [38]. In the medical and psychological fields of research, the term *proprioception* is often used. This term seems quite similar, but it is more related to a static position.

proprioception [lat. *proprius*, meaning "one's own" + perception] is the sense of the relative position of neighboring parts of the body, e.g. limbs like arms and legs.

haptic [gr. *haptikos*, from *haptesthai*, able to touch or grasp] relating to the sense of touch [185]. In correspondence with essential publications in this area of research, e.g. [123], we use this word as a general term for tactility and kinesthetics.

somatic [gr. *sōmatikos* corporeal, bodily] having to do with the body, rather than the mind [185]. Will be used in the term *somatosensory system* that describes the sensory system of the human body (e.g. cutaneous, proprioceptive, kinesthetic, pain).

modality In this book, the term modality describes one single channel of the human sense, with respect to its neurological connection. The human modalities are usually divided in: visual and auditory modalities (major modalities), and haptic modalities. The main focus will be on these haptic modalities, which are divided into tactile and kinesthetic sub modalities.

Anatomic terminology of the human hand: The terminology of the human hand is explained in Fig. 1.1. It is derived from the medical standard expressions and reduced to the termini that are important in this book.

somatic [gr. *sōmatikos*, of the body] Having to do with the body rather than the mind [185].

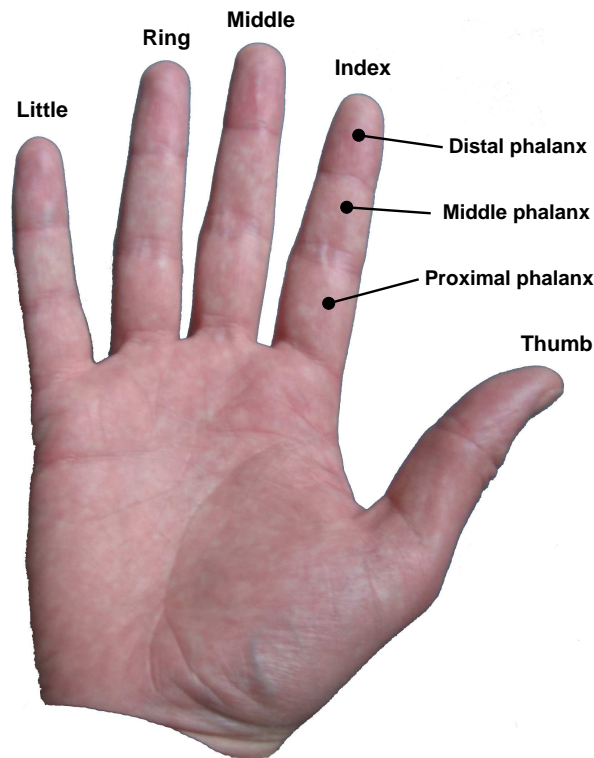


Figure 1.1: Anatomic terminology of the human hand.

1.2 The Human Tactile Sense

The tactile sense of humans, as well as of allied species, is a complex area of research, in particular because of its interdisciplinary character. As this thesis is written for readers with an engineering background, this section will summarize necessary additional information from other disciplines like medicine, biology, or psychology.

The human tactile sense can be assessed from two different viewpoints or layers. These two levels of analysis can be classified according to the research disciplines as a neurobiological level and as a psychological level.

In the functional chain, neurobiological research represents the fundamentals, as it focuses on the relationship between the physical detection of a stimulus and its further processing. This comprises the functionality of the receptors and their anatomy, as well as

the signal pathways and the signal processing in the brain. Neurobiology could be characterized as a qualitative examination of the processes involved during haptic exploration. Early publications in this research field, as can be found in [2–5], investigate the response behavior of the sensory nerve impulses. In animal models, the main classes of sensory receptors for touch, pressure and pain have been identified.

Based on these fundamental insights of neurobiological science, the higher-level processes like the integration and conjunction of the nerve signals into the human perception are usually described in a specialized research field of psychology. Founded in 1860 [48] by Gustav Fechner, who introduced quantitative methods to precisely measure the relationship between stimulus (*physics*) and perception (*psycho*), this area of research is called *psychophysics* [63]. The main focus is on the mental processing of stimuli and their conscious perception. To this end, various experimental methods and questionnaires in combination with statistical analyses are used.

The gathered knowledge concerning the functionality and performance of the human tactile sense can be used in different ways. For example, the psychophysical “benchmark” of the human perceptual system provides a valuable basis for the realization of novel haptic displays.

In this section, a combined survey of both neurobiological and psychophysical research is given. First, the anatomy of the human skin will be outlined, followed by the neurological functionality of its sensory components. The goal is to provide a comprehensive overview of the measurable quantities. Later, an introduction to psychophysics as a subdivision of perception psychology will be provided. Besides the fundamental ideas of this research direction, its methods, paradigms, and results will be described and discussed, as far as they are relevant for experiments in this thesis. The section closes with a description of different types of tactile exploration and their relation to other modalities, whereby the focus is on haptic interaction of the finger(s) with the environment.

1.2.1 Anatomy of the Human Skin

The human skin is probably the largest organ of our body. Covering us completely, it has an area of about 17 m^2 [138]. Its main function is to cover the visceral organs and to protect them against various environmental conditions like temperature, humidity, or radiation, as well as against bacteria and hazardous substances. Its structure is therefore dominated by the leather-like covering layer, which represents the borderline between our body and the environment. To handle these functions, the skin is built as a self-regenerating surface, organized in different layers [186]. The main part of the skin can be divided into hairy skin and skin without hair, known as *glabrous skin* *.

The cross-section view, as displayed in Fig. 1.2, shows the constituents of the human skin, which are mainly classified into three layers: *Epidermis*, *Dermis*, and *Subcutis*.

The **Epidermis** [gr. *epi* over, upon; *derma* skin] is the outer layer of the skin, which is directly exposed to the environment. It has a thickness of $30 - 2000\ \mu\text{m}$ and is divided into several sublayers, which are continuously renewed from beneath, whereby the horny layer of dead cells at the top is regularly repelled. Due to this continuous renewal, there

*Additionally there are also Mucous membranes lining the inside of body orifices and Mucocutaneous areas (junction of the mucous membrane, lips and tongue)[138]

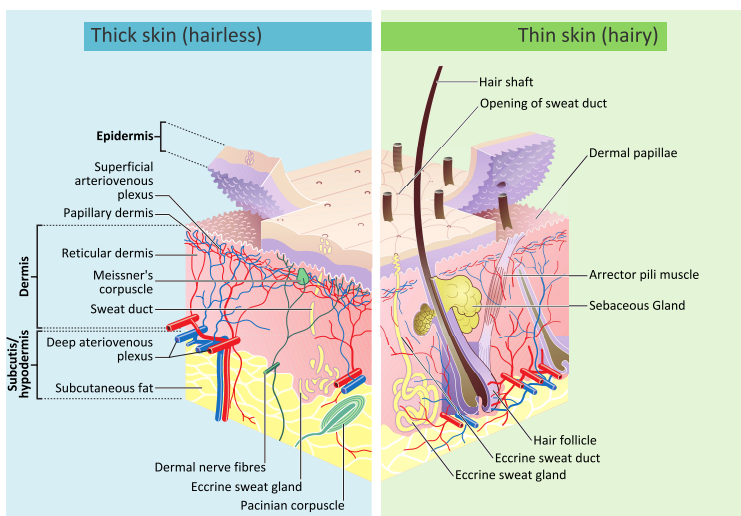


Figure 1.2: Cross-section of human skin. Reprinted from [128].

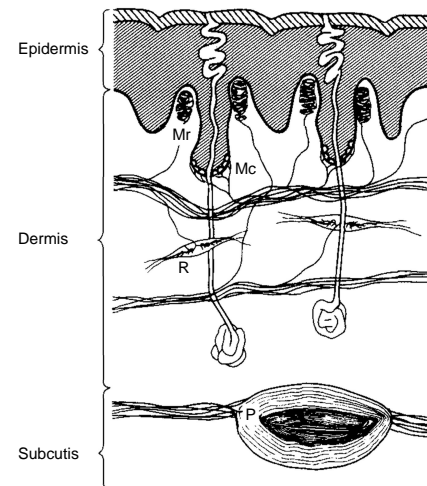


Figure 1.3: Glabrous Skin, Reprinted from [92], with permission from Elsevier.

are no receptors for physical perception in the outer layer, thus the main function of this layer is to protect us from injury and dehydration.

The second layer of the skin, called **Dermis**, has a thickness of $500 - 1500 \mu\text{m}$. It contains the main part of the receptors for physical perception as well as the perspiratory and sebaceous glands. Furthermore, this is the layer where the hair follicles with their sensory system are located, as well as a network of muscle fibers to detect and cause hair motion.

Beneath these two layers, which are commonly referred to when using the term *skin*, there is the **Subcutis** [lat. *subcutis* under-skin]. It consists of connective and adipose tissue, which contains a network of blood vessels and nerve pathways, as well as sensory receptors for high pressure perception. It varies in thickness across the human body, and it usually ends at the subjacent bone.

Fig. 1.3 shows a simplified cross-section view of the human glabrous skin, which depicts only the different layers and the location of mechanoreceptors and sweat glands. For further considerations of tactile perception in the area of the inner surface of the index finger pulp, we will restrict our focus to the glabrous skin located there.

1.2.2 The Somatosensory System

The somatosensory system is a compound of various kinds of sensory receptors that are activated by physical or chemical excitation, usually caused by interaction of the human body with the environment. In detail, it comprises specialized sensors for tactile, kinesthetic and proprioceptive stimuli (mechanoreceptors) as well as for temperature (thermoreceptors) and pain (nociceptors). These sensors are distributed within the tissue, especially beneath the skin or at the muscles and joints they correspond to. They fulfill the function of converting the physical information caused by the stimulus into an information format that is processable by the subsequent nerve system. Through a system of afferent nerve fibers, the information passes to the CNS (*central nervous system*) for further processing.

The information is transported along the nerve fibers in form of electric signals, so-called action potentials. An action signal pulse is initiated by a sensory unit (e.g. corpuscle). The nerve fiber is usually in resting state at a negative potential of -70 mV, which is the electric potential in the inner nerve fiber with respect to its surrounding. A depolarization of the potential above a certain threshold of $15 - 20$ mV triggers a positive feedback loop and thereby causes a short-time overshoot of approximately $+30$ mV and an approximate length of 1 ms. This action potential or nerve pulse travels along the nerve fiber with a characteristic velocity like a spreading wave. As the signal follows an all-or-none law, the process of triggering such a signal is termed *firing* a pulse. One action potential constitutes the minimum possible information quantum. The information content is coded in the pulse frequency of the fired pulses. In the late 60ies, a method to measure and record signals of selective somatosensory nerve fibers was developed. This technique, which is still used today, employs a coated Tungsten electrode with a diameter of $5 - 15$ μm to measure the electric potential in the inert nerve cell in situ [199].

Table 1.1: Classification of nerve fibers, according to Erlanger and Gasser. Adapted from [138]

Type	Diameter [μm]	Velocity [m/s]	Efferent fibers	Afferent fibers
A α	10 – 20	60 – 100	skeleton muscle	neuromuscular spindle (primary), tendon sensors
A β	7 – 15	40 – 90	–	neuromuscular spindle (secondary), mechanoreceptors (skin)
A γ	4 – 8	15 – 30	neuromuscular spindle	–
A δ	3 – 5	5 – 25	–	nociceptors, thermal sensors, deep sensibility sensors
B	1 – 3	3 – 15	vegetative ganglion	–
C	0.3 – 1	0.5 – 2	sympathetic effectors	nociceptors, <i>et al.</i>

Nerve fibers can communicate only unidirectionally, thus they are functionally categorized in *afferents*, which transmit nerve pulses towards the CNS, and *efferents*, which transmit nerve pulses from the CNS to muscles or adenoids. The transmission velocity of nerve fibers differs by up to a factor of 100, depending on the diameter and the consistency of their myelin coating, which ensures electrical insulation against the surroundings. Tab. 1.1 lists the classification of nerve fibers and associates them with afferent and efferent nerve fibers in the human body. It also illustrates how the transmission velocity is directly correlated with the diameter of the fiber: The thicker the diameter, the higher the velocity of the pulses. The classifying letters are given related to this velocity in descending order. All types of A and B fibers have a myelin sheath, whereas type C fibers have not.

To transform the physical and chemical information into nerve pulses, in most cases there are specialized sensory elements (receptors) located at the end of the afferent fibers.

In the following, the receptors of the somatosensory system will be described in detail. They are predominantly to be found in the glabrous skin and clustered by functions into three groups: mechanoreceptors, thermoreceptors, and nociceptors.

For the scope of our research in tactile perception, primarily the mechanoreceptors are of interest. Therefore, these receptors are described in more detail than the other two types.

Mechanoreceptors

The task of the mechanoreceptors is the transformation of the physical information of pressure and force into nerve pulses for further transportation via nerve fibers. They usually consist of a corpuscle-like structure with a pressure-sensitive membrane, which initiates pulses of a characteristic frequency. With respect to their mechanical response, they are classified into two major categories, the FA (*fast adapting*) and the SA (*slow adapting*) receptors, see Fig. 1.5. The human glabrous skin contains four different types of mechanoreceptors, which are:

- Meissner corpuscles
- Merkel receptor complexes
- Ruffini endings
- Pacinian corpuscles

In addition to these four receptors, there are mechanoreceptors specialized for inert vitals and muscle fibers. Furthermore, there are other means of sensing mechanical stimuli, which involve hair bulbs. However, these are not covered here.

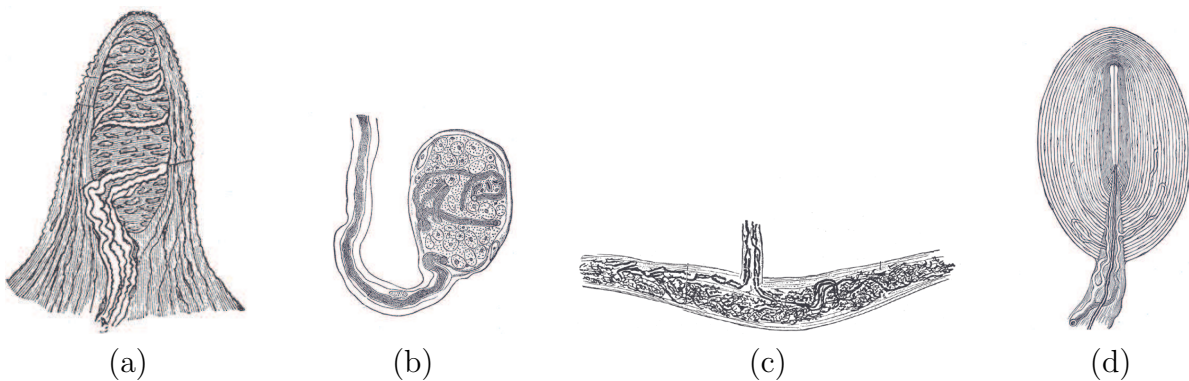


Figure 1.4: Mechanoreceptors of the human glabrous skin, drawings by Henry Vandyke Carter, adapted from [66].

Meissner corpuscles are depicted in Fig 1.4(a). They are ovoid and have a size of about $30 \times 80 \mu\text{m}$ [82]. Fig 1.3 depicts the position of the corpuscles (Mr) in the pocket-like cavities directly underneath the epidermis in upright orientation. The corpuscles consist of lamellated endings with coiled receptor axons, and they are connected to the epidermis by collagen fibers [9]. They respond very sensitively to small deformations of the epidermis. The cup-shaped sheath around the nerve terminal at the bottom of the corpuscle makes it mainly insensitive to stimuli from deeper skin layers. Meissner corpuscles are connected via nerve fibers of type $A\alpha$ to the spinal cord, they are classified as FA-I (*fast-adapting type 1*)[†].

[†]The classification is analog to the RA (*rapidly-adapting*), which is alternatively used in literature.

They respond very fast even to small indentation stimuli at the fingertip. An important property is that the receptor only fires in response to a change of the stimulus (velocity) and thus it shows differential or, in control engineering terms, *D-behavior*. The response frequency range is about 10 – 200 Hz and has its maximum sensitivity at 40 Hz [183]. The innervation density of the Meissner corpuscles within the palm of the hand varies from 25 units/cm² to 140 u./cm², where the maximum density can be found in the finger tips, especially in the index finger [90] (Fig. 1.6). With a percentage of 43%, it is the most frequent mechanoreceptor in the human hand among all four types. However, the average receptive area of one corpuscle is, with about 13 mm², marginally larger than that of the second numerous, the Merkel receptor complexes [91], see Tab. 1.2.

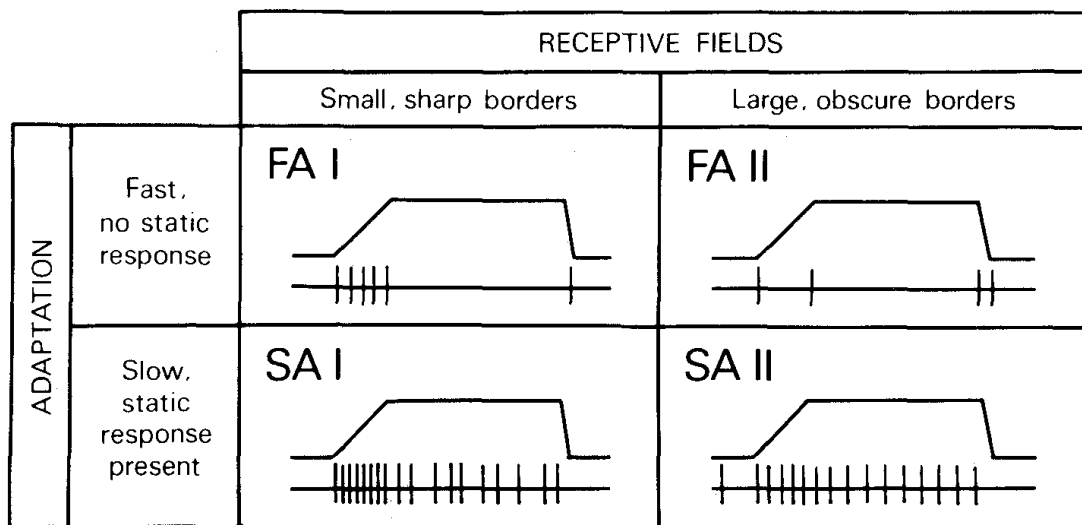


Figure 1.5: Types of mechanoreceptive response behavior. Adapted from [92], with permission from Elsevier.

Merkel receptor complexes are clustered groups of disk-shaped thin plates (Fig. 1.4(b)) with a diameter of up to 10 μm . There are 50 – 70 of these terminals bundled together to one myelinated sensory axon of the type $A\alpha$. They are located in the basal layer of the epidermis as shown in Fig. 1.3(MI)[9]. The Merkel's discs are classified as SA-I (*slow-adapting type 1*) that are characterized by general firing activities as long as a stimulus is present. As the pulse frequency additionally rises depending on the indentation velocity of the stimulus, the signal shows a proportional and differential (*PD*) behavior (Fig. 1.5). The response frequency ranges from 0.4 to 100 Hz, with a maximum sensitivity at about 50 Hz [26]. The contingent of Merkel receptor complexes amounts to 25% with a density of 10 – 70 u./mm², whereby the maximum density is found at the finger tips, likewise the Meissner corpuscles (Fig. 1.6).

Ruffini endings are based on a cylindric corpuscle core and an extensively branched plexus of collagenous endaxons as depicted in Fig. 1.4(c). Stretch of the aligned collagenous fibers also stretches the core of the Ruffini endings, such that these fibers provide the mechanical linkage for force stimuli tangential to the skin. They are located in the dermis but their fibers extend also to the subcutaneous area of the skin [9], signed with (R) in Fig. 1.3. Regarding the signal characteristics in Fig. 1.5, the Ruffini endings are classified as SA-II (*slow adapting type 2*), and in general they exhibit *PD* behavior, because the firing frequency rises proportionally to the indentation of a stimulus, and it also slightly depends

on its velocity. Early comprehensive research on Ruffini corpuscles has been undertaken on the hairy skin of cats [33]. An interesting fact is that Ruffini endings never have been observed in neurophysiological studies with monkeys [94] which caused the assumption for a long time that they are also nonexistent in the human somatosensory system [95]. Recent anatomical studies in [146] indicate, however, that there exists a small number of Ruffini corpuscles in the human index finger. The values for the response frequency are not consistently reported and lie in a range between 0 Hz and some 100 Hz. The maximum sensitivity differs from 0.5 Hz [93] up to 50 Hz [26]. In addition to the absence of perceptual sensation reported in [144] regarding Ruffini corpuscles, these values seem to be not very reliable. However, investigations in [90] have identified an innervation density of 10 – 20 units/cm² with a percentage of 19 % among all four types of receptors, with an accordingly large receptive field of about 59 mm² [91].

Pacinian corpuscles consist of a non-myelinated terminal of an A α nerve fiber embedded in a union-like lamellar structure of about 20 – 30 perineural capsules. The oval corpuscle, as depicted in Fig. 1.4(d), is located 2 – 3 mm deep within the subcutaneous tissue of the skin and can reach a length of up to 2 mm (Fig. 1.3(P)) [159]. Pacinian corpuscles respond to alternating stimuli like vibration, and they are sensitive in the range of 70 – 1000 Hz, with a maximum sensitivity at 200 – 250 Hz [183]. The skin layer above the corpuscles probably acts as a kind of mechanical *high-pass filter*. These properties classify the receptors as FA-II (*fast-adapting type 2*) and, as they measure the acceleration of the stimuli, the response can be identified as a double differentiator, or D^2 behavior. Regarding the population, Pacinian corpuscles are the least numerous type of mechanoreceptors, with a ratio of 13 %. As shown in Fig. 1.6, they are mostly uniformly distributed with a density of around 10 units/cm². They have a very large receptive area of 101 mm², due to the filtering effect caused by the deep location of the receptor.

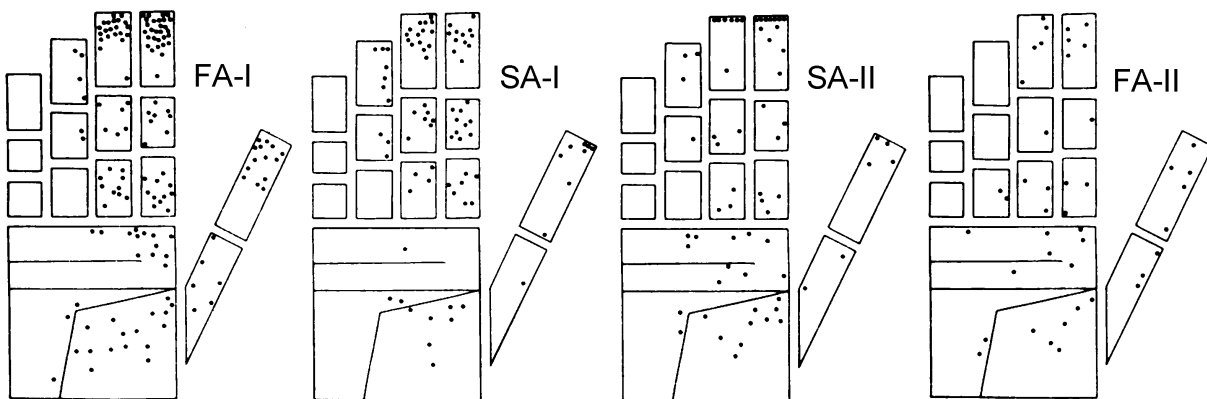


Figure 1.6: Densities of the four types of mechanoreceptors. Adapted from [90], reprinted by permission of John Wiley & Sons.

For almost all receptors described above, Fig. 1.6 shows a strong clustering tendency of mechanoreceptors towards the finger tip, especially of the index finger. Obviously, there is a strong correlation between operative functionality and sensory innervation of the hand. This makes even more sense if we consider the necessity of sensory receptors regarding the operative range of the human hand.

Table 1.2: Summary of the functional features of the four types of mechanoreceptors, extracted by neurobiological investigations.

Features	Meissner corpuscles	Merkel receptor complexes	Ruffini endings	Pacinian corpuscles
Location	Superficial dermis	Basal epidermis	Dermis and subcutis	Dermis and subcutis
Adaptation class	FA-I	SA-I	SA-II	FA-II
Control system type	D	PD	PD	D ²
Receptor size	$30 \times 80 \mu\text{m}$	$10 \mu\text{m}$	–	1 – 2 mm
Response frequency	10 – 200 Hz	0.4 – 100 Hz	0 – 100 Hz	70 – 1000 Hz
Max. sensitivity	40 Hz	50 Hz	0.5/50 Hz	200 – 250 Hz
Sensory units	43 %	25 %	19 %	13 %
Innervation density	25 – 140 /cm ²	10 – 70 /cm ²	10 – 20 /cm ²	10 /cm ²
Receptive area	13 mm ²	11 mm ²	59 mm ²	101 mm ²

In Tab. 1.2, the performance data of the human tactile sense at the hand is summarized. The data results from a large amount of neurobiological and anatomical investigation in recent years[‡]. According to the density distribution of the human hand, depicted in Fig. 1.6, the maximal values for the innervation density of Tab. 1.2 can be found in the area of the fingertip. Overall, there are about 240 – 250 sensory units, divided in 60 % Meissner, 30 % Merkel receptor complexes, 5 – 8 % Ruffini endings, and 2 – 5 % Pacinian corpuscles. Further investigations on the interplay of the mechanoreceptors during striking of several dot pattern have been conducted in [152] and [153].

Whereas nearly all mechanoreceptors have been clearly identified and measured by now, there still remain some ambiguities about the Ruffini endings. Furthermore, there seems to exist a relationship between stimulus and temperature, especially in the frequency domain, such that temperature influences the perception of stimuli with frequencies above 100 Hz [26]. This observation suggests that Pacinian and Meissner corpuscles are sensitive to temperature changes.

Thermoreceptors

In order to sense the temperature of our surroundings, we have specialized receptors, which are mainly located beneath the skin and close to important viscera (deep-body thermoreception). In glabrous skin, there are two types of receptors, one responds to *warm* temperatures and the other type to *cold* temperatures.

Cold temperature receptors consist of free nerve endings with a static temperature response of 10 – 40°C. The maximum firing rate of the nerve endings is reached at about 25°C followed by a decline of discharge frequency to almost zero at 41°C. A remarkable

[‡]The data regarding frequency response of the receptors additionally contains results of psychophysical investigations ([26])

phenomenon is a second rise of the firing rate at a temperature of 47°C, which causes the known paradox cold-perception effect. The cold-pain sensation is triggered by specialized nociceptors, to be described later. Cold temperature receptors are located in the upper part of the Dermis and they are mostly connected through A δ -fibers to the nervous system.

Warm temperature receptors also consist of free nerve endings, but these are usually located in a deeper layer of the dermis, and they are connected through non-myelinated type C nerve fibers to the nervous system. The response to temperature starts at about 30°C and rises steeply until the maximum at about 43°C, followed by a steep decay. An important consequence of the response characteristic of these two sensors is the low firing rate of nerve impulses of both receptor types in a comfortable temperature range of 31 – 36°C, which results in a neutral temperature perception.

The conscious thermo-perception system has the aim to indicate temperature changes towards critical areas of warm and cold, and it does not respond in a comfortable range of temperature. As thermal housekeeping is an important requirement for an efficiently working organism, there exists a highly sophisticated underlying control cycle for thermal regulation located at the hypothalamus region of the brain. Main actuators in the forward control loop are e.g. sweat glands and more complex metabolic processes. Mathematical models and control engineering (cybernetic) explorations can be found in [161, 209, 210]. A more detailed description of the thermo-reception and temperature regulation can be found in [42, 77].

Nociceptors

For the perception of pain, a special class of receptors are responsible, the *nociceptors*, specialized to respond to destructive (noxious) influences to the human body [§]. They are not only distributed beneath the skin, but also at several important places at which their function as alarm sensors is necessary. Nociceptors consist of free nerve endings of thin C-fibers (non-myelinated) fibers or A δ -fibers (lightly myelinated). In regular environmental and health conditions, they do not fire nerve pulses. Noxious stimuli, however, transform into electric potential and discharge as nerve pulses. Usually, nociceptors are triggered by strong pressure, temperatures above 43°C, or extremely cold stimuli. As a result of their small size, the reception field is very constricted [138]. A description of pain perception as a process of the CNS caused by nociceptors can be found in [27, 215].

1.2.3 The Somatosensory Pathway

The somatosensory pathway denotes the entire path that the generated pulse signal takes until its final destination at the parietal lobe of the primary somatosensory cortex. On this way, the signal passes several areas at which preprocessing, either by synaptic blocking, or by rearrangement takes place. The somatosensory pathway subsumes the transmission of all sensory nerve signals of proprioception and depth perception, but the pathway described here is focused on the mechanoreceptors of the skin. The signals travel along the ascending pathway (afferent nerve fibers) from sensors upwards through the spinal cord and the thalamus toward the primary somatosensory cortex of the brain. On a descending pathway (efferent nerve fibers), the commanded nerve signals reach their destination like muscles

[§]It is important to distinguish between nociception and pain, with pain denoting a subjective perception that is not necessarily caused by nociceptors.

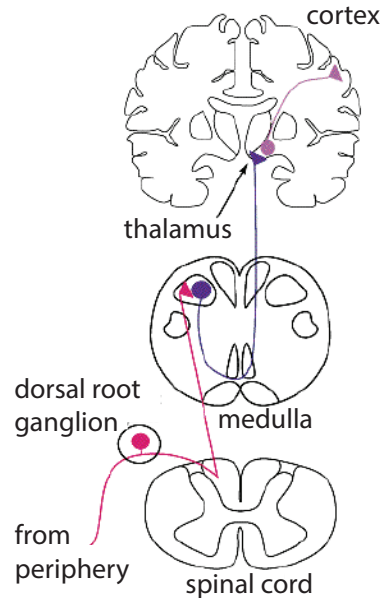


Figure 1.7: Dorsal column - Medial lemniscal system. Reprinted from [135], with permission from Dr. Diana Weedman Molavi.

or other mostly actuating elements. An overview of the afferent somatosensory pathway, containing cross section views of the important junctions and the relevant corridors in the brain, is shown in Fig. 1.7.

Once triggered by a stimulus, a nerve signal travels along the nerve fibers toward the spinal cord with the corresponding velocity, classified in Tab. 1.1. Each afferent nerve fiber enters the dorsal root of the spinal cord by passing so-called *ganglion cells*. At this entrance into the spinal cord, the nerve fibers pass a unique type of sensory neuron, the axons of which are not connected to the neuron as usual, instead they by-pass the neuron. For this reason, the axons at this stage are called *primary afferents*. Whereas the afferent axons of thermoreceptors and nociceptors terminate early in the spinal cord for synapsing, the afferent axons of mechanoreceptors ascent in the white matter (*Funiculus posterior*) of the spinal cord until they terminate on the *gracile nucleus* in the caudal medulla in a network of synapses. Not all primary afferents reach the synapses at the caudal medulla. About half of them terminate at spinal cord level, they are known as propriospinal fibers. The afferents that continue after synapsing are called *secondary afferents* and after a decussation into the *ipsilateral dorsal columns*, the fiber bundle continues to ascend through the medial lemniscal system up to the thalamus. After a further synaptic process in the somatosensory nuclei of the thalamus (*ventroposterolateral nuclei*), the resulting third (final) axons spread out to the primary somatosensory cortex in the parietal lobe, to their final destination.

The primary somatosensory cortex (*postcentral gyrus*) of the frontal lobe is located next to the primary motor cortex (*precentral gyrus*), as shown on the left side of Fig. 1.8, and it is topically organized. Each location of the area of the somatosensory cortex represents sensations from different parts of the body Fig. 1.8(a). In direct neighborhood, the primary motor cortex (*postcentral gyrus*) is located, with a similar representation map for movement regulation of the different body parts Fig. 1.8(b). The size of the body parts drawn above the sectional view of the brain indicates the size of the brain area. As this area is primarily

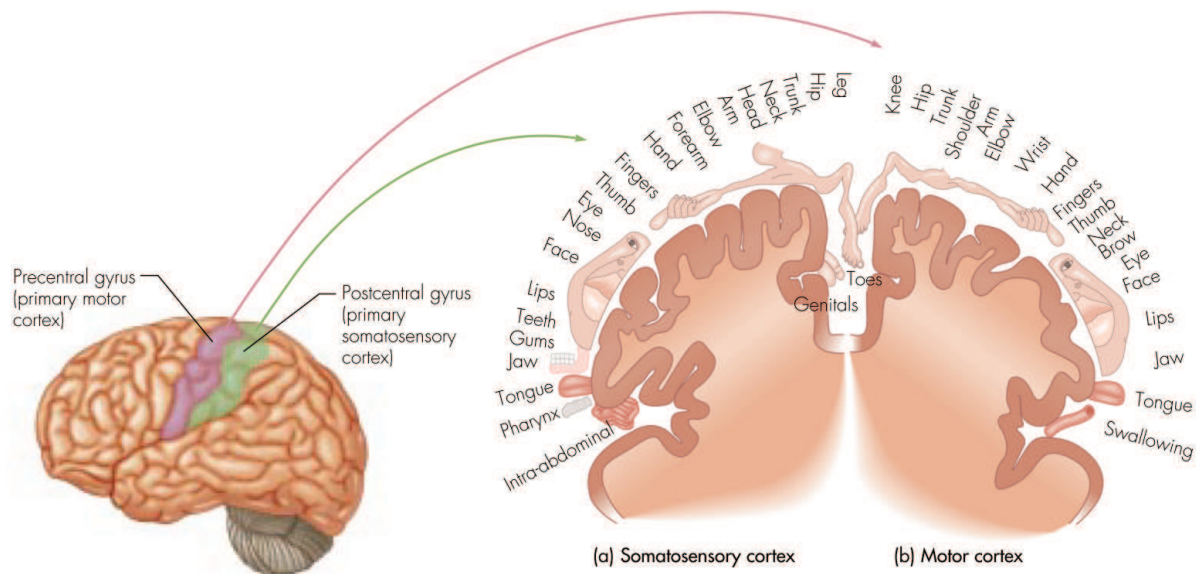


Figure 1.8: Approximate representation of sensory and motor information in the neocortex. Reprinted from [98] with permission from Cengage.

used for information processing, body parts with high innervation density, like the fingertips or the lips, have a larger representation area in the brain. The arising manikin is formally known as motor/sensory *homunculus* (lat. “little man”).

This graphical representation of the topical organization of the brain areas gives only a general overview of location and distribution. In practice, these areas are dynamic and can be changed or reorganized. It has been shown that it is possible to enlarge a specific representation area as a result of training or experience. The opposite effect is observed when areas become unused, as a result of injury, e.g. spinal cord injury or amputation. In these cases, the disused areas are re-organized to other somatosensory abilities.

From the multitude of sensory information that is induced by the large numbers of several sensory subsystems of the human body, such as haptic, visual, and auditory, only a very few amount reaches our conscious perception. The bulk of somatosensory information is selected by several filter mechanisms. Those mechanisms interfere on several states of the signal pathway, for instance at the entrance to the dorsal root by the ganglion cells or at the corresponding synapses on the way to the primary somatosensory cortex. The signal can, however, also be deflected to the vegetative nervous system, which performs autonomous functions of our organism. A very important mechanism to filter the huge amount of sensory information that is directly linked to our understanding of conscious perception is *attention*. Although not even the exact functionality of consciousness is sufficiently understood until now, there is evidence that attention is based essentially on corresponding operations that mainly occur in the neocortex and in the *paleocortex*[¶]. In this process, transient bindings in the primary somatosensory cortex seem to play an important role [39]. These may establish a kind of short-time memory that thus temporarily links the representation of physical sensations, projected to the primary somatosensory cortex, to conscious perception. A model approach based on this theory of selective attention realized for the visual domain [141] seems to explain quantitatively experimental data

[¶]The olfactory cortex of the cerebrum

obtained in neurophysiological studies presented in [136], which are performed with animals. A review that compares several theories of selective attention is presented in [140]. It supports also fundamental mechanism of *synchrony*, in which the action potentials that arrive at a neuron synchronously produce higher postsynaptic firing rates than asynchronous presynaptic signals, whose resulting firing rate can possibly be suppressed.

Electrophysiological experiments, made in [189], evidence that synchrony is a neural correlate of attentional selection. Therefore, several neuron pairs in the secondary somatosensory cortex of three animals were measured while these practiced experiments with attention shifts between tactile and visual stimuli. Results of recent experiments of the same research group can be found in [168].

The phenomenon of selective attention is of great importance. It should be of particular consideration when planing a realization of experiments to measure human perception.

To describe and model the somatosensory pathway, as well as of further information processing in the human brain, there are several approaches based on mathematics. A very famous method, which was initiated by Warren McCulloch and Walter Pitts in 1943, is the mathematical framework of Artificial Neural Networks (ANNs). This alternative form of a mathematical model differs from classical models in that it does not have to be processed sequentially. Instead, each computational element can in principle be connected to any other, whereby the connection structure has to be learned in a separate processing step. This concept is derived from the structure and functionality of the neural system of mammals, and thus it contains computational elements that have similar functionality as in the neurobiological example (e.g. neurons, synapses, axons)[166]. With introduction of digital computing technology, Neural Networks gained additional relevance, because of the possibility of recursive computation. Today, it is still a widely used method to simulate complex structures of information processing, for instance in image processing or speech recognition. The main disadvantage of this model framework, however, stems from the fact that it is very difficult, if not impossible, to formally analyze the behavior of Neural Networks, e.g. to prove stability or robustness.

Another mathematical approach has been developed by the research field of system theory, a branch of automatic control engineering, which resulted in the novel research field of *cybernetics*, which specializes on control system theory as well as on Neural Networks. The basic modeling approach in classical system theory is a mathematical representation via differential equations, because these offer are a very powerful tool to simulate nature's processes, and, moreover, can be assessed by a wide range of system analyzing methods.

Some modeling approaches regarding parts of the somatosensory pathway have been mentioned in the preceding chapter. One focus of interest is the behavior of the sensory receptors, as described in [16, 45, 49, 50, 157], where usually a relation between the stimulus and the resulting nerve signal is described mathematically. An approach to modeling the tissue of the index finger using a framework of equations built by FEM (*finite element method*), can be found in [71] and [41]. This model provides insight into the transformation of the mechanical information encoded in the stimulus on its way to the receptor. An investigation to find the optimal shape of a Pacinian corpuscle can be found in [85]. An approach based on the statistical model of Markov chains describes the firing statistics of FA mechanoreceptors [37].

Another, more general reason for modeling parts of the somatosensory pathway is to learn more about the low-level regulation mechanisms of our organism. Vegetative functions of the organism include for instance temperature regulation, which is essential for

survival. This autonomous feedback control mechanism is described and investigated in [77, 209, 210]. These vegetative control mechanisms take place in the spinal cord or in the hypothalamus and usually acquire their measurement signal (feedback signal) from the somatosensory pathway.

A closed-loop control externally processed by a computer is described in [75]. In this experiment, a limb of an anesthetized cat was used as force actuator by applying FNS (*functional neuromuscular stimulation*). The measurement input for the control loop was recorded from the skin mechanoreceptors of the footpad by using a nerve cuff. The task of the experiment was force control of the leg, in terms of preventing a gripped object from slipping, hence the implementation of an artificial gripping reflex.

1.2.4 Psychophysics

The research topic of psychophysics is designated to quantitative methods for precisely measuring relationships between stimuli in the physical domain Φ and sensations in the psychological domain Ψ . Historically, it originated at the transition from philosophical speculation of mental events to psychology.

A central role in psychophysics is attributed to the concept of *sensory threshold*. The idea of sensory threshold is based on the assumption that mental events are only registered consciously if they exceed a certain amount of sensory stimulation. The sensation that is caused by a stimulus can generally be described in four dimensions: intensity, quality, extension, and duration.

The sensory threshold is classified in absolute and difference threshold. Absolute threshold is defined as the minimum amount of stimulation energy that is necessary to produce a sensation, also known as *stimulus threshold* or *RL* ^{||}. Difference threshold is the smallest necessary amount of change in physical stimulation that is perceived, which is defined as JND (*just noticeable difference*).

A considerable step towards the measurement of differential sensitivity has been made by E. H. Weber. He discovered that the relation between a rise of differential threshold (JND) and the rise of its initial intensity of the stimulus is constant. This relationship can be described with the *Weber fraction*:

$$\frac{\Delta\Phi}{\Phi_0} = c \tag{1.1}$$

The constant value (c) that results of the JND ($\Delta\Phi$) and the starting intensity of the stimulus (Φ_0) can be seen as an individual constant for the related perception modality. However, the characteristics of Eq. (1.1) against the intensity of a stimulus Φ_0 delivers generally constant values. Only for lower values of intensities, the results diverge strongly from the constant value.

Later on, the founder of psychophysics, G. T. Fechner, enhanced *Weber's law* by adding a logarithmic relation between the physical stimulus intensity (Φ) in units above threshold and the perceived sensation magnitude (Ψ). Thus, the so-called *Fechner's law* can be formulated as:

$$\Psi = k \cdot \log(\Phi), \tag{1.2}$$

^{||}From the German expression: Reiz Limen

where k is a constant multiplier that depends on the particular sensory dimension and modality. An essential assumption for valid results of *Fechner's law* is the validity of *Weber's law* in the considered range of values. Eq. (1.1) and Eq. (1.2) provide a basic mathematical relation between a selected physical stimulus intensity and its sensation magnitude. This is useful for systematic interpretation of experimental results.

An additional phenomenon that should be considered is the more or less pronounced effect of adaption, which strongly depends on the perceived modality. The origin of adaption can be found on the signal layer of the neurons. It is caused by the temporal change until saturation of sensory response to a stimulus. Adaption is mostly related to all type A nerve fibers, thus the entire haptic perception is affected by adaption. However, nerve fibers of type C are unconcerned of the adaption effect, which explains that e.g. pain can persist over a long time. The devolution of adaption in the time domain can be mathematically approximated as logarithmic decline of the stimulus-caused sensory value with variable decay constant[143].

As indicated above, one central topic of psychophysics is the measurement of sensory threshold concerning mental events. The three classical methods that are used practically to determine absolute as well as differential thresholds are: *the method of constant stimuli*, *the method of limits*, and *the method of adjustments*. In the following, a very brief snapshot of the classical methods used for psychophysical measurement is given. This overview is oriented along the three described methods in [60], which is referred to for more detailed information.

Method of constant stimuli

To detect the absolute threshold using the method of constant stimuli, a certain amount of about five to ten stimuli with usually equidistant intensity has to be defined. The range of stimuli has to be chosen starting from a low stimulus intensity that is likely to be not noticeable by the subject up to a stimulus intensity that is detected almost always. This way, the expected threshold is located in-between. During the experiment, the subject is presented a stimulus for a fixed time duration. Afterwards, the subject has to decide whether or not he felt a stimulus. Therefore, each stimulus is presented repeatedly about 100 times or more. Furthermore, it is mixed with the other stimuli in random order. To analyze the result, a function of the perceptual amount of detected responses per intensity is determined. For each discrete presented intensity value, the perceptual proportion of "yes" answers is plotted against the corresponding stimulus, with stimuli sorted in ascending order. The data points should scatter around an ogive-shaped curve, the so-called *psychometric function*, this is due to the fact that biological and psychological measurements tend to be normally distributed. The threshold in intensity can directly be read from the diagram at the projection of the 50 % level of detected response.

To determine differential thresholds with the method of constant stimuli, the procedure and data analysis is slightly different. While performing the experiment, two stimuli are presented to the subject. One is named *reference stimulus* and the other *comparison stimulus*. The discrepancy between them varies in several finite steps of intensity regarding the measurement criteria, in analogy to the absolute measurement method. It is also important to scale the comparison stimuli in a range from not noticeable to an intensity that can be almost always detected by the subject. The order of presenting reference and comparison stimulus, as well as the presented sequence of intensity is usually randomized,

also in analogy to the absolute threshold method. After each trial, the subject has to decide whether the second stimulus differed from the first regarding a given question, like: “Was the second stimulus stronger than the first?”. Analyzing the data again consists in fitting an ogive-shaped psychometric function like described above, which displays the proportion of correct answers against the values of comparison stimuli. Now, the 50 % level characterizes the PSE (*point of subjective equality*), it represents the point that is subjectively perceived as being equal to the standard stimulus, averaged over a large number of trials. In practice, the PSE does not correspond exactly to the value of the standard stimulus, which will be considered by calculating a constant error.

Method of limits

The principle behind the method of limits is to converge to the threshold stepwise. Therefore, the trial starts either at an intensity that can be clearly perceived or from the opposite side of a not noticeable intensity. In the first case, stimulus intensity descends in small steps and terminates at the point where the presented stimulus is just not noticeable. The related level of the corresponding intensity value results from the last detected value plus half of the last intensity step. To obtain a representative value for the threshold, several trials for the same threshold have to be performed (about 10) , starting either from the perceptible or from the non perceptible area of intensity. The comparison of the results from the up and down approximation regarding one threshold usually should show an area where the successfully voted values of intensity overlap. The result can be calculated by the mean of all threshold intensity values.

The method of limits can also be used to determine difference thresholds. For this case, pairs of standard and comparison stimuli are presented and the subject has to identify whether the intensity of the comparison stimulus was higher or lower compared to the standard stimulus. Similar to the absolute threshold detection method described above, it is possible to start from a point of clearly distinguishable difference of intensity and travel in equidistant degradation of intensity toward the point where no difference between the pairs is noticeable. Additionally, several trials in opposite direction have to be performed to determine the differential threshold, which is also calculated by the mean of all trials.

A well-known derivate of the method of limits is the widely established *method of staircase*. The method starts as well with a clearly noticeable or definitely not perceptible stimulus and converges stepwise toward the threshold. After passing the threshold, the direction of step changes and the step size is reduced. This results in an asymptotic approximation of the threshold. The procedure terminates when some predetermined criterion or number of trials has been reached.

Method of adjustments

The method of adjustments is designated to measure difference thresholds, but it can also be used to measure absolute thresholds. An essential difference compared to the other standard methods is the fact that the subject controls the changing rate of the presented stimuli. To measure absolute thresholds, the procedure starts at a stimulus either far below or far above the expected threshold. The subject then ascends or descends the stimulus continuously by an almost arbitrary amount, until it is above or below the

limit of perception. Subsequently, the absolute threshold is calculated by the mean of all adjustment trials.

In case of using the method of adjustment to determine a difference threshold, a standard and a comparison stimulus are presented simultaneously. The subject is instructed to vary the comparison stimulus until it is perceived equal compared to the standard stimulus. Like in the other methods, the starting point for the comparison stimulus is well above or beneath the expected threshold and the experiment consist of several trials, which are usually conducted in randomized order. This method is also often used to determine the average error between the physical stimulation and the subject's response over a certain amount of trials. This resulting error can for instance be used as performance criterion for the psychophysical evaluation experiment.

Absolute and differential tactile thresholds

Restricted to the considered domain of tactile perception at the fingertip, there is not a large amount of publications concerning threshold determination. In the following, a selected overview of thresholds is given, mainly reduced to the later needed mechanical specifications. Thus, the kind of stimuli are focused on the indentation threshold perpendicular toward the skin and to the threshold of a stimulus that moves tangential to the skin, thus causing skin-stretch.

As shown in the section above, the parameters of the stimulus to which the mechanoreceptors may respond are displacement, velocity, and acceleration in the time domain, as well as displacement, gradient of displacement, and curvature of displacement in the spatial domain. Thus, the value of stimulation threshold can usually be determined for a static stimulus, but it can also be measured in dependence of temporal stimuli at varying frequencies.

Together with the above described absolute and differential thresholds, four possible thresholds per stimulus are conceivably (absolute-static, absolute-dynamic, differential-static, differential-dynamic).

Indentation thresholds

The absolute-static threshold for indentation in perpendicular direction varies in the skin region of the human hand. The lowest threshold value is $11.2\ \mu\text{m}$ and can be found at the distal phalanx of the index, middle, and ring finger. In contrast, the sensitivity decrease to a threshold of about $36\ \mu\text{m}$ in the palm. To find these values, the test stimulus was induced by a small probe with a diameter of $0.45\ \text{mm}$ and a hemispherical tip. It moved toward the indentation point and immediately back with the same speed of $4\ \text{mm/s}$ [89]. The sensitivity correlates with the density of mechanoreceptors, as shown in Fig. 1.6. The maximum indentation depth for a stimulus is constrained by the bone. On average, it amounts to $3\ \text{mm}$ at the fingertip, but it depends on the individual subject. The stiffness rises against the indentation depth from about $0.1\ \text{N/mm}$ in the range of $0 - 1\ \text{mm}$ over $0.4\ \text{N/mm}$ at $1 - 2\ \text{mm}$ to $1.0\ \text{N/mm}$ in the depth of $2 - 3\ \text{mm}$ [71].

Regarding the absolute-static threshold for tangential stimuli that cause skin stretch, only few values can be found in literature. This may be due to the fact that in practice it is impossible to provide pure stimulation tangential to the skin, without simultaneous stimulation of indentation perpendicular to the skin. As pointed out during the func-

tionality description of the mechanoreceptors, the SA-II typed Ruffini endings are mainly designated to receive stimuli in this direction. However, also the other receptors are inevitably involved in the perception of stimuli tangential to the skin [24]. This fact makes adds to the difficulty of stimulating in these two orthogonal directions.

In contrast to the absolute-static threshold of stimuli, there exist a few investigations regarding absolute-static force threshold values for tangential stimulation. Psychophysical experiments conducted in [147] pointed out that the subjective intensity estimates were accurately scaled to the magnitude of the shear force on the skin over a range of forces from 0.15 N to 0.75 N. Another investigation approach determining absolute-static threshold of tactile stimuli presented tangential to the skin was made by [22]. In the performed experiments, subjects received a reference stimulus in perpendicular direction and afterwards had to adjust the deflection of the comparison stimulus, given alternately in perpendicular or tangential direction, to the same length. The results show a significantly higher sensitivity in tangential displacement, as subjects chose tangential displacements 0.6 times as large as the reference displacement. Interestingly, the required force effort in tangential direction increased by a factor of four. This can be explained by the high stiffness of 0.53 N/mm at the related skin area.

If the stimulus moves at a certain frequency, the perceived impression is usually classified as vibration. The sensation of vibration again can be subdivided into a lower part and a higher part. The lower part is beneath about 80 Hz, at which the oscillation can be perceived as single distinguishable pulses. With increasing frequency, the perceived stimulus fuses to a continuous impression that is perceived as vibration [159]. This change defined also the transition from the static to the dynamic class of stimuli, as defined above. The maximum perceivable value of frequency was found to be 10 kHz[182].

Fig. 1.9 shows the sensitivity characteristics of stimuli thresholds plotted against the sinusoidal stimulation frequency. It has been determined for all three mechanoreceptors that respond to perpendicular indentation. The resulting line (red) represents the perceived sensitivity vibration with a maximal sensitivity of $0.6 \mu\text{m}$ at about 230 Hz. Like the sensitivity of vibration, also the impedance changes depending on the stimulating frequency, in nonlinear manner [70] according to its viscoelastic behavior. These results cover at least the differential-dynamic and absolute-dynamic case of stimuli thresholds, whereas for the differential-static case, as well as for differential stimuli provided tangential to the skin, no investigations have been found.

Spatial thresholds

The spatial threshold is primarily designated to the resolution of tactile events at the skin. Thus it directly results from the lateral 2-point limen, a differential-static threshold that describes the minimum distance for which two otherwise identical stimuli (needles) can be perceived as two different impressions. Based on [180] this JND is determined to 1 mm for the index finger pulp. The spatial threshold for tactile stimuli depends on the distribution and innervation density of the mechanoreceptors, depicted in Fig. 1.6 and quantified in Tab. 1.2.

Associated with the dynamic class of spatial thresholds, there are some experimental result that show a clear dependency of the JND on the stimulation frequency of the differential stimulus [181]. Thus, the spatial resolution increases with increasing stimulation frequency. This can be observed easily in everyday live, where tactile exploration of tiny

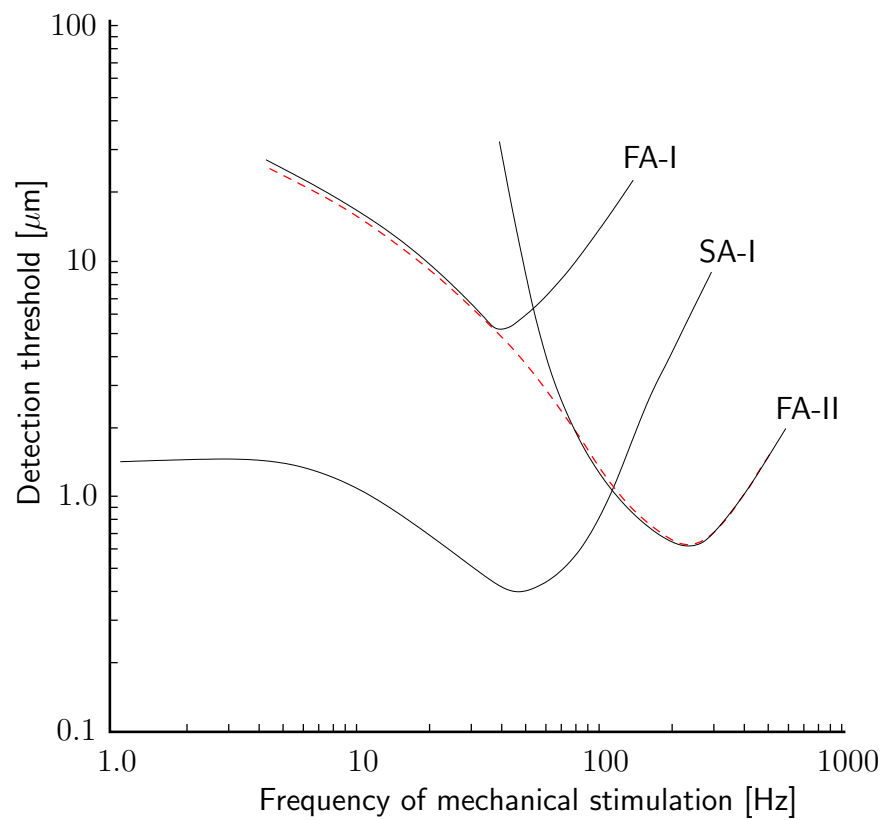


Figure 1.9: Frequency dependency of the thresholds for sinusoidal stimuli of FA-I, FA-II, and SA-I mechanoreceptors. Redrawn from [82], with permission from Cambridge University Press.

features is enhanced when vibrotactile stimulation is added by striking the fingertip over the feature. This phenomenon can be explained by the fact that static stimulation affects only the mechanoreceptors in the upper layer of the skin (Meissner corpuscles and Merkel receptor complexes). At frequencies above about 25 Hz the number of mechanoreceptors rises by the amount of the Pacinian corpuscles located deeper in the skin. Furthermore, some of the participating receptors are only sensitive to frequency stimulation. Thus, a similar characteristic as shown for the absolute thresholds in the paragraph above can be assumed.

1.2.5 Tactile Exploration

Beside the anatomical, biological and psychophysical perspectives and knowledge, this subsection completes the interdisciplinary survey concerning the human tactile sense by some fundamental considerations about the *act* of tactile exploration and its possible consequences in view of psychophysical measurement and technical realization of tactile displays. In the following, only the aspects of tactile exploration that are most relevant for the investigations in this book (attention, passive and active exploration) are considered. A more comprehensive classification and description of tactile exploration can be found in [95].

Passive Exploration

Passive touch denominates the scenario where a subject receives a stimulus while remaining in a static position. This situation occurs when the subject sits passively on a chair and someone else pokes the fingertip at several points. In everyday life, this is an almost unusual situation, most of the time we move our fingers about the objects we intend to explore. This type of exploration is called **active exploration**. However, most of the psychophysical threshold measurement experiments presented above are designed as **passive exploration** experiments. The main challenge when designing active exploration experiments is the increasing complexity due to additional perception effects (phenomena) that have to be considered in this case. However, this can also be seen as a chance to investigate the human perception more in depth.

Active Exploration

The strategy used in daily life represents a more realistic case of exploration, which is active exploration. It describes in general tactile exploration combined with additional kinesthetic movement of the sensing finger in relation to the object.

While performing such active exploration, the sensitivity of the tactile sense enhances the possibilities of tactile exploration, for instance by palpation. Since besides the tactile sense also the thermal and kinesthetic sense is involved in the process of perception, the challenge to describe this process gets more and more complex. Recent investigations try to describe the procedure of perception in an even more generic approach by including the visual modality as well [46].

The multiple possibilities to explore an object have been classified in several kinds of exploration, so-called **exploration procedures (EP)** [113]. This classification subdivides

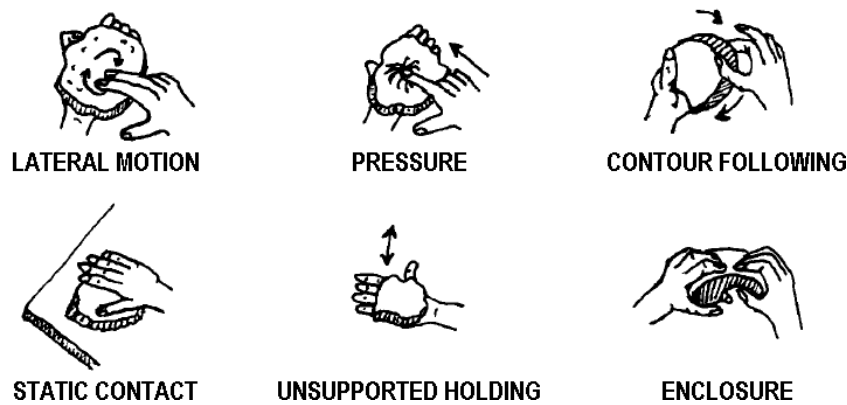


Figure 1.10: Selection of exploration procedures (EP's), reprinted from [113], with permission from Elsevier.

tactile exploration into eight procedures of tactile object observation, whereof the six most relevant EP's are shown in Fig. 1.10.

Lateral motion and pressure is important to identify consistency, whereas contour following provides essential information on the shape of an object. During static contact, heat conductance can be interpreted as a further parameter of object consistency. Unsupported holding can be used to classify weight, and enclosure grasping helps identify the overall shape of the explored object. Thus, the exploration procedure depends mainly on the question the subject was asked concerning the properties of the designated object. This is called knowledge-driven exploration of an object [114]. An additional important influence, however, is represented by the expectation or prior knowledge on object consistencies, gained by past experience. All these parameters have to be taken into account while planning experiments that target the investigation of tactile perception.

1.3 State of the Art in Actuator Technology and Tactile Displays

Whereas the preceding sections described tactile perception from the perceptual point of view including measurement and processing, this section is concerned with hardware components that are necessary to *display* tactile stimuli. Tactile displays generally consist of movable mechanisms that are driven by an energy source, which is mostly an electrical, but sometimes a fluidic actuator. Thus, most tactile displays are *mechatronic* systems. An important prerequisite during the design of new tactile devices is knowledge on suitable physical principles and the corresponding actuator technologies.

In the following subsections, an overview of the currently available principles will be given. The actuator types are described with respect to their suitability for tactile displays that stimulate the mechano- and thermo-tactile perception. Special focus is on the requirements that the device must be compact, and that it should match the capabilities of the human sensory system as closely as possible. After the definition of suitable criteria, the actuator classes are sorted according to their physical principles, and known tactile displays employing the respective actuator are briefly reviewed with respect to their functionality and performance.

1.3.1 Actuator Types and Applications

The core units of *tactile displays* usually consist of several actuators that are assembled to more complex human-machine interfaces. The fundamental idea of tactile displays is a physical stimulation of the human skin that emulates real physical objects. The physical stimulation principle depends on the kind of the desired tactile sensation. The capability of the human somatosensory system with its different sensors basically covers four different types of tactile stimulation: shape, texture, temperature, and pain. The tactile perception modes of shape and texture can both be stimulated by mechanical actuators that are capable of generating movement in an adequate range of position and velocity. Thus, the four tactile stimulation types can be reduced to three from the technological point of view: Mechanical, thermal, and pain.

Mechanical Stimulation

The description of the sensory capability of the human tactile sense, as presented in the former part of this chapter, indicates that our tactile system is mainly focused on mechanical stimuli. For this purpose, we dispose of four different kinds of sensors in various density, which are responsible for different types of mechanical simulation. In interaction, they cover a wide range of sensitivities and frequencies. Therefore, the majority of tactile devices addresses this part of the human perception.

Mechanical stimulation is usually caused by deformation of the human skin. A tactile display can achieve this by peeking, poking, or stretching the skin. In practice, this is commonly realized by a grid of thin rigid pins. Such a design requires the definition of several parameters, which are: Size of the pin tip, density of the pins, geometry of the arrangement, direction of pin excursion (lateral or normal to the skin), and pin dynamics. These criteria are very important for the choice of the actuation principle and the transmission mechanism between actuator and pin. In Sec. 1.2.2, the human mechanoreceptors have been described in terms of performance. There, also the high receptor density at our target area, the tip of the index finger, has been outlined. The high density shows that the complex system of mechanoreceptors with its particular combinations and interconnections enables capturing a large range of mechanical stimuli. A trade-off will be necessary, because there exists currently no actuation principle that would be optimal regarding all listed criteria.

Electrical Stimulation

The perception of electrical stimulation is receiving increasing attention, especially due to its relevance for information transfer via mobile devices, like tablets and cell phones. One reason is that this principle can be exploited in a very compact and energy-efficient manner. A challenge is that targeted stimulation of specific receptors is not possible via electrical stimulation, but that the electrical impulses directly act on the closest nerve endings and receptors, such that no clear tactile stimulus can be realized, and that even pain can result. In addition, many parameters with high inter-subject variability have to be taken into account, such as anatomy, but also parameters with high intra-subject variability, such as electrical conductivity of the skin, which can even change continuously depending on emotional state.

Thermal Stimulation

The mechanical part represents the main part of the entire human tactile perception, but there is also sensation of thermo-tactile stimulation. A plain surface made of plastic is perceived differently than one made of metal, even with the same surface texture. The decisive parameter in this case is the coefficient of thermal expansion, which cannot be emulated by a mechanical actuator.

Thermal stimulation can be provided by controlling the thermal flow between the human skin and the environment. Tactile classification of several materials depending on the heat flow between the skin and the environment has been investigated in [86]. The main focus of the investigations in this work addresses the mechanical modality of the tactile sense. Thus, the thermal actuator technologies to be presented in the following are mainly included for the sake of completeness and to provide a base for later discussion.

Pain

The perception of pain has a special function in tactile perception. It uses both the information of the mechanical and of the thermal sensory system, to detect over-straining. Moreover, it contains an additional network of sensors that are specialized to detect hazardous attacks to the skin, as for instance caused by chemicals. Thus, pain can be induced using mechanical, thermal, and chemical stimulation principles. However, as the investigation of pain perception is not part of this thesis, the devices presented here only try to avoid its cause and thus neglect unwanted influence on the perception of other stimuli.

Applications

There are various areas where tactile stimulation is used. A prominent example is given by Braille generators, which display tactile signs for people with vision impairments. Virtual Reality and teleoperation scenarios also increasingly incorporate stimulation of the tactile sense, for entertainment, medical, or military applications. Growing fields of application are mobile devices [8] and gaming [69]. Many user interfaces for hand-held devices like mobile phones already integrate tactile information.

The vast majority of tactile devices is based on mechanical stimulation, and thermal or nociceptive stimulation is neglected. This can be done without loss of realistic impression, because the mechanical perception channels deliver continuous information, whereas the thermal and nociceptive perception channels predominantly serve an alerting function; this means that we only become aware of thermal and nociceptive stimuli if a certain threshold is passed. For the sake of completeness, there will be a short description of thermotactile actuator concepts and some related displays.

1.3.2 Classification and Evaluation Criteria for Mechanical Tactile Actuators

To make the performance and size of the different actuator types comparable, specific criteria are established and discussed. The criteria used are energy density, power density, strain, force or pressure, and frequency response characteristics. These will now be defined and discussed briefly.

Energy density

Energy density is a general expression for the amount of energy in relation to mass or volume. Thus, the resulting SI units can be J/kg or J/m³. For our purpose, energy is defined as the maximum amount of energy that an actuator can transform from its supply into mechanical movement at the output side, independent of its source (e.g. electricity, pneumatics, thermal).

Power density

Another reference value that can be used to compare actuator performance is power. It describes, per definition, the amount of energy transferred per time unit. To obtain comparable values, power is defined as the amount of energy per time that an actuator can transform from its source to output motion. Like energy, power can also be related to mass or volume, which results in power density with the SI units W/kg or W/m³. Because of the derivation of time, power density contains additional temporal information of the system performance.

Strain

Most tactile displays provide a translational stimulus, usually administered by a moving pin. In principle, it is always possible to transfer rotatory motion, e.g. of electrical motors, into linear motion or vice versa by using a transmission gear. However, this requires an additional mechanism that costs space and weight, and which reduces the effectiveness of the system. Thus, an actuator that provides direct linear motion is advantageous. For such direct linear actuators, a criterion can be defined that describes the maximum lengthwise extension of the actuator in a specified direction. This criterion, called strain, is especially useful for actuator principles that are able to generate direct linear motion (e.g. using the piezoelectric effect). For consistency, strain is defined relative to the actuator's length at rest, and it is described in percent [%]. Nevertheless, in most cases, a mechanical transmission is still necessary to adjust the performance of the actuator to the specified performance of the stimulus. Therefore, we have to differentiate between the strain of a *pure* actuator and an actuator system, which may include a transmission.

Density

Density is the ratio between mass and volume, thus the resulting unit is kg/m³. In the description of actuator principles, density values are usually specified for the core of the physical actuator, without any additional parts like gears or electronic control units. In special cases, however, density is used to compare actuator systems or entire display concepts.

Force, Pressure

The output force of an actuator that can be achieved by the respective physical principle is an essential performance parameter for validation and to compare the several principles among each other. The SI unit for force is Newton [N]. Pressure is defined as force in relation to area, and it has the unit Pascal [Pas] or [N/m²]. Thus, pressure describes

the force that is distributed over the contact area between the actuator system and the actuated part of the (human) body, which is here the surface of the skin, more specifically the skin at the fingertip.

Frequency Response

To compare the dynamic behavior of different actuators or tactile displays, it is useful to look at the response in the frequency domain, i.e. the possible extension or force depending on frequency. The frequency response can be approximated knowing the actuator's power and static parameters like force and strain. The frequency dependency of the response threshold of the human skin is shown in Fig. 1.9. An ideal actuator would match this behavior.

Design Constraints

Derived from the target sensory system to be stimulated, a basic calculation can give an overview of additional constraints during the design of tactile displays. This calculation refers to the stimulation of SA-I mechanoreceptors in the area of the fingertip, which have a density of 70 units/cm². This results in a minimum pin density of 1 per mm². Each pin should be capable of longitudinal movements of up to 3 mm and a peak force of about 2 N. The additional constraint that this must be valid for a frequency range of 50 Hz implies that on the contact area, a power density of about 200 W/cm² is necessary**.

This example, once more, shows the ambitious requirements for the actuators. Each actuator would have to provide 2 W output power to reach the demanded performance. In practice, the power of the actuator increases under the consideration of the efficiency of the transmission system. If the tactile display is used in combination with a kinesthetic display, for instance in a global haptic scenario, this is mostly realized by a serial coupling of both displays. In those cases, space and mass of the tactile display are very important constraints for the design of the tactile display.

The following sections are organized regarding to the physical principle of actuator technology. For a better overview, these principles are divided into subsections according to the physical sources of force, such as electromagnetic and electrostatic fields, pneumatic/hydraulic, and thermal-based actuators. Hereby, the thermal actuators take an exceptional position, because they stimulate the class of thermo-tactile receptors. Furthermore, some miscellaneous actuator types are presented that do not directly fit into the three main categories. In conclusion, the performance data of the described actuators is summarized and discussed.

1.3.3 Actuators based on Magnetic Fields

DC Motors

The most commonly used actuator for robotic applications, the DC (*direct current*) motor, uses a combination of permanent magnets, coils and a commutator to produce a rotating electromagnetic field to generate a rotatory motion at the output shaft of the motor.

**This is calculated under the assumption of a sinusoidal and undamped movement of the pin across the desired frequency range

Attached reduction gears are generally used to increase the torque and decrease the speed. DC motors in combination with encoders for position measurement and position control, so-called *servo motors*, are available in different sizes and provide good position accuracy. If DC motors are used as linear actuators, the rotary motion must be transformed into a linear motion by rocker arms or combinations of screws and nuts.

TactAct 4 is an example of a tactile normal force display which uses gear-less DC motors [101]. The rotatory motion of the four position-controlled motors is transformed into linear motion by excentric discs pushing the pins in linear direction. Each pin of the 2×2 pin-array display can reach a maximum stroke of 4 mm and is continuously controllable in position. It provides forces of up to 2.5 N and has a maximum mechanical bandwidth of about 60 Hz. In spite of the very large lateral pin spacing of 8 mm, it provides a highly realistic stimulus of soft objects with no sharp edges. An example scenario is the palpation of the human skin, which allows the detection of pulsing blood vessels or subcutaneous tumors. To enhance the impression of touching a tissue-like surface, a rubber layer between the finger tip and the pin matrix is installed for the purpose of smoothening the shape of the pins.

An evolutional hardware development of two displays using DC motors is reported in [87]. The first prototype of the FEELEX series consists of a large 6×6 pin matrix within an area of 240×240 mm. Each pin has a maximum excursion of 80 mm, with a maximum speed of 100 mm/s. This display mainly addresses bi-manual interaction of the complete palms. The pins of the device are driven by position-controlled DC motors. The motors are linked to a screw gear mechanism that converts the rotatory motion into linear motion. The displayed object can be explored from the top surface through a 3 mm thick rubber plate under which the actuator stamps are located. Additional features are force sensors at the end of the driving rod and a projector system that enhances the covering rubber plate into a flexible screen, which for instance displays touchable objects. The area of interaction of FEELEX 2 is only 50×50 mm, according to a pin assembly of 19 pins in hexagonal arrangement. As it is made for tactile interaction scenarios with two or three fingers of one hand, the pin spacing has also been reduced to 8 mm, with a diameter of 6 mm per pin. The pins are driven individually by off-the-shelf RC (*radio-controlled*) servo motors, activated by a piston-crank mechanism. They reach an excitation of 18 mm at a stroke rate of 7 Hz.

The display built by [184] has similar dimensions as FEELEX. The interaction area is 200×170 mm and contains a 64×64 pin arrangement with 3 mm pin spacing. The pins are driven by micro step motors with a diameter of 4.2 mm. A lead-screw-mechanism converts the rotation of the motors into linear motion. This actuator principle achieves pin displacement of up to 10 mm at a step resolution of 0.1 mm/step.

Another example of a tactile display using DC servo motors is presented by [204]. It consists of 36 pins arranged in a 6×6 matrix with a lateral pin spacing of 2 mm. Each pin is driven by an RC servo-motor connected through a lever-rocker mechanism similar to FEELEX 2. It is designed for a maximum pin excursion of 2 mm. This device provides frequencies of up to 7.5 Hz at full pin excursion and up to 25 Hz at amplitudes less than 0.75 mm.

Solenoids

Solenoid actuators belong to the class of electromagnetic actuators that are able to produce direct linear motion. They consist of a coil of wire (solenoid), generating a magnetic field that moves an iron core toward the coil, thus direct conversion of electric source energy to linear mechanical motion can be achieved. The output excursion is about some millimeters to some centimeters, which is usually the range that is needed for classical pin based tactile displays. Due to the physical properties of the electric field and the changes of the magnetic field intensity concerning the moving iron coil, the relation between movement and attracting force is highly non-linear. Therefore, this principle is commonly used for mechanical switches, where a binary switch in position is necessary.

A design study of a solenoid actuator for tactile displays is presented by [116]. In this paper a method for dimensioning the mechanical properties of solenoid actuator is described. The design emerges from an optimization approach, which considers the tactile sensitivity of the human cutaneous sense as a boundary condition.

A slightly modified principle of solenoid actuators is used by [100] for a 6×6 grid-based tactile pin array display. The circular pins have a diameter of 1.5 mm and a pin-spacing of 3 mm, thus the active tactile area covers 16×16 mm. The actuator for each pin consists of a coil with a fixed iron core working as an electric magnet. The electric field that arises in active mode moves a rocker lever against a retaining spring. Thereby, it actuates the linkage that in turn moves the pin. Since there is no position or force control, the pins are only able to move in binary mode. The pins can exert continuous forces of around 4.5 N at the fixed maximum stroke position of 1.6 mm. Due to the lightweight design of the movable parts, it is possible to achieve a comparatively high mechanical bandwidth of more than 100 Hz.

In [73, 74], the design and evaluation of a basic haptic display that combines tactile and kinesthetic modality is presented. The tactile part consists of only one pin that is directly connected to the iron plunger of the solenoid actuator. It is mounted on a standard kinesthetic display (PHANTOMTM); hence the entire display is able to provide a collocated kinesthetic and tactile force feedback. The tactile pin has a relatively large diameter of 6.35 mm and is specified for forces up to 2 N at frequencies of up to 200 Hz^{††}. Position and frequency of the pin are controlled by a PI controller. The second part of this publication ([74]) mainly deals with the optimization of the controller performance and arising problems due to serial coupling of a tactile device onto a kinesthetic device. This issue will be discussed more in detail in Chap. 4.

An approach for a wearable grid-based solenoid display can be found in [17, 18]. It contains 64 pins, arranged in a 8×8 matrix configuration. It is capable of displaying small-scaled tactile information with a pin excursion of about 0.2 mm and forces up to 13 mN. The micro-coils of the display are arranged in a multi-layer concept which allows a flexible configuration of the pin area. Each micro-coil can operate at frequencies up to 800 Hz.

[190] shows impressively that the solenoid concept can even be downsized to MEMS (*micro-electromechanical systems*), the so-called MMMAS (*micromagnetomechanic systems*). The core of the pin is a very strong (neodymium) magnet, with a magnetization of about 1 Tesla. This magnet is embedded in the surface membrane, which is made of PDMS (*polydimethylsiloxane*). This magnet is driven by a small coil underneath with a

^{††}with a damping on -40 dB

height of 1.8 mm and a diameter of 1.7 mm. The display consists of a 4×4 pin area with a pin spacing of 2 mm, while the thickness of the display is just around 3 – 3.5 mm. Each pin can reach a deflection of $50 \mu\text{m}$ with 2.5 mN force for a RMS driving current of 800 mA. These values are quite constant in the operating frequency range of 0 – 300 Hz.

Another concept based on mini-solenoid actuators is presented in [174]. The aim of this project is to build a 5×6 pin array within a finger cap, within an actuator diameter of 2.4 mm. The maximum force is calculated to be 73 mN. The plunger of the solenoid presses against a spring (realized by the covering membrane).

Voice coil

At first glance, the functional principle of a voice coil actuator is the inverse setup of the solenoid actuator principle. The coil is placed as a movable part around a fixed permanent magnetic core. By driving a current through the coil, a magnetic field can be established. The interaction between the generated field and the permanent magnetic fields results in a force, which causes a movement. According to this physical principle, the force between the movable coil and the permanent magnet is proportional to the current through the coil, which simplifies a force control loop. Voice coil actuators usually have a better performance, and apart from the magnetic hysteresis they exhibit no losses caused by mechanical parts. On the one hand, as they are free from backlash, they are easy to control continuously in position using an additional position sensor. On the other hand, they are more complex to fabricate.

An implementation of tactile feedback in a joystick-based pointing device for notebooks is presented by [30]. This device is designed to guide the user through menu structures, providing a vibrotactile stimulus at the borders of the guiding path. The maximum pulse rate without significant loss of amplitude is 30 Hz. Besides the development of a tactile guiding device ready for the market, the study combines visual perception and tactile stimuli.

The design of a linear motor based on a voice coil principle is described by [133]. They realized two actuators, a small one with two voice coils in series with a maximum stroke of 2.5 cm, and a larger one containing four serial coils of wire that achieve a maximum stroke of 4.7 cm. The actuators are designed to drive a robot arm. First results indicate that these types of voice coil actuators are able to provide sufficient power at a very small package size and with a justifiable effort in design.

In [14] an off-the-shelf voice coil actuator with a maximum continuous output force of 2.42 N is used to drive a surface table on which the finger can be moved. To increase realism, the authors use exchangeable “real” surface material, such as wood or cloth, and they only slightly modify the experienced roughness via actuation. Finger movement is captured by a camera and used for closed-loop control of the stimuli.

Magnetostrictive Actuators

Magnetostrictive actuators are based on the property of ferromagnetic materials to change their size when exposed to a magnetic field. This effect, discovered by James Joule in 1842, causes a saturated magnitude of around $10^{-5} - 5 \cdot 10^{-5}$ times of its length. In the 1960's, an alloy with the giant magnetostrictive coefficient of strain magnitude in the order of 10^{-3} was developed, described in [58]. This magnetostrictive material, commercially known as

Terfenol-D ($\text{Tb}_3\text{-Dy}_7\text{-Fe}_2$ alloy), makes this principle interesting for actuators in tactile displays. With an energy density of $2.4 \cdot 10^{-3} - 3.6 \cdot 10^{-3} \text{ J/m}^3$ and a strain magnitude of $0.16 - 0.24\%$, it shows better performance than piezo-based actuators. The major drawback of this actuator principle is the effort in control [19] and the high magnetic fields that are necessary to operate. This indeed makes it difficult to arrange these actuators in compact clusters, as necessary for the design of tactile devices.

Some approaches of single-actuator designs using this principle are presented by [19, 67], mainly addressed to the question of position control using FEM methods.

Actuators based on Rheological Fluids

Rheology is the study of deformation, force and flow of matter. It is applicable to all materials from gas to solids. The two most important rheological fluids are ER-fluids (*electro-rheological fluids*) and MR-fluids (*magneto-rheological fluids*). ER-fluids consist of a suspension of semiconducting particles and dielectric carrier liquid, while MR-fluids are compounds of solid ferromagnetic particles in a carrier fluid, for instance hydraulic oil. In the case of ER-fluid based actuators, an electro-static field applied to the fluid causes a change of viscosity. The solidification related to the strength of the electric field starts usually at a field strength above 2 kV/mm . Generating a sufficiently strong field requires large voltages (several thousand Volt), thus this principle is not very practicable to build tactile displays in a direct way. However, [188] proposed to use ER-fluids for flow control in hydraulic actuators. One example for using ER-fluids for tactile displays is described in [132], where the fluid is used to vary the hardness of the click button of a computer mouse.

More interesting for tactile displays are actuators based on MR-fluids. Compared to the ER-fluid, MR-fluids are actuated by a magnetic field, whose strength is related to the solidification of the MR-fluid. As a magnetic field is technically easier to realize with low voltage supply (about 12 V) and the MR-fluids yield greater strength, up to 20 times more than ER-fluids, MR-fluids seem to be more appropriate for tactile devices. Ongoing research, reported by [21], presents first results of an HBB (*haptic black box*) display. The first prototype of this HBB consists of a cubic box containing the MR-fluid [163, 179]. The operator moves the hand inside the box containing the magnetically excited fluid. A cluster of magnetic coils is arranged below the box generating individual magnetic fields causing spatial changes of density in the MR-fluid.

1.3.4 Actuators based on Electric Fields

Piezoelectric Actuators

The piezoelectric effect describes the ability of some materials to generate an electric potential in response to mechanical stress or strain. This direct piezoelectric effect is reversible, thus the converse piezoelectric effect describes the stress/strain of the material while applying an electric field. The piezoelectric effect occurs on crystalline structures like tourmaline, quartz, topaz, cane sugar or Rochelle salt. Today's most used standard piezo ceramic material is made of lead, zirconate, and titanate (PZT) ceramics. During the polarization procedure after manufacturing - necessary to extend the piezoelectric effect - PZT material achieves relative expansion strains up to 0.2% . Using mono-crystalline material

like lead zinc niobate-lead titanate (PZN-PT) or lithium niobate crystals lead magnesium niobate-lead titanate (PMN-PT), expansion strain up to 0.6% can be achieved [148].

For a full extension of PZT crystal, an electric field of 1–2 V/mm is necessary. Thus, for substantial extensions in the range of several 100 μm , voltages up to 1000 V are necessary. To lower the driving voltage, it is possible to stack several PTZ's to one multi-layer PZT. Each layer usually has a thickness of 20 to 100 μm , separated by thin metal plates between. The layers are arranged in alternately poled order, where the metal plates can also be supplied in alternating order and at least wired in parallel manner to reduce the operation voltage to around 100 V. In this configuration, the driving voltage of the entire stack is nearly independent of the length of the entire actuator.

Another conceptual type of piezo actuators is the bending or bimorph piezo actuator. Similar to the stack piezo concept, it consist of two layers of PTZ material, separated by thin metal layers and with two additional metal plates on the bottom and top. By actuating the two plates in the opposite direction, one plate will bend and while the other one contracts. As the two plates are connected to each other at one side, the entire actuator performs bending motion. If one side of the actuator is fixed, the opposite side of the cantilever can be used as mechanical tap. This principle considerably improves excursion but lowers the force output to ~ 1 N. This principle is often used by Braille generators.

Electrically, a piezo actuator behaves like a capacitor, thus, it can be operated by applying voltage or using a “charging pump”. A drawback of operating the piezo actuator by voltage is a hysteresis effect between input voltage and mechanical expansion of the piezo. However, drift and hysteresis can be eliminated by using position/force feedback control. With a position-controlled piezo actuator, high position accuracy and output forces can be achieved. Several approaches in modeling and position control regarding voltage control as well as using the charge pump approach can be found in [62, 102–104]. A direct force control approach of a piezo actuator, based on sliding mode can be found in [1]. Beside a position control for the piezo actuator, in some cases it is useful to know the contact force between actuator and object. An approach to estimate the external force without an additional force sensor is presented in [167]. The force can be calculated by a force estimation model that needs the supplied voltage and current and the resulting displacement of the actuator.

A tactile shear force display based on piezoelectric actuators is presented by [76]. The prototype display is made of 64 upright piezoelectric actuators that produce a coupled, swinging motion of 112 pins whose ends stimulate the skin. Due to the differential displacement of two neighboring actuators, a lateral displacement of the pin in tangential direction to the skin is possible. A feasibility study of a tactile display that can provide shear force stimulation is presented by [119]. The fundamental idea of this study is the essential knowledge that the tactile perception is very sensitive to small displacements of the skin under lateral stretch, especially for temporal displacements. This is demonstrated effectively in a simple experiment, by using an ordinary comb [76]. Thus, the display consists of 12 stacked piezoelectric bender plates. Each plate has a thickness of 0.38 mm, fixed at their base and separated against each other, with about the same distance as the thickness. The bender plates can be controlled independently in one axis of motion, with a spatial deflection of 0.7 mm and a maximum frequency up to 500 Hz. The target application of this display is the simulation of a Braille display by using lateral skin stimulation

only. A modified version of this display (STRESS²) is used in [205] to perform a haptic memory game.

In [191] a 10×10 pin array display with 100 bending piezoelectric elements is presented. The pins are arranged in a 1×1 mm matrix. Each pin can be moved binary in a frequency range of 25 – 400 Hz with an amplitude of around $50 \mu\text{m}$ at 40 Hz and $5 \mu\text{m}$ at 320 Hz. Two psychophysical experiments have been performed to investigate the temporal resolution of the tactile perception. The subjects had to identify direction and motion of different line array elements. The results of the experiments confirm that the sensitivity of our tactile perception increases with frequency of stimulation.

Another example where piezoelectric actuators are used for vibrotactile texture exploration has been presented in [83]. The tactile display unit is attached to the end-effector of a haptic device (PHANTOMTM) that provides kinesthetic force feedback. Each pin of the 5×2 array matrix is driven by a bimorph piezoelectric actuator with a fixed frequency of 250 Hz. The maximum amplitude at this frequency is about $22 \mu\text{m}$.

Similarly compact is the tactile display KAST (KAIST Artificial Touch) presented in [109, 110]. A cluster of 30 bimorph piezoelectric actuators is integrated into a computer mouse, and they drive a 5×6 pin array. The diameter of each pin is 0.7 mm, and pins are arranged with a spacing of 1.8 mm. Each pin can reach a maximum deflection of $> 700 \mu\text{m}$ and a bandwidth of about 350 Hz. Pins are driven by a voltage of 150 VDC and can gain a blocking force of 0.06 N. The advantage of this display could be the additional use of position information from the mouse. To control the pins of the tactile display, a software with a graphical user interface has been developed, which additionally provides thermal display functions for further implementations.

The VirTouch mouse follows the same concept of integrating a tactile display into a computer mouse. The mouse exhibits three 4×8 dot matrix pin arrays. According to the target application to display Braille messages, the pin spacing is slightly higher. The pins are driven separately by a bending piezo, and they can extend in 16 steps. The entire display can be connected via standard serial communication connection (RS232).

Nowadays, the principle of bending piezos seems to be widely used for Braille generators to display a tactile alphabet for blind people. There are commercial available modules (e.g.[79, 80]) in different overall configuration and sizes. They usually consist of a discriminable pin space with a dot spacing of 2.5 mm and a pin stroke of about 0.7 mm and can achieve forces of up to 0.3 N/pin.

Electro-Static Actuators

Electro-static actuators take advantage of the force that arises from a static electric field. This arises for instance between two electro-conductive plates with differently polarized charge. This effect additionally depends on the dielectric medium, e.g. dielectric polymers between the plates. This physical principle can be described by Coulomb's law, where the attracting force between the two plates is proportional to the electric charge. Similar to stack piezo actuators, thin films of dielectric polymers, e.g. made of silicon or polyurethane, are usually assembled in a stack design, to reach sufficient extension at justifiable effort of supply voltage. The maximum strain can rise up to 32 %, at a pressure of about (~ 0.2 MPa). An review of electro-static actuator technologies is given by [72, 126]. This physical principle is also one of the key technologies for MEMS.

In [96], a promising actuator concept is presented, which aims at a use in a tactile dot matrix display design. The proposed actuator is built by a stack of polymer-based elastic layers covered in alternating poled layer electrodes. To realize an actuator that can be supplied with voltages in the 1 kV range, the elastic layers can only have a thickness of about $10\ \mu\text{m}$. At a strain of up to 30 %, there is a need of about 1000 layers to obtain a range of motion that is adequate for tactile stimulation. The advantages of this concept are the low cost and the light weight ($1\ \text{g}/\text{cm}^2$) of the actuators, whereas the high operation voltage of some 100 Volts is mostly a drawback for design issues. It seems also difficult to manufacture the multilayer stack with up to 1000 layers at a layer thickness of around $10\ \mu\text{m}$. A recent update of the actuator design, including a possible method of fabrication, has been given in [175]. Furthermore, this paper presents an approach to mathematical modeling and performance analysis of those actuators.

Electrostrictive Actuators

The physical principle of electrostrictive actuators is similar to the magnetostrictive principle. Where magnetostrictive material is able to change properties caused by a magnetic field, electrostrictive material can change properties when exposed to an electric field. In general, electrostrictive material has dielectric and non-poled properties, wherefore it cannot be used in bipolar mode like piezoelectric actuators. The relationship between strain and the driving electric field is nonlinear, but because of its quadratic characteristics, the material allows still exact placement. Disadvantages are the four to five times higher electrical capacity compared to piezoelectric actuators, which cause higher energy consumption, and the high sensitivity regarding temperature changes. The electrostrictive effect occurs in rigid multi-crystalline ceramic with a tension modulus of 120 GPa, like lead magnesium niobate (PMN) [25], as well as in soft polymer elastomers with a mechanical modulus of about 560 MPa. Both materials reach strains of up to 4 % at an electric field of 20 – 100 V/mm for polymers and about 400 – 500 V/mm for the ceramic PMN. The electrostrictive polymers can be divided into two groups: **Copolymers** consist of a crystalline polar phase and flexible chains, linking the crystals together, where **polymer chains** are cross-linked by polar polymer crystals [72]. Electrostrictive material can also be used as force sensors, by measuring the electrostrictive coefficients of polymer film [68].

Conductive Polymer Actuators

The principle of conductive polymer actuators is similar to electrostrictive actuators. The main difference is the composition of the smart material usually being a composite of electrically conducting organic material between two flexible electrodes. The most effective way to deform conductive polymers is bending. Drawbacks of this technology are the low response frequency and that the actuator needs to be in a solvent, to prevent evaporation. A new composition of materials is tested in [35]: It consists of a three-layer conductive polymer/electrolyte polymer/conductive composite material, whose conductive polymer layers are chemically integrated in the electrolyte polymer material during fabrication. Furthermore, a novel tactile display concept made of this material is presented [36].

A wearable version of this kind of device consisting of five rows with 12 cilia, is presented by [107], where the whole ciliary display can be attached to the finger tip by a flexible wiring strip. The evaluation experiment aims to find out the perceptual intersections

between normal and vibratory stimulation as well as the maximum intensity of vibrotactile stimulation.

A promising approach using EAPs (*electromechanically active polymers*) is proposed in [32]. The actuator is based on a fluid-filled bubble whose lower half of the surface is made of an EAP and the upper half is designed as a passive membrane. By activating the EAP, the lower membrane buckles outwards and the passive membrane follows inwards, caused by hydrostatic transmission. The presented prototype consists of one actuator that can be attached to the finger tip.

[115] shows a very small, highly integrable solution of an SMT (*surface-mount technology*) actuator. It is based on a disc-shaped DEA (*dielectric elastomer actuator*) membrane that can be flipped from straight to convex shape. The membrane compresses the fluid in a chamber above it, which acts as a transmission to a smaller membrane on top and thus amplifies its deflection. With this hybrid principle, a displacement of the upper membrane, which is in contact with the finger, of $62 - 197 \mu\text{m}$ can be reached. The frequency of the system can be up to 40 Hz.

1.3.5 Fluid Actuators

Pneumatic Actuators

Pneumatic actuators use the pressure or flow of air to drive pins with a piston system or to inflate air chambers. The benefit of pneumatic actuators is that the compressor generating the pressure can be placed at peripheral locations. Therefore, a good local power density is achieved. Disadvantages are the non-linearities of either pressure or flow posing high requirements on the control. Furthermore, aerodynamic effects cause limitations on actuator bandwidth.

In [29], a 4×4 pin display with pneumatic actuators is presented. In this display, the pins consist of steel needles with a diameter of 1.75 mm, driven by pneumatic micro-cylinders. The pin array has a size of 15×15 mm and the entire display unit is very compact, with a size of $30 \times 30 \times 15$ mm and a weight of 20 g. The maximum stimulation frequency is about 20 Hz.

The display presented in [137] uses an array of pressurized chambers to drive a 5×5 dot matrix display. The chambers consist of silicone tubes covered by a thin common membrane with a thickness of 0.4 mm, thus the inflated chamber provides the tactile stimuli. The displacement of the pulps is up to 0.6 mm at maximum pressure of about 4 bar. For performance reasons, the driving pressure can only be controlled in binary mode.

A special type of pneumatic display is represented by [129]. The working principle of this display is based on the tactile illusion of substituting a pushing stimulus to the skin by sucking the skin instead, e.g. through an injector. As only a surface with holes arranged in a grid-like manner is needed, this principle simplifies the technical design. Each actuator hole is driven by a small valve, connected to a central vacuum pump. Current investigations are engaged with the shape of the suck pins and an effective arrangement as well as with the two-point discrimination threshold that seems to be different to the usual pin display approaches. This principle is also used in [158] for an investigation of tactile-based torque illusions.

In [139], pneumatic pressure is used in combination with a solenoid actuator, which is attached beneath a PDMS membrane on top of the device. The membrane can either be

pushed by pneumatic pressure in the chamber or pulled by the electromagnetic force the solenoid generates. The presented setup consists of a 2×2 array where the pins are moved in a binary fashion. Each pin can move individually, and forces of up to 100 mN and a displacement of up to $700 \mu\text{m}$ are possible.

Hydraulic Actuators

Hydraulic actuators may be built similar to pneumatic actuators, replacing air by oil as medium. Usually, this increases cost and effort, but as oil is much less compressible than air, hydraulic actuators can provide higher forces at higher frequencies and are more precise in positioning.

A hybrid actuator concept including a hydraulic mechanism is presented by [99]: This micro-manipulator magnifies the displacement of a piezoelectric membrane by a hydraulic system that drives the oil bellows. The piezohydraulic actuator provides movement from a micrometer range to up to $500 \mu\text{m}$.

The same concept, scaled down to MEMS size and addressed for tactile stimulation, is presented in [206]. A chamber filled with glycerin is used as the hydraulic transmission system. The larger membrane on the bottom is driven by a piezoelectric actuator, whereas the top membrane acts directly as tactile actuator. Both membranes are made of PDMS. The device consists of 9 actuators, arranged in a 3×3 array with a pin spacing of 4 mm. Each pin has a diameter of $480 \mu\text{m}$ and can reach a displacement of up to $50 \mu\text{m}$, the frequency can reach 100 Hz.

1.3.6 Thermal Actuators

Shape Memory Alloy Actuators

Wires or pins manufactured with SMA (*Shape Memory Alloys*) can easily be deformed at room temperature. Heating the alloy forces the wire to return to its prior form, hence it “remembers” its original shape. The most common material with this characteristic is based on nickel-titanium alloy. As an actuator, SMA can exert thrusts of up to 200 N/mm^2 , in direct linear drive mode. The recovery strain is in the order of 5 – 8%, and thus very large compared to piezoelectric actuators. Although SMA actuators appear to have the highest force per area and large displacement, their slow speed of response, fatigue problems (e.g. short lifetime) and thermal management problems make them of limited use for tactile display applications. A mathematical model of SMA, based on mechanical and thermodynamic considerations, is proposed in [84]. The evaluation of the model in a coil spring scenario shows convincing evidence.

An approach to control SMA wire-based tactile displays is presented by [78]. The longitudinal contraction of a SMA wire during thermal changes is used to drive a pin through a lever transmission. Main focus in this paper is the approach to position control of the tactile pins that is able to compensate hysteresis of the SMA wire. The pin of this display reached a bandwidth of 7 – 8 Hz (at a drop down of amplitude of -3 dB).

The mechanical design and control of an entire display is presented in [208]. It contains 10 pins in one line, with a pin spacing of 2 mm. Each pin is driven by a SMA wire that moves the pin by contraction. The heat of the wire is also controlled by the current flow through it. For reasons of better evacuation of the heat, all wires are water-cooled. With

this setup, pin excitations of 3 mm at frequencies of about 40 Hz (-3 dB point) and forces around 1.5 N can be achieved.

A pin-array-based tactile normal-force display containing 64 pins is presented by [193]. The pin area is arranged in a 8×8 comb manner and thus reaches an overall size of 20×40 mm, with a pin spacing of 3.8 mm. The pins are held by springs and drawn by SMA wires. Thus, in an unactuated case, the pins are extended to their maximal excitation level. If the temperature of the SMA wires rises, they contract and thus pull the pins against the spring, lowering them. The wires are controlled by energy-related PWM signals, while the positions of the pins are determined by measuring the resistance of the SMA wires. Each pin of the device reaches an excitation of up to 1.8 mm and maximal stimulation frequencies of about 3 Hz.

An interesting actuator concept using SMA wires is presented in [64]. It consists of a number of thin SMA fibers, woven in a counter-rotating helical pattern around supporting disks. The wires are connected in a way that the disks move in parallel and perform a highly efficient transformation between force and displacement. This design overcomes the main mechanical drawbacks of SMA. The presented prototype has the form of a cylinder with a diameter of 17 mm and a length of 30 mm, and it weighs only 6 g. It performs smooth linear motion of 2.5 mm and can exert forces of up to 4 N. The performance in the frequency domain covers response times between 92 ms and 50 ms with an enhanced control approach, as described in [65].

The project described in [130, 131] aims at a SMA-based 5×5 pin array display with a pin spacing of 5 mm that can display a shape as well as stiffness. Each pin has a diameter of 2 mm and is driven by two SMA springs in serial arrangement. One of them will be responsible for the deflection and the other one displays the stiffness by varying its spring constant. Position, force and current are measured to realize position/stiffness control. So far, a pin displacement of 5 mm can be reached within 5 s, by using PI position control.

1.3.7 Thermo-Tactile Actuators

Thermo-tactile actuators are in general dedicated to a different class of receptors in the human somatosensory system. As this modality of our tactile perception is not a central topic of this work, possible thermo-tactile actuators are presented mainly for reasons of completeness, but not covered in depth.

Electric Heaters

Electrical heaters can easily be built by electric resistors dissipating electric energy as heat. One possible material is constantan (an alloy of copper and nickel). These actuators can be controlled in a closed loop by measuring the temperature with a sensor attached to the resistor. The advantages of electric heaters are the compact design and simple technology as well as low cost. A drawback is that, for physical reasons, it is only possible to heat and not to cool.

Peltier Elements

A part of the human thermo-tactile perception is sensitive to temporal temperature changes, for instance while discriminating materials like wood or different kinds of metal.

Therefore, temperature transport from the material to the skin (heating) and from the skin to the material (cooling) must be possible. A physical principle that satisfies this demand is the Peltier effect. This thermo-electric effect is based on the caloric effect of electric current at the conjunction of semiconductive materials. Physically, the Peltier element consists of two ceramic plates, separated by alternated n- and p-doped semiconductor elements that are connected in a serial manner. The direction of heat flux depends on the polarity of supplied voltage and the potential of the heat flow that can be controlled by the supplied current, causing temperature differences of 30 K and more between the two plates. With a temperature sensor, a closed-loop temperature control for cold and warm stimuli (related to the environment temperature) can be realized. Peltier elements are available in different sizes, and their heat transfer power ranges up to 40 W. Thus, a very compact bidirectional thermo-electric heat pump can be realized. An additional advantage of this principle is that no mechanical parts or fluids are necessary.

An example for a thermo-tactile display using Peltier element technology is described by [86]. The display is composed of a 16 mm^2 Peltier element with a cooling radiator attached to the lower side for additional convective heat transfer. This display addresses investigations to identify different materials like aluminum, glass, rubber, polacrylate, and wood, only by displaying their characteristic thermal conductivity and capacity.

In [214], a concept of a tactile display is presented that combines mechanical and thermal stimuli. The mechano-tactile part consists of a 5×6 dot matrix display, driven by bimorph piezo actuators, whereas the thermo-tactile part is realized by Peltier elements, which are integrated into the base plate of the tactile display. This concept allows to build a compact set of five display units, one for each finger.

The Peltier element setup used in [6] consists of two identical 15 mm^2 standard elements that can be controlled independently. They are placed closely together to provide two different temperature stimuli along one finger. The method achieves a thermal perception that is about 14% faster, by preconditioning the reference area of the finger within the *comfortable* range of temperature (Sec. 1.2.2).

Air Jets

An interesting principle for stimulation of thermoreceptors is presented in a hybrid tactile display based on MEMS technology, which targets both mechanoreceptors and thermoreceptors [11]: Via an array of miniature air jets, combined with injection of mist, a sense of cold can be induced in a temperature range from -5.6°C to -11.7°C , as well as spatial information about object surface.

1.3.8 Electro-Tactile Actuators

Today, electro-tactile stimulation is widely used in mobile devices. Therefore and for reasons of completeness, also several state-of-the art electro-tactile devices will be included in this survey. However, since electro-tactile actuators contain no mechanical components, they will not be quantitatively compared with the mechanical devices above.

In mobile devices, the major advantages of electro-tactile actuators are exploited, which are easy implementation, minimal size requirements, low cost, low energy consumption, and high spatial accuracy and resolution. One of the main challenges is to finely tune

the stimulus, given that there is only a small gap between a sufficient stimulus and an uncomfortable one, which can even turn into pain.

One of the specific tactile features that can be displayed well via this principle is texture. For example, experiments with a hand-held device revealed that the conveyed sensation of roughness can be modulated with pulse frequency and magnitude of stimulation current [8].

In [150], an electro-tactile device to display texture and roughness is presented. It consists of a tactile pad, like the mechanical displays. It is arranged in a 32×8 grid with a spacing of 2.5 mm. The electrodes have a diameter of 1 mm. The interaction force between finger and electrode pad is measured by two force sensors. In addition, the sound of the explored material is presented by headphones. The device is used for material class discrimination and dissimilarity tests with paperboard, wood, textile fabric, and rubber. With the exception of rubber, the performance of the display seems to be valid and robust, but it requires correct calibration.

To overcome the calibration process and to compensate for variability during exploration, control schemes with impedance feedback appear to be a promising solution [97].

1.3.9 Conclusion

A multitude of currently available actuation principles has been presented in the preceding sections. For a better overview, a summarized representation is given in Tab. 1.3, Tab. 1.4 and Tab. 1.5.

Table 1.3: Magnetic field principles that can be used for tactile displays

Actuator principles	Magnetic field													
	DC Motors					Solenoids					Voice coils			
Number of Tactors	4	36	19	4096	36	20	36	1	64	16	1	1	1	
Arrangement	2×2	6×6	hex.	64×64	6×6	4×5	6×6	–	8×8	4×4	–	–	–	
Pin-spacing [mm]	8	40	8	3	2	–	3	–	5	2	–	–	–	
Pin diameter [mm]	6	–	6	≤3*	1	~0.3	1.5	6.4	2	1.7	2.4	–	surface	
Contact area [cm×cm]	14×14	24×24	5×5	20×17	1.4×1.4	–	1.6×1.6	–	–	0.8×0.8	finger	–	finger	
Excursion [mm]	4	80	18	10	2	~0.6	1.6	–	0.2	5×10 ⁻⁵	–	–	4	
(B)inary or (C)ont.	C	C	C	C	C	–	B	B	C	B	B	B	C	
Max. Force [N]	2.5	–	11	–	–	0.24	4.5	2	0.013	0.0025	0.0073	–	2.42	
Max. Frequency [Hz]	60	0.2	7	15s [†]	25	–	100	160	800	300	–	30	~200	
Stimulus destination	finger	palm	finger	palm	finger	finger	finger	finger	finger	finger	finger	prototype	finger	
Resolution (steps/range)	–	–	27	100	16	–	2	2	64	–	–	2	–	
(P)osition or (F)orce control	P	P/F	F	P	P	P	P	F	P	P	P	–	P	
(O)pen or (C)losed loop	C	C	C	?	O	?	?	?	?	O	O	O	C	
Overall size (w×d×h)[mm]	portable	desktop	desktop	desktop	desktop			100g		8×8×3.5	finger cap	30×30×15	desktop	
References	[101]	[87]		[184]	[204]	[116]	[100]	[73, 74]	[17, 18]	[190]	[174]	[30]	[14]	

*Estimated value

†Average time to present a relief pattern

Table 1.4: Electric field and thermal actuation principles that can be used for tactile displays

Actuator principles	Electric field							Thermal			
	Piezoelectric			Conductive polymer				Shape Memory Alloy			
Number of Tactors	112	–	100	10	30	60	1	24	10	64	25
Arrangement	square	–	square	4×2	5×6	5×12	1	4×6	line	8×8	5×5
Pin-spacing [mm]	1.4	–	1	3	1.8	3	–	2.1	2	3.8	5
Pin diameter [mm]	0.7	0.386	1	0.5×0.5	0.7	~2×2	?	–	–	–	2
Contact area [cm×cm]	1.2×1.2	–	1×1	0.4×1	4×8	–	–	–	–	2×4	2.5×2.5
Excursion [mm]	0.01	0.7	0.05	0.022	>0.7	0.75	197*10 ⁻⁶	2.5	3	5	5
(B)inary or (C)ont.	C	C	B	C	C	C	C	C	C	C	C
Max. Force [mN]	–	–	–	–	0.06	–	?	1.2	>1.5	~1.1	2000
Max. Frequency [Hz]	1000	500	320	250	350	320	40	7	40	–	<1
Stimulation destination	finger	finger	finger	finger	finger	finger	prototype	finger	finger	finger	finger
Resolution (steps/range)	–	256	2	15	–	–	?	–	–	–	?
(P)osition or (F)orce control	P	–	P	P	P	P	F	P	P	P	P+F
(O)pen or (C)losed loop	O	O	O	O	O	O	O	C	C	C	C
Overall size (w×d×h)[mm]	–	–	–	23.5×56×24.6	40×20×23	–	10×10×5	25×25×8	–	–	desktop
References	[76]	[119]	[191]	[83]	[109, 110]	[107]	[115]	[78]	[208]	[193]	[130, 131]

Table 1.5: Fluid principles that can be used for tactile displays

Actuator principles	Fluid					
	Pneumatic				Hydraulic	
Number of Tactors	16	25	19	4	1	9
Arrangement	4×4	5×5	hex *	2×2	–	3×3
Pin-spacing [mm]	3	2.5	5	?	–	4
Pin diameter [mm]	1.75	1	2.5	5	–	4.8*10 ⁻⁴
Contact area [cm×cm]	1.5×1.5	1.2×1.2	–	~2.5×2.5	–	1.8×1.8
Excursion [mm]	3.5	~0.6	–	7*10 ⁻⁴	0.5	5*10 ⁻⁵
(B)inary or (C)ont.	C	C	C	B	C	B
Max. Force [mN]	2	0.18	–	100	–	?
Max. Frequency [Hz]	20	5	–	?	0.5	100
Stimulation destination	finger	finger	finger	finger	prototype	finger
Resolution (steps/range)	–	–	–	–	–	–
(P)osition or (F)orce control	P	F	–	–	–	–
(O)pen or (C)losed loop	C	O	C	O	–	O
Overall size (w×d×h)[mm]	30×30×15	wearable		~25×25×10		desktop
References	[29]	[137]	[129]	[139]	[99]	[206]

*Hexagonal pin arrangement

Tab. 1.3 shows a summary of magnetic field based tactile displays or feasible actuator approaches. Tab. 1.4 shows a summary of electric field and thermal tactile displays or feasible actuator approaches. Tab. 1.5 shows a summary of fluid based tactile displays or feasible actuator approaches. Some additional explanations are necessary to interpret the tables:

- The tables primarily give an overview on realized tactile displays. In addition, they also contain some actuator prototypes that could come into consideration for future tactile displays. Those actuator prototypes are, of course, not comparable regarding criteria specific to tactile displays, such as arrangement or spacing of the pins in matrix displays. These prototype actuators can (mostly) be identified by having only one factor and no arrangement.
- In general, the pins are arranged in a square matrix. Any other arrangement is assigned in *Arrangement* as hex. (hexagonal) or lin. (linear).
- The contact area refers to the pin assembly as a whole.
- Due to insufficient information from literature, the overall size either refers to size and/or weight or merely to a category of size, such as: wearable, portable, desktop (size increases in ascending order).
- The resolution (if available) is given in relation to the maximum excursion of the related pin(s).

Some actuator principles that were described above do not appear in the tables. This has the following reasons: a) Due to their fundamentally different actuation principle, the displays based on rheological fluids cannot be measured/compared in the same categories as the conventional mechanical (pin-based) displays. b) The findings on the magnetostrictive approach are purely theoretical. This means that no prototypes that could suit the needs of tactile displays are available at the moment. Therefore, it would be difficult to find performance values that are comparable to the other physical principles.

When comparing performance of currently available actuator technology to the performance of the human tactile perception, it becomes evident that *there is no actuator technology that meets all the demands*. For the conventional pin-based normal force displays, these demands are defined by the three main parameters pin excursion, force, and resolution. For a portable device, additional requirements are compact size and low weight.

1.4 Contribution and Outline of this Thesis

There are three main objectives of this work: The first objective is to investigate mechatronic hardware concepts that can match the entire range of the human tactile sense in the area of the fingertip, at least concerning mechanical stimulation (as opposed to thermal or pain stimulation). To reach this objective, fundamental questions concerning a) suitable actuator concepts and b) the device kinematics have to be answered. The second objective is to enable and to conduct first experiments on a specific sub-modality of human tactile perception that has rarely been investigated: The perception of shear force applied to the skin. The third objective is to investigate cross-modal interaction between the perception

of kinesthetic and tactile stimuli. One purpose of these psychophysical investigations is to find rules and patterns in human perception that allow a relaxation of the challenging technical requirements for tactile displays. In order to be able to conduct these experiments, the first objective first needs to be met: Hardware is needed that can match the astonishing performance of human tactile perception.

The presented literature overview shows that almost all known tactile displays use one actuator per pin to impose a tactile stimulus onto the human skin. However, as has been shown, no current actuator principle exists that could provide the required power density and mechanical compactness to display a high-fidelity tactile stimulus that satisfies the psychophysical demands. Therefore, good actuator choice alone cannot deal with the challenge, and additional options need to be explored. One possibility is to look for suitable transmission systems, in order to modulate range of motion or frequency. Another option could be to place the actuator remotely, e.g. via hydraulic, pneumatic, or mechanical (bowden-cable) transmission. Yet another option is to combine different actuators to a combined display, such that the ensemble of actuators covers the entire range of human perception. This last option is the one that is explored in the second chapter of this thesis. There, the design and realization of a combined actuator for a normal-force pin display will be presented. The concept involves two single actuators, each optimized for a specific sub-range of tactile stimulation. The design is based on target specifications from psychophysical data, and the performance of the actuator modules with respect to these specifications is evaluated experimentally.

Another result of the literature review is that almost all existing tactile displays target the perception of forces that are normal to the human skin. Very little is known on the perception of forces that are tangential, i.e. shear forces. The third chapter of this thesis is dedicated to the investigation of this sub-modality of human tactile perception. To this aim, two devices are presented that both generate shear force: The first device is the Shear-Force Display, which specifically targets skin stretch. To induce this stretch, the device uses laterally movable pins. The second device is the Slip-Friction Display, which targets the additional influence of friction effects, such as they are generated when sliding a finger across surfaces. To induce slip friction, this device uses a rotating ball. Preliminary psychophysical investigations are conducted that give first insight into the mechanisms of human shear force perception.

The fourth chapter deals with the last major aim of this thesis, which is to provide a technological basis for the investigation of cross-modal interaction between kinesthetic and tactile perception. To this aim, an experimental environment is designed that allows a large variety of tactile stimuli in combination with haptic exploration in a large workspace: An existing hyper-redundant kinesthetic base display is subsequently combined with three different tactile displays: the Shear-Force display, the Slip-Friction Display, and a commercially available normal-force display. First experimental results show that the combined setup offers a versatile platform that is suitable to investigate cross-modal phenomena caused by combined kinesthetic-tactile stimulation.

2 Normal Force Display: The Multi-Actuated Pin

In this chapter, a novel pin actuation concept for a pin-based tactile display is presented, and the general feasibility of this concept is evaluated. The main motivation of this feasibility study is to investigate whether it is technically realizable to match the full range of the human tactile capabilities in the skin region. The focused region of tactile stimulation thereby is the skin area at the index finger, one of the human's most sensitive areas regarding tactile perception.

The target specifications for the mechanical design are derived from the findings of biological and psychophysical research that were discussed in detail in Chap. 1. When comparing these specifications to currently available actuator technology, it becomes evident that there is no suitable actuation concept that would cover the whole range of human perception.

The proposed solution is to combine two individual actuation modules to a combined display. This provides the possibility to separate the development of the two modules according to their range of operation. Based on fundamental requirements, both from a physiological and technological point of view, basic design decisions are made, such as the physical actuator principle for each module. The mechanical realization then follows a strictly modular concept. Parts of the design have been presented previously in [56].

For each module, evaluation results are presented and discussed. This experimental evaluation shows that the proposed actuation concept is able to generate high-fidelity tactile stimuli that can be used for psychophysical investigations.

2.1 Design Concept

The fundamental aim is to build a tactile display that is able to generate an artificial environment. This environment should emulate a real environment in terms of physical consistency as good as possible, but at least as good as the human tactile perception is able to identify.

The envisaged tactile display follows a classical concept, according to which most tactile displays have been built: This classical tactile display design is a matrix of actuated pins, as for example in a Braille generator. Usually, a number of thin pins is arranged in a grid-like matrix, covering the area of the skin to be stimulated. The pins are generally moved orthogonally to the skin surface.

To build a matrix-based tactile display that is optimal regarding our criteria, the size and density of the pins, as well as their movement performance must at least match the human tactile perception. This requirement poses a considerable challenge to actuator and integration. Most realized displays are tailored to a special application class, which reduces requirements.

The main bottleneck that limits performance is the lack of suitable actuation mechanisms. According to the conclusion in Chap. 1, so far there seems to be no mechanical solution based on a known physical actuator principle that can directly be used for a full-scale tactile display. In most cases, a transmission is needed to adapt the actuator's range of motion to the pin's range of motion. Very often, compromises at the cost of performance have to be made.

To overcome these limitations, the solution that will be investigated in this chapter is to combine more than one physical actuator to a system of actuators. With such a combination of single actuator modules, it should be possible to achieve a mechanical performance that is adapted to the maximal tactile perception. This is possible because each single actuator can be optimized for an individual range of operation in terms of excitation range and frequency. Beyond the selection and tuning of the individual actuators, an essential consideration is the overall kinematic configuration and its consequences regarding dynamic effects.

The proposed design focuses on the base actuator that drives the individual pins within a pin matrix. The term “actuator” in this case means the combination of physical actuator and transmission mechanism that drives the pin. To prevent confusion, we will use the term “pin-actuator” in the following, to describe the entire actuator chain, which possibly is composed of several actuator modules.

The following sections present the design of such an actuator package that is optimized for the demands of human tactile perception. The first step in the design process is to extract target specifications concerning mechanical actuator performance by using data of the various psychophysical investigations that have been surveyed in Sec. 1.2.4. The next step is to decide how many actuators are used and how they can be combined.

2.1.1 Guidelines from Tactile Perception

The afore mentioned Braille generator's basic principle is used for the tactile display design here, although the Braille generator is originally intended for the opposite application. Aiming to display discriminable tactile patterns in a matrix dot combination of at least 2×3 dots, it is for instance only necessary to move the pins in a binary fashion. There, the two states are “not actuated”, where the pin tip remains at the same height as the base plate, and “actuated”, where the pin is moved toward the finger by a distance that can clearly be perceived. A further feature of the Braille generator that is not necessarily desired for tactile displays is that the pin spacing is chosen such that each pin can be identified separately. These features are necessary to discriminate displayed Braille characters, but they contradict the purpose of tactile displays, which aim to rebuild a physical *surface* at the designated skin area. For this purpose, the pin matrix density should exceed the discrimination threshold of the tactile perception. Moreover, a single pin's indentation increments must be beyond the perceivable value, to be able to present a continuous tactile stimulus.

The main focus in this chapter is on building a prototypical single-pin actuator that can be employed in a dense mesh of pins in a dot matrix display. In such a dense matrix, the coordinated pins could emulate a surface that the human tactile sense would not be able to distinguish from a real physical surface. To display such *tactile pictures* by a pin matrix based tactile display, the main issue is to minimize the size of the actuator elements. In order to formulate the minimum technical requirements, the knowledge of the

human tactile perception and its performance are core issues. Therefore, a performance criterion for the pin actuator is defined based on psychophysical investigations as surveyed in Sec. 1.2.4.

The desired pin movement performance can mechanically be characterized by two parameters, amplitude and frequency. The target that is to be stimulated by the pin is the tissue of the human skin. The tissue consistency is comparable to rubber, which reacts with spring-damper behavior to mechanical deformation. The upper bound for the actuator's indentation amplitude can be derived from an anatomical constraint, which is the distance between the skin and the underlying bone at the fingertip. According to the findings in 1.2.4, the distance is about 2.5 – 3 mm, depending on the subject. Thus, the upper bound for pin excitation is defined as 3 mm. The tissue stiffness at the fingertip increases nonlinear, caused by the compression towards the constraining bone. It reaches a value of about 1 N/mm at a pin's maximum indentation of 3 mm [71], and a maximum force of 1 N results at a static excitation of 3 mm.

With the aim to display not only static tactile pictures, but also vibrotactile effects that usually occur during tactile exploration, we also have to consider the dynamic behavior of the finger tissue, and also the tactile perception during dynamic stimulation. Investigations on the dynamic response of the fingertip pulp [178] indicate that the stiffness increases with increasing stimulation frequency. These results are based on measuring the force at the fingertip pulp during tapping at different frequencies. Furthermore, with increasing frequency, the indentation threshold of the tactile perception decreases. This means that the sensitivity of the tactile perception increases with increasing frequency. Fig. 1.9 in Sec. 1.2.4 shows the sensitivity functions of the four relevant mechanoreceptors, where the dashed line shows the frequency domain behavior of the indentation difference that can barely be perceived at the area of the fingertip. The consequence for the design of a tactile actuator is that the smallest possible pin movement of the actuator at a certain frequency should stay below this value, to ensure quasi-continuous stimulation over the entire range of human tactile perception. As common technical position sensors do not adapt their sensitivity depending on the frequency, we have to choose one with the maximum sensitivity over the whole frequency range, although this sensitivity is only needed at about 230 Hz [183].

With these findings, the ideal performance of the tactile actuator can be summarized as follows:

- **Excursion:** The overall excursion is physically limited by the compression of the tissue between the surface and the bone of the index finger. The upper limit is approximately 3 mm (static).
- **Force:** In the static case, a maximum force of 1 N and a maximum stiffness of 1 N/mm is required at an indentation of 3 mm.
- **Frequency:** The bandwidth of human cutaneous perception is about 0 – 1000 Hz. The sensitivity to indentation increases until a maximum at around 230 Hz.
- Frequency response should be adapted to the sensitivity characteristic in Fig. 1.9.
- Small packaging size and weight.
- Possibility to stack several actuators closely together for a dense pin-matrix display.

2.1.2 The Multi-Actuator Concept

As summarized in Sec. 1.3.9 there is no actuator principle that would fulfill all demanded specifications above at once. An intuitive solution is to share pin performance requirements among several actuators, which in principle need not be based on the same physical principle. In the following, a multi-actuator concept is proposed, which consists of a cluster of several actuators. Each actuator module is dedicated to a certain task or performance feature. Because of the fact that every additional mechanical coupling leads to a degradation of performance, an essential demand to the design is to use as few actuator modules as possible. For this reason, the multi-actuator concept presented here contains only two actuator modules.

In a first design step, the targeted specifications are divided into areas that are realizable with a designated actuator principle. In this stage, only the main mechanical parameters like excitation, frequency and force are of interest. This is based on the assumption that later on, the multi-actuator cluster can be assembled as a superposition of the mechanical functionalities, although this integration may pose additional challenges.

Task Division

In the following, the actuator modules are divided according to their working frequency bandwidth into a *low-frequency module* and a *high-frequency module*.

Several investigations, e.g. in [159], state that stimuli with low frequencies of < 80 Hz are usually perceived as separate pulses, whereas stimuli of higher frequencies are usually classified as vibrotactile stimuli. We use this distinction for defining the range of operation for the two actuator modules according the frequency range. Another important indication that can be used for design issues is the rapid decrease in magnitude of indentation threshold in the frequency domain, as also can be seen in Fig. 1.9. Based on the overall sensitivity (red dotted line) of this diagram, the threshold of indentation at a targeted frequency of 70 Hz is about $2 \mu\text{m}$. This threshold can be used to defines the minimum resolution of the low-frequency module on the one side and on the other side it gives a estimation of indentation amplitude for the high-frequency module. The minimum resolution can be derived from the highest sensitivity of the tactile percept system that can be found in this figure at about $0.6 \mu\text{m}$ at 230 Hz. This minimum thresholds can be used to define the minimum demands for the related actuator module, but also are useful for an estimation of the expected actuator resolution. Also important for the design specifications of the actuator modules are the maximum pin stroke. These values are difficult to define, not least because no clear investigations could be found about that issue. Experiments made in [13] result in a useful magnitude of $8 \times -10 \times$ of the minimum threshold at a related frequency. However, for the design of our modules we use $\geq 10 \times$ the maximum values of the minimal threshold of the actuator-modules working range.

In accordance with the global specifications above, the working range of the two individual actuator modules can be defined as follows:

Low-frequency actuator module:

- Min. pin stroke/resolution: $\approx 30 \mu\text{m}$
- Max. pin stroke: 3 mm

- Frequency range: 0 – 70 Hz.

High-frequency actuator module:

- Min. pin stroke/resolution: $2\ \mu\text{m}$
- Max. pin stroke: $20\ \mu\text{m}$
- Frequency range: 70 – 1000 Hz.

The magnitude of the frequency response of both modules, should have a similar characteristic as the magnitude in Fig. 1.9

With this configuration, the two actuator modules can mainly be developed separately. Nevertheless, in view of the combination of two separately developed modules, some points have to be considered from the beginning of development on. An important aspect is sensor dimensioning: The sensor modules are based on a position control that usually includes a position sensor to measure the actual position of the actuator output. Obviously, the sensor should be dimensioned for the dedicated range of excitation and frequency. This can cause problems if the module is linked to another system that produces mechanical motion, like in the envisaged multi-actuator cluster. If the modules are linked directly, for instance in a serial manner, they can excite each other in frequency ranges that are not measurable for the respective other system, possibly even leading to resonance effects that are impossible to control. This has to be considered during the design of the sensor mechanisms of the modules, as well as during the combination of the two actuator units.

Assembly of Modules

An important step while building up the actuator framework will be to merge the individual actuator modules. There are two essential possibilities to assemble the two separately developed modules: A serial or a parallel connection.

In case of a serial arrangement, the entire high-frequency module has to be mounted onto the low-frequency module. This is similar to the macro-mini concept [216] proposed for haptic displays. The advantage of this strategy is that the expected mechanical performance parameter can be calculated as a superposition of the single actuator values; only a slight correction is necessary to account for the additional weight of the high-frequency module in comparison to the low-frequency module on its own. Essential disadvantages of this kind of connection is the risk that each module excites the other one within frequency ranges that lead to resonance or instability. This is especially problematic when the low-frequency actuator is stimulated beyond its working range, as it is usually not able to measure and thus not able to compensate for the external stimulation.

An alternative is the parallel connection of the two actuator endpoints that interact with the target object. In this configuration, each actuator output is directly linked to the target object, which in our case is the tissue of the index finger. Fig. 2.1 shows one configuration of a possible parallel stimulation approach. The pins, driven by the low-frequency module, are enclosed by shucks (tubes) of a movable plate. This plate is connected with the high-frequency module and constitutes the entire contact area of the finger-tip. Both components (tubes and pins) can be moved independently with respect to the base plate to stimulate the tissue of the index fingertip, whose resting position is the base plate. With this concept, the two actuator modules are only coupled through the

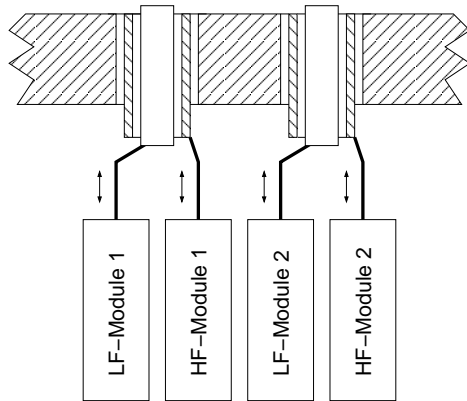


Figure 2.1: Parallel configuration

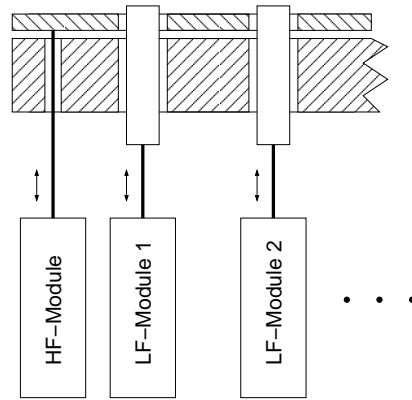


Figure 2.2: One common HF-Module

human skin. This is probably not critical, because the high frequencies, which might excite the low-frequency module and lead to uncontrollable resonance, are mostly damped by the skin.

There is yet another advantage of the parallel assembly: Due to the fact that high-frequency stimuli cannot correctly be localized by the human tactile perception, there might be potential to reduce effort in actuator hardware by providing only one high-frequency stimulus. Fig. 2.2 shows a possible realization of such a concept. The clearly discriminable amount of tactile information at lower frequencies is still provided by separate low-frequency modules, whereas the information that usually is perceived as not clearly identifiable vibration is provided by only one common high-frequency module. This does not only reduce the number of actuators, but it also allows more possibilities in placing the low-frequency modules.

Regardless of the chosen kinematics, the design requirements regarding performance of both modules are basically identical. This means that prototypes for the two modules can be developed and evaluated nearly independent of each other, and general conclusions can be drawn without having to decide a priori for a serial or parallel configuration.

Actuation of Modules

In Sec. 1.3, general considerations about possible physical actuator principles are outlined. This comparison is very useful to choose the optimal actuator for the correspondent module. The broad variety of physical actuator principles, as listed in this survey, suggests a large freedom of choice. However, it finally concludes that there is usually no distinguished principle that satisfies all demands at once. As there is consequently no actuator that fulfills these requirements of mechanical stroke and frequency response directly, the strategy is to shift and tune actuator characteristics to the required range via additional constructive elements. The common used method, from the mechanical point of view, is to transform the excursion by mechanical transmission, although this is mostly accompanied by a deterioration in frequency response.

A comparison of demands for the multi-module concept with available actuator principles leads to the decision that a stack piezo actuator can be used for both actuator modules. As briefly described in the actuator survey in Sec. 1.3, a stack piezo actuator consists of several thin layers of single piezo crystals that are electrically connected in a parallel

manner. Fig. 2.3 shows the structure of a stack piezo actuator. The thickness of the

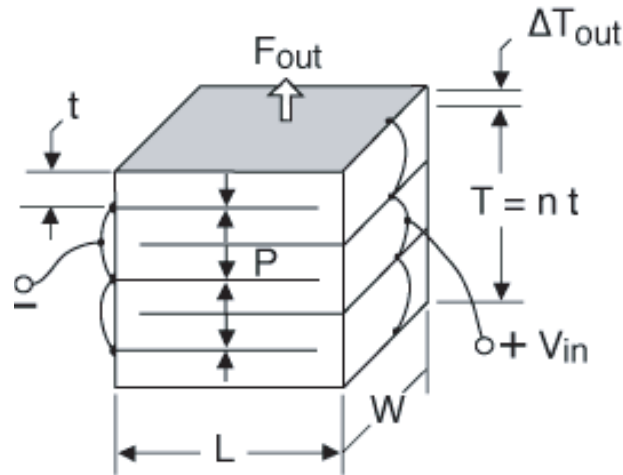


Figure 2.3: Stack piezo configuration. Reprinted from [154], with permission from Piezo Systems, Inc.

piezo crystal slices are in a sub-mm range and separated by electrodes. These electrodes are arranged in alternated polarity. With the parallel arrangement, the entire actuator movement can be calculated by the sum of all single stacks, while the supply voltage of the entire actuator is divided by the number of the stacks. Thus, this structure makes it possible to drive the piezo crystal with relatively low supply voltages in the order of some 100 V.

An further advantage of piezo based actuator in general is the high flexibility in design and that they are commonly available. The main disadvantage is the nonlinear response behavior, which can be overcome by using a more sophisticated control strategy.

2.1.3 Control Strategy

The aim of the combined actuator concept is the precise position-control of a linear movement at the output of the entire actuator. As the proposed actuator concept on the other hand consists of two separate actuator elements, a implementation of a cascaded control strategy would be reasonable. However, to keep the idea of a modular design concept, each module consists of a individual control loop, optimized for its targeted range of motion. To ensure the desired range of motion for the entire combined actuator system, an outer-control loop that covers the independent controlled actuator modules is mandatory. For the first design, the outer control loop will be independent from the inert loops. To optimize the overall performance, it might be useful to cross-link the several control loops in further steps. As the entire feedback control of both modules is processed and executed at the same hardware-layer, there should be enough margin to try more sophisticated combined control strategies in the future.

The driving unit of both modules are composed of piezo-electric elements. Thus, known nonlinear behavior between the supplied voltage and the expansion of the crystal that manifests oneself in a characteristic hysteresis, can be expected. These nonlinearities can be compensated by PI-control concepts. There are a large number of publications about the control of piezo-electric actuators, including the compensation of its nonlinearities. So for

the high frequency module a standard PI-controller would be sufficient, whereas the more complex mechatronics concept of the low frequency-module needs an more sophisticated control concept for position control. In this case a model based control approach, based on a Kalman-Bucy-Filter will be implemented.

In the following, design, construction, and evaluation of the two actuator modules will be described separately.

2.2 Low-Frequency Module

After defining the specification and the choice of actuator type, this section describes the module for the low-frequency part of the multi-actuated pin. The target specification are defined as follows:

- Min. pin stroke/resolution: $\approx 30 \mu\text{m}$
- Max. pin stroke: 3 mm
- Frequency range: 0 – 70 Hz.

The following section describes the construction of the mechanical rocker-lever system. Its passive design is driven by a stack piezo actuator and optimized by FEM analysis. The position sensor and the model of the mechanical construction, described in Sec. 2.2.2 and Sec. 2.2.3 are essential parts for the closed loop position controll that is described and evaluated in the last two sections.

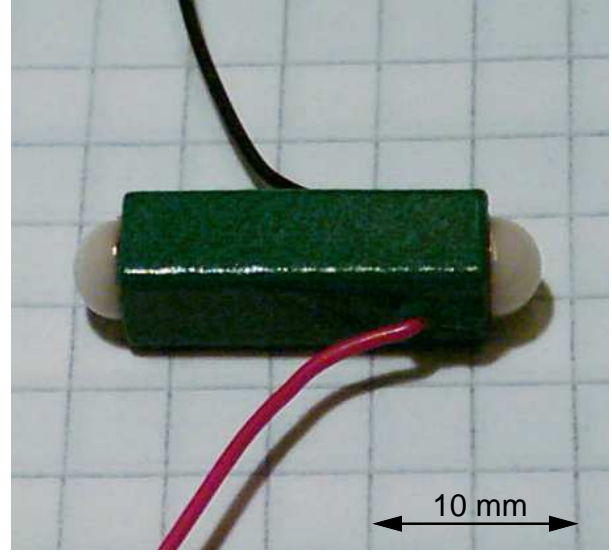
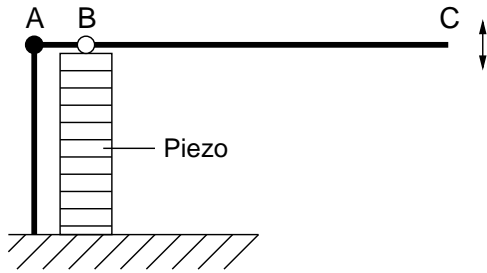
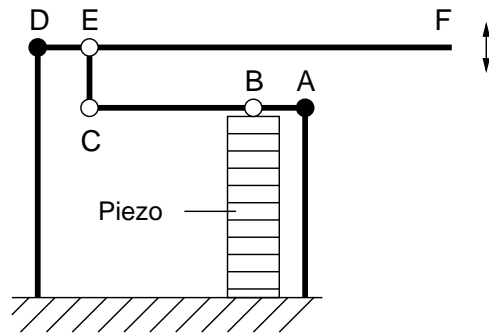
2.2.1 Construction

After investigations in off-the-shelf stack piezo actuators in terms of size, force, and excursion, a stack piezo from Piezomechanik GmbH were chosen. Tab. 2.1 shows the technical data for the selected stack piezo. An essential feature of this stack piezo series is its high expansion ratio of 0.16 %. For an optimal load transmission, a stack with hemispherical ceramic caps on bottom and top (Fig. 2.4) is chosen, which leads to a fitting size of 23 mm. Piezo crystals have a linear force-excursion characteristic between maximum force at zero excursion and zero force at maximum excursion. The following mechanical calculations for actuation dimensioning are based on half the maximum excursion ($15 \mu\text{m}$). In this range, the piezo can provide forces of up to 900 N. To reach a pin excursion of 2.5 mm, a mechanical system of levers has to augment actuator movement by a transmission ratio of 500 : 3. The simplest way to realize this is to use a lever system as shown in Fig. 2.5. Given a minimum distance \overline{AB} of 3 mm, predetermined by the width of the piezo, the length of the lever \overline{AC} would need to be 50 cm. That would contradict the demand of compactness. The same transmission ratio at a smaller size can be achieved by a cascaded two-lever transmission, as shown schematically in Fig. 2.6. Swiveling joints are displayed as circles; filled circles show joints with fixed axes. The first stage (A,B,C) is complemented by a second (D,E,F), which acts in the opposite direction to reduce the overall size of the lever. The transmission ratio of the combined lever system can be calculated as:

$$i_{BF} = i_{BC} i_{EF} = \frac{\overline{AC} \overline{DF}}{\overline{AB} \overline{DE}} = 166.6\bar{6}. \quad (2.1)$$

Table 2.1: Stack piezo data

Type	PSt 150/5 × 5/20
Max. excursion	30 μm
Max. force	1800 N
Stiffness	60 N/μm
Resonance freq.	35 kHz
Supply voltage	−30 – 150 V
El. capacity	1800 nF
Dimensions (stack)	5 × 5 × 18 mm
Weight (stack)	5 g

**Figure 2.4:** Stack piezo actuator**Figure 2.5:** One-lever transmission**Figure 2.6:** Cascaded two-lever transmission

With the additional constraints of:

$$i_{EF} = 2 i_{EF}, \quad \overline{DE} = 3 \text{ mm}, \quad (2.2)$$

the lever lengths result to be:

$$l_{\text{lower}} = \overline{AC} = 27.38 \text{ mm}; \quad l_{\text{upper}} = \overline{DF} = 54.75 \text{ mm}. \quad (2.3)$$

Based on this kinematic dimensioning, a mechanical construction can be realized. A major issue is to find a solution for the construction of the joints A, C, D, E and F. After a comparison between different standard techniques in fine mechanics [162], the method of solid state joints has been selected. These joints are realized by elastic bending of thin beams at the pivot points. They need no assembling or adjustment, have no abrasion, nearly no friction and zero backlash. One disadvantage of this technique, the high restoring force, can be used to provide the necessary pre-load for the stack piezo actuator. As a consequence of this design, the whole lever transmission mechanism has to be built out of one piece.

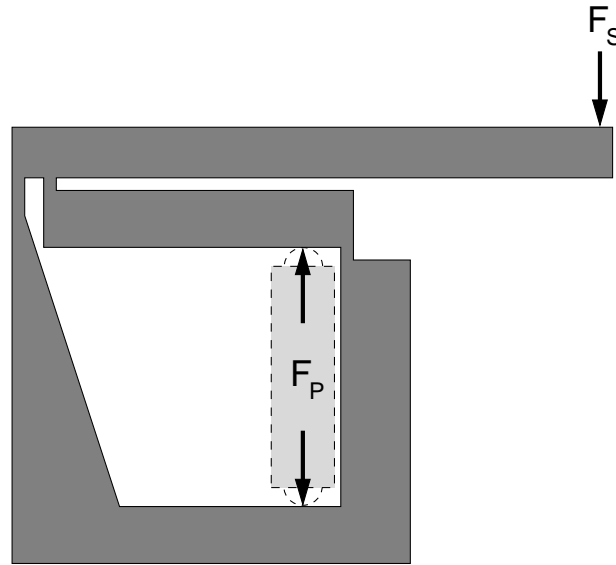


Figure 2.7: First layout of combined lever system

Fig. 2.7 shows the first layout of the cascaded two-lever system designed according to the described principle. The picture displays the side view of a cut out metal plate with a thickness of ≈ 2 mm. The lever system must be designed in a way that the stack piezo actuator (adumbrated) fits in with some initial loading. At the endpoint of the second lever, the pin can be attached to use the amplified motion in vertical direction. The force of the stack piezo F_P and the load of the pin F_S , caused by skin impedance, are displayed at their action points.

As a further step in analyzing the range of motion and the tension at the bending joints, the finite elements method (FEM) is used to optimize shape and functionality of the combined lever system. As a simplification for the FEM computation, only the load of the stack piezo actuator in direction of the first lever has been considered. This is acceptable, because at the bottom point of contact, no deformation or critical stress is expected. Fig. 2.8 shows the results of the first FEM calculations. The left picture displays the

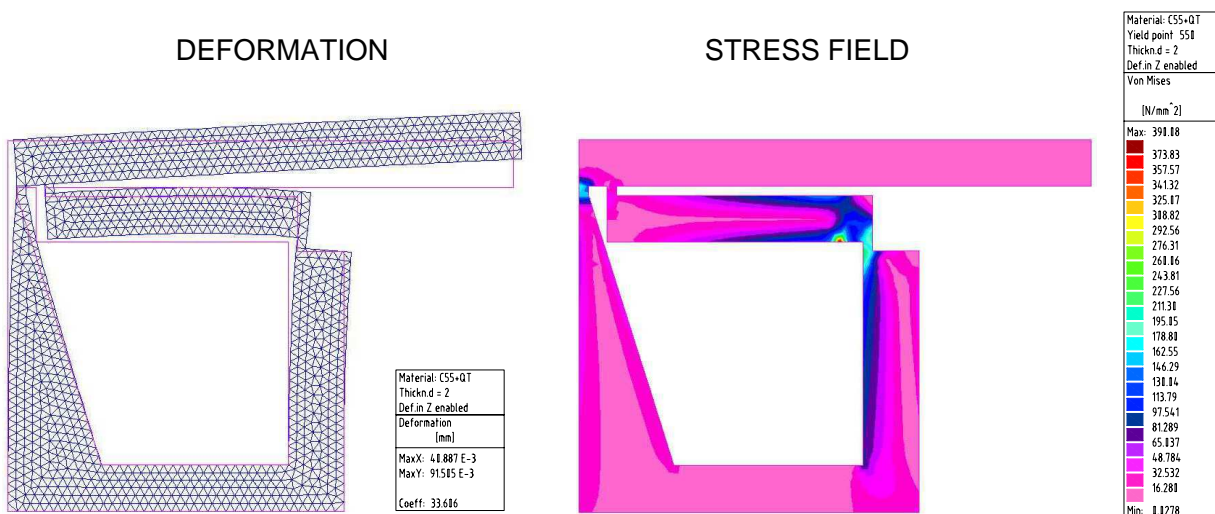


Figure 2.8: First FEM design loop of the combined lever system



Figure 2.9: Final FEM design loop of the combined lever system

deformation of the lever system at maximum load generated by the stack piezo actuator. Furthermore, the arrangement of the nodes used for the computation can be seen. The colored picture on the right side of Fig. 2.8 displays the stress fields with a table of the color-related stress forced aside. For the first three design loops, quality steel (C55) with a thickness of 2 mm has been used. This steel has an elastic modulus of $E = 210000 \text{ N/mm}^2$ and a fatigue resistance of 500 N/mm^2 . All three bending joints are realised as prismatic bonding bridges between the levers. Their base area measures $1 \times 2 \text{ mm}$ and they have a height of 1 mm. The cross-sectional area of the prismatic levers is calculated to $5 \times 2 \text{ mm}$.

First calculations results in an movement of $91 \mu\text{m}$ at the end of the second lever, when activated by an actuator extension of $23 \mu\text{m}$ at a force of 470 N. The reason for this low excursion can be found in the accidental bending behavior of the levers and the body. The stress field picture indicates low tensions in the joints that causes less bending as expected in the joints. It also shows high stress values elsewhere that results in undesired shape adaptation.

This result makes necessary to re-design the shape of the lever-structure. In this process, the findings of the former design-step can be used to optimize the shape in terms of stability and low inertia. Essentially, the following values for the lever-system have been varied:

- Decrease of thickness of the base plate down to 1.6 mm.
- Re-design of shape, based on stress field results of previous designs.
- Decrease of cross-sectional area of the bending joints.
- Elongation of upper and lower lever, to adapt transmission ratio.

The FEM analysis of some re-design steps toward the optimal structure for the lever-system is shown in Fig. 2.9. Due to the implementation of the described items the movement at the end of the second lever has been improved to 1.6 mm at a stack piezo extension of $25 \mu\text{m}$. In this maximum (end) position, the lever system applies a pre-load of 310 N to the stack piezo. The stress field picture in Fig. 2.9 shows that the maximum stress areas

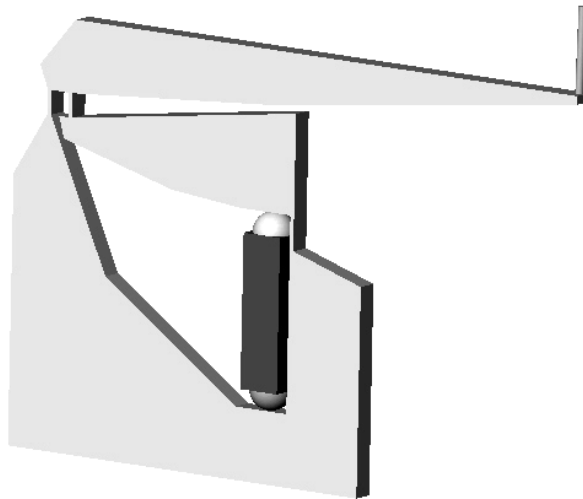


Figure 2.10: Final combined lever system with stack piezo

at the bending joints are safely in the non-deformable range when using heat-treated steel (50CrNi4) with a fatigue resistance of up to 900 N/mm^2 .

Fig. 2.10 shows the final designed body of the combined lever system with attached stack piezo. The fixation point for the attached pin is indicated at the end of the second lever. Technical drawings can be found in App. A. Because of the filigree structure, the body of the low-frequency module was manufactured, using the method of wire-electro discharge machining.

2.2.2 Position Sensor

Although the mechanical structure of the lever-system is designed very light weight, classical dynamical effects take effect while driving the system at higher frequencies. Furthermore the usual hysteresis behavior of the driving piezo element complicate the accurate control of the actuator-module. However, to obtain a precise positioning of the pin, a closed-loop position-control is necessary.

To enable this, a position sensor is desirable. The most efficient point to measure the position is directly at the attachment point of the tactile pin. A closed-loop position control of the actuator module then allows to compensate for the nonlinear behavior of the stack piezo. As the second lever is designed to be longer than the first, some space remains at the end of the second lever, beneath the fixation point (see Fig. 2.10). The specification for the sensor result from the expected performance of the actuator module as follows:

- Range of measurement: $0 - 3.5 \text{ mm}$
- Frequency range: $0 - 70 \text{ Hz}$

No suitable off-the-shelf position measurement system could be found, so a position sensor needs to be customized. The chosen sensor principle is optical; a schematic drawing is shown in Fig. 2.11. This self-made sensor is based on a PSD (*position sensitive diode*) from IC-Haus Ltd.* [81]. With this sensor, the position of an small infrared light spot

*<http://www.ichaus.com>

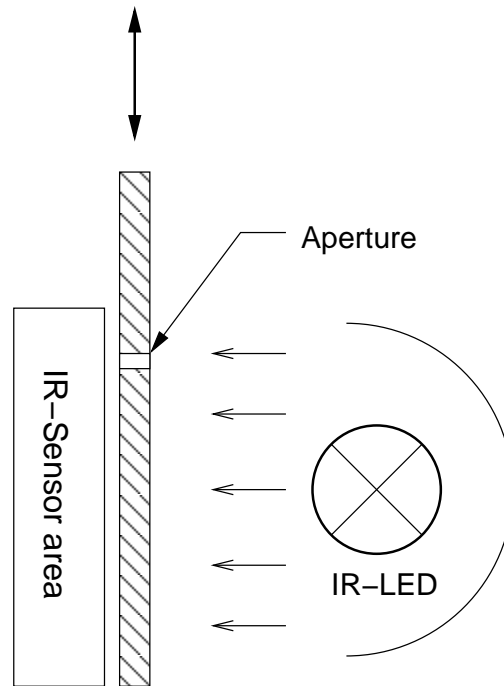


Figure 2.11: Schematic drawing of the position sensor concept (pin in upper position)

can be detected precisely within a sensing area of 2.6×0.88 mm. The light source is realized by a pulsed IR diode, and its light passes through an aperture with a diameter of 0.3 mm. The aperture is integrated in an aluminum beam attached to the end of the lever system, and thus reflects the moving part of the sensor nearby the pin position. In this configuration, the sensor is capable of measuring a position range of 0 – 2.5 mm. To augment the measurement range to the demanded range, the measurement point of the sensor is shifted by 21 mm toward the pivot point of the second lever. Using the lever effect, the range of measurement increases to 0 – 3.5 mm, which is within the demanded range.

2.2.3 Model Identification

In this subsection, a model for the combined lever-system is derived. This can be useful to analyze the mechanical behavior but mainly it is required for the observer-based control strategy. For this purpose, at first the kinematic relations of the lever-system has to be examined.

Fig. 2.12 shows the kinematic chain of the lever-system including the external acting forces. The force F_P , generated by the stack piezo represents, the control input, whereas F_S , caused by the impedance of the human skin, enter the control system as disturbance input. The mass of the moving part of the sensor is denoted by m_s and the capacity of the stack piezo by c_P .

Compared to Fig. 2.6, used to calculate the lever-transmission, the connections at the points C and E are now modeled explicitly as bending beams instead of simple joints. However, all dynamically relevant components, as for instance the sensor rod at point F and the pin rod attached at G are now considered in the computation of the dynamical model.

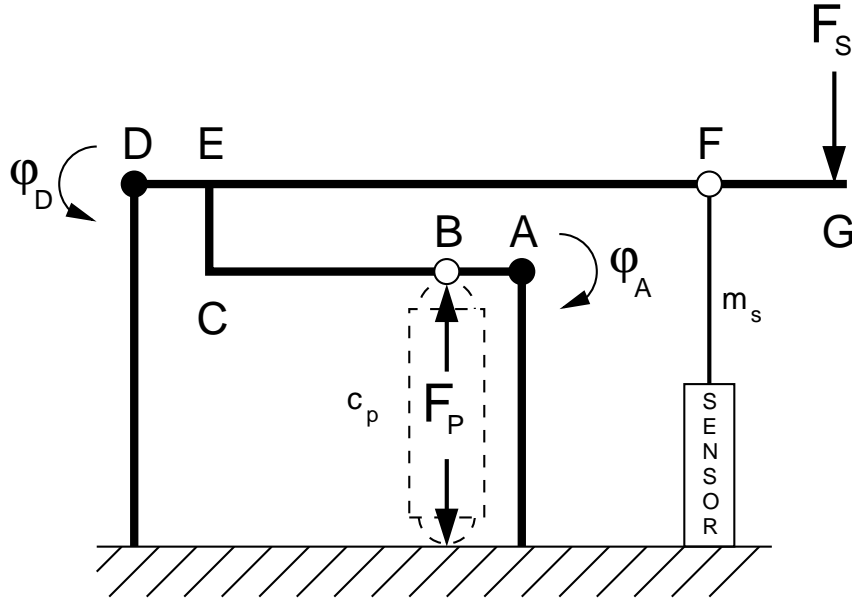


Figure 2.12: Mechanical model

The mechanical equations of motion can be obtained by solving the Lagrangian differential equations:

$$\frac{d}{dt} \left(\frac{\partial L}{\partial \dot{q}_i} \right) - \frac{\partial L}{\partial q_i} + \frac{\partial R}{\partial \dot{q}_i} = Q_i, \quad (2.4)$$

with the Lagrangian equation:

$$L = T - V, \quad (2.5)$$

where T represents the kinetic energy, V the potential energy of the considered mechanical system. R contains dissipation energy (e.g. as a result of damping) and Q_i the external torque to the mechanical system, related to the generalized coordinate q_i .

The generalized coordinates q_i are chosen as the angles of the lower (φ_A) and upper (φ_D) lever. They are subsumed to the vector \mathbf{q} :

$$\mathbf{q} = \begin{pmatrix} \varphi_A \\ \varphi_D \end{pmatrix}. \quad (2.6)$$

Expressed in these generalized coordinates \mathbf{q} , the equations of the kinetic energy T , the potential energy V and the dissipation energy R of the mechanical system can be calculated

to:

$$T = \frac{1}{2} J_{AC} \dot{\varphi}_A^2 + \frac{1}{2} J_{DG} \dot{\varphi}_D^2 + \frac{1}{2} m_s l_{DF}^2 \cos^2(\varphi_D) \dot{\varphi}_D^2 \quad (2.7)$$

$$\begin{aligned} V = & \frac{1}{2} c_A \varphi_A^2 + \frac{1}{2} c_D \varphi_D^2 + \frac{1}{2} c_{CE} (\varphi_A - \varphi_D)^2 + \frac{1}{2} c_P l_{AB}^2 \sin^2(\varphi_A) \\ & + m_{AC} g \left[\frac{1}{3} l_{AC} \sin(\varphi_A) + y_{AC} (\cos(\varphi_A) - 1) \right] \\ & + m_{DG} g \left[\frac{1}{3} l_{DG} \sin(\varphi_D) + y_{DG} (\cos(\varphi_D) - 1) \right] \\ & + m_s g l_{DF} \sin(\varphi_D) \end{aligned} \quad (2.8)$$

$$R = \frac{1}{2} d_A \dot{\varphi}_A^2 + \frac{1}{2} d_D \dot{\varphi}_D^2 + \frac{1}{2} d_{CE} (\dot{\varphi}_A - \dot{\varphi}_D)^2 \quad (2.9)$$

Where J describes inertia, g gravitational acceleration, c stiffness coefficient, d damping coefficient, and m mass, with their indices referring to the schematic in Fig. 2.12. The variables y_{AC} and y_{DG} represent the vertical position shifts of the centers of gravity from the corresponding centers of rotation.

The following simplifications have been made in the energy equations (2.7)-(2.9):

- The kinetic energy of the stack piezo and of the joints (beams) are neglected in (2.7).
- Only the vertical velocity component has been considered in (2.7)
- The potential energy of the piezo body has been neglected in (2.8).
- Due to the FEM optimization in Sec. 2.2.1, elasticity of the lower and upper lever is negligibly small. As a result, both are modeled as rigid bodies, and their dissipation energy are neglected in (2.9).

Solving the Lagrangian differential equations (2.4) results in the two equations of motion:

$$\begin{aligned} J_{AC} \ddot{\varphi}_A + c_A \varphi_A + c_{CE} \varphi_A - c_{CE} \varphi_D + c_P l_{AB}^2 \sin(\varphi_A) \cos(\varphi_A) \\ + \frac{1}{3} m_{AC} g l_{AC} \cos(\varphi_A) - m_{AC} g y_{AC} \sin(\varphi_A) \\ + d_A \dot{\varphi}_A + d_{CE} \dot{\varphi}_A - d_{CE} \dot{\varphi}_D = Q_{\varphi_A} \end{aligned} \quad (2.10)$$

$$\begin{aligned} J_{DG} \ddot{\varphi}_D + m_s l_{DF}^2 \cos^2(\varphi_D) \ddot{\varphi}_D + c_D \varphi_D + c_{CE} \varphi_D - c_{CE} \varphi_A \\ + \frac{1}{3} m_{DG} g l_{DG} \cos(\varphi_D) - m_{DG} g y_{DG} \sin(\varphi_D) + m_s g l_{DF} \cos(\varphi_D) \\ + d_D \dot{\varphi}_D + d_{CE} \dot{\varphi}_D - d_{CE} \dot{\varphi}_A - m_s l_{DF}^2 \sin(\varphi_D) \cos(\varphi_D) \dot{\varphi}_D^2 = 0 \end{aligned} \quad (2.11)$$

The torque load in (2.10) is caused by the piezo-actuators force and can be calculated with:

$$Q_{\varphi_A} = F_P l_{AB} \quad (2.12)$$

The force of the piezo, on the other hand, depends direct of the electrical charge, applied to piezo-crystal. By assume the capacity of the piezo as constant and neglecting the hysteresis effects that usually occur between supply voltage and force, the following simplified electromechanical relation between the piezo-force F_P and supplied voltage U_0 can be used:

$$F_P = K_P U_0, \text{ with } K_P = \frac{\Delta F_P}{\Delta U_0}. \quad (2.13)$$

ΔF_P and ΔU_0 can be obtained from a the maximum working range of the force and the corresponding range of voltage, respectively. With a force range of $F_P = 1800 \text{ N}$ and a voltage range of $U_0 = 150 \text{ V}$, the gain K_P results to $K_P = 12$.

Electrically, the stack piezo can be modeled in a simplified way as a capacitor with capacitance C_P [104]. Fig. 2.13 shows the equivalent circuit diagram of the piezo stack

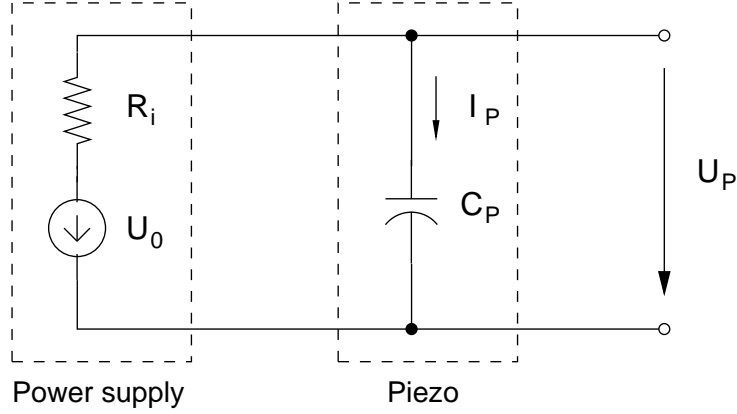


Figure 2.13: Electrical model of the piezo, attached to the power supply

connected to the power supply, containing of a source voltage U_0 and an internal resistance R_i . The voltage applied to the piezo is labeled with U_P and the current with I_P . Using Kirchhoff's voltage law ($\sum U_i = 0$), results to the following equation:

$$U_0 = U_P + R_i I_P. \quad (2.14)$$

The fundamental relation between voltage and current of an capacitor is given by:

$$I_P = C_P \dot{U}_P. \quad (2.15)$$

Combining (2.14) and (2.15), the dynamic behavior of the applied source voltage U_0 and the piezo voltage U_P , which represents mechanical excitation, can be described by:

$$\dot{U}_P = -\frac{U_P}{R_i C_P} + \frac{U_0}{R_i C_P}. \quad (2.16)$$

For further system analysis and controller design, the dynamic equations of the lever system (2.10), (2.11), as well as the electromechanical equations (2.13), (2.16) are transformed to state-space form:

$$\dot{\mathbf{x}} = \mathbf{A} \mathbf{x} + \mathbf{b} u + \mathbf{z}(\varphi_D, \dot{\varphi}_D), \quad y = \mathbf{c}^T \mathbf{x}. \quad (2.17)$$

The state vector \mathbf{x} and the control input u are defined as:

$$\mathbf{x} = \begin{pmatrix} U_P \\ \varphi_A \\ \dot{\varphi}_A \\ \varphi_D \\ \dot{\varphi}_D \end{pmatrix}, \quad u = U_0. \quad (2.18)$$

Based on this, the system matrix \mathbf{A} , the input vector \mathbf{b} and the output vector \mathbf{c} are given by:

$$\mathbf{A} = \begin{pmatrix} -\frac{1}{R_i C_P} & 0 & 0 & 0 & 0 \\ 0 & 0 & 1 & 0 & 0 \\ \frac{K_P l_{AB}}{J_{AC}} & \frac{-c_A - c_{CE} - c_P l_{AB}^2 + m_{AC} g y_{AC}}{J_{AC}} & \frac{-d_A - d_{CE}}{J_{AC}} & \frac{c_{CE}}{J_{AC}} & \frac{d_{CE}}{J_{AC}} \\ 0 & 0 & 0 & 0 & 1 \\ 0 & \frac{c_{CE}}{J_{DG} + m_s l_{DF}^2} & \frac{d_{CE}}{J_{DG} + m_s l_{DF}^2} & \frac{-c_D - c_{CE} + m_{DG} g y_{DG}}{J_{DG} + m_s l_{DF}^2} & \frac{-d_D - d_{CE}}{J_{DG} + m_s l_{DF}^2} \end{pmatrix},$$

$$\mathbf{b} = \begin{pmatrix} \frac{1}{R_i C_P} \\ 0 \\ 0 \\ 0 \\ 0 \end{pmatrix}, \quad \mathbf{c} = \begin{pmatrix} 0 \\ 0 \\ 0 \\ l_{DG} \\ 0 \end{pmatrix}. \quad (2.19)$$

The disturbance vector $\mathbf{z}(\varphi_D, \dot{\varphi}_D)$ containing constant and nonlinear terms of (2.11) is:

$$\mathbf{z}(\varphi_D, \dot{\varphi}_D) = \begin{pmatrix} 0 \\ 0 \\ \frac{m_{AC} g l_{AC}}{3 J_{AC}} \\ 0 \\ -\frac{m_s l_{DF}^2 \sin(\varphi_D) \cos(\varphi_D) \varphi_D^2 - \frac{1}{3} m_{DG} g l_{DG} + m_s g l_{DF}}{J_{DG} + m_s l_{DF}^2} \end{pmatrix}. \quad (2.20)$$

Before the transformation of (2.10) and (2.11) into the state space form (2.17) the trigonometric functions have been replaced by:

$$\sin(\varphi) \approx \varphi, \quad \cos(\varphi) \approx 1, \quad \text{for } \varphi \ll 1. \quad (2.21)$$

These simplifications have been made to linearize parts of the differential equation. They are practicable because of very small angles φ_A and φ_D .

In the following, the parameters of the system matrix \mathbf{A} are specified mathematically. The stiffness coefficients c of the joints A and D are calculated based on a homogeneous, straight bending beam. They can be calculated departing from the deflection curve that is given by Bernoulli's hypothesis:

$$w''(x) = -\frac{M(x)}{EI(x)} = -\frac{M_0}{2EI} \left(1 - \frac{x}{l}\right), \quad (2.22)$$

where $w''(x)$ is the beam deflection in relation to the distance of its fixation x , M_0 is the maximum momentum at the fixation point, E represents the shear modulus of the employed steel, and I is the geometrical momentum of inertia. Solving the definite integral of (2.22) from the fixation point to the maximum length ($x = l$) under consideration that there is no bending at the fixation point ($w'(0) = 0$), results in the bending deflection at the endpoint l :

$$w'_l = -\frac{M_0}{4EI} l. \quad (2.23)$$

Table 2.2: Stiffness coefficients

Joint	b [mm]	h [mm]	l [mm]	c [Nm]
A	2.5	0.6	4	2.363
B	2.5	0.5	2.9	1.886
CE	2.5	0.5	2.9	1.886

As w'_l represents the gradient of the beam deflection at its end point. The relation to the bending angle φ_l is given to:

$$w'_l = \tan(\varphi_l) \approx \varphi_l, \text{ for } \varphi_l \ll 1. \quad (2.24)$$

This simplification only can be made under the assumption of a very short beam and it is only valid for tiny angles. By inserting the specific values:

$$I = \frac{bh^3}{12}, \quad (2.25)$$

(2.23) can be transformed under assumption of (2.24) into an relation of the torque in relation to the bending-angle:

$$M_0(\varphi_l) = E \frac{bh^3}{3l} \varphi_l. \quad (2.26)$$

The potential energy of the beam caused by bending can be calculated to [40]:

$$E_{pot} = \frac{1}{2} \int_0^{\varphi_l} M_0(\varphi'_l) d\varphi'_l = \frac{1}{2} E \frac{bh^3}{6l} \varphi_l^2 \approx \frac{1}{2} c \varphi_l^2. \quad (2.27)$$

Hence, the stiffness of the bending beams in relation to the geometrical form and the modulus of elasticity E can be estimated to:

$$c = E \frac{bh^3}{6l^3}. \quad (2.28)$$

Tab. 2.2 displays the stiffness of the three bending joints, with $E = 210000 \text{ N/mm}^2$. The stiffness coefficient of the stack pie According to Tab. 2.1, the stiffness coefficient of the stack piezo can determined to $c_p = 60000 \text{ N/mm}^2$.

The inertia of the lower and upper lever can directly computed by the CAD program based on the geometrical data and the density of the employed steel to:

$$J_{AC} = 17.92 \cdot 10^{-7} \text{ kg m}^2, \quad J_{DG} = 57.64 \cdot 10^{-7} \text{ kg m}^2 \quad (2.29)$$

Tab. 2.3 summarizes the geometrical data of the lever-system that are necessary to compute the system coefficients. The only values that remains to complete the linear part of the state-space system (2.17) are the damping values d_A, d_{CE}, d_D . In general it is very difficult to determine the damping values mathematically. As the mechanical hardware is already available, it is possible to derive these values with system-identification methods, like step response or measuring the frequency response at different frequencies. To simplify the identification of the damping values, four substitute variables that summarizes the damping coefficients of the system matrix (2.17) are established:

$$D_1 = -\frac{d_A - d_{CE}}{J_{AC}}, \quad D_{12} = \frac{d_{CE}}{J_{AC}}, \quad D_2 = -\frac{d_A - d_{CE}}{J_{AC}}, \quad D_{12} = \frac{d_{CE}}{J_{AC}}$$

Table 2.3: Deviations and masses of the combined lever system

1st lever	2nd lever	Sensor	Piezo
$l_{AC} = 33 \text{ mm}$	$l_{DG} = 72 \text{ mm}$	$l_{DF} = 51 \text{ mm}$	$l_{AB} = 3.5 \text{ mm}$
$m_{AC} = 3.862 \text{ g}$	$m_{DG} = 6.381 \text{ g}$	$m_s = 0.65 \text{ g}$	–
$y_{AC} = 10 \text{ mm}$	$y_{DG} = 5.9 \text{ mm}$	–	–

Based on pre-knowledge of geometrical relations and initial observations of the mechanical setup, the following specifications can be made:

- Initially, quantitative comparisons between the step-response of the real system with the step-response of the mathematical model constrain the damping values $D_1, D_2 \leq 5000$.
- Due to the geometrical relations of the lever system, the following assumptions can be made $D_1 : D_2 \approx 1 : 8$.
- Likewise geometrical motivated are the relations $D_{12} \approx 2D_2$ and $D_2 \approx 2D_{21}$

These assumptions reduce the order of unknown damping values to one. This remaining damping values D can be determined while the validation process of the calculated dynamic model.

To use the dynamic system model for controller design, it is necessary to validate it with the real hardware setup. Therefore, the frequency response of the hardware setup is compared to the frequency response of the computed model. Fig.2.14 shows the open-loop frequency-response characteristics of the real system and the result of computation, using the linear state-space model (2.19), within a range of 10 Hz–10 kHz. For the determination of the real system, the hardware-setup was stimulated by a sine-sweep signal. Signal generation, measurement and processing has been made by a HP35665 Dynamic Signal Analyzer. The solid line shows the measured frequency-response of the hardware-setup. The dashed line shows the computed frequency-response of the state-space model, where the damping value D is chosen such that the frequency-response of the model fits best to the real hardware-setup. The first resonance frequency of the system can be identified clearly at a frequency of 88 Hz. For the frequency band of 0 – 250 Hz, the model represents the real system very precisely in gain and phase. In this range the model is suitable for later applications. At frequencies above 250 Hz the divergence between model and hardware response rises more and more. The second resonance peak at about 2.8 kHz, which is clearly identifiable in the state-space model, is much less pronounced in the hardware, similarly the phase is considerably smoother. This difference between theory and practice is probably due to nonlinearities, which are not considered in the simulation. These nonlinearities are included in the disturbance term of the state-space model (2.20), and thus not used for the simulation. As a result, the model shows sufficient exactitude for the frequency range of the planned low-frequency actuator module.

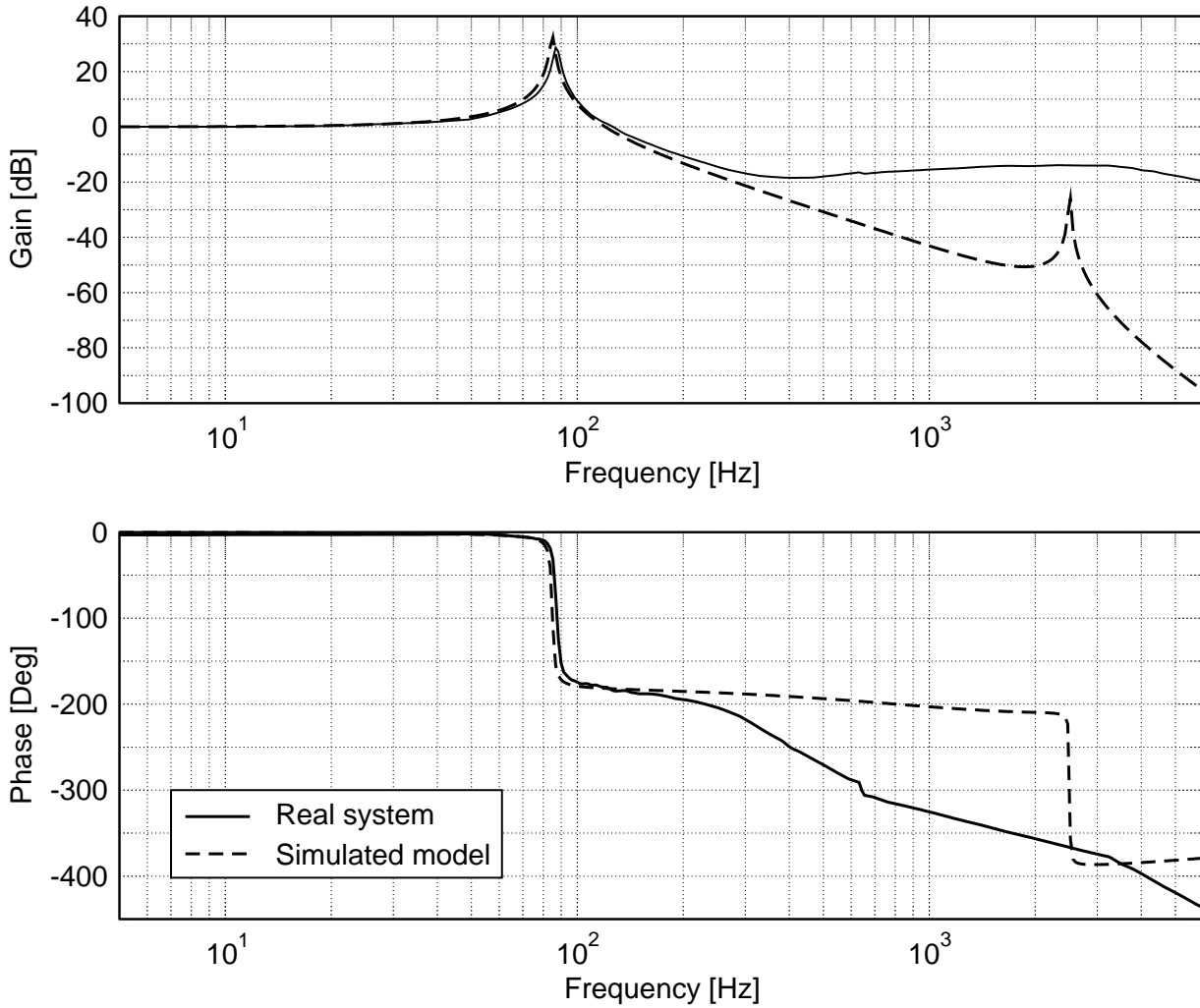


Figure 2.14: Open-loop frequency response, measured in experiment

As the damping value D is found iteratively by fitting the model's frequency response to the measured one of the hardware, finally the parameters of the system matrix \mathbf{A} in (2.19), for the state-space system (2.17) result to:

$$\mathbf{A} = \begin{pmatrix} -7936 & 0 & 0 & 0 & 0 \\ 0 & 0 & 1 & 0 & 0 \\ 4.946 \cdot 10^8 & -2.476 \cdot 10^8 & -100 & 5.7 \cdot 10^5 & 24 \\ 0 & 0 & 0 & 0 & 1 \\ 0 & 1.425 \cdot 10^5 & 6.25 & -2.85 \cdot 10^5 & -12 \end{pmatrix}$$

Fig. 2.15 shows the step response at a range of $150 \mu\text{m}$ to $750 \mu\text{m}$ of the real setup in comparison with the computed dynamic model. The computed model follows the real system with a small phase shift. Furthermore, the amplitude decay is not exactly as fast as in the real system. However, the characteristics of the real system is sufficiently approximated by the computed model. This will be a solid basis for further control design.

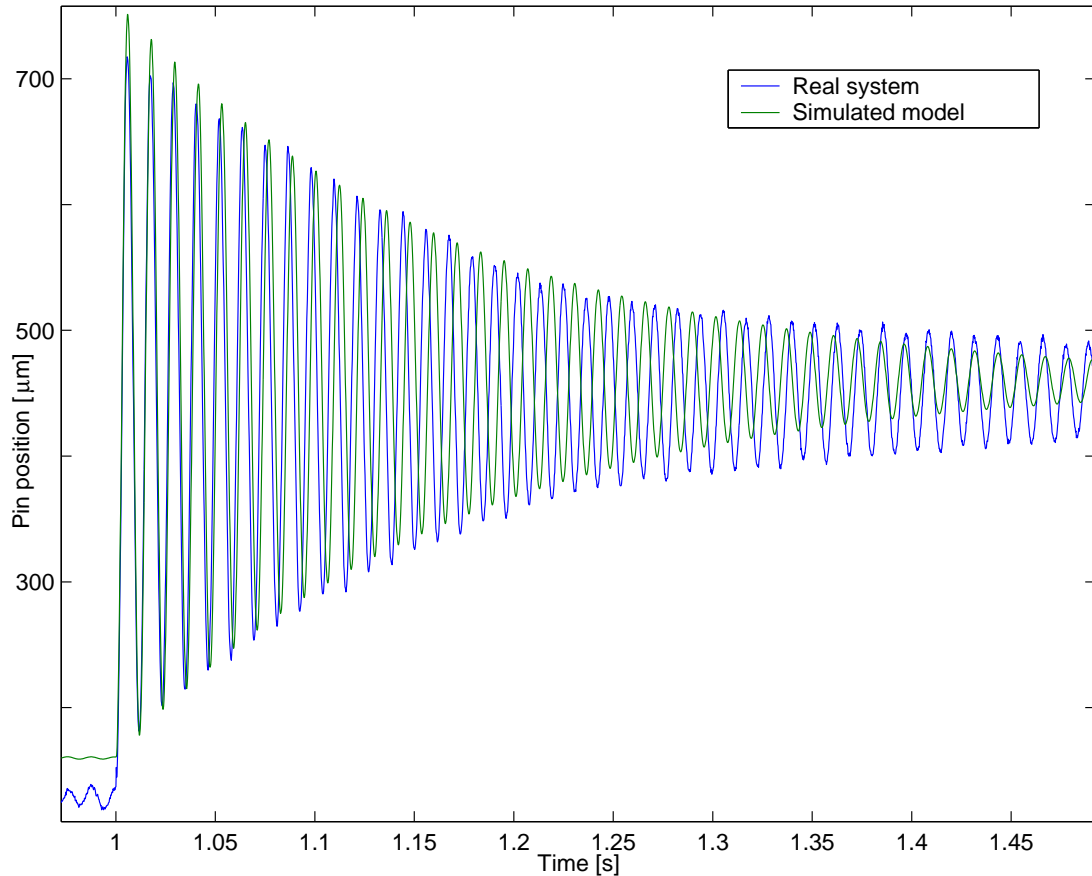


Figure 2.15: Step response of the real system compared to the model.

2.2.4 Control Concept

Based on the dynamic model of the combined lever system described above, now the concept and parameterization of the position controller for the low-frequency module is described. Fig. 2.16 shows the overall control concept of the low-frequency module. The desired position w is the reference value to be tracked by the pin. The pin position y is measured by the position sensor at the endpoint of the lever system. Basically, the entire control structure can be divided into two cascaded control loops:

- An **output control** loop at the outer control structure ensures steady-state reference tracking. It consists of an integral action controller.
- The **state-space control** in the inner control loop is implemented to enhance the dynamic behavior of the plant, and it is realized by an observer-based control structure.

In the following, controller design will be described first, followed by observer design.

Controller Design

The gains for the outer integral action control loop and the gains for the inner state-space loop are found simultaneously using an LQ-control approach [125]. To include integral

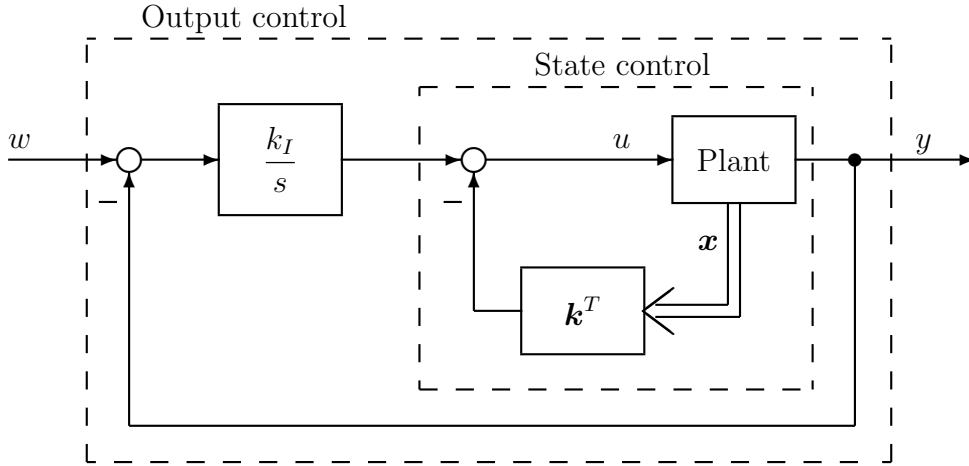


Figure 2.16: Control structure

action, the equations of the dynamic system in state-space form (2.17) are extended by an integrator to:

$$\begin{pmatrix} \dot{\mathbf{x}} \\ \dot{x}_I \end{pmatrix} = \begin{pmatrix} \mathbf{A} & 0 \\ -\mathbf{c}^T & 0 \end{pmatrix} \begin{pmatrix} \mathbf{x} \\ x_I \end{pmatrix} + \begin{pmatrix} \mathbf{b} \\ 0 \end{pmatrix} u + \begin{pmatrix} 0 \\ 1 \end{pmatrix} w, \quad (2.30)$$

Matrix and vectors are the same as in (2.19). In closed loop, the input u to the plant becomes a function of the system state vector:

$$u = -\mathbf{k}^T \begin{pmatrix} \mathbf{x} \\ x_I \end{pmatrix}, \text{ with } \mathbf{k}^T = (k_1 \ k_2 \ k_3 \ k_4 \ k_5 \ k_I). \quad (2.31)$$

The coefficients of the gain vector \mathbf{k} are calculated by solving the optimization problem:

$$\min_{\mathbf{k}} J(\mathbf{x}, u, \sigma) = \int_0^\infty e^{2\sigma t} [\mathbf{x}^T(t) \mathbf{Q} \mathbf{x}(t) + u^2(t) r] dt, \quad (2.32)$$

with $Re(\lambda_i) < -\sigma$.

The matrix \mathbf{Q} weighs the states \mathbf{x} of the system, and the coefficient r weighs the control input u . The stability margin σ in (2.32) is used to determine the settling time. To prevent saturation of the control input, caused for instance by the maximum supply voltage of the stack piezo (150 V), the control input weight coefficient is set to $r = 1 \cdot 10^6$, whereas the weighting matrix for the states is set to $\mathbf{Q} = \text{diag}(1)$. The standardized step response in Fig. 2.17 shows the result of the LQ-controller design at the reference input regarding different stability margins. In each case, the signal response is stable and shows the desired aperiodic characteristic. Fig. 2.18 shows the computed and standardized actuation value during the step response in terms of the maximum set voltage of 150 V. It can be seen that stability margins lower than $\sigma < -678$ would end up in a saturation of the stack piezo amplifier. For this reason, a stability margin of $\sigma = -678$ is chosen. With this value, we

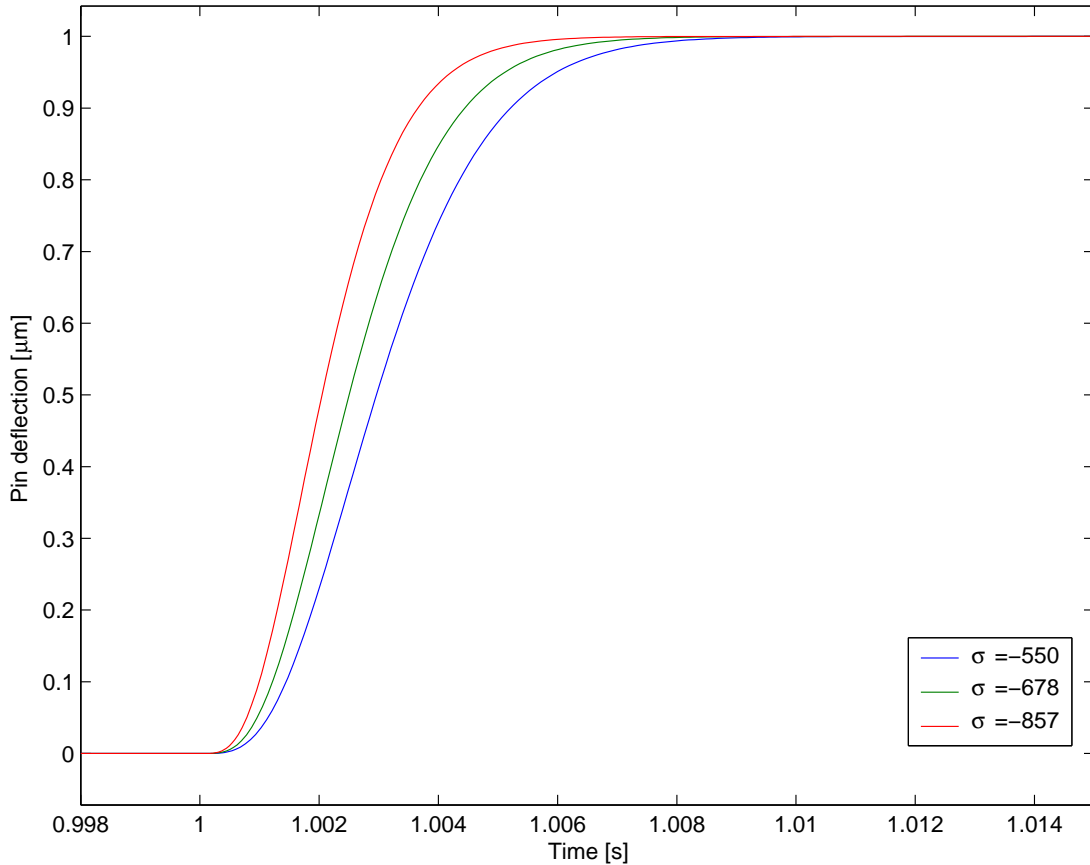


Figure 2.17: Standardized step response at different stability margins

obtain a step response time of $t = 7$ ms, and the gain coefficients result to:

$$\begin{pmatrix} \mathbf{k} \\ k_I \end{pmatrix} = \begin{pmatrix} 10,676 \\ -0,64 \\ 1,0715 \cdot 10^{-3} \\ 62,473 \\ 0,074536 \\ 26439 \end{pmatrix} \quad (2.33)$$

Observer Design

As a basis for inner state-feedback controller, which enhances the dynamic behavior of the actuator-module and also compensates the sensor noise of the position sensor, an observer according to Fig. 2.16 is realized. This controller is designed using the well-known *Kalman-Bucy-Filter* approach. Fig. 2.19 shows the diagram of the used Kalman-Bucy-Filter, adapted from [176]. It essentially consists of a parallel observer in form of a state-space system $(\hat{\mathbf{A}}, \hat{\mathbf{b}})$, based on the computed model in Sec. 2.2.3. The input of the state-space model is calculated by the difference of the measured and the computed output (y, \hat{y}) of the plants, weighted by the vector \mathbf{l} . The estimated states of the system are given by the state vector $\hat{\mathbf{x}}$. Under assumption of full equality between the real plant and the computed

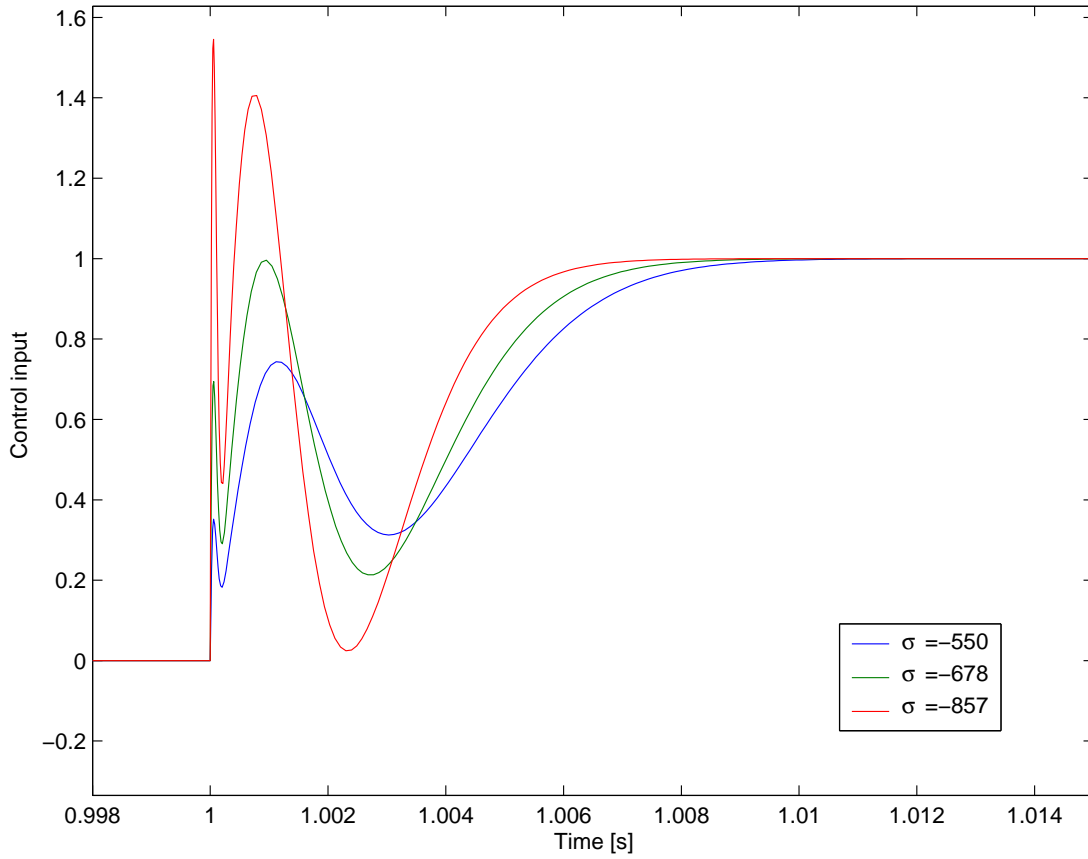


Figure 2.18: Standardized computed actuating value at different stability margins

model ($\hat{\mathbf{A}}=\mathbf{A}$, $\hat{\mathbf{b}}=\mathbf{b}$, and $\hat{\mathbf{c}}=\mathbf{c}$), the state-space form of the observer results to:

$$\dot{\hat{\mathbf{x}}} = (\mathbf{A} - \mathbf{l}\mathbf{c}^T)\hat{\mathbf{x}} + \mathbf{b}u + \mathbf{l}y. \quad (2.34)$$

The Kalman gain vector \mathbf{l} has been determined by minimization of the performance index of the state vector error $\tilde{\mathbf{x}}(t) = \hat{\mathbf{x}}(t) - \mathbf{x}(t)$ between the observer (2.34) and the system model (2.17), more explicitly by minimization of variance:

$$\begin{aligned} J[\tilde{\mathbf{x}}(t)] &= E [\|\tilde{\mathbf{x}}(t)\|^2] \\ &= \lim_{T \rightarrow \infty} \frac{1}{2T} \int_{-T}^{+T} \|\tilde{\mathbf{x}}(t)\|^2 dt \longrightarrow \min. \end{aligned} \quad (2.35)$$

With the equation for the Kalman gain \mathbf{l} :

$$\mathbf{l} = \Pi_+ \mathbf{c} w^{-1}. \quad (2.36)$$

The covariance matrix Π_+ consists of the positive definite solution as a result of solving the *Matrix-Riccati-Equation*:

$$-\mathbf{A}\Pi - \Pi\mathbf{A}^T + \Pi\mathbf{c}w^{-1}\mathbf{c}^T\Pi - \mathbf{V} = 0 \quad (2.37)$$

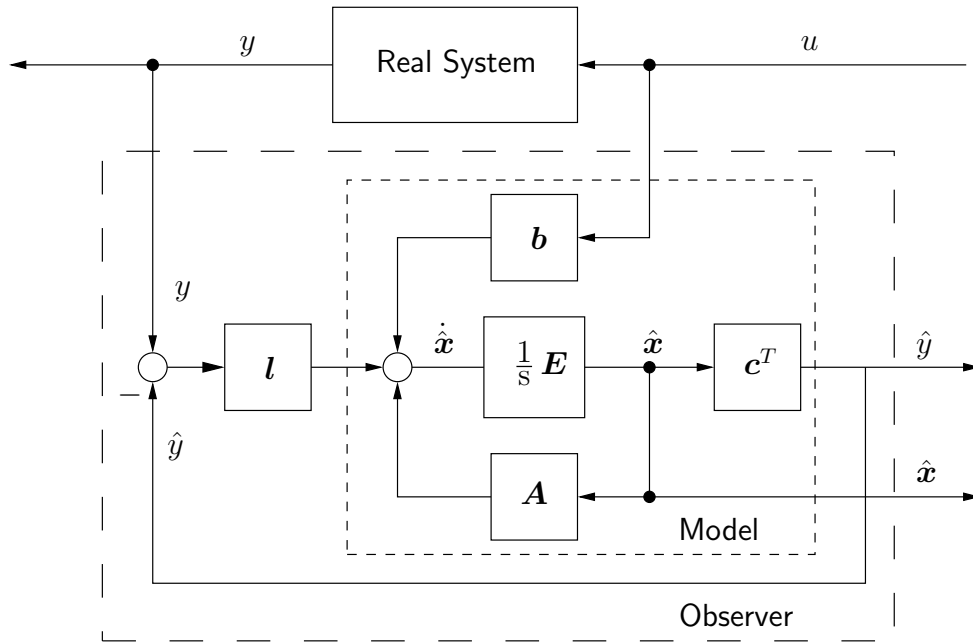


Figure 2.19: Kalman-Bucy-Filter block diagram [176]

The weighting matrix \mathbf{V} is determined by the process noise, whereas the weighting value w depends on the measurement noise. They are specified by measurements on the real system in an iterative process to: $\mathbf{V} = \text{diag}(10^{-4})$, $w = 1.2 \cdot 10^{-7}$. The Kalman gain vector l results to:

$$l = \begin{pmatrix} 3546, 2 \\ -52643 \\ -1, 304 \cdot 10^9 \\ 5176, 8 \\ 1, 34 \cdot 10^7 \end{pmatrix} \quad (2.38)$$

2.2.5 Controller Performance

The entire dynamic system of the low frequency actuator containing an output control loop at the outer and an observer-based state-space controller at the inner control loop can be summarized in state space form as:

$$\begin{pmatrix} \dot{x} \\ \dot{x}_I \\ \dot{\hat{x}} \end{pmatrix} = \begin{pmatrix} \mathbf{A} & k_I \mathbf{b} & -\mathbf{b} \mathbf{k}^T \\ 0 & 0 & -\mathbf{c}^T \\ l \mathbf{c}^T & 0 & \mathbf{A} - l \mathbf{c}^T \end{pmatrix} \begin{pmatrix} x \\ x_I \\ \hat{x} \end{pmatrix} + \begin{pmatrix} 0 \\ 0 \\ \mathbf{b} \end{pmatrix} u + \begin{pmatrix} 0 \\ 1 \\ 0 \end{pmatrix} w \quad (2.39)$$

Due to the fact of using the LQ-control approach both for controller and observer design, the entire controller for the low-frequency module is inherently stable. For measuring the

performance of the entire controller, a step response in both directions of the pin moving space has been performed.

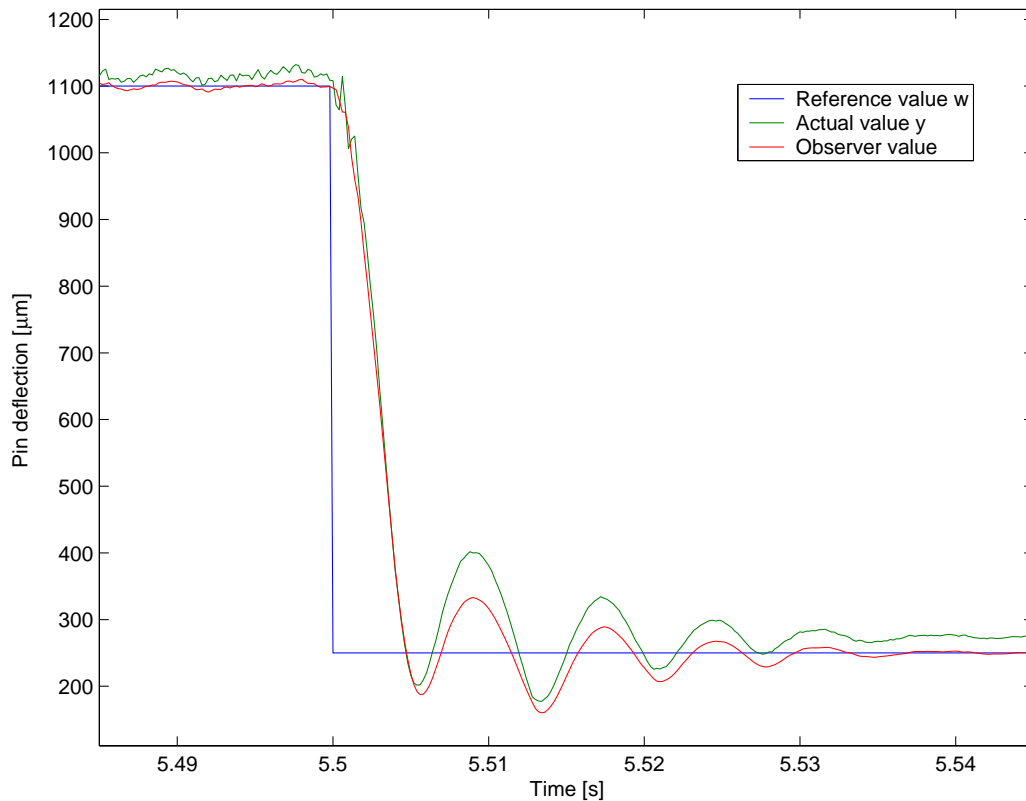


Figure 2.20: Closed-loop response to a reference step from 1100 μm to 250 μm

Fig. 2.20 shows the measured pin position of a step response from 1100 μm down to 250 μm , as well as the pin position, calculated by the observer. After a small overshoot, the system reaches a nearly steady state after approximately 20 ms. In Fig. 2.21 the corresponding characteristic of the control voltage for the stack piezo amplifier is shown. This values are give as a percentage of the maximum input value of $U_{max} = 150 \text{ V}$. The measured observer pin position on a step response from 250 μm up to 1100 μm is shown in Fig. 2.22. Compared with the step downward it has a longer setting time supposed by the countering influence of inertia. Other reasons could be the neglected nonlinearities. The corresponding control voltage is shown in Fig. 2.23.

Compared with the open loop step response in Fig. 2.15 a clear improvement of the positioning accuracy has been reached. Even if the specifications are not reached completely, the resulting low frequency actuator represents a promising approach in actuator technology for tactile pin actuators. Finally, Fig. 2.24 shows a picture of the realized hardware setup of the low frequency actuator, inclusive position sensor.

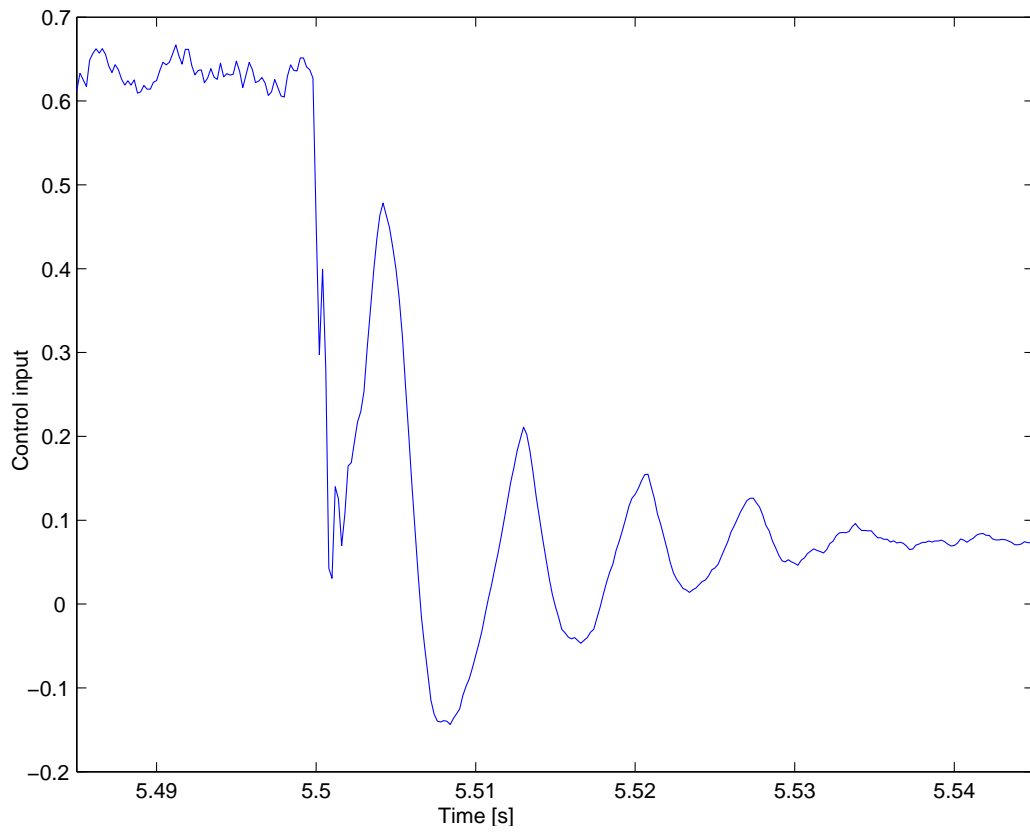


Figure 2.21: Control input for a reference step from $1100 \mu\text{m}$ to $250 \mu\text{m}$ with respect to U_{max}

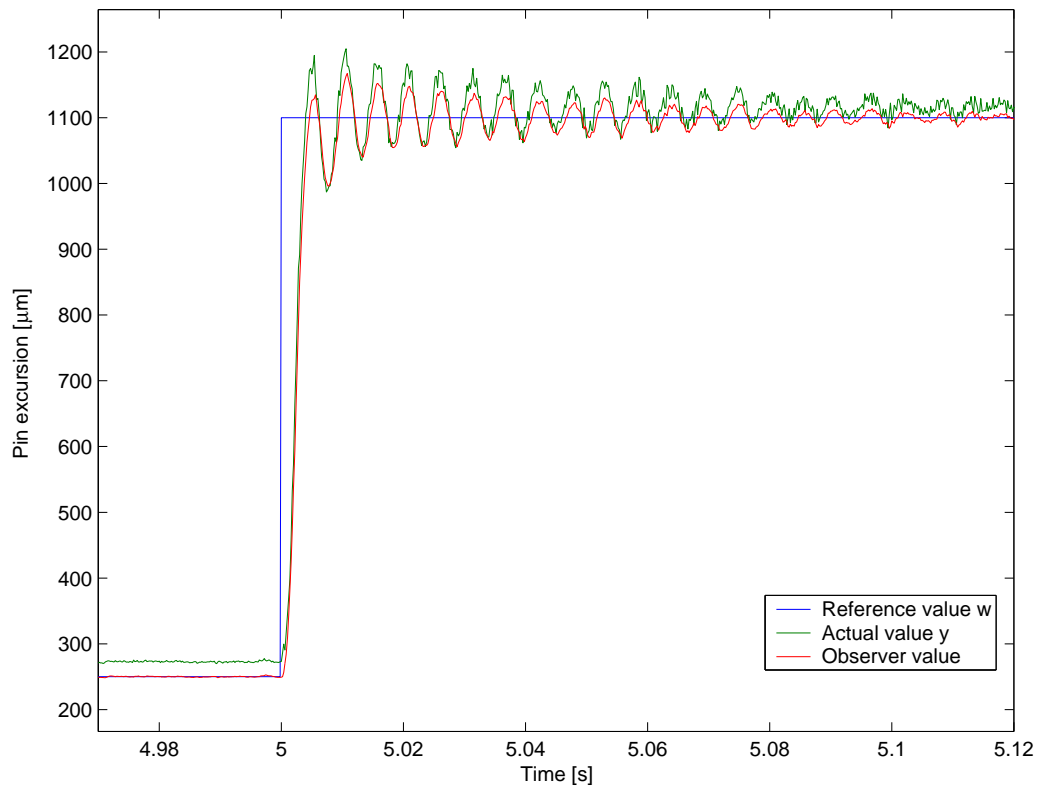


Figure 2.22: Closed loop step response from $250 \mu\text{m}$ to $1100 \mu\text{m}$

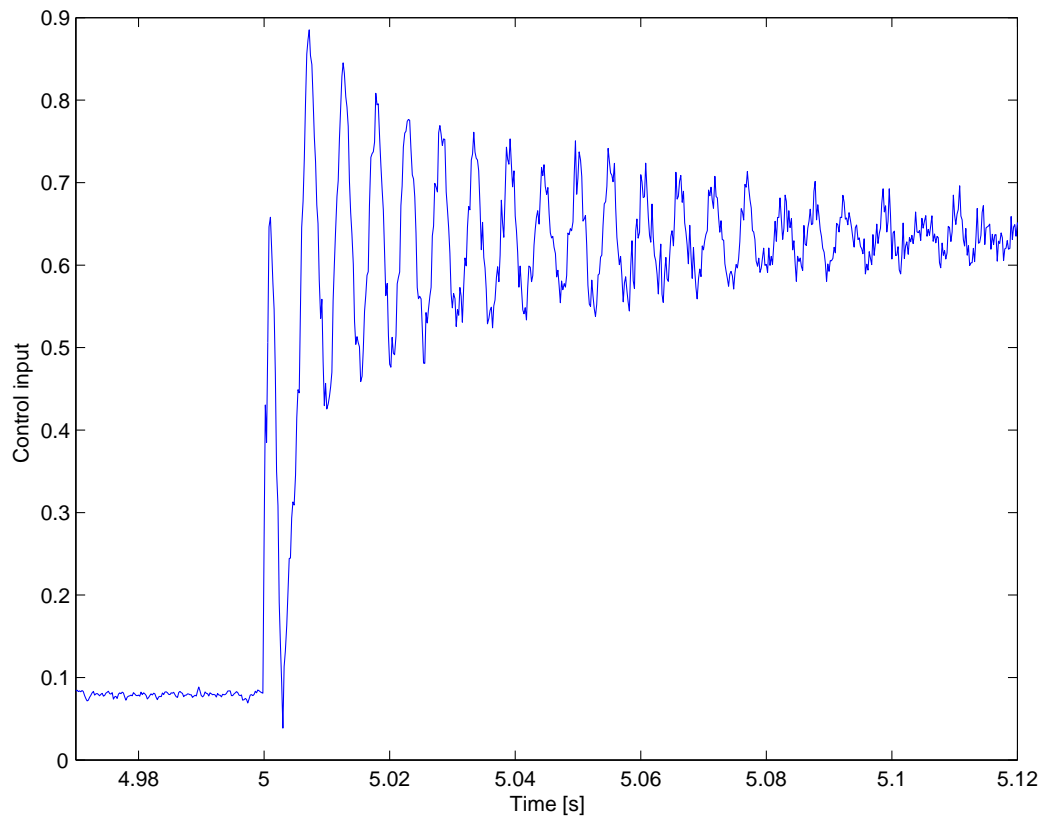


Figure 2.23: Control input at a step from $250 \mu\text{m}$ to $1100 \mu\text{m}$ with respect to U_{max}

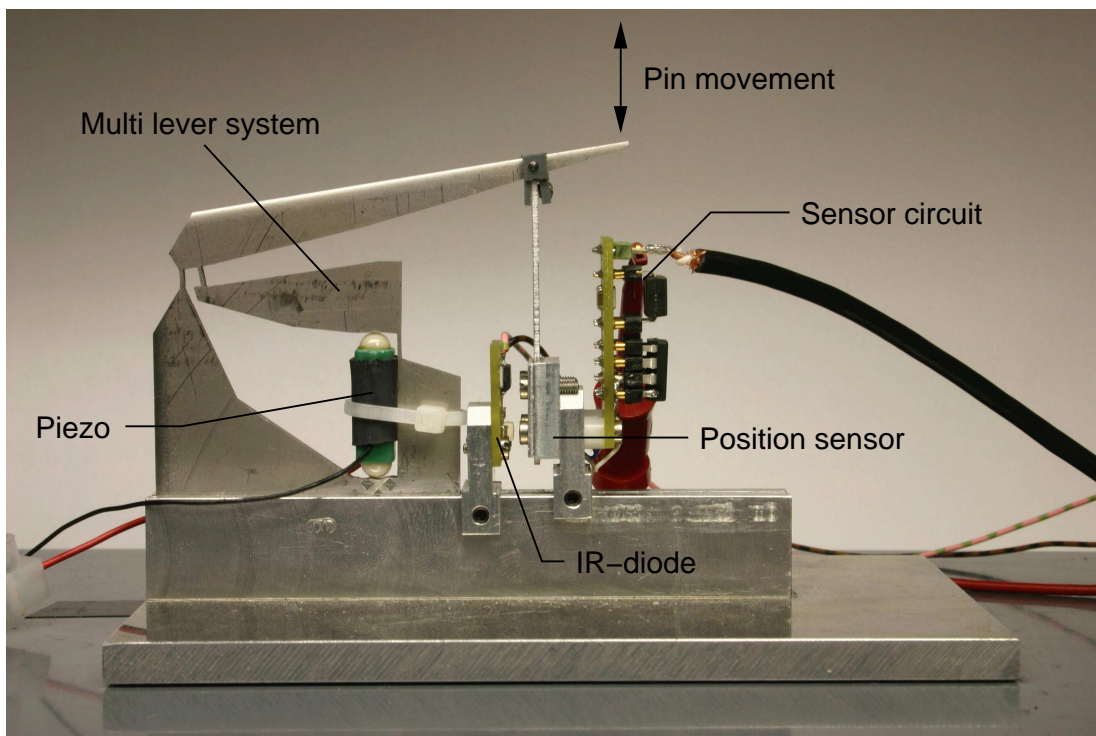


Figure 2.24: Complete setup of the low-frequency module

2.3 High-Frequency Module

The high-frequency module of the combined actuator concept is appropriate for the frequency range above 70 Hz. According to the specifications above, it should be able to reach a pin excursion of about $20\ \mu\text{m}$ and stimulation frequencies up to 1 kHz.

These requirements can also be met by a standard stack piezo actuator. In this case, an off-the-shelf stack-piezo module without mechanical transmission will be used. Fig. 2.25

Table 2.4: Stack piezo data

Type	PSt 150/5/40
Max. stroke	$55\ \mu\text{m}$
Max. force	800 N
Prestress	150 N
Stiffness	$12\ \frac{\text{N}}{\mu\text{m}}$
Resonance freq.	20 kHz
Supply voltage	-30 – 150 V
El. capacity	1600 nF
Pos. sensitivity	0.05 nm
Length (L)	46 mm

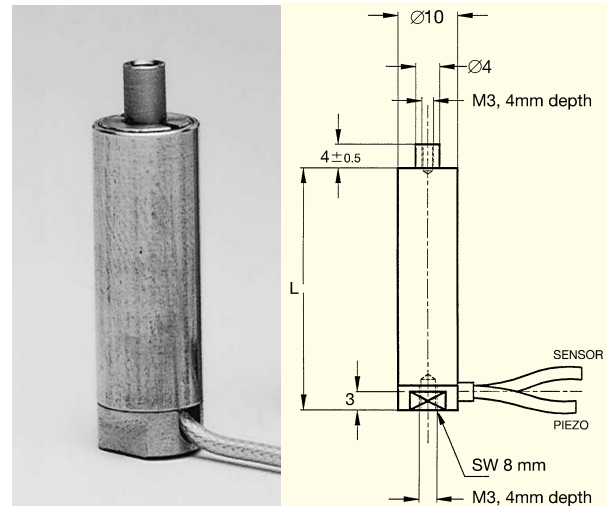


Figure 2.25: High-frequency stack piezo

shows a picture and a technical drawing of the chosen stack-piezo actuator. It comes with a strain gauge based position sensor that is customized for the possible range of motion of the actuator. The performance data of the module is summarized in Tab. 2.4.

Similar to the piezo actuator that was used for the low-frequency module, nonlinearities in form of hysteresis dominate the objectives for the closed control loop. The control concept however can be realized much simpler, compared to the low-frequency module. This is due to the fact that the output motion of the piezo-crystal is directly used for stimulation. As the piezo-module also contains a position sensor solution innately, a standard PI-control approach can be used for position control.

The sensor contains a strain gauge implemented in full Wheatstone bridge configuration for deformation measurement. A signal amplifier was built that makes this passive sensor accessible for the Sensoray DAQ-card. The circuit diagram of the amplifier and the pin assignment of the strain gauge can be found in App. B.

2.3.1 Position Control

Model Identification

The high-frequency module is a stack piezo element. Similar to the core actuator of the low-frequency actuator above, the dynamic behavior can be modeled by capacity, resistance and a power (charging) source, as shown in Fig. 2.13. The result is a PT_1 system (first

order lowpass), with the transfer function:

$$F_{hf}(s) = \frac{\text{excursion}}{\text{supplied voltage}} = \frac{y}{U_0} = \frac{k_g k_{piezo}}{Ts + 1}, \quad (2.40)$$

with the amplification k_g from command signal voltage to piezo supply voltage, and K_p denoting the maximum excursion divided by the maximum input voltage. The time constant can be determined from the piezo capacity C_{piezo} and the internal resistance of the virtual power supply R_i : $T = R_i C_{piezo}$.

Control Concept

A controller with proportional combined with integral action is chosen. This concept is a frequently used, robust concept, and it provides sufficient accuracy for the envisaged application. Fig. 2.26 shows the control structure of the high-frequency module. The sensor

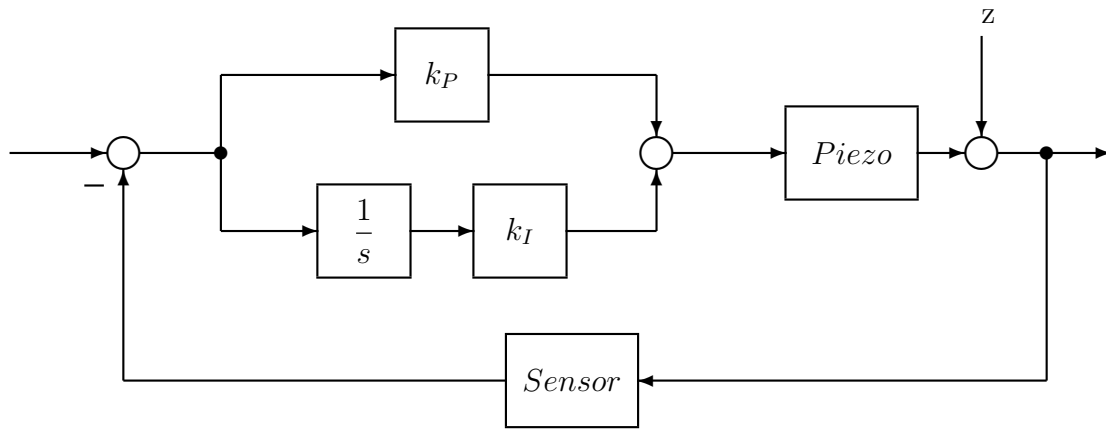


Figure 2.26: High-frequency module control structure

is assumed as ideal ($F_s = 1$), and the controller proportional and integral coefficients are k_P and k_I , respectively.

For the demanded frequency range of up to 1 kHz, a settling time of $T_{set} = 1$ ms is necessary. Thus, a stability margin of $\sigma_g = -3000$ results. A root locus analysis was performed to ensure that the roots comply with these stability margins. The resulting control gains were: $k_P = 0.3368$ and $k_I = 3200$.

2.3.2 Controller Performance

Fig. 2.27 shows the behavior of the stack piezo in its entire range of movement, where the characteristic hysteresis can be seen.

The results of the position-controlled stack piezo are displayed in Fig. 2.28 and Fig. 2.29. They show the sine and pulse responses at the same frequency (250 Hz). There, the measured voltage in the range of 0 to 10 V is proportional to the pin excursion of 0 to 40 μm . In comparison with measurements of the real system, the computed model differs by about 10% in terms of bandwidth, with $f_{max} = 950$ Hz. With this performance, the controlled high-frequency actuator can be used as part of the multi-actuated pin concept, as intended.

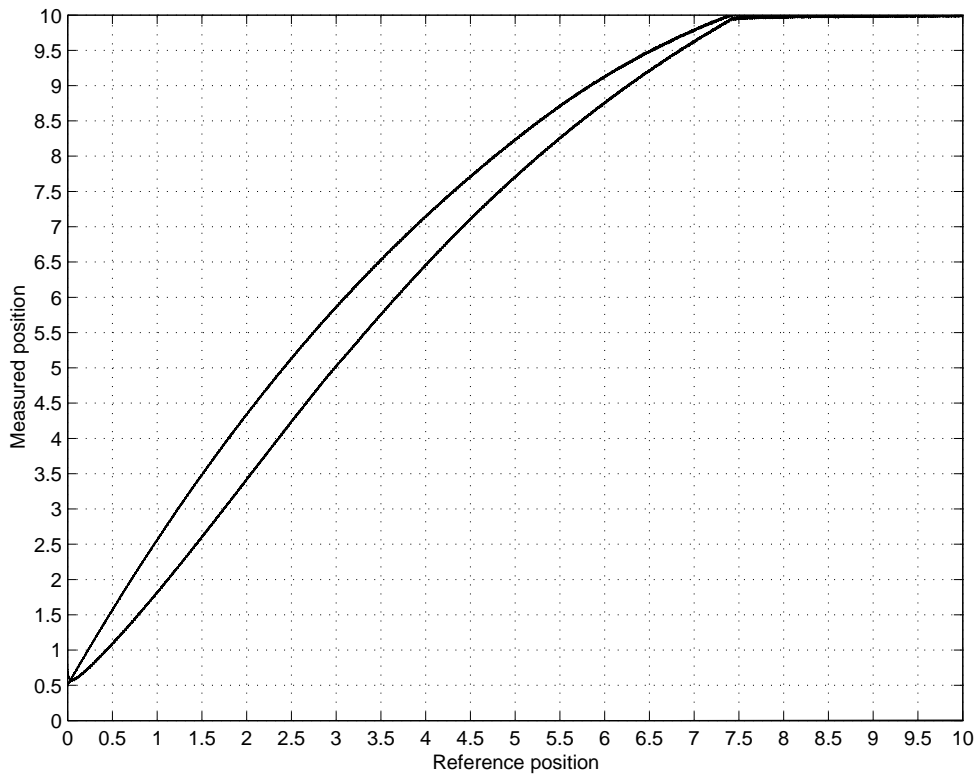


Figure 2.27: Hysteresis of the stack piezo

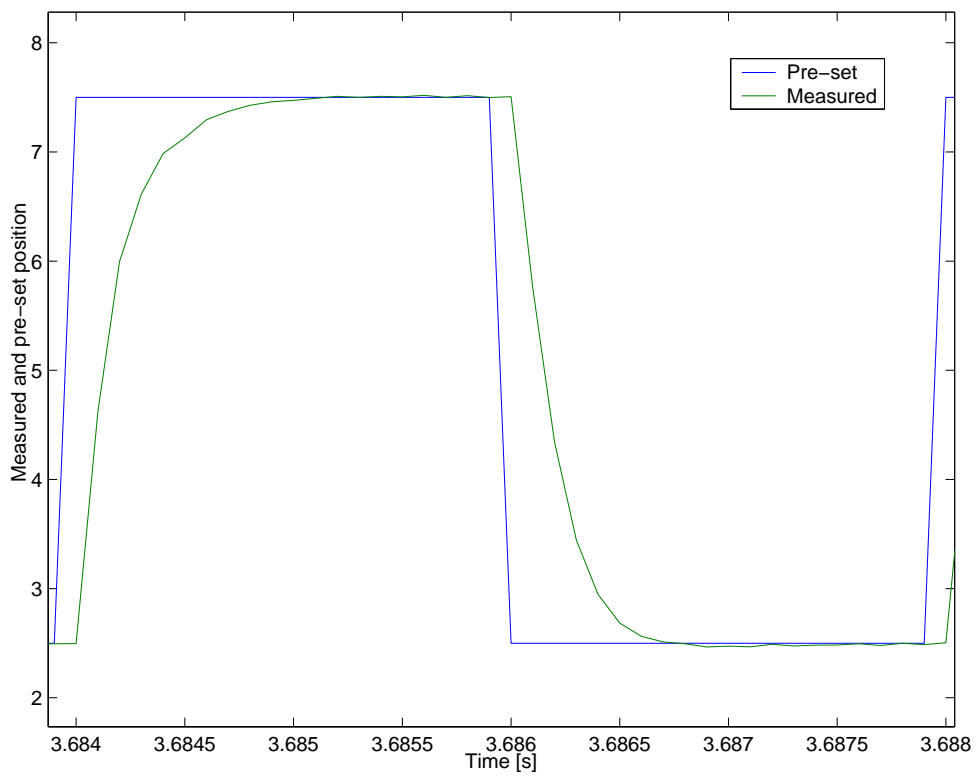


Figure 2.28: Pulse signal tracking performance at 250 Hz

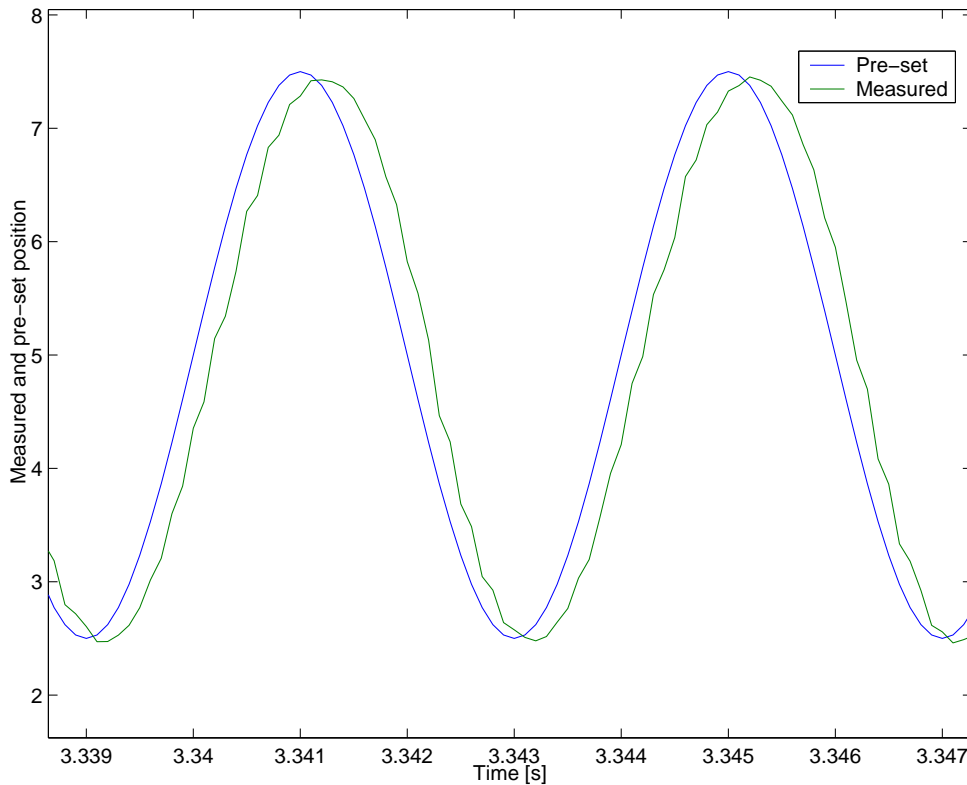


Figure 2.29: Sine wave tracking performance at 250 Hz

2.4 Conclusion

In this chapter, a novel concept for a pin-based tactile display was presented. The challenge was to match the entire range of human perception at the finger-tip, which is not possible with current actuator technology. The proposed solution combines two actuators in a way that both need to cover only part of the required operating range. This division is done so that one module covers high-frequency, low-amplitude stimuli, the other covers low-frequency, high-amplitude stimuli.

The strictly modular concept allows to design and analyze both modules separately. Correspondingly, individual prototypes for the two modules have been realized and evaluated. The results show that the performance of the two modules in combination is sufficient to match human perception.

In theory, yet improved tracking performance could be achieved by modified electronics and an alternative control scheme for the piezo actuator: The use of charge control instead of voltage control offers the advantage of a linear input-output relationship, particularly eliminating the problem of hysteresis [10]. However, the electronics would be complicated to realize in practice.

The redundant actuation concept causes increased size and weight of an individual pin compared to a single-actuator design. However, this disadvantage becomes marginal when the single-pin concept is extended to an extensive tactile display, e.g. according to the classical pin-matrix tactile display concept: Then, it is not necessary to multiply both module components. As described in Sec. 2.1.2 and illustrated in Fig. 2.2, it is sufficient to fabricate many low-frequency modules and a single high-frequency module component.

In conclusion, a display that follows the proposed concept could be used for psychophysical investigations, where high-fidelity tactile stimuli are needed.

3 Lateral Force Displays

The survey on tactile displays (see Sec. 1.3) shows that the conventional method to provide tactile stimuli is to emulate tactile information of the real environment via mechanical stimulation. In the majority of cases, solely active tactile stimuli in direction normal to the skin are used for tactile stimulation. Normal forces require a considerable effort on the technical realization to achieve realistic stimulation. An explicit example is the effort necessary to built a single actuated pin intended for an ideal pin-matrix based tactile actuator, as shown in Chap. 2. This prototype setup demonstrates insistently that it is currently impossible to built an ideal tactile display with economically justifiable effort.

However, the biophysical properties of the human tactile sense (Chap. 1.2) suggest that there may be an additional kind of tactile cues that has been widely neglected, which is skin stretch. Recent results of psychophysical investigations in conjunction with anatomical findings [146] indicate that a special type of mechanoreceptor, namely the Ruffini endings, are designated to detect this kind of stimulation. Skin stretch can for instance be induced by applying shear forces to the skin surface. This facet of human perception could open up new possibilities for the design of tactile displays, but it could also impose even more rigid requirements.

The fundamentals of tactile perception caused by skin stretch have been investigated much less until now compared to the perception of normal forces. To learn more about the outer psychophysical relations of this sub-modality of tactile perception, key questions concern the isolated effect of skin stretch alone, as well as accompanying friction effects, which are for instance related to a fingertip sliding along a surface.

To address these key questions, two different experiments were designed, requiring two separate displays. The first series of experiments focused on a psychophysical investigation of stimulation with spatial constraint. For this purpose, a display with an ability to stimulate isolated regions on the fingertip was necessary. The second series of experiments addressed the perception of several types of friction between the entire skin surface of the fingertip and the surface of an object that it is in contact with. For this purpose, a display with an ability to stimulate the entire surface of the fingertip was necessary.

The design process was similar for both displays. It started with a concept and a specification part, followed by the description of hardware components and hardware setup, and it closed with associated evaluation experiments.

The design specifications were driven by the intended psychophysical experiments. to achieve reliable results, it was important to ensure sufficient performance and resolution, regarding actuation as well as sensing. To achieve this aim, the known performance of tactile perception (see Sec. 1.2) was used as a guideline.

First, a pin-based tactile display was designed to explore the spatial resolution of lateral skin stretch. The device allowed to identify the JND for angular resolution of lateral tactile stimulation, based on classical psychophysical methods. Second, a display is presented that has the capability to provide two-dimensional slip friction relative to the surface of

the fingertip. Both displays were designed in a compact manner, in consideration of the ability to later combine them with a kinesthetic display.

The following sections contain a description of the entire work flow for both displays, covering specifications, hardware setup, and evaluation experiments.

3.1 Shear-Force Display

The first display in the series of tactile shear force displays is built to explore the human tactile perception of isolated skin stretch in more depth. Therefore, only point contact between the device and the fingertip is desired, in order to induce skin stretch within a spatially constrained region of the human skin. These contact points are directly attached to the skin of the fingertip, and they should be able to move laterally with respect to the skin.

The concept for this design was inspired by a basic experience that can be made with an ordinary comb, as reported in [76]. This experiment only requires a comb and a pencil: When touching the tooth of the comb with the fingertip, a slight striking along the long side of the tooth, e.g. using a pencil, causes a kind of running wave sensation under the index finger. This indicates that very small excitations, in the sub-mm range of the teeth, cause skin stretch that can clearly be perceived as tactile sensation. This suggests the promising conclusion that the tactile perception of skin stretch might be very sensitive.

At the end of this chapter, two psychophysical experiments are described, to explore whether the stimuli produced by the display are appropriate for human perception. These evaluation experiments studied the discrimination performance of humans for distinguishing between different directions of pin movement.

3.1.1 Concept and Specification

The conceptual idea of the Shear-Force Display is based on one or more rigid pins, like the ones used for normal-force displays. A major difference is that the Shear-Force Display must be able to move the pin(s) lateral to the surface of the human skin. This augments the movement space to a two-dimensional space, with the consequence that two actuators are needed to drive a single pin.

The next points to consider are the shape and the size of the pin. In order to cause skin stretch, the pin must be able to remain in contact with the skin over the entire range of motion it covers. On the other side, the pin must not be perceived as punctual (needle-like) tactile sensation. Both demands could be satisfied by maximizing the contact area of the pin at the skin. However, arguments against a large contact area are movement constraints, especially if there is more than one pin present. Resulting from this trade-off, a round pin with a plain top surface and a diameter of 1 mm was chosen. The desired pin movement was determined to be 2 mm in each direction. This value results mainly from the comb experiments described earlier. Previous pilot experiments with a similar setup showed that even a amplitude of lateral pin movement below 1 mm beneath the skin causes a clear perceptual sensation of skin stretch. Therefore, the chosen dimensions seem to be a good compromise concerning pin size and motion, and they allow to install four lateral movable pins within the area of the fingertip of the human index finger.

The skin reacts to stretching with a resistive force. To push against this resistance, the pin needs a certain force. In addition, there must be sufficient performance left to ensure an appropriate velocity of the pins, to provide the intended stimuli. The skin can physically be described as viscoelastic material, where force reactions in normal direction are nearly independent of tangential force reaction. Investigations on these viscoelastic properties of the skin show that the force response clearly depends on the strain rate. In a steady state, the force response solely depends on skin stretch [23].

However, more quantitative knowledge on the exact physical properties of the human skin at the tip of the index finger is needed to specify the required force and power of the actuator driving the pins. To this aim, an initial experiment was performed.

The experiment on skin stretch was performed by providing sinusoidal pin excitations of up to $150\ \mu\text{m}$ perpendicular to the skin at several frequencies in the range of 2–200 Hz. The pin size was 0.5 mm in diameter and the stimulation time was 10 s per trial. The results, based on the viscoelastic model, show a steady-state shear modulus of $90\ \text{kN/m}^2$ *. In the range of the stimulation frequency of 2 – 20 Hz, the shear modulus is about $70\ \text{kN/m}^2$. At stimulation frequencies from 30 Hz up to 200 Hz, the shear modulus increases from $454\ \text{kN/m}^2$ to $8.09\ \text{MN/m}^2$.

According to the demands of the envisaged experiments, the maximum kinetic frequency of the pins was specified to 20 Hz. For this range, a maximum shear modulus of $90\ \text{kN/m}^2$ can be expected. The maximum bulk modulus in this frequency range is $55\ \text{kN/m}^2$. With the specified dimensions of the pin and a pin movement of 2 mm in each direction, a maximum driving-force of 0.355 N is required, according to the equations for purely elastic behavior of the hand tissue [23]. Tab. 3.1 lists the key specifications that are demanded

Table 3.1: Specifications for the Shear-Force Display.

Property	Specification
Number of pins	4
Pin shape	circular
Pin tip area	$0.7854\ \text{mm}^2$ ($\varnothing 1\ \text{mm}$)
Pin movement	two axes, workspace $2 \times 2\ \text{mm}$
Max. lateral force	0.355 N
Max. frequency	20 Hz

from the Shear-Force Display. Besides these quantitative specifications, it must also be considered that the display should be as compact and lightweight as possible.

Mechanical Concept

The main objective is to find a mechanical solution that transfers the rotatory motion of two servo motors to one pin, generating two-dimensional lateral pin motion. Fig. 3.1 shows the design concept of the tactile Shear-Force Display. The side view illustrates the

*Measured at a stimulation-frequency of 2 Hz.

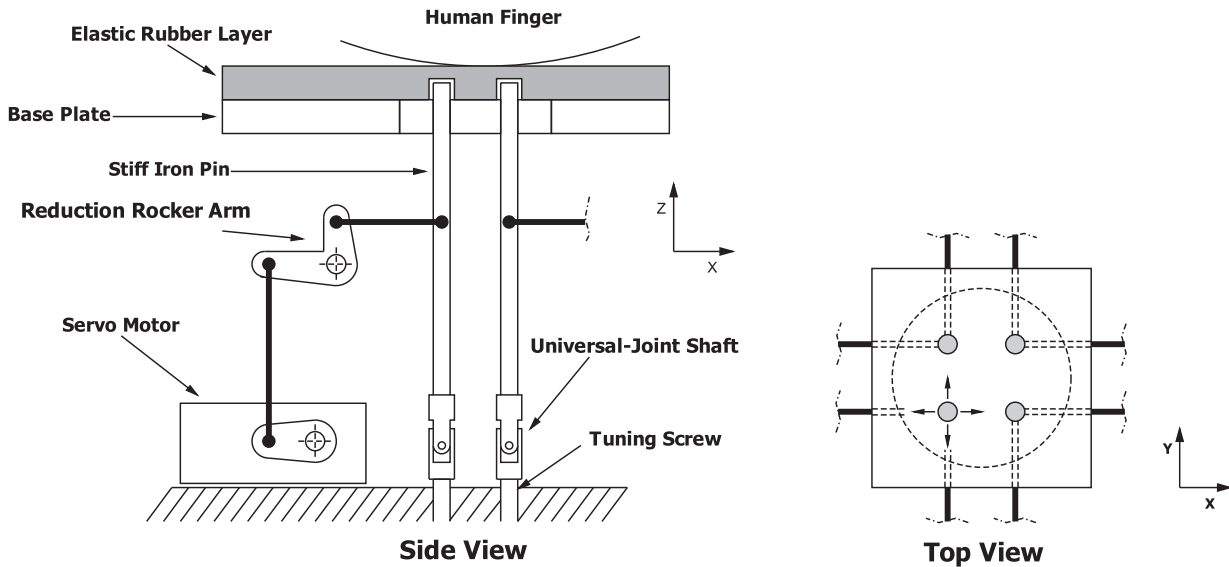


Figure 3.1: Functional principle of the Shear-Force Display.

mechanism to operate one pin in one axis of motion. All four pins are connected to the base plate by universal-joint shafts. This locks the rotatory motion of the pins and thus allows only pitch motion. The pin must be long enough to prevent undesired motion normal to the skin during pitch motion. Each pin is actuated by two servo motors. The figure shows one of the two actuator chains: The rotatory motion of the servo motor is transformed by the reduction rocker arm, which in turn moves the pin. These components are connected via lever linkages with ball joints on both ends. This ensures explicit transmission of linear motion with nearly zero backlash. The top view in Fig. 3.1 shows the arrangement of the four pins. The dotted cycle represents the hole in the cover plate, which enables the connection between the pins and the skin of the resting index finger.

According to this concept, an experimental prototype for one pin was built as a proof of principle [53]. The following section describes the final hardware setup of the tactile Shear-Force Display, as presented previously in [54–56].

3.1.2 Hardware Setup

As the experimental prototype demonstrated the general functionality of the desired display, the remaining issues for the hardware setup are the choice of suitable mechanical components, primarily the actuators, and the calculation of the kinematics of the described lever system.

In the further explanations, the x , y -axes of the device-related coordinate system describe the plane parallel both to the base plate and to the skin surface of the fingertip. Thus, the z -axis describes the direction orthogonal to the base plate and to the skin-surface.

Hardware Components

To avoid development of components from scratch, off-the-shelf solutions were used wherever possible.

After an investigation of the commercially available actuators, RC-servo motors were chosen. Despite the disadvantage of producing rotatory motion, which has to be translated to linear motion, they represent the best trade-off in terms of performance, usability, size, weight, pricing and availability. As these servo motors are commonly used for RC vehicles and flying objects of any type, they are available in a wide range of size and performance data. The rotatory range of motion is usually 90-180°, and the protocol of the input control signal is consistent. Among the multitude of motors, the RC-servo motor DS 3781 from Graupner was chosen as the most suitable one. The performance data for the servo motor,

Table 3.2: Performance data of the RC-servo motor DS 3781

Type	Graupner DS 3781
Supply voltage	4.8 – 6 V
Max. current	890 mA
Operating range	90°(±45°)
Torque	18 Ncm
Stall torque	47 Ncm
Operating speed	0.05 s/40° (no load)
Dimensions	33 × 15 × 26.5 mm
Weight	28 g

listed in Tab. 3.2, are related to the maximum supply voltage of 6 V. Further features of the servo motor are the high precision digital controller and the double ball bearing-mounted metal gear. To actuate all four pins independently in two directions, eight RC-servo motors are needed.

Custom-made parts are necessary for the pins of the display. As mentioned above, the basic idea is to connect the lower end of each pin to a base plate using a universal joint. With sufficient pin length, movement of the pin tip in z direction is negligible for small excursions, such that the pin tip moves only in x and y direction. However, this requires a pin length of several 10 mm, in order to constrain motion in z -direction below the desired specifications. Given the pin's circular cross section area with a diameter of 1 mm, this is not possible, because such a thin and long pole would not have the necessary stiffness to resist bending. The chosen solution is to mount a shorter pin on top of a long base rod with larger cross section, which then is connected to the base plate. The left side of Fig. 3.2 shows the design of one pin mounted on its base rod. In this way, the essential pin length can be reduced to 10 mm, thus the pin bending is reduced to an insignificant amount.

The base rod also provides an easy possibility to attach the control rods that actuate the pin. The right side of Fig. 3.2 shows the top view on the full arrangement of all four pins with their steering rods. Here, it becomes evident why it is essential to place the pins on the inside edge of the prismatic base rods: It allows adjacent quadratic pin workspaces of 2 mm² per pin, regarding the x, y -plane.

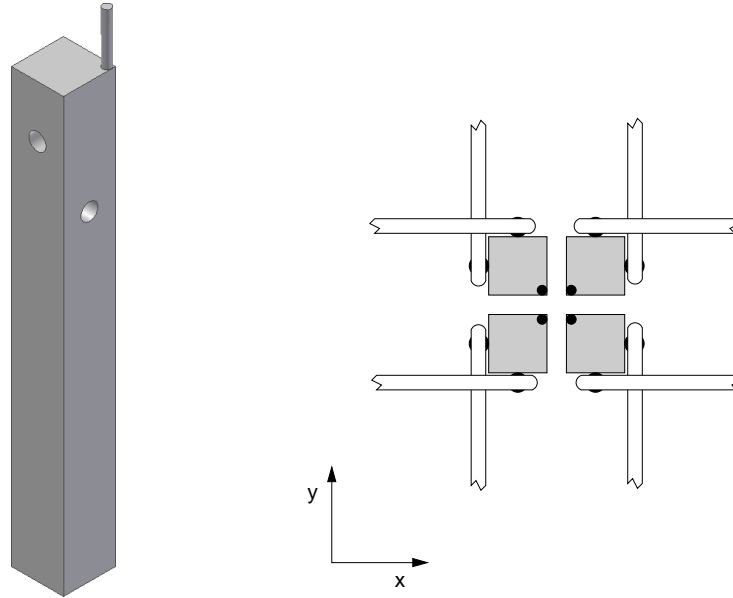


Figure 3.2: Realization of one pin on top of a base rod with fixation points for the steering rods; top view of the arrangement of the four pins with base and control rods.

The mechanical parts of the display are predominantly manufactured from aluminum. This simplifies the mechanical processing and keeps the device lightweight. All custom-made mechanical parts were fabricated at the institute’s workshop.

The proposed gimbal-mounting of the pins is realized by universal-joint shafts. These are available in the needed size from a standard retailer for mechanical components. To connect the control linkage between the lever of the servo-motors and the base rod of the pin, linkage rods with ball joints were used. Also here, easily available standard components are used. The chosen ball joints exhibit nearly no backlash on reversal movement, and they have very low friction.

Kinematics

The dimensions of design components, like pin rod or transmission levers, mostly depend on the desired pin movement and on the kinematics of the used actuators and.

The selected servo motors provide a rotation in an angle range of $\pm 45^\circ$. A system of lever and steering rods transforms the rotation of the servo motor to a translatory movement of the pin tips. Fig. 3.3 describes the kinematic chains between servo motors and the pin tips. The revolute joints are displayed as circles; the filled circles show joints with fixed axes. The left and right figure describe the kinematic chain for actuating the x - and y -axis, respectively. In both cases, the rotation point of the servo motor is located in point A . The first lever \overline{AB} transmits the rotation to a quasi-longitudinal motion of the steering rod \overline{BC} . After the reduction lever \overline{CE} , mounted at point B , a further rod \overline{EF} tilts the pin \overline{GH} along the corresponding axis, which causes a spherical movement of the pin tip. The displayed configuration is the zero-position state of pins and servo motors. The levers at the servo-motors are specified to $l_1 = 6 \text{ mm}$. Assuming a motion range of the servo-motors of $\alpha = \pm 45^\circ$, the horizontal displacement of point B can be calculated to:

$$\Delta x_B = \Delta y_B = l_1 \sin(\alpha) = \pm 4.247 \text{ mm} \quad (3.1)$$

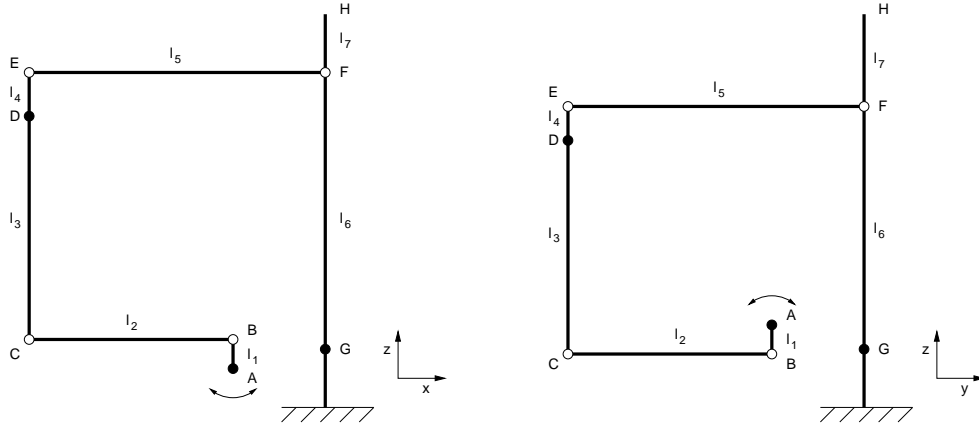


Figure 3.3: Kinematic actuation chain for the x -axis (left) and y -axis (right) of one pin.

Considering the additional lever transmission ratio on the lever \overline{GH} and the demand of $\Delta x_H = \Delta y_H = \pm 1$ mm horizontal pin tip movement in point H , the overall horizontal reduction ratio between point B and H can be calculated to:

$$n_{BH} = \frac{\Delta x_H}{\Delta x_B} = \frac{\Delta y_H}{\Delta y_B} = \frac{l_4}{l_3} \frac{(l_6 + l_7)}{l_6} = 0.235 \quad (3.2)$$

The lengths $l_2, l_{CE} = (l_3 + l_4), l_5, l_6, l_7$ are given due to constraints of the mechanical design, thus only the lengths l_3 and l_4 can be chosen freely. By using the reduction ratio (3.2), they can be calculated by:

$$l_3 = \frac{l_{CE} (l_6 + l_7)}{l_6 (n_{BH} + 1) + l_7}, \quad l_4 = l_{CE} - l_3 \quad (3.3)$$

Thereby, the lengths l_3 and l_4 must be calculated for the current axis.

Table 3.3: Dimensions of the kinematic chain

Length	x -axis	y -axis
l_1	6 mm	6 mm
l_2	42 mm	42 mm
l_3	46.5 mm	44 mm
l_4	9 mm	7.5 mm
l_5	61 mm	61 mm
l_6	57 mm	50 mm
l_7	12 mm	19 mm

In Tab. 3.3, the resultant dimensions of the kinematic chain in both axes are summarized.

Due to the fact that the pins pivot at their base point, the pin tips essentially describe a spherical motion. As a consequence, the tips move also in z -direction. The high pin length constrains this deviation in z -direction to a tolerable amount of $7.25 \mu\text{m}$. A similar deviation of the pin position occurs in the x, y -plane, caused by the steering poles. At one end, their motion is constrained to either the x -axis or to the y -axis. At the other end, their motion is constrained to the z -axis. In combination, this constrains the motion at the pin-connection to the x, y -plane, more specifically to a spherical motion within the x, y -plane. The resulting position deviation has the same amount for each axis and can be calculated to $8.2 \mu\text{m}$. These values are beyond the perceptual limit, as discussed in Sec. 1.2.

The positioning resolution of the pin movement is constrained by the actuator type and its control. Driving the entire 2 mm pin movement of one axis by a linearly scaled PWM-signal (*pulse wide modulation*) that is at last quantized by 8-bit, an achievable positioning resolution of $7.81 \mu\text{m}$ per bit can be achieved. Therefore, the above mentioned mechanical deviations are in the range of ± 1 bit and can be neglected.

Larger deviations are caused by the transmission of the rotatory motion of the servo-motor to the final linear motion of the pin tips. The largest deflection thereby occurs at the transmission in point B , caused by the large rotatory range (90°) of the servo motor. By introducing the angles α at pivot-point A , β at pivot-point D , and γ at pivot-point G , the kinematics can be described by the following equations:

$$\begin{aligned} (l_{2,x} - l_{1,x}\sin(\alpha_x) + l_{3,x}\sin(\beta_x))^2 + (l_{1,x}(\cos(\alpha_x) - 1) + l_{3,x}(\cos(\beta_x) - 1))^2 &= 0 \\ (l_{5,x} - l_{4,x}\sin(\beta_x) + l_{6,x}\sin(\gamma_x))^2 + (l_{4,x}(1 - \cos(\beta_x)) + l_{6,x}(\cos(\gamma_x) - 1))^2 &= 0 \\ \tilde{x}_H &= (l_{6,x} + l_{5,x})\sin(\gamma_x) \end{aligned} \quad (3.4)$$

$$\begin{aligned} (l_{2,y} - l_{1,y}\sin(\alpha_y) + l_{3,y}\sin(\beta_y))^2 + (l_{1,y}(1 - \cos(\alpha_y)) + l_{3,y}(\cos(\beta_y) - 1))^2 &= 0 \\ (l_{5,y} - l_{4,y}\sin(\beta_y) + l_{6,y}\sin(\gamma_y))^2 + (l_{4,y}(1 - \cos(\beta_y)) + l_{6,y}(\cos(\gamma_y) - 1))^2 &= 0 \\ \tilde{y}_H &= (l_{6,y} + l_{5,y})\sin(\gamma_y) \end{aligned} \quad (3.5)$$

Caused by the different configuration of the lever l_1 of the servo motor, the kinematic equations for the x -chain (3.4) and the y -chain (3.5) differ in the second implicit equation. Fig. 3.4 shows the deviation of the pin position related to the angle of the servo motor within its working range of $\pm 45^\circ$. Caused by the differing dimensions of the kinematic chain, the deviations in $(\tilde{x}_H - x_H)$ (solid line) and $(\tilde{y}_H - y_H)$ (dotted line) direction are slightly different. Both deviations are larger than the position resolution of the servo-motors, so they can not be neglected. However, as the deviation can be determined uniquely as a nonlinear function of the desired position, it can be compensated by an according lookup table.

Prototype Setup

According to the design specification and to the kinematic calculations above, a prototype of the pin-based Shear-Force Display was built. The custom-made parts were manufactured from aluminum standard components, i.e. from plates and profiled rods. Fig. 3.5 shows the mechanical details of the display such as the pin bodies, the control rods, and the servo motors. Fig. 3.6 shows the display in use with a close-up view of the pin area, which is in contact with the finger tip through a hole in the cover plate.

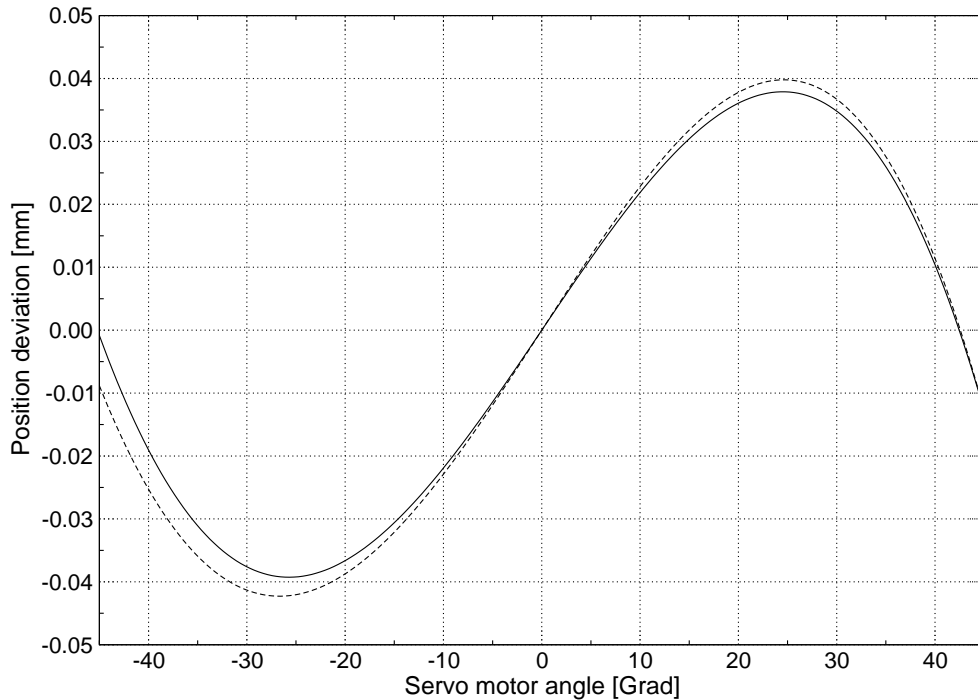


Figure 3.4: Position error in dependence of the servo motor lever angle

Computer Interface

The Shear-Force Display is controlled using a personal computer. The control interface consists of a hardware- and a software part. Fig. 3.7 shows the modules of the entire interface. The main task of the computer interface is to generate PWM-signals that contain position information for the servo motors. The timing of the PWM-signal is shown in Fig. 3.8. Each pulse starts with an initialization part ($t_1 - t_0$) of 1 ms. The remaining part of the pulse ($t_2 - t_1$) has a length of 0–1 ms and it contains the desired position information for the servo motor. Thus, the rotation range of the servo, which is ($0^\circ - 90^\circ$), maps to the pulse width range of 1–2 ms. The standard repeating time of the pulse sequences ($t_3 - t_0$) is 20 ms. The specifications of the servo motors, however, allow also pulse repeating times down to 10 ms. This enhances the performance of the servo motors and allows an update frequency of the position information of up to 100 Hz.

The driver module that realizes this timing for all eight servo motors is written in C, and it runs as a real-time thread on a RTLinux operating system. It generates the PWM-signals for all eight servo motors at an update frequency of 100 Hz in parallel, according to the position information received from any other application program via a defined fifo-buffer. This buffer has a length of 8 Byte, one Byte for each servo-motor position. Thus, the angular position range of one servo motor has a resolution of 8 bit. This results in a quantization of 0.352° . The driver module converts the input value linearly to the PWM-signal for the angular position of the servo motors. Therefore, the position correction, shown in Fig. 3.4, has to be calculated in the application program. An additional ring counter is implemented, which is triggered after each PWM-sequence. This counter can be polled from the driver-module via fifo-buffer, to synchronize the application.

The signals are directly routed to the eight data lines (pin 2 - pin 9 at printer connector) at the centronics printer port of the computer. Fig. 3.9 shows the wiring of the connecting

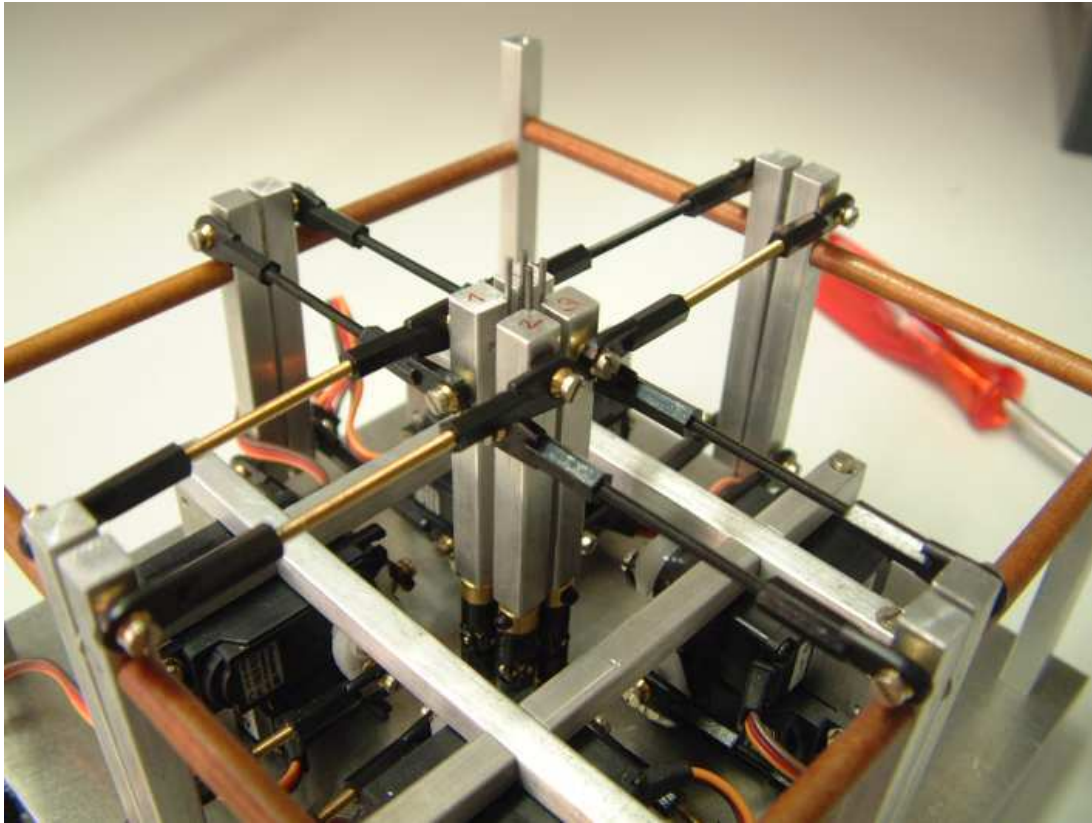


Figure 3.5: Mechanical details of the prototype setup.

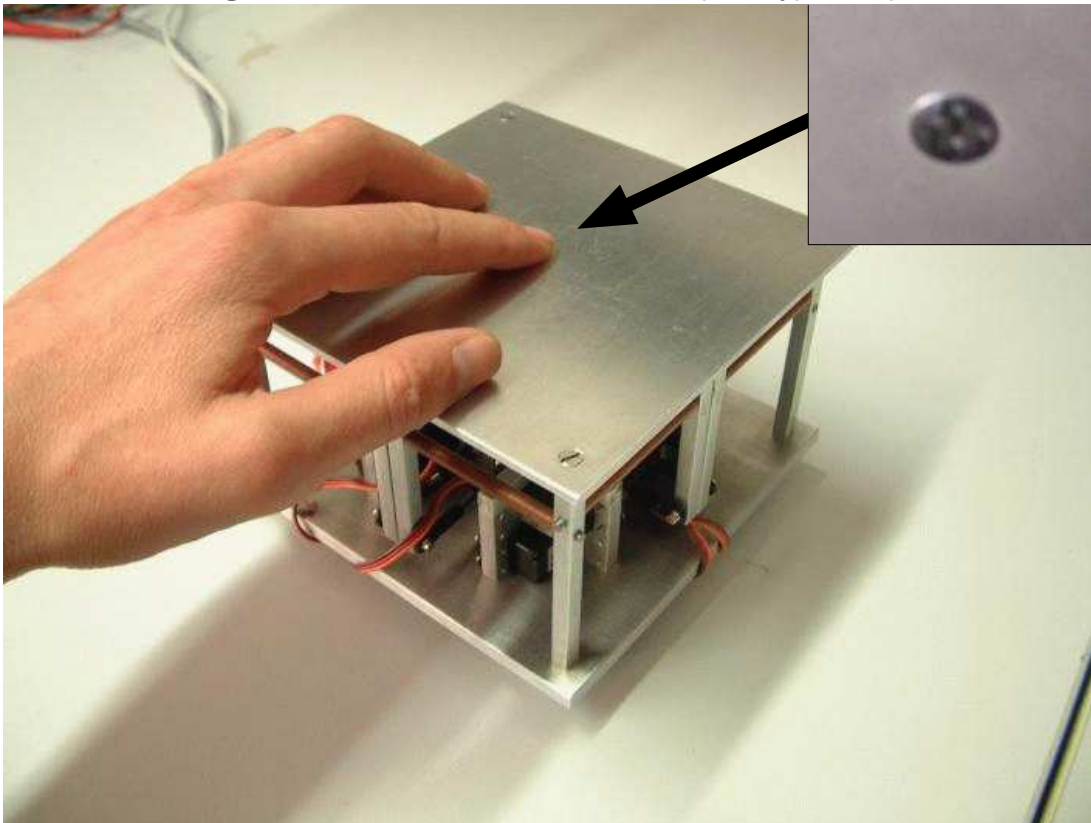


Figure 3.6: Hardware setup of the pin-based Shear-Force Display

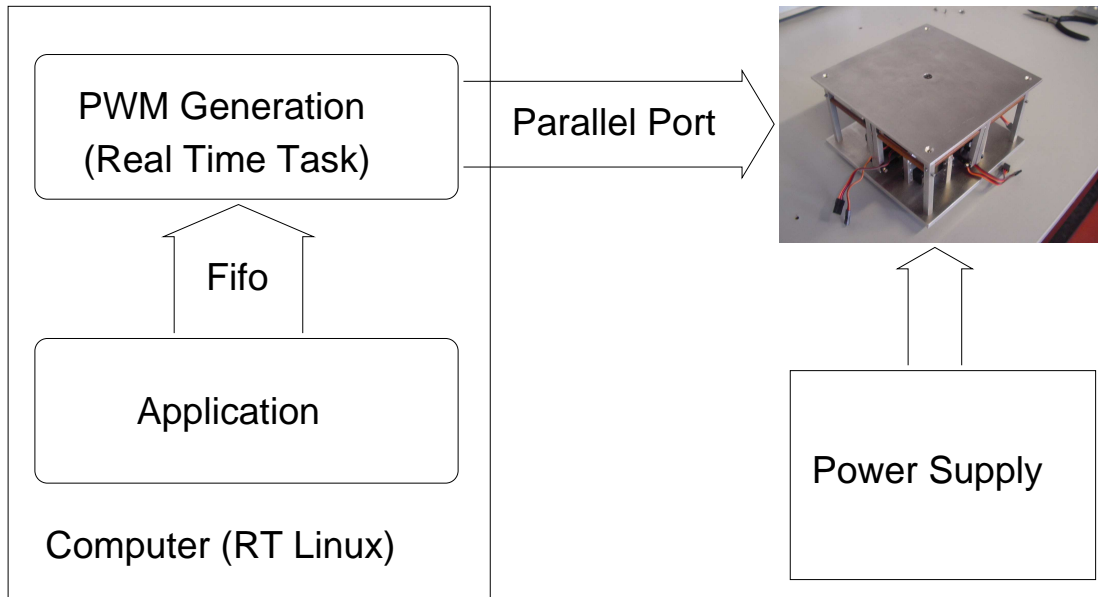


Figure 3.7: Structure of the computer interface.

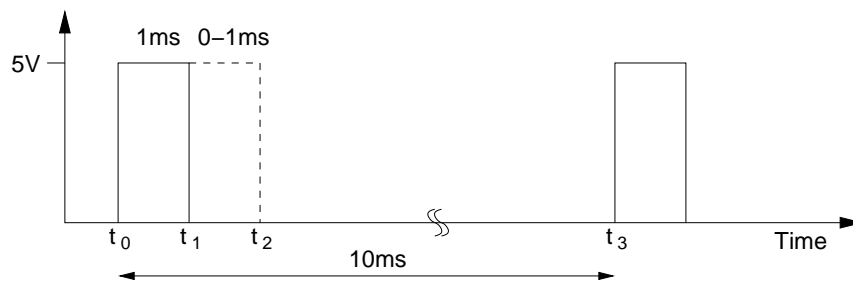


Figure 3.8: Composition of the PWM-signal

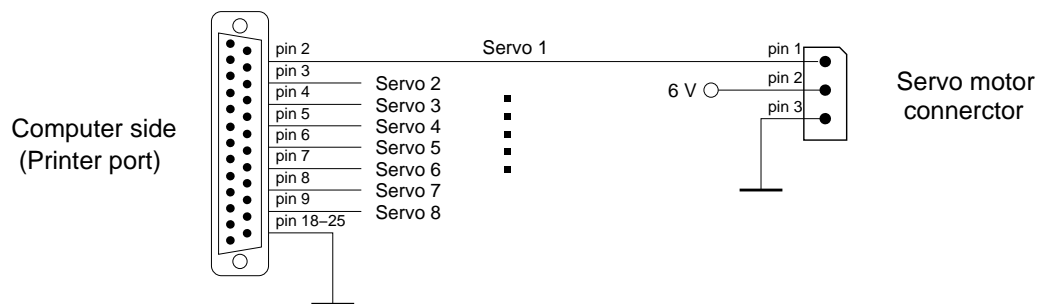


Figure 3.9: Connecting cable

cable between the printer port and the three-pin connectors of the servo-motors. As the data-lines of the centronics interface have a signal level of 5 V, they can directly be connected to the signal input of the servo-motors (pin 1 at servo-motor connector), which operates at the same signal level. To enhance the quality of the signal and to protect the centronics interface, it is recommended to implement some additional TTL line-drivers (e.g. SN 74 LS 07) or actually some optoelectronic coupler. In this setup we used TTL line-drivers. An additional power supply providing the 6 V operating voltage (pin 2 at servo-motor connectors) is necessary to ensure the desired performance of the servo-motors.

Technical Data

Table 3.4 summarizes the technical data of the tactile Shear Force Display.

Table 3.4: Technical data of the Shear-Force Display.

Property	Value
Pin excursion (lateral)	± 1 mm (per axis)
Position quantization	8 bit (256 Steps)
Positioning resolution	7.8 μ m
Max. pin force (per axis)	4.23 N
Max. pin velocity	22.8 mm/s
Pin workspace	2 \times 2 mm
Size	150 \times 150 \times 90 mm
Weight	1100 g

3.1.3 Evaluation Experiment

The first experiments performed with the Shear-Force Display address basic psychophysical questions. They were conducted in collaboration with the Max Planck Institute for Biological Cybernetics in Tübingen. A key question was whether the stimuli produced by the Shear-Force Display are appropriate for human perception, which is directly related to the usability of the Shear-Force Display for further investigations. The presentation here focuses on the results relevant to this question. The complete experiments, including detailed discussions, are presented in [44].

In Experiment 1, the discrimination performance for different directions of single-pin movement was studied. To our knowledge, there is just a single study on human direction discrimination on the finger tip [105]. In Experiment 2, the integration of parallel movement of multiple pins was studied. From well-established theories on sensory integration in humans, we expected that discrimination performance should profit from multi- as compared to single-pin stimuli - at least if the brain processes movements displayed by the single pins independently from another [46].

Experiment 1

Methods. 14 right-handed participants (9 females, age range 21 to 40 years, average age 26) took part for pay. None of them had any known tactile deficit.

The participants sat in a quiet room in front of a table with their left elbow resting comfortably on a custom-made support. By using robust tape, their left hand was attached to the Shear-Force Display in a way that the tip of their left index finger was reliably centered on the midpoint of the pin display. We used the Shear-Force Display with a single pin only (for this experiment the other three pins were removed) and a particular modified base plate (Fig. 3.10 right, upper) that allowed for individual adaptation of gap size and,

thus, maximal spread of skin stretch. A blind prevented participants from seeing the display, and white noise displayed via headphones masked the sounds of the display during pin movement. A custom-made program on a PC controlled the stimulus presentation and collected the responses, using a basic input device (switch).

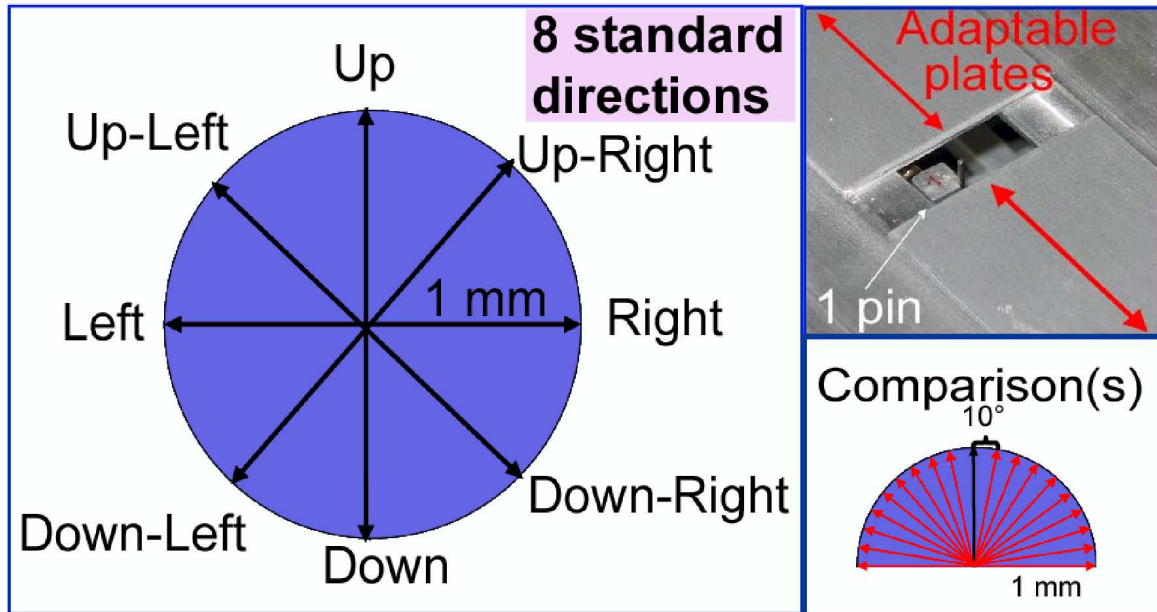


Figure 3.10: Setup in Experiment 1.

Tactile stimuli were unidirectional single strokes of 1 mm length (velocity 1 cm/s) starting at the midpoint of the display. For the strokes, we defined eight standard directions with respect to the finger (separated by 45° , Fig. 3.10 left). For each standard stroke, a set of 19 comparison strokes was chosen, the directions of which were distributed in 10° steps around the corresponding standard within an area of $\pm 90^\circ$ (Fig. 3.10 right, lower). In each single trial, the participants successively felt a standard and a comparison stroke and then had to decide by a button press which of the two strokes had been oriented more in clock-wise direction. Between the strokes, participants had to lift their finger to allow for moving the pin back to the midpoint without evoking tactile stimulation. Required finger movements were signaled by different sounds on the headphones.

Each pair of standard and comparison stroke was presented twelve times during the experiment. The order of standard and comparison was balanced across repetitions, and the order of pairs was completely random. For each individual participant, the experiment lasted about four hours, performed within two sessions (including three breaks) on different days.

Using the *psignifit* toolbox for Matlab [211, 212], we fitted individual psychometric functions (cumulative Gaussians; Maximum Likelihood procedure) to the proportion of trials in which the comparison stroke was perceived as more clockwise-oriented than the standard stroke, plotted against the comparison direction. From the fits, we obtained individual 84%-discrimination thresholds per standard.

Results and Discussion. After the experiment, all participants reported that they had felt pin translation and most that they had also perceived skin stretch. Figure 3.11

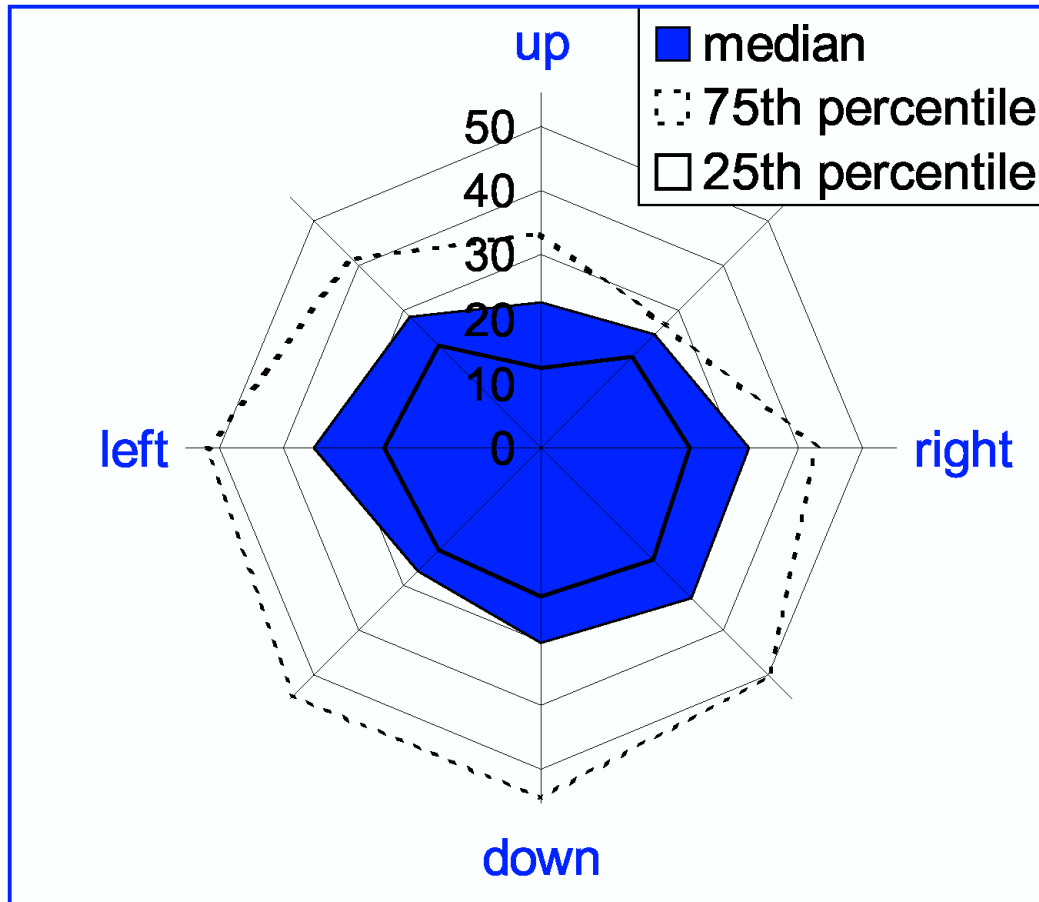


Figure 3.11: Medians and quartiles of 84%-thresholds by standard direction.

depicts medians and quartiles of the individual discrimination thresholds by standard direction. Median thresholds ranged from 23° to 35° , thresholds quartiles ranged from a maximal 75%-percentile of 54° down to a minimal 25%-percentile of 12° . Further, the individual thresholds per standard direction were subjected to a Friedman test [51, 52]. The test reached significance, $\chi^2(7) = 20.7, p < .01$, indicating a perceptual anisotropy, i.e., participants discriminated better between movements in up-direction as compared to the other directions.

Most importantly here, threshold magnitudes demonstrate that humans can well discriminate the directions of the movements displayed. It is also important to note that the technical directional resolution of the shear-force device clearly exceeds the perceptual thresholds we observed. Thus, the Shear-Force Display produces tactile stimuli that are appropriate for human perception, and shear forces seem to be usable to obtain a differentiated impression of at least one environmental aspect. Consequently, the next experiment explored to which extent shear forces displayed by more than one pin are integrated in perception.

Experiment 2

Methods. Twelve paid right-handed participants without known tactile deficits took part in Experiment 2 (6 females, age range 19 to 40 years, average age 27). The same setup, procedure and stimuli as in Experiment 1 were used. However, just two standard directions were included (up and down, with respect to the finger), and 19 corresponding comparison directions. Directions were displayed either with one, two or four pins. The

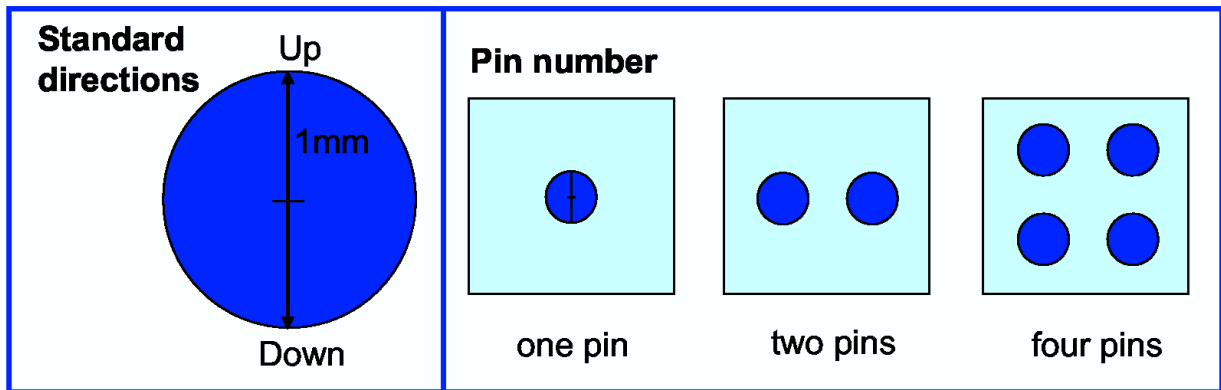


Figure 3.12: Setup in Experiment 2.

other pins were removed (see Fig. 3.12 for directions and pin configuration). In the multi-pin conditions, all pins moved simultaneously and with identical velocity and direction; the pins were separated by 3 mm (center-to-center). Trials with one, two or four pins were performed in three sessions spread over different days. The order of sessions was balanced between participants according to a Latin square design [15]. The whole experiment lasted about three hours.

Results and Discussion. Fig. 3.13 depicts medians and quartiles of the individual discrimination thresholds by standard direction and pin number. Median thresholds ranged from 19° to 23° , threshold quartiles ranged from a maximal 75%-percentile of 33° down to a minimal 25%-percentile of 16° . The individual thresholds per standard direction and pin number were subjected to a Friedman test. The test clearly failed to reach significance, $\chi^2(5) = 6.7$, $p > .20$, indicating that the participants' discrimination performance depended neither on movement direction nor on the number of pins.

In general, the magnitude of discrimination thresholds in Experiment 2 confirmed that humans well discriminate between the directions of the movements displayed and that the perceptual resolution did not exceed the technical resolution. Thresholds in this experiment tended to be slightly lower than in Experiment 1. However, given that there were substantially less different standard directions compared to the last experiment, memory effects may have played a role. Surprisingly, we were not able to replicate the advantage of up-directions observed in Experiment 1.

Most importantly, we did not find any effect of pin number on discrimination performance. Well-established models on human signal processing state that the human brain integrates independent redundant signals on the same physical property to a combined estimate, which is more reliable than the single signals [46]. The lack of an integration

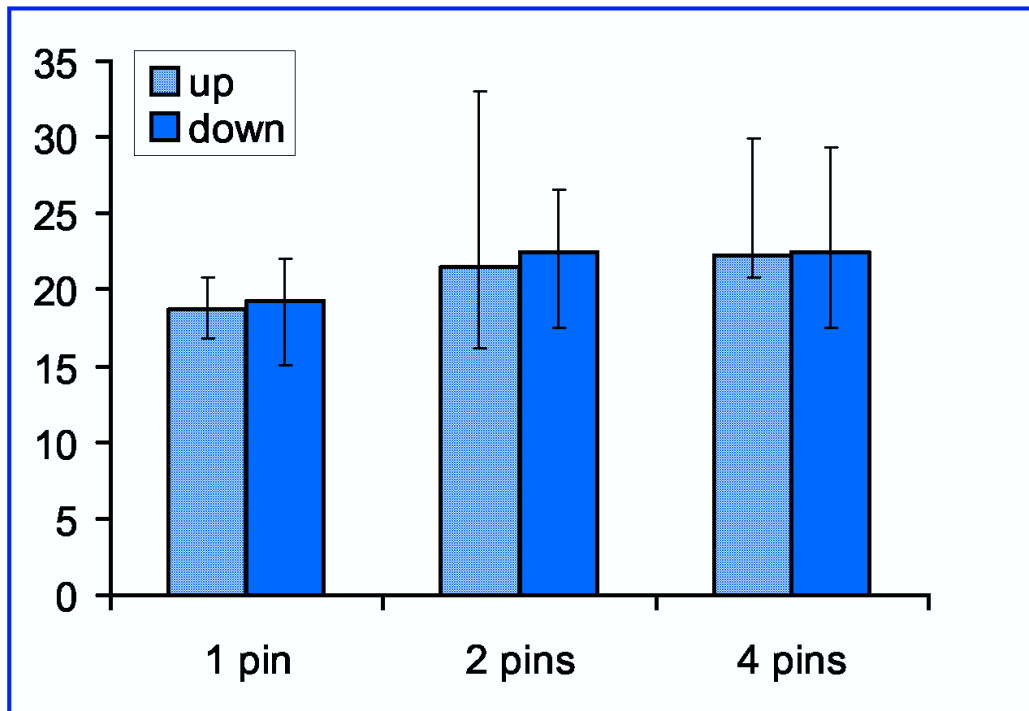


Figure 3.13: Medians and quartiles of 84% -thresholds by standard direction and pin number.

benefit in the present study may indicate that the movements of the different pins of the shear force device were not independently processed in the perceptual system.

3.2 Slip-Friction Display

In this Section, the second type of lateral force display is presented. Unlike the stimulation of partial regions of the fingertip, as targeted by the Shear-Force Display or by normal force devices, the display described in the following is made predominantly to display skin stretch as a cause of friction to the entire surface of a fingertip.

An equivalent sensation for this stimulation in the real world would be active sliding of the entire fingertip across a surface. During this action, two general physical effects can be observed: Initially, a shear force is generated between the finger and the surface, which causes deformation of the fingertip tissue. As soon as the shear forces between the finger and the surface overcome static friction, the situation will switch to a slip motion, which is physically governed by slip friction. Experimental investigations on this topic can be found in [120].

The basic idea of the display is based on a rotating object beneath the fingertip, which could be a ball or a drum. To realize a great range of imaginable sliding scenarios, the rotating medium of choice will be a ball, driven by two motors that can be operated at precisely controlled speeds. The motors are arranged orthogonal to each other, to allow a Cartesian movement of the ball. The only movement that cannot be reached at the contact area in this configuration is pure rotation about the vertical axis.

Based on a survey of similar existing displays and additional demands, the concept of the display will be outlined in the following section. First, required specifications are stated, which are derived from perceptual characteristics of the tactile perception in the skin in the area of the index fingertip. Sec. 3.2.2 describes the choice of components and the hardware setup.

3.2.1 Concept and Specification

Existing concepts of sphere-based slip friction displays are either based on rotating drums [172] or spherical objects [105, 171, 207]. Using such a sphere-based display, Webster *et al.* [207] pointed out the significance of slip for human force modulation during a delicate manipulation task. Within their experiment, the user had to slide a virtually displayed sheet of paper across a table to a target position. The subject had to modulate the normal contact force accurately, in order to make the paper follow the movement of his finger and thus place it to a defined target. The result was that if slip sensation was additionally provided, the subject's performance in modulating the normal force increased significantly.

Derived from the general idea of providing a spatial stimulus of slip force caused by lateral friction beneath the index fingertip, we decided to realize the display by using a ball-based design. In contrast to existing sphere-based slip force displays, the interest was not only in high-fidelity, but also in compactness and lightweight design, in view of further use in serial combination with the kinesthetic display ViSHARD 10. In this combination, as described in the following chapter, we wanted to validate previous psychophysical findings concerning the perception of superposed tactile and kinesthetic stimuli. More specifically, we were interested in a quantification of the effect of tactile suppression in different configurations.

Previous psychophysical investigations with drum- or sphere-based devices have revealed essential characteristics of human perception: In [171], two experiments were conducted using highly sophisticated custom-made hardware. The first experiment aimed at determining the JND in speed and direction of the perception of slip on two different surface textures. In the second experiment, the relative importance of kinesthetic feedback versus slip feedback in perceiving surface velocity was investigated.

A display similar to the one we realized was used in [105]. It consists of a ball driven by two servo motors, and it provides slip forces in both lateral axes to the fingertip of the index finger. This setup has been used to determine the JND of the tactile perception regarding direction sensitivity to a tactile point stimulus that strikes across the index finger pad. However, since this display was designed to be mounted on the end-effector of the comparably small kinesthetic force feedback device PHANToM, the ball had only about half the diameter of the devices mentioned above. To determine appropriate dimensions for the ball diameter of our display, specifications about the maximum curvature of spherical objects to be still perceived as flat surfaces resulted useful. According to [172], the diameter of a rotating drum of 58.4 mm proved sufficient to create the illusion of a flat surface stimulus. In search of a commercially available ball of this size, we decided to use a billiard ball. The chosen white standard ball, usually used on pool billiard tables, has a diameter of 60.2 mm. The standard billiard ball is made of phenolic resin and comes with a polished glossy white surface, which is in general too smooth to be used in our experiments. As the surface is also too regular for the optical position measurement sensor, we made it rougher by sandblasting.

The ball is supported by an arrangement of ball bearings, and it is rotated by two servo motors.

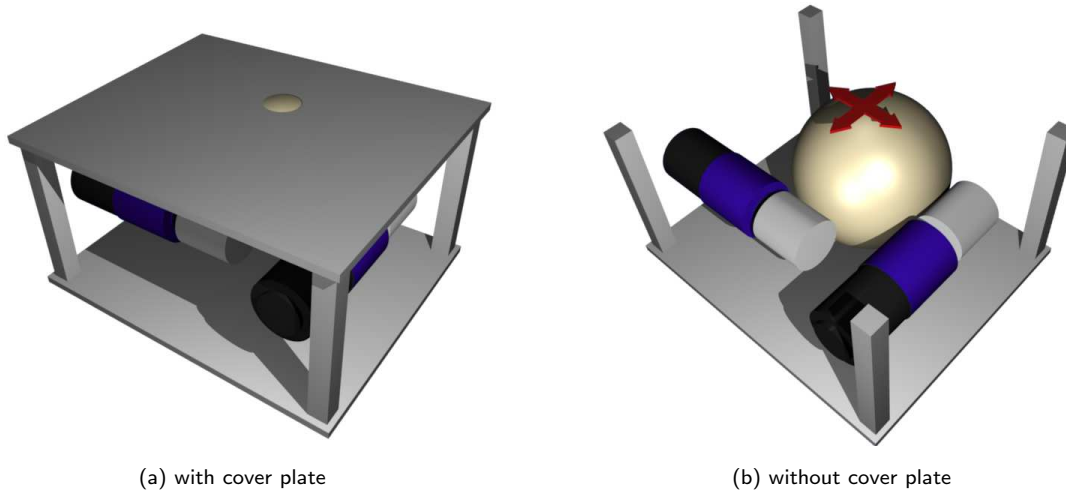


Figure 3.14: Design of the sphere-based tactile Slip-Friction Display

Fig. 3.14(a) shows the setup of the display. The hand of the user needs to be fixed relative to the device in such a way that the index finger is not mechanically constrained and that its tip touches the ball through an aperture in the cover plate. The dimensions are based on findings in [173], which indicate the optimal aperture size of the casing and the optimal distance between fingertip and the moving part of the device.

Fig. 3.14(b) provides a view into the inside of the display. Two servo motors are orthogonally arranged, each with a driving wheel attached to its output shaft. These wheels rotate the ball in the two lateral axes of motion, thus causing slip friction to the fingertip of the user. As a consequence of the orthogonal arrangement of the driving wheels, each of the two lateral axes can be actuated independently using only one motor. Using both motors in combination, any linear combination of the axes is possible. With this arrangement, a wide range of movements can be achieved. Only the rotation of the ball around its vertical axis (z -axis) is not possible, since the axes of the wheels are coplanar and placed at the ball's equator. However, in the intended experiments, this rotational motion can be performed by the supporting kinesthetic device.

The two servo motors used are small DC-motors with a power of 8.7 W each and a maximum speed of 7100 rpm. An attached reduction gear is used to lower the speed by a ratio of $I_1 = 14 : 1$ and to provide a maximum torque of 523 mNm at the output shaft connected to the driving wheels. The reduction gear combined with the ratio of $I_2 = 4.01 : 1$ between wheel diameter and ball diameter provides a theoretical maximum slip speed of 393 mm/s. The minimum slip speed is limited to 0.56 mm/s by the servo motor controller.

In the experiments, the display shall be mounted on the hyper-redundant kinesthetic display ViSHARD 10, therefore a compact and light-weight design is essential. With the chosen components as described above, we realized a display with a size of $150 \times 150 \times 150$ mm and a weight around 1.5 kg.

3.2.2 Hardware Setup

The central component of the display is the ball. Fig. 3.15 shows the hardware setup of

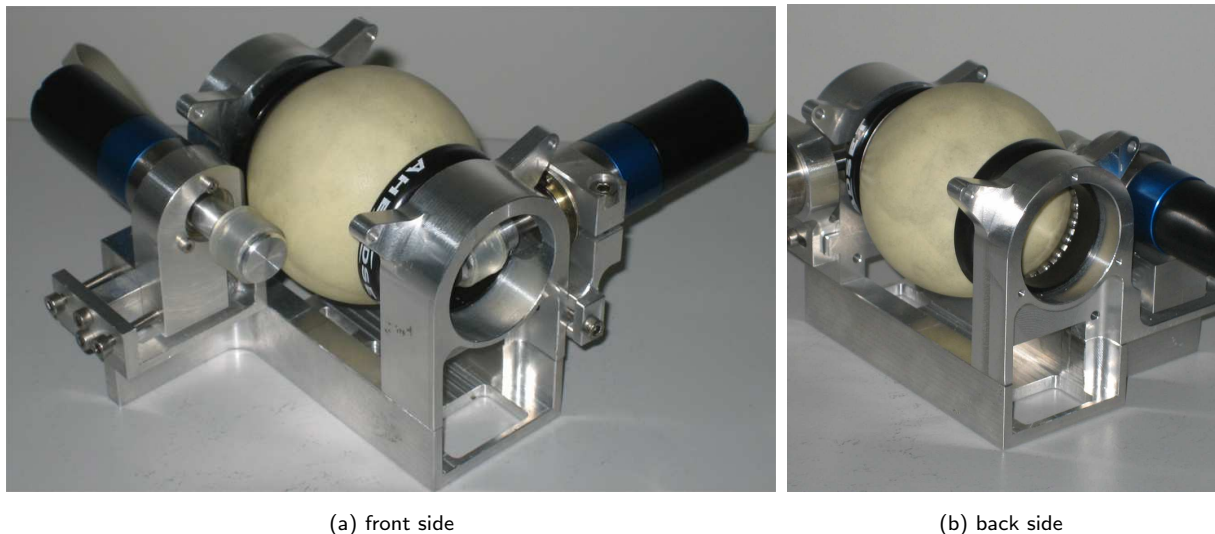


Figure 3.15: Hardware setup of the tactile Slip-Friction Display

the sphere-based tactile Slip Force Display. The front view displays the sandblasted billiard ball, which is embedded in the driving unit consisting of servo motors and friction gears. The back view shows the ball ring bearing mechanism of the billiard ball in detail.

Each motor driver module includes an internal closed-loop position/velocity control. It is accessed via a serial RS-232 connection from the operating PC. These driver modules ensure a tracking of the commanded reference position and velocity, and they transmit the measured position and motor current back to the PC.

One objective was to display a fixed flat surface texture that can be explored in a large workspace using tactile perception. To this aim, the current interface receives the position data from the kinesthetic display VISHARD 10 on which it is mounted, and it uses this information to control both motors that guide the ball beneath the finger of the operator.

This display aims to realistically display surfaces when a finger slides over them. Therefore, an isolated evaluation of this display is not meaningful, and movement of the hand needs to be enabled. The corresponding experimental setup with VISHARD 10 will be described in the next chapter.

3.3 Conclusion

This chapter was dedicated to the investigation of a human sensory modality that has not been investigated much so far: Tactile perception caused by skin stretch. Two devices were realized, each dedicated to a key question: A pin-based display was realized to study isolated effect of skin stretch, and a sphere-based display was realized to study the influence of accompanying friction effects that occur when sliding along a surface. Both displays were designed in a compact manner, in consideration of the ability to later combine them with a kinesthetic display.

A series of experiments with the pin-based display allowed to explore the spatial resolution of lateral skin stretch, and also the influence of the number of pins. Both experiments demonstrated that humans can well discriminate between the shear forces displayed, and also that their perceptual resolution does not exceed the technical resolution of the device. Future device development can take advantage of these facts and pursue less challenging specifications.

A first experiment with a single pin revealed that humans can discriminate direction of skin stretch well. Surprisingly, a second experiment with a pin matrix array showed that the number of pins has no influence on human discrimination performance, at least concerning movement direction. Based on the knowledge that sensory integration of multiple information channels improves performance [46], this finding suggests that the perceptual system processed the movement of the individual pins as one single combined stimulus.

Future investigations with the present prototype could explore to what degree non-simultaneous, differential multi-pin patterns of movement evoke discriminable percepts. To allow in-depth investigations, new devices to produce shear force could include mechanisms that allow for an increased pin distance.

The second display provides two-dimensional slip friction relative to the surface of the fingertip. In contrast to the pin-based display, which aims to investigate isolated effects of skin stretch, this display aims to produce a realistic haptic experience when a finger slides along a virtual surface. As such an exploration requires movement of the hand in space, an experimental evaluation is only meaningful when the display is combined with a kinesthetic display that allows this movement. This combined setup will be presented in the next chapter.

A possible improvement to the current prototype of the Slip-Friction Display concerns position sensing. Currently, the system relies on position information from the kinesthetic base display. To reach a more accurate measurement of the displayed virtual surface, an additional optical position sensor could be integrated. For this, off-the-shelf components from optical mouse systems could be used. The sensor could be placed beneath the ball, opposing the user's fingertip, thus the measured position could easily be mapped to the position of the virtual surface. Those sensors usually have a minimum resolution of 300 dpi, which would map to the sufficiently precise position resolution of 0.085 mm.

4 Integrated Kinesthetic and Tactile Stimulation

The displays that have been discussed in the previous chapters are all tactile displays. Their main focus is the direct stimulation of the human skin. However, as stated in Chap. 1, the human haptic perception comprises the tactile and kinesthetic sense. Simple observations made in everyday life, for example when grasping an object, show that the stimulation of the tactile and kinesthetic perception is often merged to a general haptic experience. For an enhanced psychophysical investigation, as well as for a more realistic presentation of an extensive (complex) haptic impression, simultaneous stimulation of the tactile and the kinesthetic modality is essential [108].

In the practical realization of haptic displays, mostly isolated devices for the kinesthetic or tactile modality have been developed. Also most basic research studies on human haptic perception investigate both modalities independently. Most known applications for haptic displays can indeed be divided into either purely kinesthetic or purely tactile applications, but there are applications where *complete* haptic displays would be needed. Complete haptic displays are definitely interesting for psychophysical experiments, in particular to investigate cross-modal effects between kinesthetic and haptic perception and movement.

In this chapter, a conceptual framework to combine kinesthetic and tactile systems is presented, which enables a great variety of haptic stimulation. The novel feature is the possibility to use several tactile displays, e.g. those that are described in the previous chapters, in combination with the same kinesthetic base display.

The flexibility of configuration will be a benefit for psychophysical investigations of cross-modality effects between the kinesthetic and tactile domain. One example is to investigate the quality of perception of several similar, but not equal tactile stimuli in combination with the same kinesthetic stimulus. Another possibility that will be emphasized are investigations in cross-modal phenomena, e.g. suppression effects that later on can be used for technical simplification.

After some basic design consideration, Sec. 4.1 contains a brief description of the kinesthetic and tactile hardware components that are used for the integrated system, as well as the system integration in terms of hardware realization and inter-module communication. To evaluate the integrated system, Sec. 4.2 describes a series of psychophysical experiments that address the quality of tactile perception in the context of simultaneous kinesthetic stimuli. These experiments prove the functionality of the developed framework and its usability as a toolchain for psychophysical investigations, and they allow some first insight into the phenomenon of tactile suppression.

The described conceptual framework has been previously presented in [57].

4.1 Combining Tactile and Kinesthetic Displays

There are only a few publications on combined tactile/kinesthetic approaches, such as [73, 74, 83]. The described systems combine custom-made tactile displays with a commercially available kinesthetic display (PHANToM) in a serial manner. As this kinesthetic display is not made for heavy loads at the end-effector, the tactile display design is very limited. The combined kinesthetic and tactile display described in [111] uses a five-bar parallel linkage in combination with a mouse-like tactile display. However, the linkage is limited to a small workspace with only 2 DOF *degrees of freedom*. There have also been attempts to combine kinesthetic with thermo-tactile stimulation [213].

In general, the most important drawbacks of previous combined display concepts are the restricted workspace of the kinesthetic interfaces and insufficient payload of the end-effector. This imposed narrow restrictions on the design of the tactile display.

In the following, a concept is proposed that is based on a powerful hardware solution for the kinesthetic part, allowing a combination with high-performance tactile displays that are mostly developed within this thesis. The first issue concerning the conceptual design of the combined display is its kinematic configuration. Afterwards, hardware components, hardware connection, and software interfacing will be described.

4.1.1 Link Configuration

From the perspective of the user, there are two different kinematic principles to combine two devices for kinesthetic and tactile stimulation: a serial or a parallel connection of the displays, as defined in [108]. Advantages and drawbacks of both configuration types will be discussed, followed by a novel design that combines major advantages of both and avoids their drawbacks for this particular application of haptic exploration.

Serial kinematic configuration

The most intuitive approach is to combine the two devices in a serial manner, which would mirror the human kinematic chain from shoulder to fingertip. In this configuration, the tactile display basically is mounted at the end-effector of the kinesthetic device, and the user is in contact only at the finger tip. Fig. 4.1 shows this configuration schematically during haptic interaction via fingertip.

External force and torque stimuli ($F_{ext.}$, $M_{ext.}$) to the operator can only be transferred at the finger-device contact point. Forces pointing in direction away from the finger, as well as torques can be provided if the finger tip is fixated to the device.

The main advantage of this configuration is that the most realistic interaction would be possible. The user would interact with virtual objects in the same way as he would interact with real-world objects. However, both the mechanical realization as well as control of this type of display is complicated. All kinesthetic forces would need to be transmitted through the tactile display, such that it needs to have sufficient structural stability and strong actuators. Furthermore, synchronization of kinesthetic and tactile stimuli requires sophisticated control of the resulting redundant structure. Insufficient stiffness or control performance of the kinesthetic device, which could e.g. result in force errors, can not be hidden easily from the sensitive receptors in the human fingertip. This means that the tactile display needs to fulfill two purposes: a) Suppress or compensate force and position

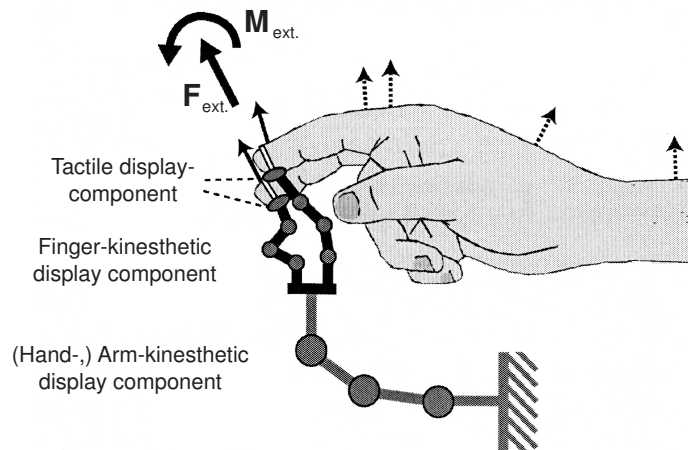


Figure 4.1: Serial kinematic approach; adapted from [108].

errors from the kinesthetic display, similar to a macro-mini approach[216], and b) render the desired tactile stimuli.

Parallel kinematic configuration

The parallel design of integrated haptic displays differs from the serial kinematic approach mainly in the number of force bindings to the operator's hand.

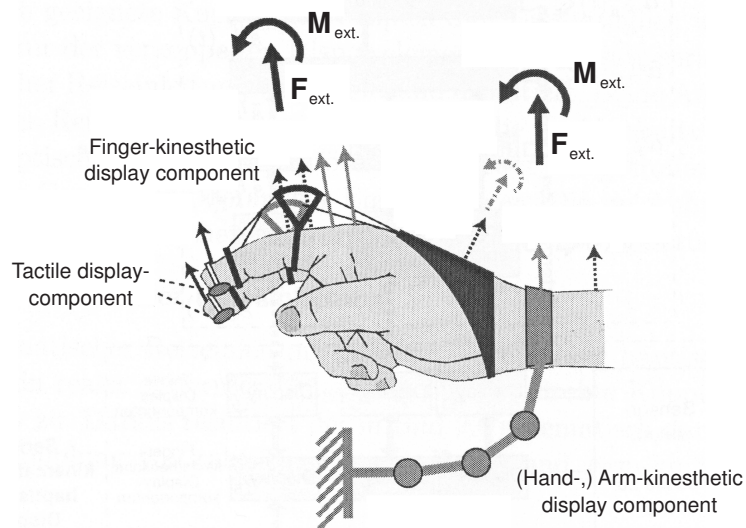


Figure 4.2: Parallel kinematic approach; adapted from [108].

Fig. 4.2 shows schematically an exemplary combined haptic display based on parallel arranged kinematics. In this case, the external kinesthetic stimuli in form of forces and torques ($F_{ext.}$, $M_{ext.}$) are conducted partly through the wrist and partly through the finger

limbs. An additional tactile display component is mounted separately at the fingertip and provides tactile stimuli.

The main advantage of this approach is a balanced imprinting of forces and torques according to the related human haptic abilities. This is particularly advantageous for the tactile display component in terms of rendering smooth tactile texture and shape information of the object surface. Another advantage of this architecture is that the kinesthetic and the tactile display components can be developed separately in a modular manner. The tactile device does not need to compensate for force nor position errors of the kinesthetic module, as they are decoupled.

A drawback of this approach are erroneous tactile stimuli due to the numerous kinesthetic force initiation points, e.g. at the wrist. Due to the properties of the human nervous system, this is not a serious drawback though: The density of mechanoreceptors in these regions is much lower compared to the sensitive human fingertip [28]. Therefore, tactile stimuli are perceived less strongly there. Instead, the perception of force at the arm is dominated by the muscle activations provoked by kinesthetic stimuli. A serious disadvantage of this design, however, is that the human needs to carry the weight of the tactile display. Furthermore, reaction forces/torques of the tactile stimuli are transferred to the human finger or hand as well, which could hamper the illusion.

Combining advantages of both

The goal is to combine the main advantages of serial and parallel connection: The user should not feel the weight of the tactile display, and yet the tactile display should be decoupled from the kinesthetic display to ensure maximal accuracy and precision of tactile stimuli. To enable such a device design, an additional property of human haptic exploration can be exploited: Bergamasco *et al.* [20] investigated which contact forces haptic devices would have to provide to the human arm and hand during general exploratory and manipulative procedures. For haptic exploration, he concluded from [112] that even if the hand moves relative to the object, the contact areas over finger and palm remain almost unchanged.

In the suggested solution, the tactile display is mounted on top of the kinesthetic device as in a serial connection. However, in contrast to a purely serial design, the user's wrist is strapped to the cover of the tactile display, which is rigidly connected to the kinesthetic display. Only one finger receives tactile stimuli, the other fingers may rest on the cover surface and are thereby connected to the kinesthetic display's end effector. When the wrist is strapped onto the surface, passive elastic joint moments in the fingers make it easy to stay connected to the cover with some pre-tension, without any muscle activation required.

In this special configuration, the kinesthetic display supports the weight of the tactile display, but it does not influence the relative motion between wrist and finger tip. Also forces between the kinesthetic display and the user are almost entirely transmitted via the large surface contact areas at wrist, palm, and the other fingers. Therefore, forces administered to the finger tip can be controlled by the tactile display in an independent manner.

Table 4.1: Specifications of ViSHaRD 10

Property	Value
workspace	cylinder $\varnothing 1.7 \text{ m} \times 0.6 \text{ m}$ 360° for each rotation
peak force	170 N
peak torque	pitch, yaw: 13 N m roll: 4.8 N m
translational velocity	> 1 m/s
maximum payload	7 kg
mass of moving parts	$\approx 24 \text{ kg}$

4.1.2 Kinesthetic Feedback: ViSHaRD 10

As hand/arm kinesthetic base display component for the integrated device, we designed the hyper-redundant kinesthetic display ViSHaRD 10 * [198], which provides spacious force feedback to the operator’s hand.

The driving motivation for the design is the vision of a general-purpose haptic interface that can be used in a large variety of application domains. Distinct advantages compared to existing solutions include an unlimited orientation workspace free of singularities; large translational workspace; human matched force capability; high payload capability and comparatively large mounting room to accommodate various (actuated) application specific end-effectors; redundancy to avoid user interference; dual-arm kinesthetic haptic interaction with full 6 DOF capability (again redundancy facilitates collision avoidance between the two arms). Fig. 4.3 shows ViSHaRD 10 mounted at the floor with a cylindric standard grip at the end-effector (another option is the ceiling assembly). Technical device specifications are summarized in Table 4.1. A detailed description of the mechatronic design is provided in [196, 197].

4.1.3 Tactile Feedback

Three tactile displays were used in the combined experiments: The first two, the Shear-Force Display and the Slip-Friction Display, have been presented in the previous chapters. The third display is the commercially available VirTouch mouse.

Tactile Shear-Force Display

The Shear-Force Display, as described in Sec. 3.1, has been used for a number of psychophysical experiments studying the angular spatial discrimination in the finger tip. This aspect of human perception has been assessed by inducing pin strokes in different directions [44]. These investigations also indicated that the technically realized accuracy in pin positioning is far superior to the requirements posed by human perceptual performance.

*Virtual Scenario Haptic Rendering Device with 10 DOF

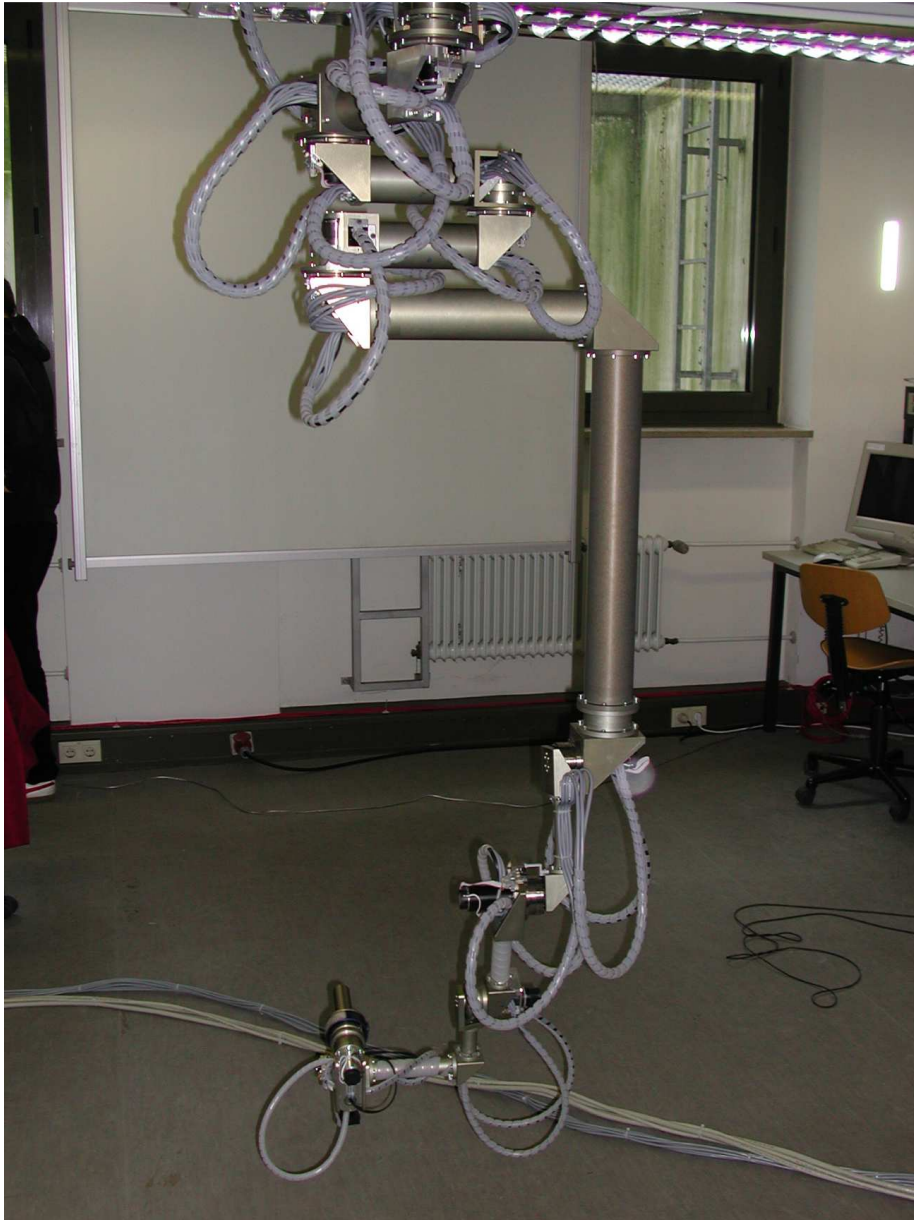


Figure 4.3: ViSHaRD 10 with standard end-effector.



Figure 4.4: VirTouch Mouse [124].

Tactile Slip-Friction Display

The design of the tactile Slip-Friction Display has been extensively described in Sec. 3.2. The display is based on a rotating ball that is in contact with the user's fingertip. Using two actuators, the ball can rotate around any axis in the horizontal plane. This rotation creates the illusion of sliding over a flat surface with the fingertip.

VirTouch Mouse

Due to its capability of displaying tactile normal force to the fingertip, the commercially available VirTouch Mouse is used. It contains three Braille generator modules for the index, the middle finger, and the ring finger of the operator's hand. The Braille generator modules are integrated in an enhanced computer mouse, connected to the serial port of an ordinary personal computer. Each Braille generator module consists of a dot matrix array in 4×8 configuration. Each of the 96 pins is movable independently in normal direction toward the skin of the operator's finger tip. The range of motion is 1 mm per pin, divided into 16 incremental steps.

Fig. 4.4 shows the VirTouch Mouse. The close-up view of the Braille module section illustrates the pin arrangement of the Braille units, inserted into the corresponding finger molds. The pins are driven by bending piezo actuators. The interface, as well as electrical drivers and power supply, is integrated and used as bought without any modifications.

4.1.4 Hardware Integration

The proposed concept envisages a serial connection between the kinesthetic base display, ViSHaRD 10, and the three tactile displays. These integrated systems take advantage of the good extensibility of the ViSHaRD 10 device, due to its high payload capability, large workspace, and the hyper-redundant joint design.

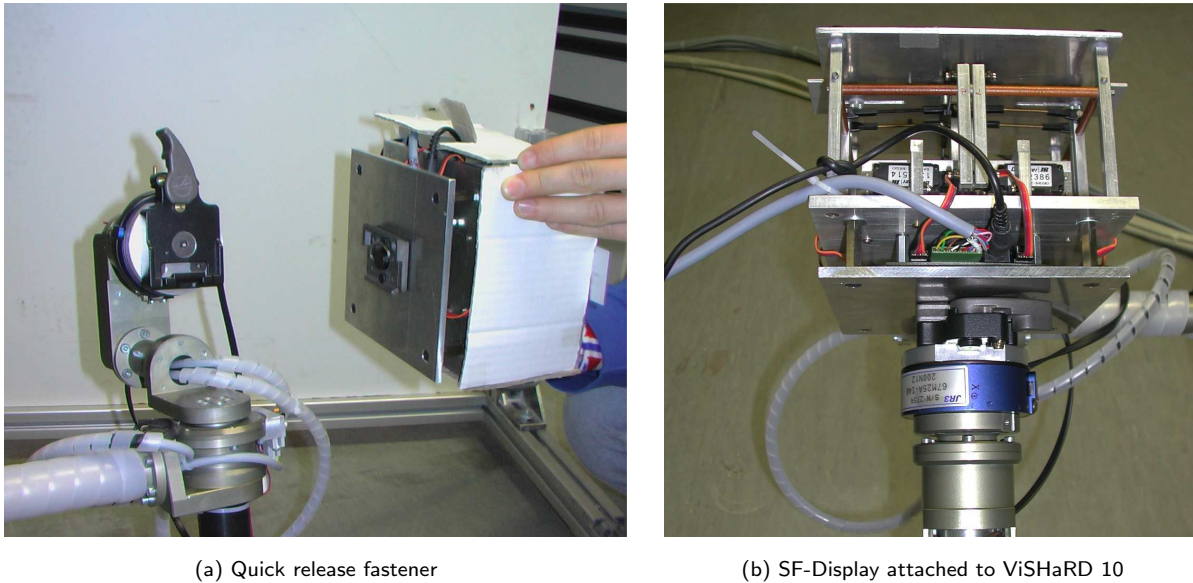


Figure 4.5: Mounting mechanism on ViSHaRD 10.

Each tactile display is mounted on ViSHaRD 10 via a quick-release fastener. Regarding the control and interface level, both devices are connected via standard LAN connections. This is realized by an enhanced UDP protocol, specialized for telepresence applications. In this manner, the modular concept is realized on the hardware as well as the control/interface level.

The end-effector of ViSHaRD 10 is connected to the fitting flange located at the upper end of the force/torque sensor. This sensor measures contact forces and torques caused by the interaction of the operator and the virtual environment, transmitted via the device. This connection is realized by a bolted joint, normally not designed for frequent changes of the end-effector. For using ViSHaRD 10 as kinesthetic base display for several additional attachable devices, dependent on the task to perform, we have implemented a quick-release fastener between the force/torque sensor and the additional device to facilitate the changing procedure of the end-effector or other mounted devices.

The left part of Fig. 4.5(a) shows the base plate of the quick-release fastener with release lever open, fixated on top of the force/torque sensor. In the right part of the picture, the counterpart of the fastener is shown, fixed to the bottom of the tactile Shear-Force Display, which has been described above. Regarding the fastener, we chose an off-the-shelf quick-release fastener usually used as photography equipment. In this case, we selected a robust fastener made of metal to ensure a stiff connection between ViSHaRD 10 and the end-effector that is free from backlash.

Fig. 4.5(b) shows the tactile Shear-Force Display mounted on the force/torque sensor (blue) via the locked quick-release fastener. The SF-Display is kinetically connected in a serial manner. Thus, with this configuration it is possible to exert tactile shear force stimuli to the finger tip as well as kinesthetic forces to the hand.

In the following, the three possible hardware setups are presented. The specific setups can be mounted and changed very quickly without much reinitialization or calibration effort. Thus, the modular concept of the components works mostly autonomously and communicates via the UDP-socket based LAN connection.

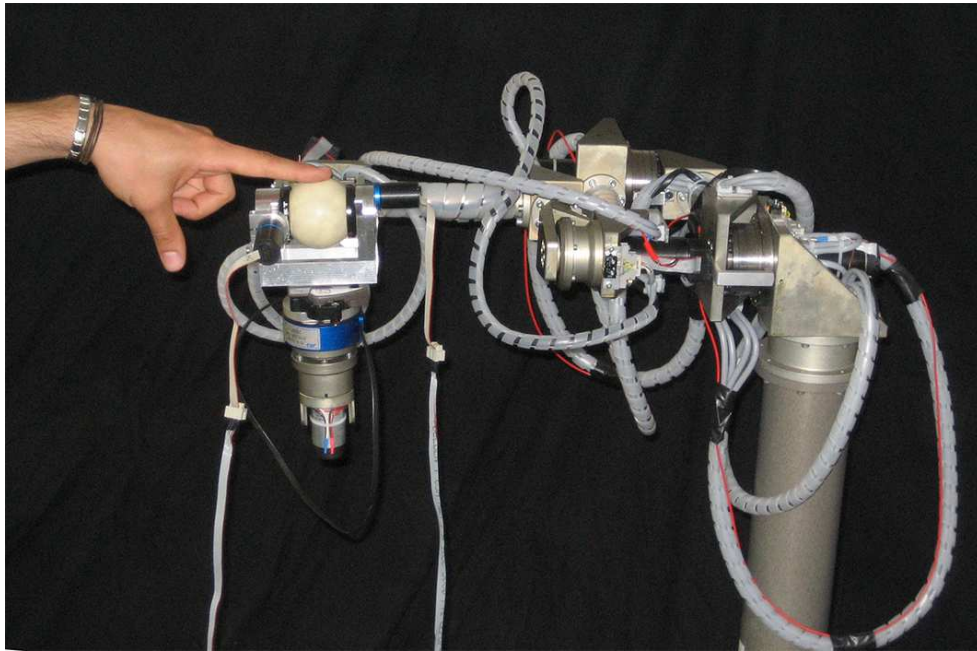


Figure 4.6: Slip-Friction Display mounted on ViSHaRD 10.



Figure 4.7: Shear-Force Display mounted on ViSHaRD 10.



Figure 4.8: VirTouch Mouse mounted on ViSHaRD 10.

ViSHaRD 10 + Slip-Friction Display: Fig. 4.6 shows the setup, realized by combining ViSHaRD 10 with the tactile Slip-Friction Display. For later experiments, an additional fixation for the finger will be used.

ViSHaRD 10 + Tactile Shear-Force Display: Fig. 4.7 shows the combination of ViSHaRD 10 with the tactile Shear-Force Display. The wrist needs to be fixed to the tactile Shear-Force Display by an elastic strip. A more detailed view of the mounted Shear-Force Display is shown in Fig. 4.5, which also displays the applied connection mechanism described above.

ViSHaRD 10 + VirTouch Mouse: The third setup combines the VirTouch Mouse (VTM) with ViSHaRD 10, displayed in Fig. 4.8. The VTM is attached to an aluminum plate that contains the counterpart of the quick-release fastener at the bottom of the plate.

4.2 Evaluation and Application

4.2.1 Evaluation of the Integrated Kinesthetic–Tactile Setups

In this section, a series of experiments conducted with the three hardware setups presented in Sec. 4.1 are described. The objective is to study the psychophysical correlation between the tactile and the kinesthetic portion of haptic information. Furthermore, the influence of different kinds of tactile stimulation is estimated. To this aim, a sinusoidal surface is presented via kinesthetic feedback in combination with a varying amount of tactile information.

Experimental Setup

For these experiments we used the three hardware setups as described in Sec. 4.1. The experiments took place in a quiet room, specifically designated to this series of experiments. The participants sat comfortably on a height-adjustable working stool. For all experiments, the left index finger was stimulated, thus its root was attached on top of the tactile device with a robust tape, such that the tip of the finger was able to touch the stimulation area of the tactile device. In this configuration, the longitudinal active motion of the operator's arm moves the kinesthetic part of the setup, whereas the fingertip is decoupled from this motion.

Each presented stimulus is a combination of a kinesthetic and a tactile component. The kinesthetic component was a constant guided movement along one designated axis of ViSHaRD 10 (y -axis). During the stimulation phase, an additional sinusoidal movement normal to the operators finger tip (z -axis), synchronized to the movement along the y -axis is presented. Thus, it imitates a rigid and spatially fixed sinusoidal surface in the area of the stimulus. It is oriented in longitudinal direction with respect to the operator, and the chosen parameter set is: Amplitude 1 mm, wavelength 10 cm, overall length: 35 cm. Thus the tactile display performs a vertical movement, which is transmitted to the base of the index finger.

Superposed to the kinesthetic stimulus, a tactile stimulus is provided by one of the three described devices. The intensity of this additional tactile stimulus can be varied and it will be changed from trial to trial. In case of the VTM, the surface is displayed by moving the appropriate pins of the pin matrix to form the lateral sinusoidal surface aligned with the direction of movement. Thus, the VTM has to generate a "walking" sinusoidal shape during active exploration. Due to the fact that the Shear-Force Display as well as the Slip Friction Display are not able to provide a proper stimulus in normal direction, they only move laterally to the skin at the fingertip and thus generate shear forces to the index finger. This horizontal movement is also synchronized with the kinesthetic stimulus, but 180° shifted in phase. Such a phase lag enhances the impression of bumps and holes in the virtual sinusoidal surface. The shifted lateral motion causes deformation of the skin and thus produces shear forces as if the user explores the object; however, the stimulus only contains the lateral component of the contact force of the surface.

For the experiments, all movable parts of the several tactile devices were covered, in order to avoid possible visual cues by pin or ball movement. Moreover, white noise displayed via headphones masked the sound of the displays during stimulation.

Protocol

Six persons (five male, one female) participated in the experimental series. Their age ranged from 21 to 36 years (average 27 years). None of them reported any known tactile deficit due to accident or illness concerning the left index finger. Three of the participants were partly familiar with the hardware setup but with the exception of one, all were naïve concerning the purpose of the experiments.

The experimental procedure was the same for all three used hardware setups. Based on the *two interval forced choice* paradigm, the participant received two stimuli, among which he had to make a decision. In our experiment, one trial is defined according to the following sequence:

- a) The participant has to move the display to its starting position ($y_{start} = -40$ cm).
- b) ViSHaRD 10 accelerates the tactile device, and thus the attached finger up to an exploration velocity of $v_{exp} = 20$ cm/s.
- c) Between the area of $y_{begin} = -20$ cm and $y_{end} = 15$ cm, the stimulus containing sinusoidal movement along the z -axis of the kinesthetic display and the corresponding movement of the tactile device is presented. In this range, the velocity is held constant at v_{exp} .
- d) The kinesthetic display slows down and moves back to the to starting position ($y_{start} = -40$ cm).
- e) After the first stimulus, the comparison trial is performed in analogy to items **b)** to **d)**. After the second stimulus, the participant has to vote which one of the two stimuli has been more "realistic".

The participants thus consecutively felt a standard stimulus, containing kinesthetic movement only, and a comparison stimulus, consisting of kinesthetic and tactile information. As described above, the tactile information consists of a sinusoidal movement, synchronized with the kinesthetic base display. Whereas the level of kinesthetic information is kept constant, the additional tactile information about the sinusoidal shape varies linearly in 10 steps between the amplitudes of 0 – 1 mm.

Each pair of stimuli was presented 20 times. The order of the pairs, as well as the order of presentation of a pair was randomized.

Based on preliminary studies, we decided to guide the entire kinesthetic motion by trajectory tracking, to ensure constant velocity exploration. This proved to be important for the comparability of obtained results.

As the velocity for exploration was predetermined, we told the participants to let themselves be guided and not to act against the movement.

Results and Discussion

Fig. 4.9 shows the results (obtained from 6 subjects) of the combined setup of ViSHaRD 10 and the Shear-Force Display. Displayed are mean and standard deviation of the proportion of trials where the combined kinesthetic and tactile stimulus was perceived as more realistic than the purely kinesthetic one. These values are plotted against the rising intensity of the tactile part of the stimulus. The range from 0.2 – 0.6 mm amplitude of the Shear-Force Display is sensed as realistic in 80% or more of the cases. Interestingly, when the amplitude of the force stimulus is further raised, it starts to feel disturbing. One participant reported that in case of the full excursion of the shear force stimulus, the combined stimulus felt more like two separate stimuli.

The results of the combination with the Slip-Friction Display in Fig. 4.10 indicate that that the perceived realism peaks to about 90% for slip friction amplitudes between 0.2 mm and 0.5 mm. Even higher amplitudes up to the maximum value of 1 mm are rated with more than 70% "realistic". A possible explanation is that the provided shear force interacts via a planar contact with the operator's finger tip. This prevents the sensation of a separation of kinesthetic and tactile information and leads to a more harmonic combination.

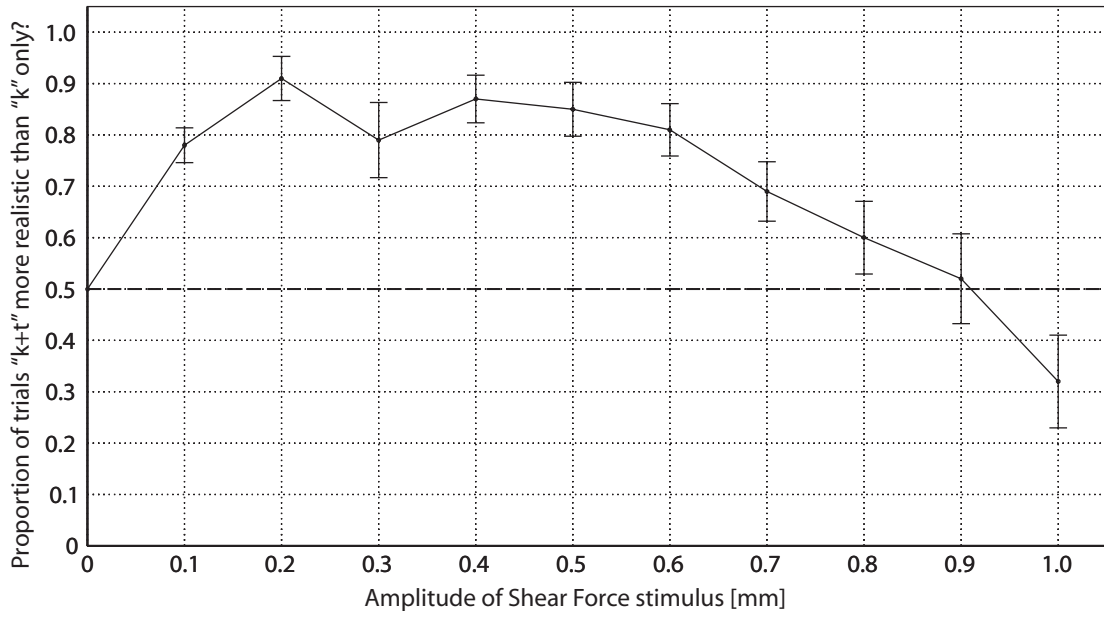


Figure 4.9: ViSHaRD 10 + Shear-Force Display.

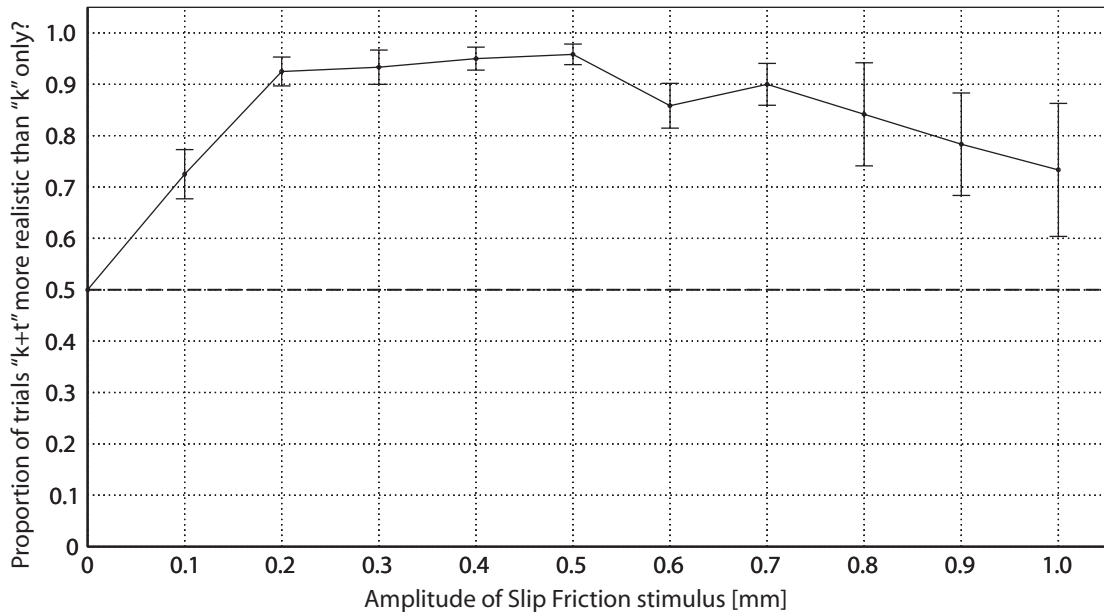


Figure 4.10: ViSHaRD 10 + Slip-Friction Display.

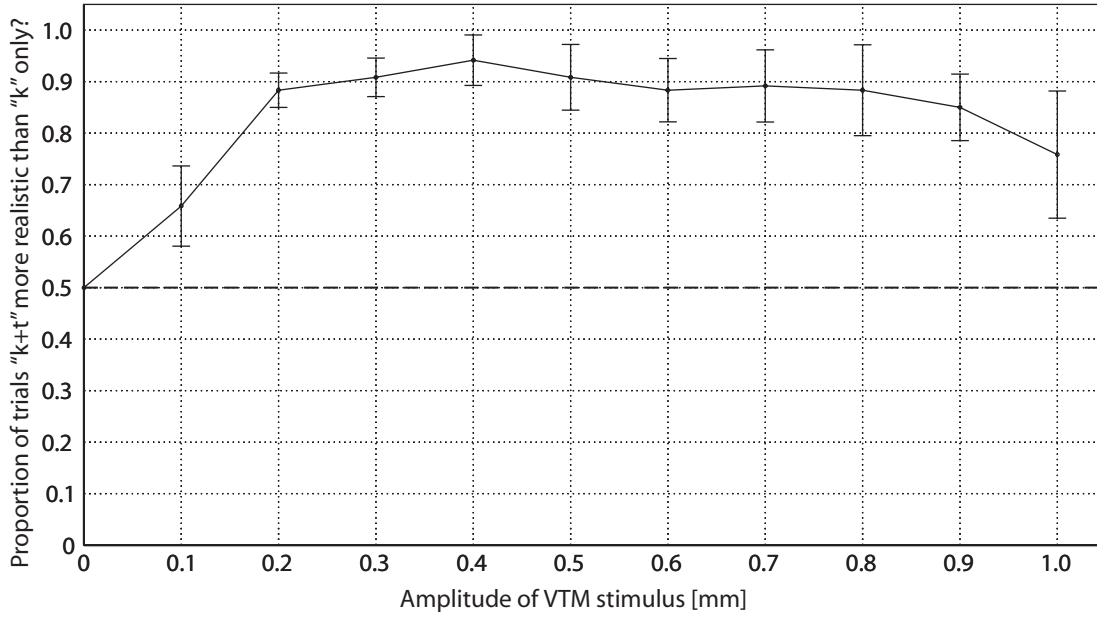


Figure 4.11: ViSHaRD 10 + VirTouch Mouse.

The results of the combination of ViSHaRD 10 and the VTM, which are displayed in Fig. 4.11, show a relatively constant percentage of perceived realism level of percent of around 80% regarding the combined stimulus beyond 0.2 mm. That proves the assumption that a tactile stimulus built by a normal force display with the objective to rebuild the shape of the virtual surface can be augmented without losing the feeling of a real surface. In other words, the tactile stimulus is scalable.

4.2.2 Psychophysical Application: Perception of Virtual Stairs

To evaluate the combination of the ViSHaRD 10 and the Shear Force Display, a 3D experiment was set up. In this experiment, subjects were to explore a virtual stair. This experiment aimed to investigate perception of sharp edges.

Experimental Setup

A VR system is developed to investigate the haptic-visual interaction with rigid walls and sharp edges. A virtual stair is created by using simple geometrical objects. The avatar is again a virtual proxy. If the avatar collides with the stairs, then the resulting force is calculated as:

$$F = k_s x_s + b_s v_s, \quad (4.1)$$

where k_s, b_s are spring and damping coefficients of the stairs. The penetration depth of the avatar into the stairs is x_s and the avatar velocity is v_s . Addition of the damping element is necessary to manage high stiffness of the stairs. The important point here is, when the user changes the direction and wants to leave the stairs, b_s has to be set to 0. Otherwise the avatar sticks to the virtual stairs. The virtual scene of "stairs" is shown in Fig. 4.12.

For the tactile rendering of the step, only one pin of the Shear-Force Display is used. The position of the finger is traced while exploring the surface and the pin is pre-orientated

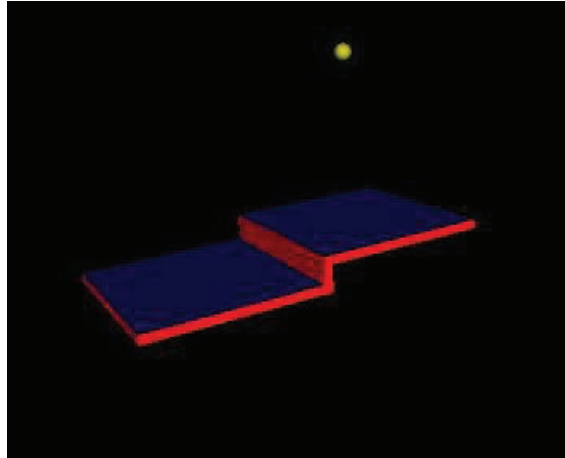


Figure 4.12: Virtual stairs.

in moving direction with maximum excursion. In the area of the edge ($x_{edge} \pm 1 \text{ mm}$) the pin position is mapped to the stationary position of the edge.

According to the virtual model, the kinesthetic subsystem renders the two x-y plane of the stairs shown in Fig. 4.12. Hence, the subjects feels a smooth surface when moving across the two planes. Thereby the user can only perform translatory movements. Rotational movements were not allowed. That means, the subjects fingertip always points at a certain direction. The fingertip position is indicated by the yellow ball. When the subject reaches the edge of the virtual step, the Shear-Force Display exerts a constant shear force exactly in that moment when the fingertip strokes over the edge. In the real situation, the fingertip would only partially touch the object when it strokes over the edge. The other part of the fingertip is not in contact with the object. In that moment, shear forces are imprinted on the fingertip.

Protocol 1: Qualitative Evaluation of Presence

By the use of the tactile Shear-Force Display, we expected an increasing immersion of the subjects compared to a haptic interface that is only capable of exerting kinesthetic stimuli.

To quantify immersion, we conducted an experiment with five subjects. Their task was to compare their impression of the realistic rendering of the stair when rendered either using the purely kinesthetic display of the ViSHaRD 10, or using the combined setup of the ViSHaRD 10 plus the Shear-Force Display and a real step. The subjects got visual information as shown in Fig. 4.12. After one trial to accommodate with the experimental testbed, the experiments were conducted.

Presence Results and Discussion

All subjects reported the highest immersion in the case of the real step. This indicates that the experimental setup was chosen correctly, since the real situation was perceived as most realistic. The condition using the purely kinesthetic setup yielded the least immersion. Subjects reported the condition with added tactile feedback in the combined ViSHaRD 10 plus Shear-Force Display condition to be more realistic than with kinesthetic feedback

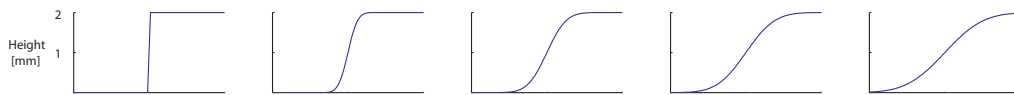


Figure 4.13: Edge stimuli for haptic rendering in the evaluation task.

only. However, subjects still stated a distinct difference to the reference situation of the real step.

Protocol 2: Quantifying Feature Detection Performance

In the following experiment the setup of ViSHARD and the tactile Shear Force Display has been used. The aim was a verification and quantification of the enhancement in feature detection while using combined kinesthetic and tactile sub-modalities. For this, we used the scenario described above, but without visual feedback. To evaluate the performance, we chose the magnitude estimation technique. As stimulus, an edge of 2 mm height with varying steepness was used. The steepness is varied in 5 steps and is calculated based on cumulative normal distributions. This results in five different stimuli (Fig. 4.13)

The maximum length of the edge is 10 mm (step 5). These slope profiles can be displayed in z -direction (height) by ViSHaRD 10. For this experiment, the six DOF of ViSHaRD 10 have been constrained to one axis of free motion (y -direction). ViSHaRD 10 is driven by an admittance control from a separate control computer. It communicates via LAN using UDP-communication protocol. The experiment control computer receives the current position, drives the Shear-Force Display, and returns the z -position. For this experiment, we used only one pin of the Shear Force Display, the other three pins were removed.

Three right-handed participants (all male) participated voluntarily. None of them reported any known tactile deficit concerning the right index finger, e.g. due to accident or illness. All participants were familiar with the device from earlier experiments.

The participants stood in front of the integrated device and attached their right index finger on the top of the Shear-Force Display, so that the phalanx of their index finger was reliably centered at the midpoint of the pin of the Shear-Force Display. The position of the participant was chosen in a way that the remaining degree of free motion of ViSHaRD 10 ran horizontally and easy to follow in front of the subject. White noise via headphones masked the sounds of the mechanics. The participants had to move the device about 10 cm to the right, to reach the starting position. Then they had to explore the edge along the movable axis of motion with adequately low speed. In all trials, the edge was placed at the same place. Before the actual experiment started, each of the edges, was presented two times in regular order as a training task, with and without shear force. During the experiment, the 10 different stimuli were presented five times in randomized order. After each exploration of a stimulus, the participant was asked to estimate the explored edge regarding sharpness by a number on a scale from 1 to 5. To analyze the data, first the average of each subject and stimulus was calculated across the replications. To allow for a comparison of the results among the participants, these values were normalized.

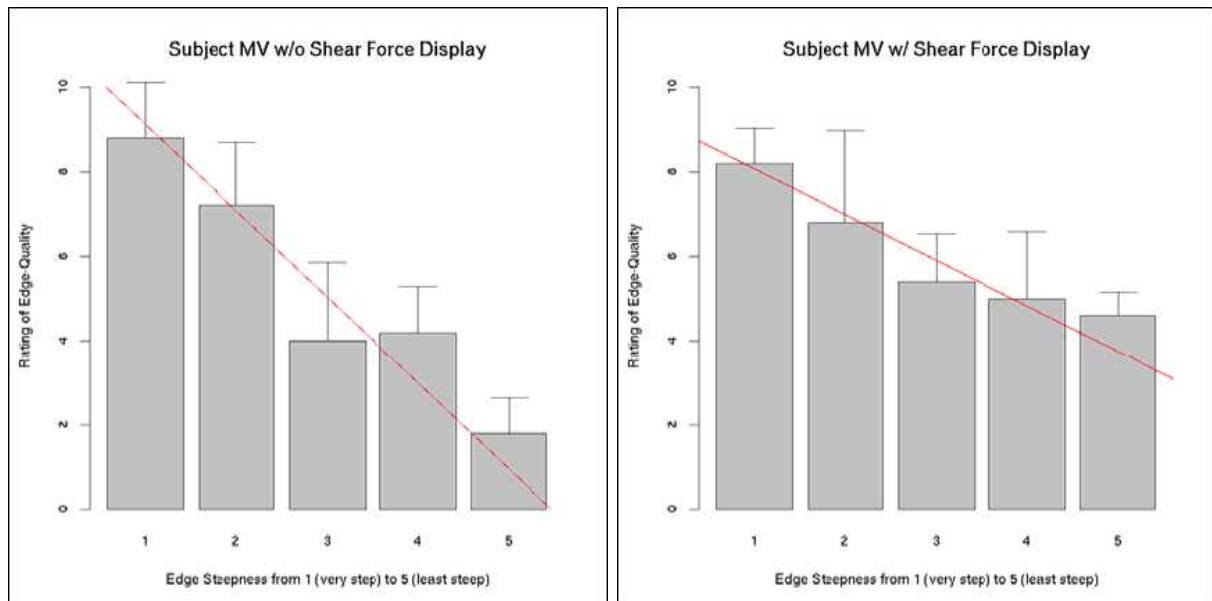


Figure 4.14: Mean ratings and SD for five ratings each of different steepness. Data of one subject in condition with and without additional tactile feedback.

Feature Detection Results and Discussion

Of the three tested subjects, only one showed different ratings between the condition without and the one with activated Shear-Force Display (Wilcoxon-Test: $N = 25, W = 159, p = 0.002$). On the other hand, there is no reasonable scaling of the edge quality rating with respect to the steepness of the presented edge. For both remaining subjects, we did not find any difference between ratings with and without Shear-Force Display.

These results for the tested subjects are rather inconsistent. In the only case with reasonable scaling of rating in relation to edge steepness, we cannot find a difference between ratings for the condition with in contrast to without shear force display. However, the different slope of decrease between the two conditions suggest that indeed the rating of less steep edges is better with Shear-Force Display. Therefore we conclude that for edges that are steep and easily displayed by kinesthetic means, we don't have an advantage in using an additional tactile display. For shallow edges, however, ratings of edge quality increase with the addition of tactile feedback.

4.3 Conclusion

In this chapter, a flexible approach to combine kinesthetic and tactile displays has been presented. The concept is based on a high-performance kinesthetic base display, which allows haptic interaction in a large workspace. Three different tactile displays have been used in combination with this base display. Such a flexible configuration opens up a large domain of possible psychophysical experiments that target cross-modal interaction of kinesthetic and tactile perception.

A series of exemplary psychophysical experiments has been conducted to assess usability of the proposed approach. A first important result concerns the feeling of immersion or

presence when exploring virtual scenes: Consistently, subjects judged the display to be more realistic when tactile information was added to the kinesthetic channel. However, concerning subject performance, a clear, general benefit of additional tactile information could not be found. Only for information that is not easily displayed by kinesthetic means (like shallow edges), performance of perception seems to benefit from the addition of tactile feedback. Beyond the scope of this thesis, the described hardware framework has already been used to explore the phenomenon of tactile suppression [202].

These exemplary findings indicate that the developed framework will be a valuable toolchain for further investigations.

5 Conclusion and Perspective

The overriding motivation of this work was to enable combined tactile-kinesthetic interaction of human subjects with robotic devices. Regarding this aim, this work contributed three main jigsaw pieces: The first was to provide novel device hardware and actuator concepts that outperform human perception and thereby enable the investigation of phenomena in haptic perception. This allowed a second contribution, which is insight into a yet almost unexplored human tactile sub-modality: the perception of shear force. Finally, the set of mechatronic tools also paved the way for a third contribution, which is exemplary work on inter-modal coherence between tactile and kinesthetic perception.

With this set of tools at hand, the focus could move towards the specific experiments that can be conducted with it, and which questions future research projects could target.

5.1 Investigating Mechanisms of Human Perception

On the way to explaining human perception in a mathematical way, there are some fundamental neurobiological properties that need closer investigation: Attention, interaction between modalities, and interaction between sub-modalities.

5.1.1 Selective Attention

Attention plays an important role in the context of sensory integration. In reaction to the general over-availability of sensory information, there are several mechanisms that shade or shut off sensory information selectively on the way to our conscious perception [39, 136, 140].

A famous example stems from the auditive domain, the so-called “cocktail party effect” [34]: Human subjects are able to selectively perceive sound sources from preferred directions, allowing them to filter out the voice of a conversation partner within a noisy crowd. This is only possible when hearing with two ears. It is yet unclear which mechanism is responsible for the phenomenon of selective attention. It is also not clear whether the mechanisms of selective attention are uniform when switching between modalities. There are some indications that this is not the case, but that there are some asymmetries. For example, it seems to be easier to focus on vision than on tactility when there are competing stimuli [195]. A survey on the role of attention in tactile perception can be found in [187].

5.1.2 Interplay of Somatosensory Modalities

Concerning the interplay of somatosensory modalities, pioneering work on the integration of information has been presented in [46], but more detailed experiments need to be done for the tactile sense. First results from literature indicate that other modalities heavily influence tactile perception, sometimes even making this information channel superfluous. One example concerns applications where vision can be used alternatively, for example in

robotic surgery with visual feedback. There, it has been shown that the lack of tactile feedback did not negatively influence surgeons' performance [194]. They simply compensated by using vision, leading even to an illusory perception of tactility. This so-called "reverse Braille phenomenon" has been explained by intersensory integration [194]. A close investigation of the reverse Braille phenomenon, or more general the influence of vision in the context of tactility, could be a milestone on the way to explaining interplay of modalities.

5.1.3 Interplay of Haptic Sub-Modalities

It is not only important to consider the influence of other sensory modalities (visual and auditory), but also of sensory interactions *within* haptic perception or even tactile perception alone: It is known that there can be a considerable influence of other sensors besides those that react to mechanical stimuli. For example, humans manipulate objects that are cold with a firmer grasp than those that are warm. An obvious explanation is that fingers could be more numb, and a fail-safe mechanism increases grasp force in the absence of sensory feedback. Another possible explanation could be that cold objects are perceived as more wet, so that a lower friction coefficient is expected [31]. The mechanical part of the human tactile perception has the highest number of sensors. Other important characteristics are that it delivers tactile information continuously; our perceptual system can dim it, but not switch it off. However, these facts indicate, but they do not prove that mechanical stimuli really enter the dominant channel. It would be interesting to investigate potential correlations between mechanical, thermal and pain stimulation during the combined perception of tactile stimuli. This could clarify whether the hypothesis can be defended that thermal perception can be neglected as long as thermal stimuli stay within a comfortable range. The same question arises for nociception: Is there only an influence when stimuli exceed the pain threshold, or already below? Interesting findings from neurobiology already hint at an important influence of pain, more specifically they indicate that pain facilitates tactile perception [156].

5.2 Outlook on Future Device Design

The devices presented in this thesis are research platforms to study human perception; practical usability or portability was of little interest. To be relevant for real-world applications, tactile devices must be much simpler, lighter, and less bulky. With this premise, there are two major possible research directions:

- One aim could be to maintain or even enhance the degree of realism of haptic devices by exploiting a large amount of perceptual phenomena to "cheat" the human sensory system, which was also an idea behind this thesis.
- A fundamentally different approach on the way to reducing complexity is to step back again and to explore openly what the added value of robotic tactile devices can be in the future. What is probably more relevant than realism in itself is the *performance benefit* that humans can gain when using such devices. Here, the idea of reproducing real-world tactile stimuli is abandoned, instead the tactile perceptual channel is simply considered as a way of conveying information of any type.

Both research directions require profound knowledge on characteristics of human perception.

5.2.1 Exploiting Perception Phenomena to Reduce Complexity

When considering the mentioned neurobiological principles, the goal when developing haptic devices can not be to identify and to match all relevant channels of information. With the currently available technology and the usual 1:1 approach in realization of displays, it is impossible to find a satisfying solution. The main challenge in realizing displays that are able to provide the whole range of haptic stimulation (kinesthetic and tactile) is the difficulty to provide sufficient DOF. This is true even for the kinesthetic modality alone, where each joint, including individual fingers would need its robotic counterpart. The system becomes unrealistically complicated already when the whole range of human mechanical receptors in the arm should be covered, not mentioning thermal or nociceptive sensations.

Instead, haptic device development must aim for an optimal technical compromise between perceived realism and technical complexity. The solutions presented in this thesis already represent compromises, exploiting a multitude of known physiological properties to cheat the human sensorimotor apparatus. However, there are probably many more options to create a holistic haptic impression with less technical effort.

Some indications how devices could be simplified can be drawn from knowledge on ways to “cheat” human tactile perception. For example, an interesting phenomenon that allows to induce the illusion of continuously moving stimuli with only two discrete stimulation sites is the “cutaneous rabbits” illusion: When tapping wrist and elbow in a rapid sequence, it seems that taps are running up the forearm. Similar effects have been called “tactile phi phenomenon” or “phantom sensation” [7, 88]. As there are many illusions known from vision, these could offer inspiration. For example, inspired by the barberpole illusion*, it has already been shown that visual and tactile perception are very similar in the way they can be deceived [177]. Another example for the apparent similarity between the two modalities is the inability to notice changes in scenes or patterns when disruptions or distractions mask these changes. This phenomenon, called “change blindness”, is well-known for vision, and it also seems to exist in the tactile sense [59]. Exploiting this would allow to hide technological deficits far above the perception threshold by suitable masking stimuli. Ideally, these masks would not disturb the task but rather be task-inherent: For example, discrete or quasi-discrete events like grasping/releasing objects or steep edges could be used to secretly re-adjust a stimulation bias, reducing requirements for range of motion. Further findings on isolated tactile phenomena [119, 165], perception mechanisms of localized haptic features like bumps and holes [134], or the fact that frequency changes can induce height illusions [121] may also offer ways to simplify devices. A particularly interesting phenomenon in the context of combined kinesthetic-tactile devices is tactile suppression [43], where concurrent kinesthetic stimuli hamper tactile perception. Models for underlying mechanisms, such as a temporal abstraction network [127] to explain the “cutaneous rabbits” illusion, might be tools to predict further phenomena.

*Barberpole illusion: This is a well-known visual illusion where a pole with diagonal stripes rotates about its vertical axis. The stripes then seem to move up or down.

5.2.2 Tailoring Tactile Devices to Convey Information in Novel Applications

It is known that in certain areas, added tactile information is beneficial to improve human work performance. One example is the automobile industry, where human workers inspect metal surfaces with their hands. There, it has been long known that an additional tool to enhance tactile perception is beneficial to improve performance: They found that a simple knitted glove acts like a tactile magnifying glass for small surface defects. Correspondingly, a performance-enhancing “haptic contact lens” has been developed based on this principle [106], and it has been shown to improve human bump detection accuracy.

However, there are also domains where the added value of tactile information is questionable. One example concerns applications where vision can be used alternatively, as in the example of robotic surgery given above. This finding demonstrates that the benefit of tactile information depends strongly on the application and on the availability of other sensory information.

Therefore, a promising way is to abandon the goal of realism, but to use tactile stimulation as a means to convey information in an abstract way. The example of the surgeon suggests that this information has to be non-redundant with other channels. One example where tactile feedback could prove beneficial is substitute feedback for impaired subjects, like amputees or the blind. Another example could be to augment senses of non-impaired subjects, to increase their performance in certain tasks. A third example is feedback for man-machine interfaces like communication devices.

On the example of substitute sensory feedback for patients that have lost arms or legs, particular strengths and weaknesses of different tactile devices become evident. Several experiments indicate that amputees can generally benefit from artificial sensory feedback and improve motor performance [117, 164]. However, it is still disputed which would be the optimal way to convey this sensory information. The seemingly most intuitive way to reproduce sensations at a prosthetic limb would be to provide a stimulus of the same type at another location, meaning pressure sensors on the prosthesis are mapped to actuators that can again produce pressure on the human skin elsewhere. The advantage of this method is that it allows higher discrimination performance compared to vibration or electro-tactile feedback [149]. This may be explained by the additional transformation that the human perceptual system needs to perform when stimulus and conveyed information are not congruent [151]. However, there are problems in practical usability. This in turn is a strength of vibrotactile or electro-tactile stimulation. A weakness of this method is habituation, meaning an undesired adaptation of the perception threshold to increasing values. A solution could be high-frequency electro-tactile stimulation: This type of feedback avoids habituation, such that it has been successfully used for hand prosthetics [12].

A crucial aspect to gain added value from tactile information is avoiding redundancy with other modalities. One example is the substitution of lost senses in impaired subjects, not only for amputees, but also for blind patients. Several tactile displays have been developed that help the blind navigate. For example, oral stimulation allowed a very clear distinction between right and left direction indicators [192]. Another option is to display feedback to the feet, called podotactile feedback. Also this type of display proved successful in navigation assistance [200].

Tactile feedback in non-impaired subjects can be used to further augment the sensory system. An application that is gaining increasing popularity is the indication of direction,

be it for navigation in the real world, for example via stimulation on the torso [47] or on the fingertip/hand [61, 145, 169], or for navigation in virtual worlds in gaming applications [69]. In futuristic applications, this additional information channel could be coupled to any physically realizable sensors that detect stimuli outside the perceivable range of human subjects. For example, radiation or acoustic/electromagnetic waves outside the audible/visible spectrum could be mapped to the human body, which could be advantageous for certain applications. The main advantage of tactile feedback is that it unobtrusive, does not interfere with activities, and can rather easily be ignored when not needed.

Many current displays, particularly those used for navigation assistance, are based on simple vibrators. Their main advantage is their low technical complexity and excellent portability. For navigation tasks, this seems sufficient. It is also a frequently used technology for smart electronic devices like mobile phones, e.g. for touchpad interfaces, to provide tactile features while sliding over the screen [118, 122, 142, 170]. However, there are also tasks where it has been shown that the human tactile system is better able to interpret signals of low frequency, such as provided by normal-force or shear-force displays. One example for this is subitizing, which is the capability to instantaneously count a low number of objects. In experiments where a varying number of fingers on a human hand were simultaneously stimulated, it was shown that subitizing is possible with a normal-force display [160], but not with vibrators [59]. This can to some extent be explained by the receptor type and the respective signal propagation, as outlined in the introduction, which shows that spatial resolution is not good for high-frequent stimuli.

The most important conclusion from this diverse list of future applications is that there is no one-fits-all solution. Instead, each application has its very specific demands, both in terms of the optimal perceptual mechanism to convey information to the human, and in terms of technological constraints. Therefore, it is crucial to know the specific benefits of each perceptual sub-modality.

5.2.3 The First Step

For both research directions in tactile devices, be it illusion-based realism enhancements or task-specific information transmission, the first step is identical: Finding out more about human tactile perception. This information can then be used either to find ways to cheat, or to determine which information can best be transferred by which type of tactile stimulus.

The mechatronic solutions presented in this thesis offer a versatile experimental platform to uncover and quantify hidden mechanisms of human perception, which can then be exploited to deceive human subjects. Going further in this direction (which is beyond the scope of this work), there have already been psychophysical experiments with the combined tactile-kinesthetic setup [201, 203]. These investigations confirm that haptic perception in general implies a strong inter-correlation of tactile and kinesthetic perception. This is in congruence with simple observations made in everyday life: Even for the most basic tasks like grasping objects, the complete haptic perception is used.

To find the optimal device for a given task, it is important to know the specific characteristics and benefits of each perceptual sub-modality. A large uncharted territory is still in the domain of shear force perception, in contrast to normal force, vibration, and electrotactile stimulation. In case shear force perception turns out to have similar characteristics as normal force perception, the technological constraints alone can determine which display type is more beneficial. For example, it could be very attractive to investigate new forms

of producing shear force on the human body. Probably, such displays could be designed very flat, for example using contractile elements in textiles. This could bring a considerable technological advantage. Furthermore, if shear force and normal force perception show such striking differences as there are between vibration and normal force perception, this could open up even more Degrees of Freedom during the design and optimization of task-specific tactile displays. Therefore, it is essential to find out more about how humans perceive shear force. Many questions need to be answered, for example how learning and adaptation influence task performance. The shear force displays presented in this thesis provide dedicated experimental platforms to acquire this knowledge.

In conclusion, knowledge of how humans perceive tactile stimuli and how they merge them with kinesthetic and other perceptual channels will be a crucial benefit for the design of tactile displays. The technological principles presented in this thesis offer suitable tools to acquire this knowledge, paving the way to smart, simple solutions in the future.

A Technical Documents: Low-Frequency Actuator

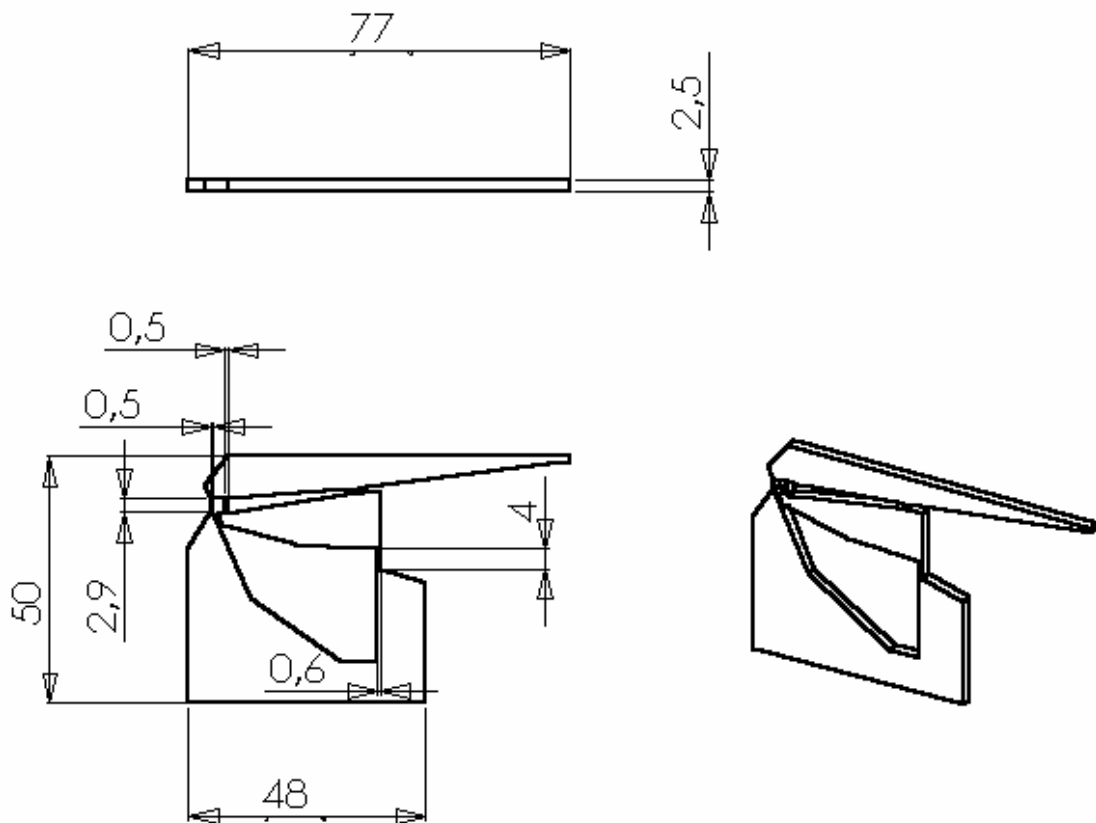


Figure A.1: Technical drawing of the lever system (unit of length = mm)

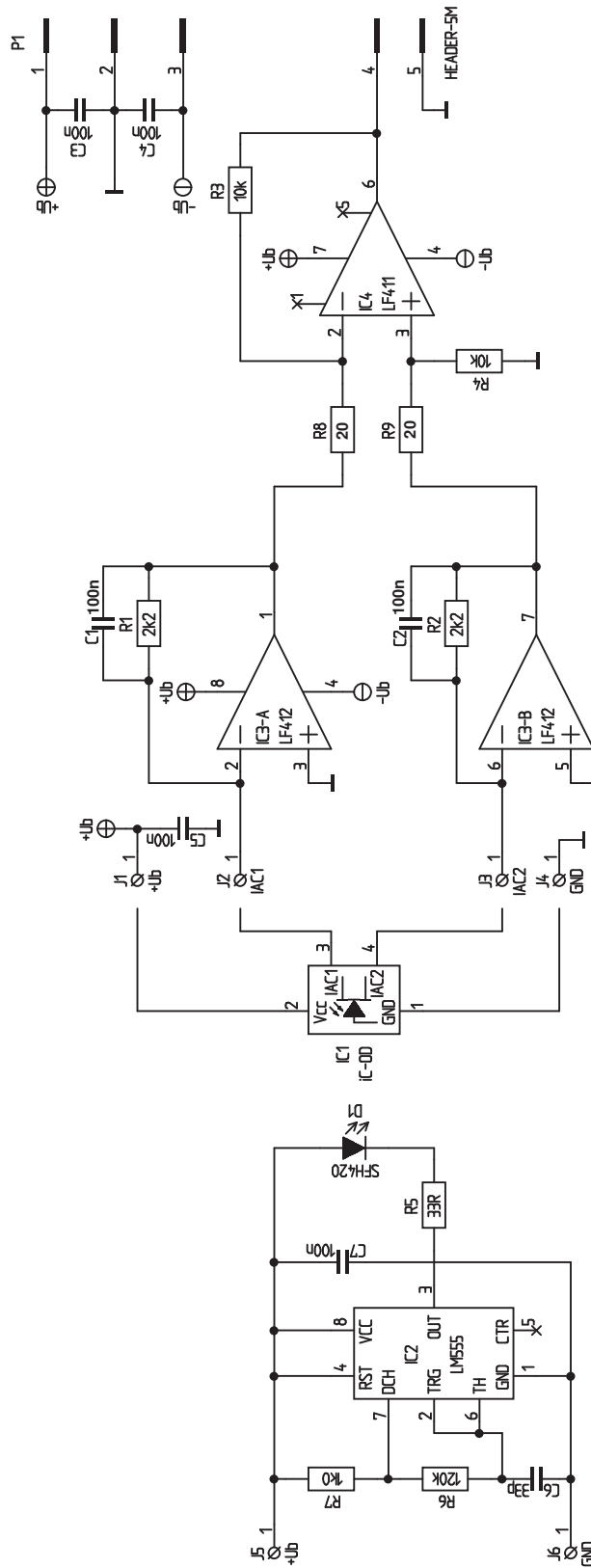


Figure A.2: Circuit diagram of the IR-Position sensor

B Technical Documents: High-Frequency Actuator

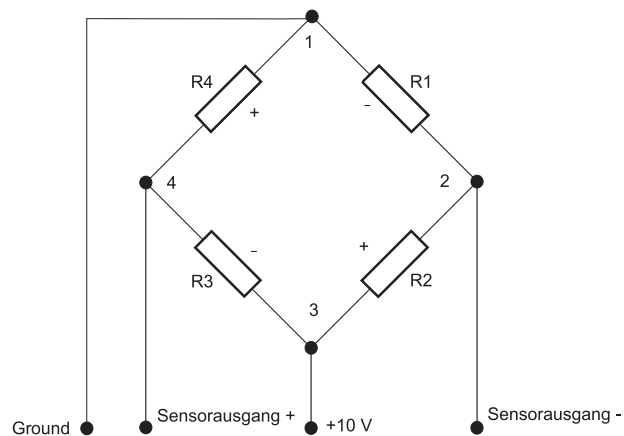


Figure B.1: Connector pin assignment of the strain gauge (full Wheatstone bridge) of the PSt 150/5/40 piezo actuator module, taken from [155]

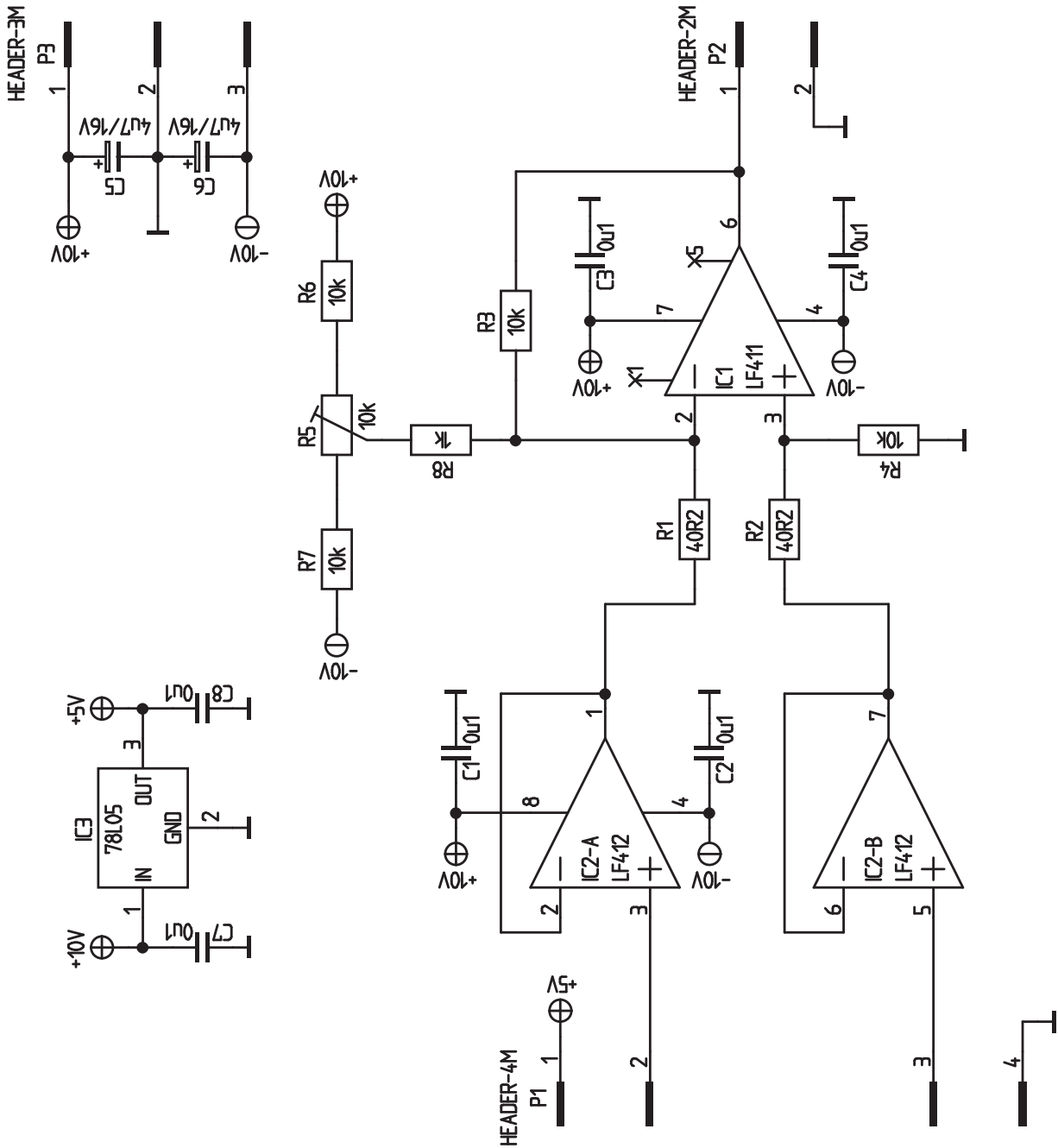
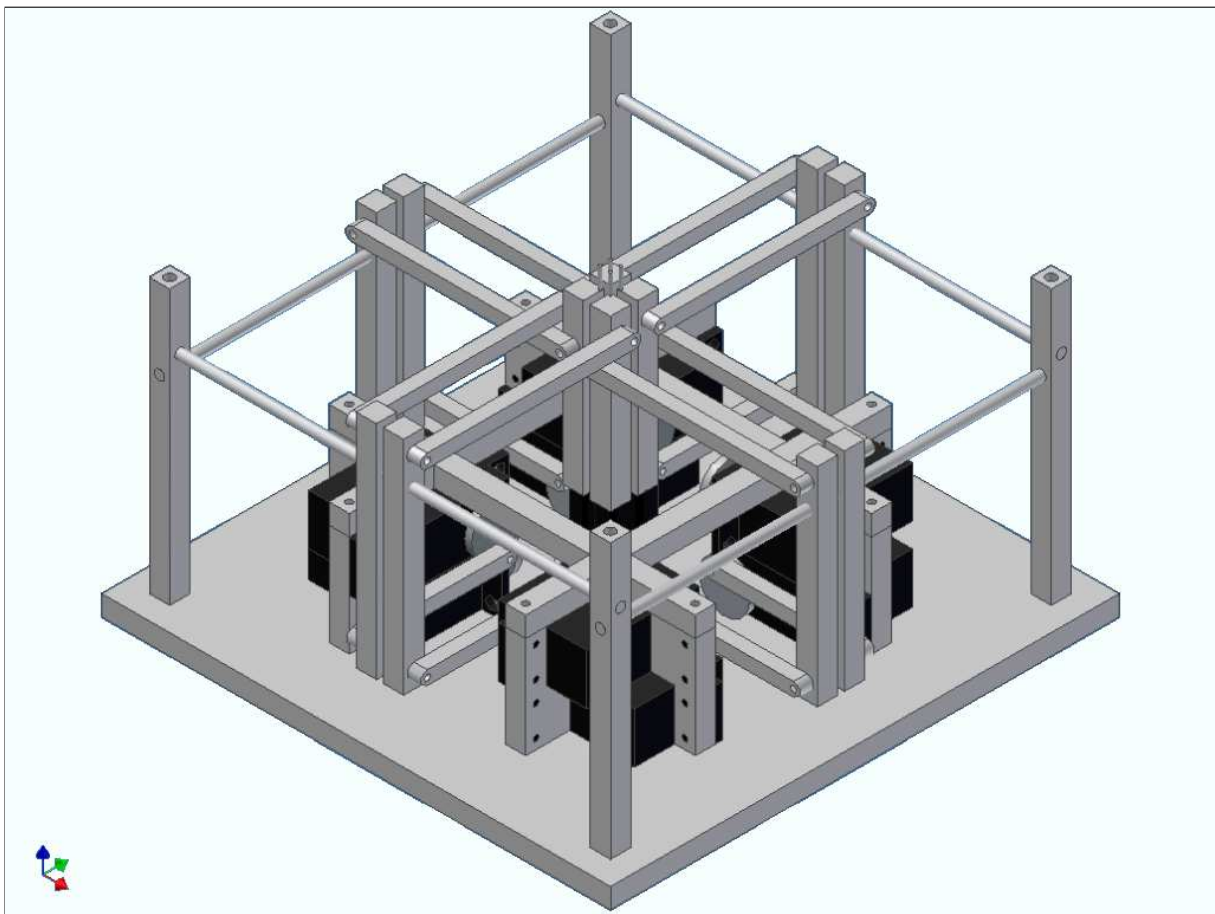


Figure B.2: Circuit diagram of the strain gauge amplifier

C Technical Documents: Pin-Based Shear Force Display

Technical Drawings (unit of length = mm)



Source code

Listing C.1: Realtime module to generate RC-Servo conform PWM Signals at the printer port

```
#include <rtl.h>
#include <pthread.h>
#include <rtl_time.h>
#include <rtl_fifo.h>
#include <asm/io.h>

#define PRINTER_PORT    0x378           // Hardware address printer port
#define PERIOD_TIME     1000000LL      // Signal refresh rate (10ms)
#define THRESHOLD_TIME  950000LL      // 1ms(-10*5us)!
#define POS_RESOLUTION  256           // (0-256 = 0-1ms)
#define MIN_TIME_STEP   3906LL        // 1ms/POS_RESOLUTION (3.906us)
#define POS_INIT        128           // Initial start position
#define FIFO_SIZE       1000         // Size of communication fifo

pthread_t thread;

void * start_routine(void *arg)
{
    unsigned char    motornr, portout;
    unsigned char    motor_pos[8], fifo_motor_pos[8];
    int              puls;
    hrtime_t         start_time, now_time;

    struct           sched_param p;

    p.sched_priority = 1;
    pthread_setschedparam (pthread_self(), SCHED_FIFO, &p);
    pthread_make_periodic_np (pthread_self(), gethrtime(), (hrtime_t)
        PERIOD_TIME);

    for (motornr = 0; motornr < 8; motornr++)
        motor_pos[motornr] = POS_INIT;

    while (1)
    {
        portout = 0xff;
        start_time = clock_gethrtime(CLOCK_REALTIME);
        outb(portout, PRINTER_PORT);
        now_time = start_time + (hrtime_t)THRESHOLD_TIME;

        if(rtf_get(1, fifo_motor_pos, sizeof(fifo_motor_pos)) ==
            sizeof(fifo_motor_pos))
            for(motornr = 0; motornr < 8; motornr++)
```

```
        motor_pos[motornr] = fifo_motor_pos[
            motornr];

    for(puls = 0;puls <= POS_RESOLUTION;puls++)
    {
        for(motornr = 0;motornr < 8;motornr++)
            if(motor_pos[motornr] == puls)
                portout&=~(0x01<<motornr);

        clock_nanosleep(CLOCK_REALTIME,TIMER_ABSTIME,
            hrt2ts(now_time),NULL);
        now_time += (hrtime_t)MIN_TIME_STEP;
        outb(portout,PRINTER_PORT);
    }

    outb(0x00,PRINTER_PORT);
    pthread_wait_np();
}

return 0;
}

int init_module(void)
{
    int dummy;

    rtf_destroy(1);
    dummy = rtf_create(1,FIFO_SIZE);

    return pthread_create (&thread, NULL, start_routine, 1);
}

void cleanup_module(void)
{
    pthread_delete_np (thread);
}
```

Bibliography

- [1] K. Abidi, A. Sabanovic, and S. Yesilyurt. Sliding-mode based force control of a piezoelectric actuator. In *Proceedings of the International Conference on Mechatronics (ICM'04)*, 2004.
- [2] E. D. Adrian. The impulses produced by sensory nerve endings: Part i. *Journal of Physiology*, 61:49–72, 1926.
- [3] E. D. Adrian. The impulses produced by sensory nerve endings: Part ii. the response of a single end-organ. *Journal of Physiology*, 61:151–171, 1926.
- [4] E. D. Adrian. The impulses produced by sensory nerve endings: Part iii. impulses set up by touch and pressure. *Journal of Physiology*, 61:465–483, 1926.
- [5] E. D. Adrian. The impulses produced by sensory nerve endings: Part iv. impulses from pain receptors. *Journal of Physiology*, 62:33–51, 1926.
- [6] S. Akiyama, K. Sato, Y. Makino, and T. Maeno. Presentation of thermal sensation through preliminary adjustment of adapting skin temperature. In *Proceedings of the 2012 IEEE Haptics Symposium (HAPTICS)*, pages 355 –358, march 2012.
- [7] D.S. Alles. Information transmission by phantom sensations. *IEEE Transactions on Man-Machine Systems*, 11(1):85–91, 1970.
- [8] M. Ercan Altinsoy and Sebastian Merchel. Electrotactile feedback for handheld devices with touch screen and simulation of roughness. *IEEE Transactions on Haptics*, 5(1):6–13, 2012.
- [9] K. H. Andres and M. v. Düring. *Handbook of Sensory Physiology 2, Somatosensory System*, chapter 1, Morphology of cutaneous receptors, pages 3–29. Springer-Verlag Berlin, 1973.
- [10] Ltd. APC International, editor. *Piezo-Mechanics: An Introduction*. Available online: www.americanpiezo.com, accessed 2011.
- [11] M. Arai, K. Terao, T. Suzuki, F. Simokawa, F. Oohira, and H. Takao. Air-flow based multifunctional tactile display device with multi-jet integrated micro venturi nozzle array. In *Proceedings of the 2012 IEEE 25th International Conference on Micro Electro Mechanical Systems (MEMS)*, pages 148 –151, 29 2012-feb. 2 2012.
- [12] A. H. Arieta, H. Yokoi, T. Arai, and Yu Wenwei. FES as Biofeedback for an EMG Controlled Prosthetic Hand. In *Proceedings of TENCON 2005*, pages 1–6, 2005.

- [13] N. Asamura, N. Yokoyama, and H. Shinoda. A method of selective stimulation to epidermal skin receptors for realistic touch feedback. In *Proceedings of Virtual Reality*, pages 274–281. IEEE, March 1999.
- [14] S. Asano, S. Okamoto, Y. Matsuura, H. Nagano, and Y. Yamada. Vibrotactile display approach that modifies roughness sensations of real textures. In *Proceedings of IEEE RO-MAN 2012*, pages 1001–1006, sept. 2012.
- [15] R. A. Bailey. *Design of Comparative Experiments*. Number 25 in Cambridge Series in Statistical and Probabilistic Mathematics. Cambridge University Press, 2008.
- [16] Jonathan Bell and Mark H. Holmes. A note on modeling mechano-chemical transduction with an application to a skin receptor. *Journal of Mathematical Biology*, 32:275–285, 1994.
- [17] M. Benali-Khoudja, M. Hafez, J.-M. Alexandre, A. Kheddar, and V. Moreau. Vital: a new low-cost vibro-tactile display system. In *Proceedings of the International Conference on Robotics and Automation (ICRA)*, volume 1, pages 721–726, 2004.
- [18] M. Benali-Khoudja, M. and Hafez, J.-M. Alexandre, and A. Kheddar. Electromagnetically driven high-density tactile interface based on a multi-layer approach. In *Proceedings of the International Symposium on Micromechanics and Human Sciences*, pages 147–152, 2003.
- [19] M. E. H. Benbouzid. Artificial neural networks for finite element modeling of giant magnetostrictive devices. *IEEE Transactions On Magnetics*, 34:3853–3856, 1998.
- [20] M. Bergamasco. Design of hand force feedback systems for glove-like advanced interfaces. In *Proceedings of the 1992 IEEE International Workshop on Robot and Human Communication*, pages 286–293, September 1992.
- [21] A. Bicchi, M. Raugi, R. Rizzo, and N. Sgambelluri. Analysis and design of an electromagnetic system for the characterization of magneto-rheological fluids for haptic interfaces. *IEEE Transactions On Magnetics*, 41:1876–1879, 2005.
- [22] James Biggs and Mandayam A. Srinivasan. Tangential versus normal displacements of skin: Relative effectiveness for producing tactile sensations. In *Proceedings of the 10th Symp. on Haptic Interfaces for Virtual Environment and Teleoperator Systems (HAPTICS'02)*, 2002.
- [23] A. S. Birch and M. A. Srinivasan. Experimental determination of the viscoelastic properties of the human fingerpad. Technical Report 632, Research Lab. of Electronics at the MIT Cambridge, Massachusetts, 1999.
- [24] Ingvars Birznieks, Per Jenmalm, Antony W. Goodwin, and Roland S. Johansson. Encoding of direction of fingertip forces by human tactile afferents. *Journal of Neuroscience*, 21:8222–8237, 2001.
- [25] Gary H. Blackwood and Mark A. Ealey. Electrostrictive behavior in lead magnesium niobate (pnn) actuators. part i: materials perspective. *Smart Materials and Structures*, 2:124–133, 1993.

-
- [26] S. J. Bolanowski, G. A. Gescheider, R. T. Verrillo, and C. M. Checkosky. Four channels mediate the mechanical aspects of touch. *Journal of the Acoustical Society of America*, 84(5):1680–1694, 1988.
- [27] Jonathan Brooks and Irene Tracey. From nociception to pain perception: imaging the spinal and supraspinal pathways. *Journal of Anatomy*, 207:19–33, 2005.
- [28] G. Bruggencate. *Physiologie*, chapter Allgemeine Physiologie sensorischer Systeme, pages 47–82. Urban & Fischer Verlag München, 1999.
- [29] D. G. Caldwell, N. Tsagarakis, and C. Giesler. An integrated tactile/shear feedback array for stimulation of finger mechanoreceptor. In *Proceedings of the 1999 IEEE International Conference on Robotics and Automation*, pages 287–292, 1999.
- [30] Christopher S. Campbell, Shumin Zhai, Kim W. May, and Paul P. Maglio. What you feel must be what you see: Adding tactile feedback to the trackpoint. In *Proceedings of Human-Computer Interaction (INTERACT '99)*, pages 383–390, 1999.
- [31] Heather Carnahan, Adam Dubrowski, and Lawrence E.M. Grierson. Temperature influences both haptic perception and force production when grasping. *International Journal of Industrial Ergonomics*, 40(1):55–58, 2010.
- [32] F. Carpi, G. Frediani, and D. De Rossi. Electroactive elastomeric actuators for biomedical and bioinspired systems. In *Proceedings of the 2012 4th IEEE RAS EMBS International Conference on Biomedical Robotics and Biomechatronics (BioRob)*, pages 623–627, june 2012.
- [33] Margaret R. Chambers, K. H. Andres, Monika v. Duering, and A. Iggo. The structure and function of the slowly adapting type 2 mechanoreceptor in hairy skin. *Q. J. Exp. Physiol. Cogn. Med. Sci.*, 57:417–445, 1972.
- [34] E. Colin Cherry. Some experiments on the recognition of speech, with one and with two ears. *The Journal of the Acoustical Society of America*, 25(5):975–979, 1953.
- [35] J. Citerin, A. Kheddar, M. Hafez, F. Vidal, C. Plesse, D. Teyssie, and C. Chevrot. Characterization of a new interpenetrated network conductive polymer (ipn-cp) as a potential actuator that works in air conditions. In *Proceedings of the IEEE/RSJ International Conference on Intelligent Robots and Systems (IROS 2004)*, volume 1, pages 913–918 vol.1, 2004.
- [36] J. Citerin, G. Turbelin, A. Kheddar, F. Vidal, C. Chevrot, and D. Teyssie. New design methods and simulation of linear actuators using ionic polymers. In G. Turbelin, editor, *Proceedings of the Robotics and Biomimetics (ROBIO). 2005 IEEE International Conference on*, pages 438–443, 2005.
- [37] Burak Güçlü and Stanley J. Bolanowski. Tristate markov model for the firing statistics of rapidly-adapting mechanoreceptive fibers. *Journal of Computational Neuroscience*, 17:107–126, 2004.
- [38] Houghton Mifflin Company, editor. *The American Heritage Dictionary of the English Language*. Houghton Mifflin Company, 2004. <http://www.answers.com>.

- [39] Francis Crick and Christof Koch. Towards a neurobiological theory of consciousness. *Seminars in the Neurosciences*, 2:263–275, 1990.
- [40] Horst Czichos and Manfred Hennecke, editors. *HÜTTE – Die Grundlagen der Ingenieurwissenschaften*. Springer, Berlin, Heidelberg, 31 edition, 2000.
- [41] K. Dandekar, B.I. Raju, and M.A. Srinivasan. 3-d finite-element models of human and monkey fingertips to investigate the mechanics of tactile sense. *Journal of Biomechanical Engineering*, 125:682–691, 2003.
- [42] Ian Darian-Smith and Kenneth O. Johnson. Thermal sensibility and thermoreceptors. *Journal of Investigative Dermatology*, 69:146–153, 1977.
- [43] D. Dente, E.P. Scilingo, N. Sgambelluri, and A. Bicchi. Does active exploration suppress tactile flow perception? In E.P. Scilingo, editor, *Proceedings of the First Joint Eurohaptics Conference and Symposium on Haptic Interfaces for Virtual Environment and Teleoperator Systems World Haptics 2005*, pages 660–661, 2005.
- [44] K. Drewing, M. Fritschi, R. Zopf, M. O. Ernst, and M. Buss. First evaluation of a novel tactile display exerting shear force via lateral displacement. *ACM Transactions on Applied Perception*, 2(2):118–131, April 2005.
- [45] Benoni B. Edin. Quantitative analyses of dynamic strain sensitivity in human skin mechanoreceptors. *Journal of Neurophysiology*, 92:3233–3243, 2004.
- [46] Marc O. Ernst and Martin S. Banks. Humans integrate visual and haptic information in a statistically optimal fashion. *Nature*, 415:429–433, January 2002.
- [47] Jan Van Erp. Presenting directions with a vibrotactile torso display. *Ergonomics*, 48(3):302–313, Feb 2005.
- [48] G. T. Fechner. *Elemente der Psychophysik (2 Bnd.)*. Breitkopf & Härtel, 2nd edition, 1889.
- [49] A. S. French, A. V. Holden, and R. B. Stein. The estimation of the frequency response function of a mechanoreceptor. *Kybernetik*, 11:15–23, 1972.
- [50] Andrew S. French, Shin-Ichi Sekizawa, Ulli Höger, and Päivi H. Torkkeli. Predicting the responses of mechanoreceptor neurons to physiological inputs by nonlinear system identification. *Annals of Biomedical Engineering*, 29:187–194, 2001.
- [51] Milton Friedman. The use of ranks to avoid the assumption of normality implicit in the analysis of variance. *Journal of the American Statistical Association*, 32(200):675–701, December 1937.
- [52] Milton Friedman. A correction: The use of ranks to avoid the assumption of normality implicit in the analysis of variance. *Journal of the American Statistical Association*, 34(205):109, March 1939.
- [53] M. Fritschi. Deliverable 6.1: Design of a tactile shear force prototype display. Technical report, EU-Project TOUCH-HapSys (IST-2001-38040), March 2003. <http://www.touch-hapsys.org>.

-
- [54] M. Fritschi, K. Drewing, R. Zopf, M.O. Ernst, and M. Buss. Construction and first evaluation of a newly developed tactile shear force display. In M. Buss and M. Fritschi, editors, *Proceedings of the 4th International Conference EuroHaptics 2004*, pages 508–511, Munich, Germany, June 2004.
- [55] M. Fritschi, K. Drewing, R. Zopf, M.O. Ernst, and M. Buss. Construction and psychophysical evaluation of a novel tactile shear force display. In *Proceedings of the 13th International Workshop on Robot and Human Interactive Communication (RO-MAN 2004)*, pages 509–513. IEEE, 2004.
- [56] M. Fritschi, K. Drewing, R. Zopf, M.O. Ernst, and M. Buss. Tactile feedback systems. In *Workshop at the International Conference on Intelligent Robots and Systems (IROS 2004)*. IEEE/RSJ, Sept./Oct. 2004.
- [57] Michael Fritschi, Hasan Esen, Martin Buss, and Marc O. Ernst. *The Sense of Touch and its Rendering*, volume 45/2008 of *Springer Tracts in Advanced Robotics*, chapter Multi-modal VR Systems, pages 179–206. Springer Berlin / Heidelberg, 2008.
- [58] T. Fukuda, H. Hosokai, H. Ohyama, H. Hashimoto, and F. Arai. Giant magnetostrictive alloy (gma) applications to micro mobilerobot as a micro actuator without power supply cables. In *Proceedings of the Conference on Micro Electro Mechanical Systems (MEMS'91)*, pages 210–215, 1991.
- [59] Alberto Gallace, Hong Z Tan, and Charles Spence. Can tactile stimuli be subitised? an unresolved controversy within the literature on numerosity judgments. *Perception*, 37(5):782–800, 2008.
- [60] George A. Gescheider. *Psychophysics Method, Theory, and Application*. Lawrence Erlbaum Associates Inc., 2nd edition, 1985.
- [61] B.T. Gleeson, S.K. Horschel, and W.R. Provancher. Design of a fingertip-mounted tactile display with tangential skin displacement feedback. *IEEE Transactions on Haptics*, 3(4):297–301, Oct 2010.
- [62] Gunnar Gnad. *Ansteuerkonzept für piezoelektrische Aktoren*. PhD thesis, Otto-von-Guericke-Universität Magdeburg, 2005.
- [63] E. Bruce Goldstein. *Sensation and Perception*. Wadsworth, 6th edition, 2002.
- [64] Danny Grant and Vincent Hayward. Design of shape memory alloy actuator with high strain and variable structure control. In *Proceedings of the IEEE International Conference of Robotics and Automation*, pages 2305–2310. IEEE, 1995.
- [65] Danny Grant and Vincent Hayward. Controller for a high strain shape memory alloy actuator: Quenching of limit cycles. In *Proceedings of the 1997 IEEE International Conference on Robotics and Automation*, pages 254–259, 1997.
- [66] Henry Gray. *Anatomy of the Human Body*. Lea & Febiger, Philadelphia and New York, 20 edition, 1918. with drawings by H. V. Carter.

- [67] R.D. Greenough, J.M. Reed, and K. O'Connor. Characterisation of magnetostrictive or piezoelectric materials and transducers. In *Proceedings of the IEE Colloquium on Innovative Actuators for Mechatronic Systems*, 1995.
- [68] Francois M. Guillot, Jacek Jarzynski, and Edward Balizer. Measurement of electrostrictive coefficients of polymer films. *Journal of Acoustical Society of America*, 110(6):2980–2990, 2001.
- [69] A.L. Guinan, R.L. Koslover, N.A. Caswell, and W.R. Provancher. Bi-manual skin stretch feedback embedded within a game controller. In *Proceedings of the IEEE Haptics Symposium (HAPTICS)*, pages 255–260, march 2012.
- [70] R. J. Gulati and M. A. Srinivasan. Human fingerpad under indentation i: static and dynamic force response. In *Proceedings of the Bioengineering Conference*, volume 29, pages 261–262, 1995.
- [71] Rogeve J. Gulati and Mandayam A. Srinivasan. Determination of mechanical properties of the human fingerpad in vivo using tactile stimulator. Technical Report 605, Research Lab. of Electronics at the MIT Cambridge, Massachusetts, 1997.
- [72] M. Harders, A. Mazzone, G. Szekely, J. Citerin, M. Hafez, A. Kheddar, N. Sgambelluri, E. P E.P. Scilingo, A. Bicchi, and V.Hartwig. Deliverable 4.2: Final report on physical principles. Technical report, <http://www.touch-hapsys.org>, 2004.
- [73] C. J. Hasser and M. W. Daniels. Tactile feedback with adaptive controller for a force-reflecting haptic display. 1. design. In *Proceedings of the 5th Southern Biomedical Engineering Conference*, pages 526–529, 1996.
- [74] C. J. Hasser and M. W. Daniels. Tactile feedback with adaptive controller for a force-reflecting haptic display. 2. improvements and evaluation. In *Proceedings of the 5th Southern Biomedical Engineering Conference*, pages 530–533, 1996.
- [75] M.K. Haugland and J.A. Hoffer. Slip information provided by nerve cuff signals: application in closed-loop control of functional electrical stimulation. *IEEE Transactions on Rehabilitation Engineering*, 2:29–36, 1994.
- [76] Vincent Hayward and Juan Manuel Cruz-Hernández. Tactile display device using distributed lateral skin stretch. In *Proceedings of the Symposium on Haptic Interfaces for Virtual Environment and Teleoperator Systems*, pages 1309–1314, 2000.
- [77] Herbert Hensel. *Thermoreception and Temperatur Regulation*. Monographs of the physiological society No. 38. Academic Press, 1981. ISBN 0-12-341260-9.
- [78] R.D. Howe, D.A. Kontarinis, and W.J. Peine. Shape memory alloy actuator controller design for tactile displays. In *Proceedings of the 34th Conf. on Decision and Control*, volume 4, pages 3540–3544, 1995.
- [79] <http://hyperbraille.de/?lang=en>. Hyperbraille. Accessed: 2014-07-16.
- [80] <http://metec-ag.com>. metec ag. Accessed: 2014-07-16.

-
- [81] <http://www.ichaus.com/>.
- [82] A. Iggo. *Cutaneous sensory mechanisms*, chapter 17, pages 369–408. Cambridge University Press, 1982.
- [83] Y. Ikei and M. Shiratori. Textureexplorer: a tactile and force display for virtual textures. In *Proceedings of HAPTICS*, pages 327–334, 2002.
- [84] K. Ikuta, M. Tsukamoto, and S. Hirose. Mathematical model and experimental verification of shape memory alloy for designing micro actuator. In *Proceedings of Micro Electro Mechanical Systems (MEMS)*, pages 103–108, 1991.
- [85] O. B. Il'inskii, B. V. Krylov, and V. L. Cherepnov. Investigation of the optimal shape of the nerve ending of the encapsulated tissue mechanoreceptor (pacinian corpuscle). *Journal of Neurophysiology*, 9:326–331, 1977.
- [86] S. Ino, S. Shimizu, T. Odagawa, M. Sato, M. Takahashi, T. Izumi, and T. Ifukube. A tactile display for presenting quality of materials by changing the temperature of skin surface. In *2nd Proceedings of the IEEE Workshop on Robot and Human Communication*, pages 220–224, 1993.
- [87] Hiroo Iwata, Hiroaki Yano, Fumitaka Nakaizumi, and Ryo Kawamura. Project feelex: Adding haptic surface to graphics. In *Proceedings of ACM SIGGRAPH*, pages 469–475, 2001.
- [88] T. Izumi, N. Hoshimiya, A. Fujii, and Y. Handa. A presentation method of a traveling image for the sensory feedback for control of the paralyzed upper extremity. *Systems and Computers in Japan*, 19:87–96, 1988.
- [89] R. S. Johansson and A. B. Vallbo. Detection of tactile stimuli. thresholds of afferent units related to psychophysical thresholds in the human hand. *Journal of Physiology*, 297:405–422, 1979.
- [90] R. S. Johansson and A. B. Vallbo. Tactile sensibility in the human hand: receptive and absolute densities of four types of mechanoreceptive units in glabrous skin. *Journal of Physiology*, 286:283–300, 1979.
- [91] R. S. Johansson and A. B. Vallbo. Spatial properties of the population of mechanoreceptive units in the glabrous skin of the human hand. *Brain Research*, 184:353–366, 1980.
- [92] R.S. Johansson and A.B. Vallbo. Tactile sensory coding in the glabrous skin of the human hand. *Trends in Neurosciences*, 6:27–32, 1983.
- [93] Kenneth Johnson. *Stevens Handbook of Experimental Psychophysik: Sensation and Perception*, volume 1, chapter 13, Neural basis of haptic perception, pages 537–583. Wiley, New York, 3rd edition, 2002.
- [94] Kenneth O. Johnson. The role and function of cutaneous mechanoreceptors. *Current Opinion in Neurobiology*, 11:455–461, 2001.

- [95] Lynette A. Jones and Susan J. Lederman. *Human Hand Function*. Oxford University Press, 2006.
- [96] M. Jungmann and H. F. Schlaak. Miniaturised electrostatic tactile display with high structural compliance. In *Proceedings of the 2nd International Conference EuroHaptics*, 2002.
- [97] H. Kajimoto. Electrotactile display with real-time impedance feedback using pulse width modulation. *IEEE Transactions on Haptics*, 5(2):184–188, april-june 2012.
- [98] James W. Kalat. *Biological Psychology*. Wadsworth Publishing, 1997.
- [99] Pasi Kallio, Mikael Lind, Hannu Kojola, Quan Zhou, and Heikki N. Koivo. An actuation system for parallel link micromanipulators. In *Proceedings of the IEEE International Conference on Intelligent Robots and Systems (IROS)*, 1996.
- [100] P. Kammermeier, M. Buss, and G. Schmidt. Actuator array for display of distributed tactile information - design and preliminary experiments. In *Proceedings of the ASME Dynamic Systems and Control Division*, 2000.
- [101] P. Kammermeier, A. Kron, M. Buss, and G. Schmidt. Towards intuitive multifingered haptic exploration and manipulation. In *Proceedings of the 2001 Workshop on Advances in Multimodal Telepresence Systems*, pages 57–70, 2001.
- [102] C. Kasuga and F. Harashima. Characteristics analysis of multi-layer piezo-ceramic actuator. iii. In *Proceedings of the IEEE International Conference on Industrial Electronics, Control, Instrumentation, and Automation (IECON)*, volume 2, pages 1214–1218, 1995.
- [103] C. Kasuga, Y. Nakagawa, F. Harashima, T. Nishimura, and M. Ban. Characteristics analysis of multi-layer piezo-ceramic actuator. ii. In *Proceedings of the IEEE International Conference on Industrial Electronics, Control, Instrumentation, and Automation (IECON)*, volume 3, pages 1573–1576, 1993.
- [104] C. Kasuga, T. Nishimura, and F. Harashima. Characteristics analysis method of multi-layer piezo-ceramic actuator simulation of equivalent circuit using the state space method. In *Proceedings of the IEEE International Conference on Industrial Electronics, Control, Instrumentation, and Automation (IECON)*, volume 1, pages 336–339, 1992.
- [105] David V. Keyson and Adrianus J. M. Houtsmma. Directional sensitivity to a tactile point stimulus moving across the fingerpad. *Perception and Psychophysics*, 57:738–744, 1995.
- [106] Ryo Kikuuwe, Akihito Sano, Hiromi Mochiyama, and Naoyuki Takesue. Enhancing haptic detection of surface undulation. *ACM Transactions on Applied Perception*, 2:46–67, 2005.
- [107] M. Konyo, K. Akazawa, S. Tadokoro, and T. Takamori. Tactile feel display for virtual active touch. In *Proceedings of the IEEE/RSJ International Conference on Intelligent Robots and Systems (IROS)*, volume 4, pages 3744–3750, 2003.

-
- [108] A. Kron. *Beiträge zur bimauellen und mehrfingerigen haptischen Informationsvermittlung in Telepräsenzsystemen*. PhD thesis, Institute of Automatic Control Engineering, Technische Universität München, 2004.
- [109] Ki-Uk Kyung, Seung-Chan Kim, and Dong-Soo Kwon. Texture display mouse: Vibrotactile pattern and roughness display. *IEEE/ASME Transactions on Mechatronics*, 12:356–360, 2007.
- [110] Ki-Uk Kyung, Seung-Chan Kim, Dong-Soo Kwon, and M.A. Srinivasan. Texture display mouse kat: Vibrotactile pattern and roughness display. In *Proceedings of the IEEE/RSJ International Conference on Intelligent Robots and Systems (IROS)*, 2006.
- [111] Ki-Uk Kyung, Seung-Woo Son, Gi-Hun Yang, and Dong-Soo Kwon. How to effectively display surface properties using an integrated tactile display system. In *Proceedings of the International Conference on Robotics and Automation (ICRA)*, pages 1761–1766, 2005.
- [112] S.J. Lederman and R.L. Klatzky. *Vision and action: The control of grasping*, chapter Haptic exploration and object representation, pages 98–109. Abex, New Jersey, 1990.
- [113] Susan J. Lederman and Roberta L. Klatzky. Hand movements: A window into haptic object recognition. *Cognitive Psychology*, 19:342–368, 1987.
- [114] Susan J. Lederman and Roberta L. Klatzky. Haptic classification of common objects: Knowledge-driven exploration. *Cognitive Psychology*, 22:421–459, 1990.
- [115] Hyung Seok Lee, Hyeok Yong Kwon, Dae Gyeong Kim, Ui Kyum Kim, Nguyen Ngoc Linh, Nguyen Canh Toan, Hyungpil Moon, Ja Choon Koo, Jae do Nam, and Hyouk Ryeol Choi. Smd pluggable tactile display driven by soft actuator. In *Proceedings of the 2012 IEEE International Conference on Robotics and Automation (ICRA)*, pages 2731–2736, may 2012.
- [116] Jung-Hoon Lee, Ihn-Seok Ahn, and Jong-Oh Park. Design and implementation of tactile feedback device using electromagnetic type. In *Proceedings of the International Conference on Intelligent Robots and Systems (IROS)*, 1999.
- [117] Ming-Yih Lee, Chih-Feng Lin, and Kok-Soon Soon. Balance control enhancement using sub-sensory stimulation and visual-auditory biofeedback strategies for amputee subjects. *Prosthetics and Orthotics International*, 31(4):342–352, 2007.
- [118] V. Levesque, L. Oram, and K. MacLean. Exploring the design space of programmable friction for scrolling interactions. In *Proceedings of the IEEE Haptics Symposium (HAPTICS)*, pages 23–30, march 2012.
- [119] Vincent Levesque, Jerome Pasquero, Vincent Hayward, and Maryse Legault. Display of virtual braille dots by lateral skin deformation: feasibility study. *ACM Trans. Appl. Percept.*, 2(2):132–149, 2005.

- [120] Jung-Chi Liao and Mandayam A. Srinivasan. Experimental investigation of frictional properties of the human fingerpad. Technical Report 629, Research Lab. of Electronics at the MIT Cambridge, Massachusetts, 1999.
- [121] Soo-Chul Lim, Seung-Chan Kim, Ki-Uk Kyung, and Dong-Soo Kwon. Quantitative analysis of vibrotactile threshold and the effect of vibration frequency difference on tactile perception. In *Proceedings of the International Joint Conference SICE-ICASE*, pages 1927–1932, 2006.
- [122] Jiaqing Lin, H. Nishino, T. Kagawa, and K. Utsumiya. A tangible medical image processing assistant with haptic modality. In *Proceedings of the Sixth International Conference on Complex, Intelligent and Software Intensive Systems (CISIS)*, pages 723–728, july 2012.
- [123] J. M. Loomis and S. J. Lederman. *Handbook of perception and human performance*, chapter Tactual perception, pages 31/1–31/41. Wiley New York, 1986.
- [124] Virtouch Ltd. <http://www.skerpel.com/mouse.htm>.
- [125] Jan Lunze. *Regelungstechnik 2: Mehrgrößensysteme, Digitale Regelung (Springer-Lehrbuch)*. Springer, 2006.
- [126] John D. W. Madden, Nathan A. Vandesteeg, Patrick A. Anquetil, Peter G. A. Madden, Arash Takshi, Rachel Z. Pytel, Serge R. Lafontaine, Paul A. Wieringa, and Ian W. Hunter. Artificial muscle technology: Physical principles and naval prospects. *IEEE Journal of Oceanic Engineering*, 29:706–727, 2004.
- [127] Neil Madden and Brian Logan. Modelling perceptual phenomena using temporal abstraction networks. In *Proceedings of Modeling Natural Action Selection Workshop*, 2005.
- [128] By Madhero88 and M.Komorniczak. Layers of the skin. Wikimedia Commons, <https://commons.wikimedia.org/w/index.php?curid=21986708>, Oct 2012. CC BY-SA 3.0.
- [129] Yasutoshi Makino, Naoya Asamura, and Hiroyuki Shinoda. Multi primitive tactile display based on suction pressure control. In *Proceedings of the 12th IEEE International Symposium on Haptic Interfaces for Virtual Environment and Teleoperator Systems (HAPTICS)*, 2004.
- [130] N.A Mansour, AM.R.F. El-Bab, and M. Abdellatif. Design of a novel multi-modal tactile display device for biomedical applications. In *Proceedings of the 4th IEEE RAS EMBS International Conference on Biomedical Robotics and Biomechatronics (BioRob)*, pages 183–188, June 2012.
- [131] N.A Mansour, AM.R.F. El-Bab, and M. Abdellatif. Shape characterization of a multi-modal tactile display device for biomedical applications. In *Proceedings of the First International Conference on Innovative Engineering Systems (ICIES)*, pages 7–12, Dec 2012.

-
- [132] K. Matsuura, T. Yakoh, T. Aoyama, H. Anzai, K. Sakurai, and K. Isobe. Smooth tactile display in mouse using electro-rheological gel. In *Proceedings of the International Symposium on Industrial Electronics (ISIE)*, volume 2, pages 424–429, 2002.
- [133] John McBean and Cynthia Breazeal. Voice coil actuators for human-robot interaction. In *Proceedings of the IEEE/RSJ International Conference on Intelligent Robots and Systems (IROS)*, 2004.
- [134] Paul Andrew Millman. *Haptic Perception of Localized Features*. PhD thesis, Northwestern University, 1995.
- [135] Diana Weedman Molavi. Neuroscience tutorial. The Washington University School of Medicine, <http://www.bioon.com/bioline/neurosci/course/index.htm>, accessed 2016.
- [136] J. Moran and R. Desimone. Selective attention gates visual processing in the extrastriate cortex. *Science*, 229(4715):782–784, Aug 1985.
- [137] G. Moy, C. Wagner, and R.S. Fearing. A compliant tactile display for teletaction. In *Proceedings of Proceedings of the IEEE International Conference on Robotics and Automation (ICRA)*, 2000.
- [138] Ernst Mutschler, Hans-Georg Schaible, Gerhard Thews, and Peter Vaupel, editors. *Anatomie, Physiologie, Pathophysiologie des Menschen*. Wissenschaftliche Verlagsgesellschaft Stuttgart, 6th edition, 2007.
- [139] Kyoungwan Na, Ji-Seok Han, Duk-Moon Roh, Byung-Ki Chae, Eui-Sung Yoon, Ji Yoon Kang, and Il-Joo Cho. Flexible latching-type tactile display system actuated by combination of electromagnetic and pneumatic forces. In *Proceedings of the IEEE 25th International Conference on Micro Electro Mechanical Systems (MEMS)*, pages 1149–1152, 29 2012-feb. 2 2012.
- [140] Ernst Niebur, Steven S. Hsiao, and Kenneth O. Johnson. Synchrony: a neuronal mechanism for attentional selection? *Current Opinion in Neurobiology*, 12:190–194, 2002.
- [141] Ernst Niebur and Christof Koch. A model for the neuronal implementation of selective visual attention based on temporal correlation among neurons. *Journal of Computational Neuroscience*, 1:141–158, 1994.
- [142] H. Nishino, Y. Fukakusa, A. Hatano, T. Kagawa, and K. Utsumiya. A tangible information explorer using vibratory touch screen. In *Proceedings of the IEEE 26th International Conference on Advanced Information Networking and Applications (AINA)*, pages 671–677, march 2012.
- [143] Kenneth H. Norwich. *Information, Sensation and Perception*. Academic Press, Inc., 1993.
- [144] Jose Ochoa and Erik Torebjörk. Sensations evoked by intraneural microstimulation of single mechanoreceptor units innervating the human hand. *Journal of Physiology*, 342:633–654, 1983.

- [145] S. Okumoto, Feng Zhao, and H. Sawada. Tactoglove presenting tactile sensations for intuitive gestural interaction. In *Proceedings of the IEEE International Symposium on Industrial Electronics (ISIE)*, pages 1680–1685, may 2012.
- [146] Michel Pare, Catherine Behets, and Olivier Cornu. Paucity of presumptive ruffini corpuscles in the index finger pad of humans. *The Journal of Comparative Neurology*, 456:260–266, 2003.
- [147] Michel Pare, Heather Carnahan, and Allan M. Smith. Magnitude estimation of tangential force applied to the fingerpad. *Experimental Brain Research*, 142:342–348, 2002.
- [148] Seung-Eek Park and Thomas R. ShROUT. Ultrahigh strain and piezoelectric behavior in relaxor based ferroelectric single crystals. *Journal of Applied Physic*, 82:1804–1811, 1997.
- [149] P. E. Patterson and J. A. Katz. Design and evaluation of a sensory feedback system that provides grasping pressure in a myoelectric hand. *J Rehabil Res Dev*, 29(1):1–8, 1992.
- [150] M. Peruzzini, M. Germani, and M. Mengoni. Electro-tactile device for texture simulation. In *Proceedings of the 2012 IEEE/ASME International Conference on Mechatronics and Embedded Systems and Applications (MESA)*, pages 178–183, july 2012.
- [151] C. A. Phillips. Sensory feedback control of upper- and lower-extremity motor prostheses. *Crit Rev Biomed Eng*, 16(2):105–140, 1988.
- [152] J. R. Phillips, R. S. Johansson, and K. O. Johnson. Responses of human mechanoreceptive afferents to embossed dot arrays scanned across fingerpad skin. *Journal of Neuroscience*, 12:827–839, 1992.
- [153] J. R. Phillips, R. S. Johansson, and K. O. Johnson. Representation of braille characters in human nerve fibres. *Exp. Brain Research*, 81:589–592, 1990.
- [154] Inc. Piezo Systems. Co-fired multi-layer stack motor. Introduction to piezo transducers, <http://www.piezo.com/tech2intropiezotrans.html>, accessed 2016.
- [155] Piezomechanik - Dr. Lutz Pickelmann GmbH. *Piezo-Mechanics: An Introduction*. <http://www.piezomechanik.com>.
- [156] Markus Ploner, Bettina Pollok, and Alfons Schnitzler. Pain facilitates tactile processing in human somatosensory cortices. *Journal of Neurophysiology*, 92(3):1825–1829, 2004.
- [157] Seppo Pohja. Survey of studies on tactile senses. Technical Report R96-02, RWCP Neuro SICS Laboratory, 1996.
- [158] L.B.C. Porquis, M. Konyo, and S. Tadokoro. Tactile-based torque illusion controlled by strain distributions on multi-finger contact. In *Proceedings of the IEEE Haptics Symposium (HAPTICS)*, pages 393–398, March 2012.

-
- [159] F. Reynier and V. Hayward. Summary of the kinesthetic and tactile function of the human upper extremities. Internal report, McGill Research Centre for Intelligent Machines, Montreal, 1993.
- [160] Kevin J Riggs, Ludovic Ferrand, Denis Lancelin, Laurent Fryziel, Gérard Dumur, and Andrew Simpson. Subitizing in tactile perception. *Psychol Sci*, 17(4):271–272, Apr 2006.
- [161] J. W. Ring and Richard de Dear. Temperature transients: A model for heat diffusion through the skin, thermoreceptor response and thermal sensation. *Int. Journal of Indoor Environment and Health*, 1:448–456, 1991.
- [162] H. Ringhandt and Ch. Wirth. *Feinwerkzeugelemente*. Carl Hansa Verlag, München, 1992.
- [163] R. Rizzo, N. Sgambelluri, E.P. Scilingo, M. Raugi, and A. Bicchi. Electromagnetic modeling and design of haptic interface prototypes based on magnetorheological fluids. *IEEE Transactions on Magnetics*, 43(9):3586–3600, 2007.
- [164] Barbara Susan Robinson, Jeanne L Cook, Cynthia McCormick Richburg, and Stephen E Price. Use of an electro-tactile vestibular substitution system to facilitate balance and gait of an individual with gentamicin-induced bilateral vestibular hypofunction and bilateral transtibial amputation. *Journal of Neurology and Physical Therapy*, 33(3):150–159, Sep 2009.
- [165] Gabriel Robles-De-La-Torre and Vincent Hayward. Virtual surfaces and haptic shape perception. In *Proceedings of the Haptic Interfaces for Virtual Environment and Teleoperator Systems Symposium, ASME International Mechanical Engineering Congress and Exposition*, 2000.
- [166] Raül Rojas. *Theorie der neuronalen Netze*. Springer-Verlag Berlin Heidelberg New York, 4th edition, 1996.
- [167] Pekka Ronkanen, Pasi Kallio, and Heikki N. Koivo. Simultaneous actuation and force estimation using piezoelectric actuators. In *Proceedings of the 2007 IEEE International Conference on Mechatronics and Automation*, 2007.
- [168] A. Roy, P. N. Steinmetz, S. S. Hsiao, K. O. Johnson, and E. Niebur. Synchrony: A neural correlate of somatosensory attention. *Journal of Neurophysiology*, 98:1645–1661, 2007.
- [169] Dongseok Ryu, Gi-Hun Yang, and Sungchul Kang. T-hive: Bilateral haptic interface using vibrotactile cues for presenting spatial information. *Systems, Man, and Cybernetics, Part C: Applications and Reviews, IEEE Transactions on*, 42(6):1318–1325, nov. 2012.
- [170] S. Saga and K. Deguchi. Lateral-force-based 2.5-dimensional tactile display for touch screen. In *Proceedings of the IEEE Haptics Symposium (HAPTICS)*, pages 15–22, march 2012.

- [171] M. Salada, P. Vishton, J.E. Colgate, and E. Frankel. Two experiments on the perception of slip at the fingertip. In *Proceedings of the 12th Symp. on Haptic Interfaces For Virtual Environment and Teleoperator Systems (HAPTICS)*, pages 146–153, 2004.
- [172] Mark Salada, J. Edward Colgate, Margaret Lee, and Peter Vishton. Fingertiphaptics: A novel direction in haptic display. In *Conference Proceedings of the 8th Mechatronics Forum*, 2002.
- [173] Mark A. Salada, J. Edward Colgate, Margaret V. Lee, and Peter M. Vishton. Validating a novel approach to rendering fingertip contact sensations. In *Proceedings of the 10th Symp. on Haptic Interfaces For Virtual Environment and Teleoperator Systems (HAPTICS)*, 2002.
- [174] F. Salsedo, S. Marcheschi, M. Fontana, and M. Bergamasco. Tactile transducer based on electromechanical solenoids. In *Proceedings of the IEEE World Haptics Conference (WHC)*, pages 581–586, June 2011.
- [175] Helmut F. Schlaak, Markus Jungmann, Marc Matysek, and Peter Lotz. Novel multilayer electrostatic solid state actuators with elastic dielectric. In *Smart Structures and Materials 2005: Electroactive Polymer Actuators and Devices (EAPAD)*, volume 5759, pages 121–133, 2005.
- [176] Günther Schmidt. *Regelungs- und Steuerungstechnik 2*. Institute of Automatic Control Engineering (LSR) at TU München, 2000.
- [177] Enzo Scilingo, Nicola Sgambelluri, and Antonio Bicchi. The role of tactile flow in processing dynamic haptic stimuli. In Antonio Bicchi, Martin Buss, Marc Ernst, and Angelika Peer, editors, *The Sense of Touch and its Rendering*, volume 45 of *Springer Tracts in Advanced Robotics*, pages 39–60. Springer Berlin / Heidelberg, 2008.
- [178] Elaine R. Serina, C. D. Mote, and David Rempel. Force response of the fingertip pulpnext term to repeated compression - effects of loading rate, loading angle and anthropometry. *Journal of Biomechanics*, 30:1035–1040, 1997.
- [179] N. Sgambelluri, R. Rizzo, E.P. Scilingo, M. Raugi, and A. Bicchi. Free hand haptic interfaces based on magnetorheological fluids. In *Proceedings of the 14th Symposium on Haptic Interfaces for Virtual Environment and Teleoperator Systems*, pages 367–371, 2006.
- [180] C. E. Sherrick and R. W. Cholewiak. *Handbook of human perception and human performance*, volume 1, chapter 12: Cutaneous Sensitivity, pages 1–57. John Wiley & Sons, New York, 1986.
- [181] Carl E. Sherrick, Roger W. Cholewiak, and Amy A. Collins. The localization of low- and high-frequency vibrotactile stimuli. *Journal of the Acoustical Society of America*, 88:169–179, 1990.
- [182] K.B. Shimoga. A survey of perceptual feedback issues in dexterous telemanipulation. i. finger force feedback. In *Proceedings of the Annual International Symposium on Virtual Reality*, pages 263–270, 1993.

-
- [183] K.B. Shimoga. A survey of perceptual feedback issues in dexterous telemanipulation. ii. finger touch feedback. In *Proceedings of the Annual International Symposium on Virtual Reality*, pages 271–279, 1993.
- [184] Masami Shinohara, Yutaka Shimizu, and Akira Mochizuki. Three-dimensional tactile display for the blind. *IEEE Transactions on Rehabilitation Engineering*, 6:249–256, 1998.
- [185] C. Soanes, A. Spooner, and S. Hawker, editors. *The Oxford Paperback Dictionary, Thesaurus and Wordpower Guide*. Oxford University Press, 2001.
- [186] Johannes Sobotta and Ulrich Welsch, editors. *Atlas Histologie*. Elsevier, Urban & Fischer, München, 2005.
- [187] Charles Spence and Alberto Gallace. Recent developments in the study of tactile attention. *Can J Exp Psychol*, 61(3):196–207, Sep 2007.
- [188] R. Stanway. The development of force actuators using ER and MR fluid technology. In *Proceedings of the IEE Colloquium on Actuator Technology: Current Practice and New Developments*, 1996.
- [189] P. N. Steinmetz, A. Roy, P. J. Fitzgerald, S. S. Hsiao, K. O. Johnson, and E. Niebur. Attention modulates synchronized neuronal firing in primate somatosensory cortex. *Nature*, 404:187–190, 2000.
- [190] J. Streque, A Talbi, P. Pernod, and V. Preobrazhensky. New magnetic microactuator design based on pdms elastomer and mems technologies for tactile display. *IEEE Transactions on Haptics*, 3(2):88–97, April 2010.
- [191] I.R. Summers, C.M. Chanter, A.L. Southall, and A.C Brady. Results from a tactile array on the fingertip. In *Proceedings of the 2nd International Conference EuroHaptics*, 2001.
- [192] Hui Tang and David J Beebe. An oral tactile interface for blind navigation. *IEEE Trans Neural Syst Rehabil Eng*, 14(1):116–123, Mar 2006.
- [193] P.M. Taylor, P.M. Taylor, A. Moser, and A. Creed. The design and control of a tactile display based on shape memory alloys. In *Proceedings of the IEEE International Conference on Robotics and Automation*, volume 2, pages 1318–1323, 1997.
- [194] Ashutosh K. Tewari, Nishant D. Patel, Robert A. Leung, Rajiv Yadav, E. Darracott Vaughan, Youssef El-Douaihy, Jiangling J. Tu, Muhul B. Amin, Mohammed Akhtar, Mark Burns, Usha Kreaden, Mark A. Rubin, Atsushi Takenaka, and Maria M. Shevchuk. Visual cues as a surrogate for tactile feedback during robotic-assisted laparoscopic prostatectomy: posterolateral margin rates in 1340 consecutive patients. *BJU International*, 106(4):528–536, 2010.
- [195] Massimo Turatto, Giovanni Galfano, Bruce Bridgeman, and Carlo Umiltà. Space-independent modality-driven attentional capture in auditory, tactile and visual systems. *Exp Brain Res*, 155(3):301–310, Apr 2004.

- [196] M. Ueberle, N. Mock, A. Peer, C. Michas, and M. Buss. *Advances in Telerobotics: Human Interfaces, Control, and Applications*, chapter Design, control, and evaluation of a hyper-redundant haptic device. Springer, STAR series, 2007.
- [197] Marc Ueberle. *Design, Control, and Evaluation of a Family of Kinesthetic Haptic Interfaces*. PhD thesis, Lehrstuhl für Steuerungs- und Regelungstechnik, Technische Universität München, 2006.
- [198] Marc Ueberle, N. Mock, and M. Buss. Vishard 10, a novel hyper-redundant haptic interface. In *Proceedings of the 12th International Symposium on Haptic Interfaces for Virtual Environment and Teleoperator Systems*, pages 58–65, 2004.
- [199] A. B. Vallbo and K. E. Hagbarth. Activity from skin mechanoreceptors recorded percutaneously in awake human subjects. *Experimental Neurology*, 21:270–289, 1968.
- [200] Ramiro Velazquez and Omar Bazan. Preliminary evaluation of podotactile feedback in sighted and blind users. *Proceedings of the Annual International Conference of the IEEE Engineering in Medicine and Biology Society (EMBC)*, 2010:2103–2106, 2010.
- [201] Marco Vitello. *Perception of moving tactile stimuli*. PhD thesis, Max-Planck Institute of Biological Cybernetics, 2010.
- [202] Marco P. Vitello, Michael Fritschi, and Marc O. Ernst. *Immersive Multimodal Interactive Presence*, chapter Active Movement Reduces the Tactile Discrimination Performance, pages 7–34. Springer Series on Touch and Haptic Systems. Springer Berlin / Heidelberg, 2012.
- [203] M.P. Vitello, M.O. Ernst, and M. Fritschi. An instance of tactile suppression: Active exploration impairs tactile sensitivity for the direction of lateral movement. In *Proceedings of the EuroHaptic International Conference*, pages 351–355, 2006.
- [204] C.R. Wagner, S.J. Lederman, and R.D. Howe. A tactile shape display using rc servomotors. In *Proceedings of the 10th International Symposium on Haptic Interfaces for Virtual Environment and Teleoperator Systems (HAPTICS'02)*, 2002.
- [205] Qi Wang, Vincent Levesque, Jerome Pasquero, and Vincent Hayward. A haptic memory game using the stress2 tactile display. In *CHI '06 extended abstracts on Human factors in computing systems*, pages 271–274, New York, NY, USA, 2006. ACM Press.
- [206] J. Watanabe, H. Ishikawa, X. Arouette, and N. Miki. Surface texture and pseudo tactile sensation displayed by a mems-based tactile display. In *Proceedings of the IEEE/RSJ International Conference on Intelligent Robots and Systems (IROS)*, pages 4150–4155, oct. 2012.
- [207] Robert J. Webster, Todd E. Murphy, Lawton N. Verner, and Allison M. Okamura. A novel two-dimensional tactile slip display: Design, kinematics and perceptual experiments. *ACM Transactions on Applied Perception*, 2:150–165, 2005.

-
- [208] Parris S. Wellman, William J. Peine, Gregg E. Favalora, and Robert D. Howe. Mechanical design and control of a high-bandwidth shape memory alloy tactile display. In *Proceedings of the International Symposium on Experimental Robotics*, pages 56–66, 1997.
- [209] J. Werner. Zur Temperaturregelung des menschlichen Körpers. *Biological Cybernetics*, 17:53–63, 1975.
- [210] J. Werner. Mathematical treatment of structure and function of the human thermoregulatory system. *Biological Cybernetics*, 25:93–101, 1977.
- [211] Felix A. Wichmann and N. Jeremy Hill. The psychometric function: I. fitting, sampling, and goodness of fit. *Perception & Psychophysics*, 63:1293–1313, 2001.
- [212] Felix A. Wichmann and N. Jeremy Hill. The psychometric function: Ii. bootstrap-based confidence intervals and sampling. *Perception & Psychophysics*, 63:1314–1329, 2001.
- [213] Gi-Hun Yang, Ki-Uk Kyung, Young-Ju Jeong, and Dong-Soo Kwon. Novel haptic mouse system for holistic haptic display and potential of vibrotactile stimulation. In *Proceedings of the International Conference on Intelligent Robots and Systems (IROS)*, pages 1980–1985, 2005.
- [214] Gi-Hun Yang, Ki-Uk Kyung, M.A. Srinivasan, and Dong-Soo Kwon. Quantitative tactile display device with pin-array type tactile feedback and thermal feedback. In *Proceedings of the International Conference on Robotics and Automation (ICRA)*, pages 3917–3922, 2006.
- [215] Manfred Zimmermann. Neurophysiologische Grundlagen von Schmerz und Schmerztherapie. *Langenbecks Archiv for Chirurgie*, 342:64–74, 1976.
- [216] M. Zinn, B. Roth, O. Khatib, and J.K. Salisbury. New actuation approach for human-friendly robot design. *The International Journal of Robotics Research*, 23:379–398, 2004.